UMCEE 98-12 June 1998

DEVELOPMENT OF A GUIDE FOR EVALUATION OF EXISTING BRIDGES PART I

PROJECT 97-0245 DIR

Report submitted to the Michigan Department of Transportation

Andrzej S. Nowak and Sangjin Kim

Department of Civil and Environmental Engineering
University of Michigan
Ann Arbor, Michigan 48109-2125

Testing and Research Section
Construction and Technology Division
Research Project No. RC-1362
Part I

This report, authorized by the transportation director, has been prepared to provide technical information and guidance for personnel in the Michigan Department of Transportation, the FHWA, and other reciprocating agencies. The cost of publishing 40 copies of this report at $7.57 per copy is $302.84 and it is printed in accordance with Executive Directive 1991-6.

Technical Report Documentation Page

1. Report No. Research Report RC-1362	2. Government Accession No.	3. Recipient's Catalog No.
4. Title and Subtitle Development of a Guide for Evaluation of Existing Bridges, Part I		5. Report Date May 1998
7. Author(s) Andrzej S. Nowak and Sangjin Kim		6. Performing Organization Code
9. Performing Organization Name and Address University of Michigan 2340 G. G. Brown Bldg. Ann Arbor, MI 48109-2125		8. Performing Org Report No. RC-1362
12. Sponsoring Agency Name and Address Michigan Department of Transportation Construction and Technology Division P.O. Box 30049 Lansing, MI 48909		10. Work Unit No. (TRAIS)
		11. Contract/Grant No. 97-0245 DIR
15. Supplementary Notes		13. Type of Report & Period Covered Final Report, 5-97/5-98
		14. Sponsoring Agency Code

16. Abstract

The objective of this report is to present the results of the field tests carried out in 1997 by the team at the University of Michigan. The field tests were performed to determine the load distribution factors needed for evaluation of exisiting bridges. In some of the previous tests it was observed that the currently girder distribution factors can be conservative. However, the analytical study carried out in conjunction with the development of the AASHTO LRFD Code showed that for short spans and girder spacings, the current code provisions can be too permissive. Therefore, this study focused on short span steel girder bridges. The tests also included measurement of dynamic loads, and proof load testing. The research work involved formulation of the testing procedure, selection of structures, installation of equipment, measurements, and interpretation of the results. The work was based on experience gained in the previous study. Equipment included the data acquisition systems available at the University of Michigan. The measurements included strains and deflections. Five bridges were tested; including one proof load test. All selected structures are located in South Michigan. The results are summarized in the final chapter of this report.

17. Key Words bridges, field testing load distribution, proof load, dynamic load	18. Distribution Statement No restrictions. This document is available to the public through the Michigan Department of Transportation.		
19. Security Classification (report) Unclassified	20. Security Classification (Page) Unclassified	21. No of Pages	22. Price

Form DOT F 1700.7 (8-72)

DISCLAIMER

The contents of this report reflect the views of the authors, who are responsible for the facts and the accuracy of the information presented herein. This document is disseminated under the sponsorship of the Michigan Department of Transportation and Great Lakes Center for Truck Transportation Research at the University of Michigan Transportation Research Institute, in the interest of information exchange. The Michigan Department of Transportation assumes no liability for the contents or use thereof.

Executive Summary

The research work carried out as a part of this project is documented in two reports: Part I and Part II. This report presents the results of the field tests carried out in 1997. The other report, Part II, provides a guide for field testing. The field tests were performed to determine the load distribution factors needed for evaluation of existing bridges. Prior analytical studies showed that in most cases the current code provisions are too conservative, however, for short spans and girder spacings, they can be too permissive. There are many short span steel girder bridges in Michigan. Therefore, this study focused on these structures to verify the validity of the code specified distribution factor.

The research work involved formulation of the testing procedure, selection of structures, installation of equipment, measurements, and interpretation of the results. The work was based on experience gained in the previous study. Equipment included the data acquisition systems available at the University of Michigan. The measurements included strains and deflections. An important part of this project was further development of practical procedure for the proof load tests. The proof load was applied in form of military tanks (M-60) provided by the Michigan National Guard. Application of proof load required traffic control.

Bridges were selected for tests based of the following criteria: structural type (steel girder bridges), span length (less than 18 m), accessibility for testing equipment (unacceptable because of deep water or height), traffic volume (requirement for traffic control), and future repair/replacement schedule (bridges scheduled for major repairs/replacements in the near future were excluded). The five bridges selected for field tests are: Bridge B02-46032, M-156 over Silver Creek in Morenci, Bridge B05-46041, M-34 over Raisin River in Adrian, Bridge

B02-12021, US-12 over Swan Creek near Bronson, Bridge B02-38051, M-106 over Portage River Drain near Munith, and Bridge B01-70041, M-45 over Bass River near Grand Rapids.

For all tested bridges, the strains were measured under a single truck in various transverse positions within the roadway width, and under two trucks side-by-side. The measurements were taken for a crawling speed and a normal traffic speed. The observed girder distribution factors were compared to analytical values obtained using the formulas specified in the AASHTO specifications (1996) and AASHTO LRFD Code (1994).

The test results confirmed that the response is linear. The comparison of strain values for a single truck indicates that for two trucks side-by-side tests, the results are equal to superposition of single truck results. The absolute value of measured strains is lower than expected. The main reasons for low strains are: unintended composite action, partial fixity of supports and increased actual stiffness due to sidewalks, parapets and railings. For a single truck, girder distribution factors observed in the tests are lower than those specified by AASHTO. For two trucks side-by-side, the girder distribution factors are equal to those specified in AASHTO.

Dynamic load were measured in terms of the ratio of dynamic and static strains. It was observed that dynamic load is lower than specified and the dynamic load factor decreases with increasing static load effect. For two trucks side-by-side it is about 0.10.

Proof load test performed on bridge B02-12021 confirmed that it is adequate to carry the normal truck traffic. The measured deflections and strains were relatively low, and considerably lower than expected.

TABLE OF CONTENTS

Note:

Intentionally left blank

Acknowledgments

The presented research has been sponsored by the Michigan Department of Transportation, and the Great Lakes Center for Truck and Transit Research (GLCTTR) at the University of Michigan which is gratefully acknowledged. The authors thank the technical staff of the Michigan DOT, Roger Till, Sonny Jadun, Sudhakar Kulkarni, and David Juntunen, for their useful comments, discussions and support, and Thomas Gillespie, of the University of Michigan Transportation Research Institute (UMTRI) for his support.

The project team received help from other researchers, current and former students and staff of the University of Michigan. In particular, thanks are due to Dr. Vijay Saraf, Junsik Eom, Chris Eamon, Chan-Hee Park, Tom Murphy, Dr. Ahmet Sanli, Dr. Maria Szerszen, Manu Puri, and Angela Campbell. They were involved in field instrumentation, measurements, and processing of the results.

Thanks are due to the Michigan State Police for their cooperation. Traffic control was provided by the Michigan DOT and several counties. Proof load test was carried out using military tanks provided by the Michigan National Guard which is gratefully acknowledged.

The realization of the research program would not be possible without in kind support of the Michigan DOT and the University of Michigan. Measurements were taken using equipment purchased by the University of Michigan.

Thanks are due to Junsik Eom who served as a technical editor of this Report. He was assisted by Dr. Ahmet Sanli and Chris Eamon.

Note:

Intentionally left blank

1. Introduction

A rational bridge management requires a good knowledge of the actual loads, load distribution, load effects and structural condition (load carrying capacity). Therefore, evaluation of existing structures is very important. However, there is a considerable number of bridges that are very difficult, if not impossible, to evaluate using traditional inspection methods and analysis. For example, this applies to many deteriorated structures (severe corrosion, cracking), and those for which the documentation is missing. It also may apply to structures showing difficult to explain behavior (excessive vibration, deflection, accelerated deterioration).

A considerable number of Michigan bridges show signs of deterioration. In particular, there is a severe corrosion on many steel and concrete structures. By analytical methods, many of these bridges are not adequate to carry the normal highway traffic. However, the actual load carrying capacity is often much higher than what can be determined by analysis, due to more favorable load sharing, effect of non-structural components (parapets, railing, sidewalks), composite deck action without shear developers, and other difficult to quantify factors. Field testing can reveal the hidden strength reserve and thus verify the adequacy of the bridge.

The research work carried out as a part of this project is documented in two reports: Part I and Part II. The objective Part I is to present the results of the field tests carried out in 1997. The other report, Part II, provides a guide for field testing, including weigh-in-motion truck measurement, measurement of dynamic loads, measurement of fatigue loads, verification of girder distribution factors, and proof load testing.

The field tests were performed to determine the load distribution factors needed for evaluation of existing bridges. In some of the previous tests it was observed that the currently used S/4.27 (S = girder spacing in meters; or S/14 where S = girder spacing in feet, and in both expressions, the resulting load distribution factor is a fraction of the entire truck weight) can be conservative. However, the analytical study carried out in conjunction with the development of the AASHTO LRFD Code (1994) showed that for short spans and girder spacings, S/4.27 or even S/3.36 (=S/11, where S is girder spacing in feet) can be too permissive. There are many such bridges in Michigan, in particular with steel girders. Therefore, the study focused on short span steel girder bridges to verify the validity of this distribution factor.

The research work involved formulation of the testing procedure, selection of structures, installation of equipment, measurements, and interpretation of the results. The work was based on experience gained in the previous study. Equipment included the data acquisition systems available at the University of Michigan. The measurements included strains and deflections. An attempt was made towards the development of an approach to difficult to access spans, spans over water, and spans over busy roads. Therefore, a special reach-all truck was used. Equipment for wireless transfer of the signal was purchased for this project. However, the system did not work and was sent back to the manufacturer for repairs and adjustments.

An important part of this project is further development of practical procedure for the proof load tests. The parameters which determine the proof load level include a live load factor, dynamic factor, number of lanes, and traffic volume and weight. The proof load was applied in form of military tanks (M-60) provided by the Michigan National Guard. The Project Team had an experience of using these

tanks for bridge testing. Application of proof load required traffic control.

Five bridges were tested, including one proof load test. All selected structures are located in South Michigan. The results are summarized in the final chapter of this report.

2. Selected Bridges

Bridges were selected for tests based of the following criteria:

- Structural type; it was decided to focus on steel girder bridges.
- Span length; the verification of distribution factors is needed mostly for shorter spans, less than 18 m.
- Accessibility; not all the structures can be accessed to install the testing equipment because of deep water, heavy traffic, or height.
- Traffic volume; very busy bridges can be difficult from the traffic control point of view.
- Future repair/replacement schedule; it was decided to exclude bridges scheduled for major repairs/replacements in the near future.

The five bridges selected for field tests are listed in Table 2.1.

Table 2.1. List of selected bridges.

MDOT ID Number	Location	Span (m)	Number of Girders	Girder Spacing (m)	Year of Construction	Skew
B02-46032	Morenci (M-156)	13.7	10	1.32	1935	30°
B05-46041	Adrian (M-34)	16.8	11	1.44	1932	0°
B02-12021	Bronson (US-12)	9.9	12	1.36	1922	10°
B02-38051	Munith (M-106)	13.7	9	1.46	1939	20°
B01-70041	Grand Rapids (M-45)	11.7	10	1.42	1929	0°

Bridges in Table 2.1 were selected from two lists prepared by the Michigan DOT. The first list includes 28 structures, Table 2.2, and the other one - 36 bridges, Table 2.3.

Table 2.2. List of Bridges Provided by MDOT, April 1997.

	Bridge ID	Facility	Feature	Location	Yr Blt	Br Type	Max Span	Condition Rtgs						Beam Spacing		District
								Deck	Surface	Super	Paint	Subs	Load Rtg	Feet	Inches	
1	12021-B03	US-12	COLDWATER R	W LT OF COLDWATER	1939	3	75	3	5	3	0	5	9	73	5	1	7
2	13032-B02	M-66	WANONDAGER CR	3.2 MI SW OF BARRY CO LIN	1940	3	50	4	4	5	0	8	9	88	4	9	7
3	13061-R01	I-94BL	CONRAIL	1.0 MI E OF BATTLE CREEK	1937	3	40	3	5	4	1	5	9	82	4	6	7
4	38051-B02	M-106	PORTAGE R DRAIN	4.7 MI S&W OF INGHAM CO	1939	3	45	5	6	5	0	6	9	89	4	9	8
5	46032-B02	M-156	SILVER CR	IN MORENCI	1935	3	45	5	6	5	0	7	9	89	4	4	8
6	46041-B05	M-34	BEAN CR	IN HUDSON	1930	3	65	4	7	4	0	4	9	82	4	4	8
7	47014-S04	M-34	S BR RAISIN R	IN ADRIAN (BEECHER ST)	1932	3	55	4	7	4	5	6	9	78	4	8	8
8	47061-B03	CROUSE RD	US-23	1.6 MI N OF M-59	1961	3	60	6	6	5	0	7	9	81	6	0	8
9	47065-S09	I-96 BL	S BR SHIWASSE R	1.9 MI OF HOWEL	1918	3	40	5	7	4	0	6	9	80	4	5	8
10	50011-S04	DORR RD	I-96	1.6 MI SE OF I-96 BL	1961	3	91	6	6	4	0	6	9	78	6	0	8
11	58032-B01	CLINTON R RD	M-53	1.2 MI S OF M-59	1966	3	88	6	6	4	0	7	9	81	6	0	9
12	58053-B04	M-50	RAISIN R	IN DUNDEE MONROE ST	1937	3	60	3	5	3	0	4	9	82	4	11	8
13	63022-S03	US-24	HURON R	@WAYNE CO LINE	1933	3	81	4	8	3	0	4	9	55	4	11	8
14	63022-S04	SOUTH HILL RD	I-96	4.0 MI E OF LIVINGSTON CO	1957	3	71	6	6	5	5	7	9	80	4	5	9
15	63022-S06	OLD PLANK RD	I-96	5.1 MI OF LIVINGSTON CO	1957	3	71	6	7	5	1	6	9	82	4	5	9
16	63022-S09	BECK RD	I-96	IN NOVI	1957	3	72	4	5	4	0	6	9	82	4	11	9
17	63022-S10	HAGGERTY RD	M-102	E LTS OF NOVI	1957	3	73	4	5	4	0	7	9	87	4	5	9
18	63022-S11	10 MI RD(GD R)	M-102	2 MI W OF FARMINGTON	1957	3	68	5	6	5	1	6	9	89	6	2	9
19	63081-B02	DRAKE RD	M-102	4.0 MI NW OF WAYNE CO LN	1957	3	69	4	5	4	0	6	9	80	4	7	9
20	63081-S112	M-10 NB	ROUGE R	IN SOUTHFIELD	1929	3	60	5	6	5	0	5	9	88	4	8	9
21	63081-S12	EVERGREEN RD S.B	M-10	IN SOUTHFIELD	1963	3	88	6	7	4	0	6	9	86	5	1	9
22	63172-S13	10 MI RD	M-10	IN SOUTHFIELD	1963	3	84	4	5	4	0	4	9	82	5	3	9
23	63172-S13	WALDON RD	I-75	2.5 MI SE OF M-15	1962	3	119	4	6	4	0	7	9	77	6	0	9
24	63172-S14	SASHABAW RD	I-75	2.2 MI SE OF M-15	1962	3	111	6	8	4	0	6	9	77	6	0	9
25	77091-B01	M-25	BLACK R SPILLWA	IN PORT HURON	1932	3	55	4	5	4	0	5	9	83	4	8	9
26	78011-B01	M-103	WHITE PIGEON R	0.5 MI N OF INDIANA STATE	1931	3	50	3	4	3	0	4	9	80	4	8	7
27	80024-S02	PAW PAW RD	I-94	1.2 MI W OF M-40	1960	3	92	6	7	4	0	7	9	82	4	2	7
28	81074-S05	EARHART RD	US-23	3.0 MI N OF M-17 & US-23	1962	3	109	5	6	4	0	7	9	83	5	2	8

Table 2.3. List of Bridges Provided by MDOT, June 1997.

	Bridge ID	Facility	Feature	Location	Yr Blt	Yr Recon	Bridge Type		Condition Rtgs Deck	Supr	Subst	Oper Rtg	Max Span	Bridge Length	Deck Width	Beam Spacing	Skew
1	03072-B03	M-40	S BRANCH CR	4.0 MI SE OF OTTAWA CO LI	1935	0	3	02	3	3	6	77.0	10.6	10.6	11.7	4'-6"	0
2	03072-B04	M-40	N BRANCH CR	2.4 MI SE OF OTTAWA CO LI	1935	0	3	02	3	3	6	77.0	10.6	10.6	11.7	4'-6"	0
3	06071-B01	M-13	SAGANING CR	4.0 MI S OF STANDISH	1937	1952	3	02	4	2	7	90.0	10.0	25.3	22.0	4'-11"	0
4	06071-B02	M-13	S BR PINE R	3.0 MI S OF STANDISH	1935	1952	3	02	4	4	2	80.0	9.7	29.2	22.0	4'-11"	0
5	06072-B01	US-23 (WDN MAIN)	N BR PINE RIVER	1.8 MI NE OF STANDISH	1930	0	3	02	5	6	7	89.0	10.6	10.6	14.3	4'-8"	0
6	09011-B01	M-84	DUTCH CREEK	5.7 MI SW OF BAY CITY PO	1927	0	3	02	5	4	4	97.0	13.7	13.7	14.1	4'-8"	0
7	09012-B01	M-247	KAWKAWLIN R	4.4 MI NW OF BAY CITY PO	1935	0	3	02	4	5	4	85.0	13.7	41.1	12.6	4'-4"	0
8	12021-B02	US-12	SWAN CR	2.7 MI NE OF BRONSON	1922	1974	3	02	5	6	0	77.0	12.2	12.2	14.8	4'-6"	10
9	19031-B01	US-27	LOOKING GLASS RIVER	5.3 MI N OF INGHAM CO LIN	1941	1947	3	02	5	4	7	87.0	13.7	27.1	21.1	4'-7"	0
10	19062-B01	M-21	LITTLE MAPLE R	2.0 MI W OF OVID	1929	0	3	02	4	4	8	77.0	12.2	12.2	14.2	4'-8"	0
11	23052-B01	M-50	LITTLE THORNAPPLE R	6.4 MI N W OF CHARLOTTE	1931	0	3	02	6	8	7	80.0	10.6	10.6	14.1	4'-8"	38
12	25051-B01	M-54BR	THREAD CR	IN FLINT 2000 BLK S SAGIN	1941	0	3	02	4	4	4	90.0	12.2	12.2	28.8	5'-6"	24
13	26022-B02	M-81	MOLASSE R	4.5 MI E OF M-30	1931	0	3	02	3	3	3	94.0	10.6	20.4	10.9	4'-9"	25
14	29021-B01	M-57	PINE CRK	5.8 MI W OF US 27	1939	0	3	02	5	4	4	89.0	12.2	33.5	12.3		
15	29022-B01	M-57	BEAR CRK	3.5 MI E OF US 27	1941	0	3	02	5	7	8	85.0	13.7	13.7	13.9	4'-10"	30
16	29031-B01	US-27BR	PINE RIVER	IN CITY OF ALMA	1928	1977	2	04	4	4	7	75.0	9.7	28.6	15.1	6'-0"	0
17	32012-B02	M-25	PIGEON R	IN CASEVILLE	1930	0	3	02	3	4	6	81.0	12.2	24.3	17.0	4'-8"	15
18	34021-B01	M-50	DUCK CREEK	3.5 MI E OF KENT CO	1923	0	1	21	4	5	8	85.0	10.6	10.6	7.2		0
19	38051-B02	M-106	PORTAGE R DRAIN	4.7 MI SW OF INGHAM CO	1939	0	3	02	5	5	6	89.0	13.7	13.7	12.3	4'-10"	20
20	38101-S03	SANDSTONE RD	I-94	2.2 MI W OF M-80	1958	0	3	32	5	6	7	85.0	14.9	46.7	14.3	6'-3"	0
21	38101-S04	BLACKMAN RD	I-94	.5 MI W OF M-60	1958	0	3	32	6	6	7	85.0	14.9	49.0	10.1	6'-3"	0
22	44061-B03	M-90	FLINT R	1.0 MI W OF NORTH BRANCH	1948	0	3	32	4	4	4	90.0	12.2	33.8	10.1	5'-3"	0
23	46011-B02	US-127	BEAN CREEK	0.6 MI NE OF HILLDALE CO	1925	0	3	42	6	4	3	80.0	10.6	10.6	10.5		
24	54012-B02	US-131	PARIS CR	IN PARIS	1929	0	3	02	5	8	6	98.0	10.3	10.3	24.2	4'-5"	0
25	54032-B02	M-66	N BR CHIPPEWA R	IN BARRYTON	1927	0	3	02	4	5	4	90.0	12.2	24.3	11.1	4'-8"	
26	61153-B04	US-31 BR EB	MUSKEGON R	IN MUSKEGON	1944	0	2	01	6	6	6	78.0	12.2	32.0	14.3	4'-8"	15
27	70041-B01	M-45	BASS R	7.7 MI E OF US-31	1929	0	3	02	4	4	6	83.0	12.2	12.2	13.7	4'-8"	0
28	70041-B03	M-45	SAN CR	2.7 MI W OF KENT CO L	1929	0	3	02	3	4	6	84.0	13.7	13.7	14.3	4'-8"	0
29	73051-B05	M-13	BIRCH RUN OUTLET DR	7.1 MI S OF M-46	1941	0	3	02	6	7	7	83.0	12.2	33.5	11.7	4'-7"	0
30	74061-B02	M-46	S BR CASS RIVER	2.0 MI W OF M-19	1930	0	3	02	4	6	4	80.0	12.2	24.3	11.2	4'-8"	40
31	76021-B013	TEMP I-69	S BR LOOKING CLASS R	1.3 MI NE OF CLINTON CO L	1931	0	3	02	2	5	7	80.0	12.2	12.2	18.7	4'-4"	15
32	78042-B05	M-60 & M-66	NOTTAWA CR	1.2 MI E OF JCT M-66	1931	0	3	02	5	8	6	92.0	10.6	21.3	14.1		22
33	78062-B01	M-86	SWAN CR	IN COLON	1932	0	3	02	3	4	4	84.0	10.0	30.1	12.9	4'-8"	0
34	79081-B06	M-25	WISCOGGIN CR	0.1 MI S OF HURON CO LINE	1941	0	3	02	4	5	6	88.0	13.7	13.7	13.8	4'-10"	0
35	81062-S06	STONE SCHOOL RD	I-94	IN ANN ARBOR	1954	0	2	04	4	6	5	89.0	14.9	52.7	9.5	4'-11"	0
36	82072-R01	M-3 (GRATIOT AVE)	I-84 GTW RR	IN DETROIT	1929	1970	3	42	5	6	5	91.0	13.4	25.9	36.5		34

3. Load Testing Procedures

3.1 Instrumentation and Data Acquisition

The strain transducers were attached to the lower surface of the bottom flange of the steel girders at midspan (Figure 3.1). In addition, they were installed in selected girders at supports to measure the moment restraint provided by supports. The transducers were also installed at quarter points on Bridge B02-12021 to determine longitudinal load distribution. LVDTs were used to measure deflections and to monitor the global response of the structure during proof load testing of Bridge B02-12021. Each LVDT was placed on a tripod and connected to the bottom of the girder by a wire. Figure 3.2 shows the setup of an LVDT for the measurement of a girder deflection. Strain transducers and LVDTs were connected to the SCXI data acquisition system from the National Instruments. The data acquisition mode is controlled from the external PC notebook computer, and acquired data are processed and directly saved in PC's hard drive (Figure 3.3).

The system consists of a four slot SCXI-1000 chassis, one SCXI-1200 data acquisition module and two SCXI-1100 multiplexers. Each multiplexer can handle up to 32 channels of input data. The current system is capable of handling 64 channels of strain or deflection inputs. Up to 32 additional channels can be added if required. A portable field computer is used to store, process and display the data on site. A typical data acquisition setup is shown in Figure 3.3. The data from all instruments is collected after placing the trucks in desired positions or while trucks are passing on the bridge. The real time responses of all transducers are displayed on the monitor during all stages of testing.

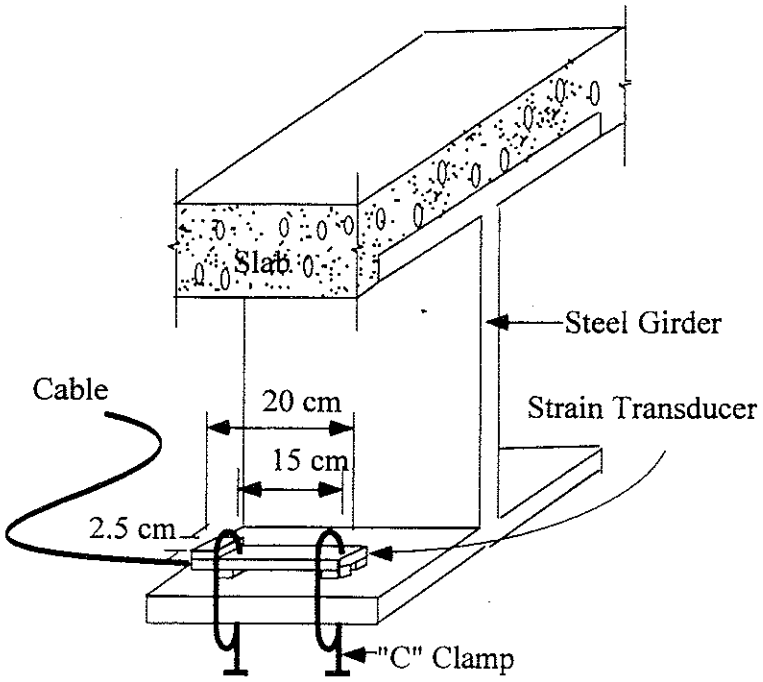

Figure 3.1 Demountable Strain Transducer Mounted to the Lower Flange.

3.2 Test Loads for Load Distribution Tests

Strain data necessary to calculate girder distribution and impact factors were taken from bottom-flanges of girders in the middle of a span. Strain data were obtained under passes of three-unit 10-axle and 11-axle trucks with known weight and configuration for all bridges except bridge B01-70041. Configurations of test trucks are shown in Table 3.1 for all bridges except bridge B01-70041. The same two trucks were used for all bridges except bridge B01-70041. Two three-unit 11-axle trucks were used in bridge B01-70041 and the test truck configurations are shown in Table 3.2. Two trucks have the same axle spacings. Strain data obtained from side-by-side truck tests were used to calculate load distribution and impact factors. Superposition of strain data from each truck provided the verification of the obtained data and the linear-elastic behavior of the bridge.

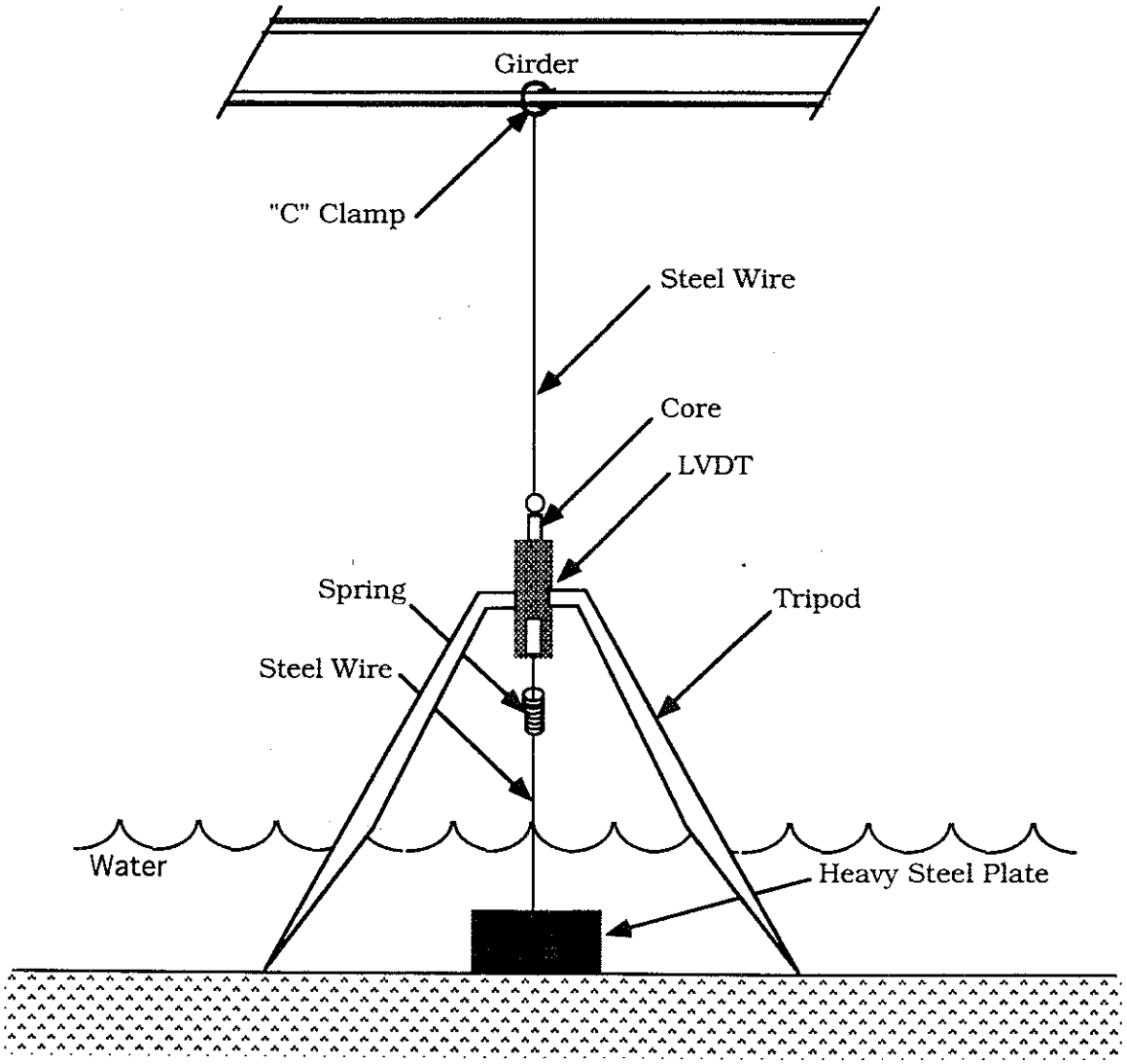

Figure 3.2 Typical LVDT setup.

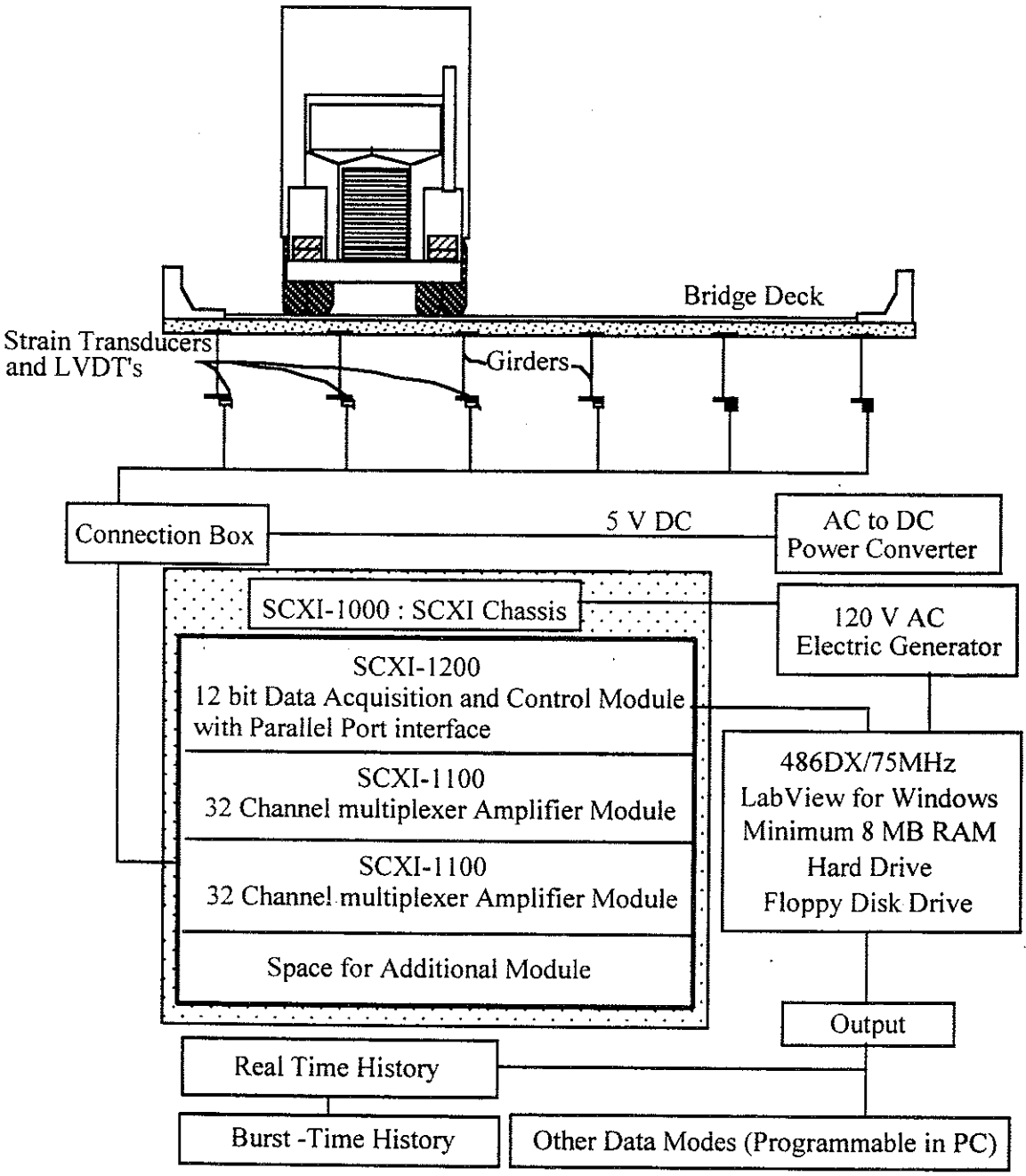

Figure 3.3 SCXI Data Acquisition System Setup.

In addition to static loading at predetermined positions, trucks were driven over the bridge at crawling speed to simulate static loads and at high speed to obtain dynamic effect on the bridge. For the bridge carrying M-156 over Silver Creek in Morenci, the locations causing maximum bending moment were analytically calculated before tests and trucks were statically placed at the analytical maximum bending position. However, the strains obtained from crawling speed tests were always greater than those from the analytical maximum bending position. Therefore, bridges except Bridge B02-46032 (M-156 over Silver Creek in Morenci) were tested under crawling speed and the maximum speed obtained by a test truck at a bridge site (high speed).

In general, the following load cases were applied for bridges with two lanes. Truck 1 is 11-axle truck or truck A for bridge B01-70041. Truck 2 is 10-axle truck or truck B for bridge B01-70041. Lane 1 and lane 2 indicate east and west lane for bridge B02-46032 and north and south lane for all other bridges.

(a) at crawling speed,

- truck 1 in the center of lane 1
- truck 1 close to the curb of lane 1
- truck 2 in the center of lane 1
- truck 2 close to the curb of lane 1
- truck 1 in the center of lane 2
- truck 1 close to the curb of lane 2
- truck 2 in the center of lane 2
- truck 2 close to the curb of lane 2
- truck 1 in the center of lane 1 and truck 2 in the center of lane 2
- truck 2 in the center of lane 1 and truck 1 in the center of lane 2

(b) at high speed,

- truck 1 in the center of lane 1
- truck 2 in the center of lane 1
- truck 1 in the center of lane 2
- truck 2 in the center of lane 2
- truck 1 in the center of lane 1 and truck 2 in the center of lane 2
- truck 2 in the center of lane 1 and truck 1 in the center of lane 2

Table 3.1 Test Truck Configurations for All Bridges except B01-70041

Ten-Axle Truck

Axle Spacing (m)

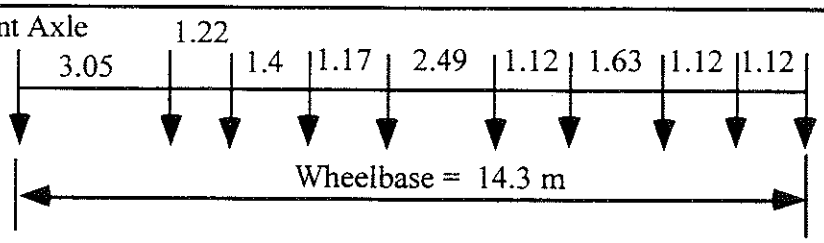

Bridge ID Number	GVW (kN)	Each Axle Weight (kN)									
		1	2	3	4	5	6	7	8	9	10
B02-46032	582	82	59	54	52	60	57	55	44	55	64
B05-46041	580	74	66	56	54	58	47	40	58	63	64
B02-12021	573	74	67	54	51	58	46	39	63	60	61
B02-38051	585	73	65	56	54	56	50	41	64	62	64

Eleven-Axle Truck

Axle Spacing (m)

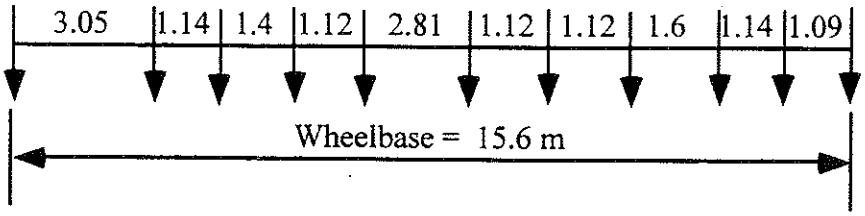

Bridge ID Number	GVW (kN)	Each Axle Weight (kN)										
		1	2	3	4	5	6	7	8	9	10	11
B02-46032	637	85	60	53	51	58	55	61	68	44	48	54
B05-46041	637	80	58	56	55	62	52	58	65	45	49	57
B02-12021	640	77	59	58	57	59	52	56	65	49	51	57
B02-38051	644	84	55	58	57	57	51	53	63	49	57	60

Table 3.2 Test Truck Configuration for Bridge B01-70041

Axle Spacing (m)	Front Axle 3.66 | 1.47 | 3.05 | 1.14 | 1.14 | 2.49 | 1.14 | 1.83 | 1.14 | 1.14 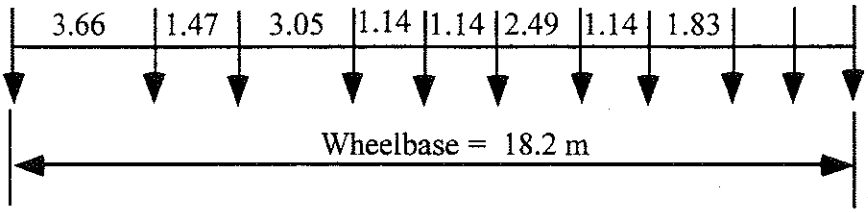											
Truck ID Number	GVW (kN)	Each Axle Weight (kN)										
		1	2	3	4	5	6	7	8	9	10	11
Truck A	696	71	71	67	57	53	80	49	64	61	57	66
Truck B	682	72	71	67	65	55	59	52	72	41	52	76

3.3 Test Loads for Proof Load Tests

3.3.1 Proof Load Level

Proof load tests were carried out to verify if the bridge can safely carry the maximum allowable legal load. In Michigan, the maximum mid-span moment in medium span bridges is caused by 11-axle two unit trucks with the wheel configuration shown in Figure 3.4. For an 11-axle truck, the gross vehicle weight (GVW) can be up to 730 kN, which is almost twice the allowable legal load in other states. Most states allow a maximum GVW of 356 kN only. It is more than twice the MS18 design load (AASHTO 1996). The proof load testing was designed to verify the moment capacity of steel girders close to mid-span. Before the proof load tests, the target proof load has to be calculated. If the test load safely reaches the target proof load level, then the operating rating factor for 11-axle two unit truck would be 1.0.

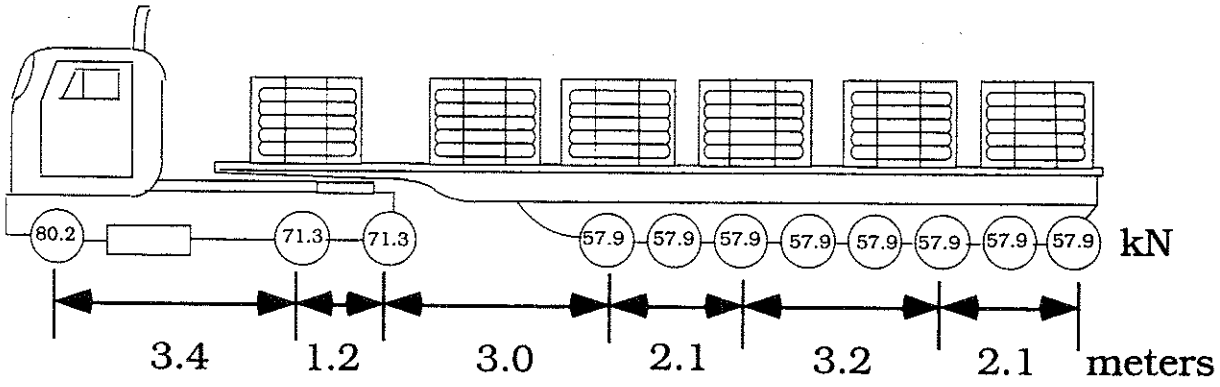

Figure 3.4 11-Axle Two-Unit Truck.

The proof load level should be sufficiently higher than that from 11-axle truck, to ensure the desired safety level. The final draft NCHRP Report 12-28(13)A titled "Bridge Rating Through Load Testing" by A.G. Lichtenstein (1993) provides guidelines for calculating the target proof load level. It suggests that the maximum allowable legal load should be multiplied by a factor Xp, which represents the live load factor needed to bring the bridge to an operating rating factor of 1.0. The guide recommends that Xp should be 1.4 before any adjustments are made. It also recommends the following adjustments to Xp, that should be considered in selecting a target live load magnitude.

- Increase X_p by 15 percent for one lane structures or for other spans in which the single lane loading augmented by an additional 15 percent would govern.
- Increase X_p by 10 percent for spans with fracture critical details.
- Increase X_p by 10 percent for structures without redundant load paths.
- Reduce X_p by 5 percent if the structure is ratable.
- Additional factors including traffic intensity and bridge condition may also be incorporated in the selection of the live load factor X_p.

Application of the recommended adjustment factors, leads to the target live load factor X_{pa}. The net percent increase in X_p (Σ) is found by summing the appropriate adjustments given above. Then

$$X_{pa} = X_p (1 + \Sigma/100) \tag{3-1}$$

The target proof load (L_t) is then:

$$L_t = X_{pa} (1 + I) L_r \tag{3-2}$$

$$1.3 \leq X_{pa} \leq 2.2 \tag{3-3}$$

where,

L_r = the comparable live load due to the rating vehicle for the loaded lanes.

I = impact factor

X_{pa} = the target live load factor.

Based on the span length, the AASHTO Standard Specifications (1996) specifies the impact factors of less than 0.3. However, previous studies by several researchers have indicated that the dynamic amplification is much smaller for heavy loads (Hwang and Nowak 1991, Nassif and Nowak 1995, Nowak, Laman and Nassif 1994). Therefore, for this study, an impact factor of 0.1 was selected.

3.3.2 Load Selection

The M-60 military tanks were selected. Each tank weighs 504 kN (obtained from tank weight information from the Michigan National Guard) and the load is distributed over a track length of 4.5 m. Hence, these tanks cause very high moments at mid-span. The tanks were provided by the Michigan National Guard. The front and side views of the M-60 tanks are shown in Figures 3.5 and 3.6.

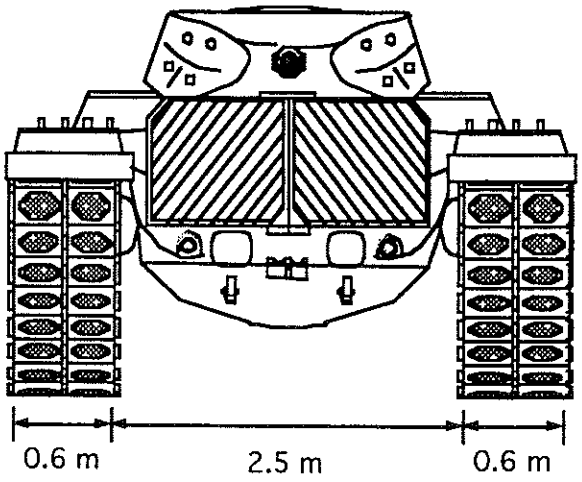

Figure 3.5 Cross-Section of M-60 Tank.

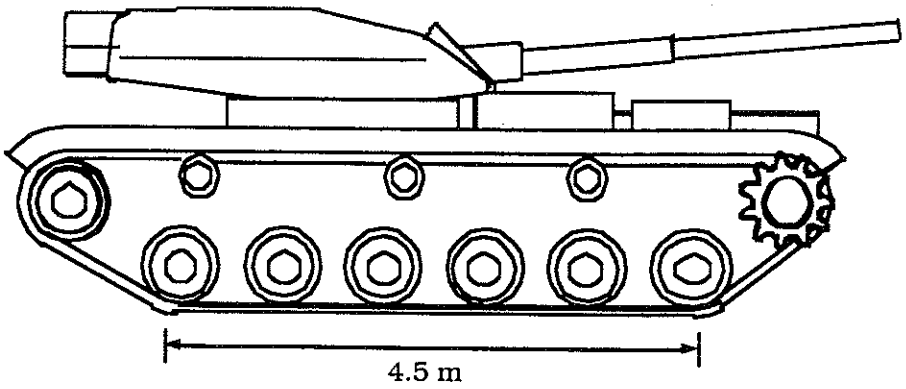

Figure 3.6 Side Elevation of M-60 Tank.

The following proof load cases were applied for Bridge US12/SC:

- one tank close to the curb of north lane
  - in the middle of span
  - 0.61 m east from the middle of span
  - 0.61 m west from the middle of span
- one tank at the center of north lane
  - in the middle of span
  - 0.61 m east from the middle of span
  - 0.61 m west from the middle of span
- one tank close to the curb of south lane
  - in the middle of span
  - 0.61 m east from the middle of span
  - 0.61 m west from the middle of span
- one tank at the center of south lane
  - in the middle of span
  - 0.61 m east from the middle of span
  - 0.61 m west from the middle of span
- two side-by-side tanks at the center of bridge width
  - both tanks 0.61 m east from the middle of span
  - one tank 0.61 m east from the middle of span, the other tank in the middle of span
  - both tanks in the middle of span
  - one tank 0.61 m west from the middle of span, the other tank in the middle of span
  - both tanks 0.61 m west from the middle of span

Detailed proof load positions are shown in chapter 7.

3.4 Load Distribution and Impact Factor Calculation from Test Results

Collected strain data from the tests were processed to identify impact and girder distribution factors. Girder Distribution Factors (GDF) are calculated from the maximum static strain obtained from the static loading at each girder at the same section along the length of the bridge. Ghosn *et al.* (1986) assumed that GDF was equal to the ratio of the static strain at the girder to the sum of all the static strains. Stallings and Yoo (1993) used the weighted strains to account for the different section moduli of the girders. Accordingly, GDF for the ith girder, GDF_i, can be derived as follows:

$$GDF_i = \frac{M_i}{\sum_{j=1}^{k} M_j} = \frac{ES_i\varepsilon_i}{\sum_{j=1}^{k} ES_j\varepsilon_j} = \frac{\frac{S_i}{S_t}\varepsilon_i}{\sum_{j=1}^{k}\frac{S_j}{S_t}\varepsilon_j} = \frac{\varepsilon_i w_i}{\sum_{j=1}^{k}\varepsilon_j w_j} \qquad (3\text{-}4)$$

where M_i = bending moment at the ith girder; E = modulus of elasticity; S_i = section modulus of the ith girder; S_t = typical interior section modulus; ε_i = maximum bottom-flange static strain at the ith girder; w_i = ratio of the section modulus of the ith girder to that of a typical interior girder; and k = number of girders. When all girders have the same section modulus (that is, when weight factors, w_i, are equal to one for all girders), Eq. (3-4) is the equivalent to that of Ghosn *et al.* (1986). Because of edge stiffening effect due to curbs and barrier walls, the section modulus in exterior girders is slightly greater than in interior girders. In other words, the weight factors, w_i, for exterior girders are greater than one. Therefore, from Eq. (3-4), the assumption of the weight factors, w_i, equal to one will cause slightly overestimated girder distribution factors in interior girders and underestimated girder distribution factors in exterior girders. In this study, the weight factors, w_i, are assumed to be one.

Impact factors are defined in several ways, as discussed in previous studies (Paultre *et al.* 1992; Bakht and Pinjarkar 1989). In this study, the impact factor was taken as the ratio of the maximum dynamic strain and the maximum static strain (Figure 3.7):

$$I = \frac{\varepsilon_{dyn}}{\varepsilon_{stat}} \qquad (3\text{-}5)$$

where ε_{dyn} = absolute maximum dynamic strain under the vehicle traveling at normal speed; and ε_{stat} = maximum static strain obtained by filtering the dynamic response. A numerical procedure is applied to filter collected data.

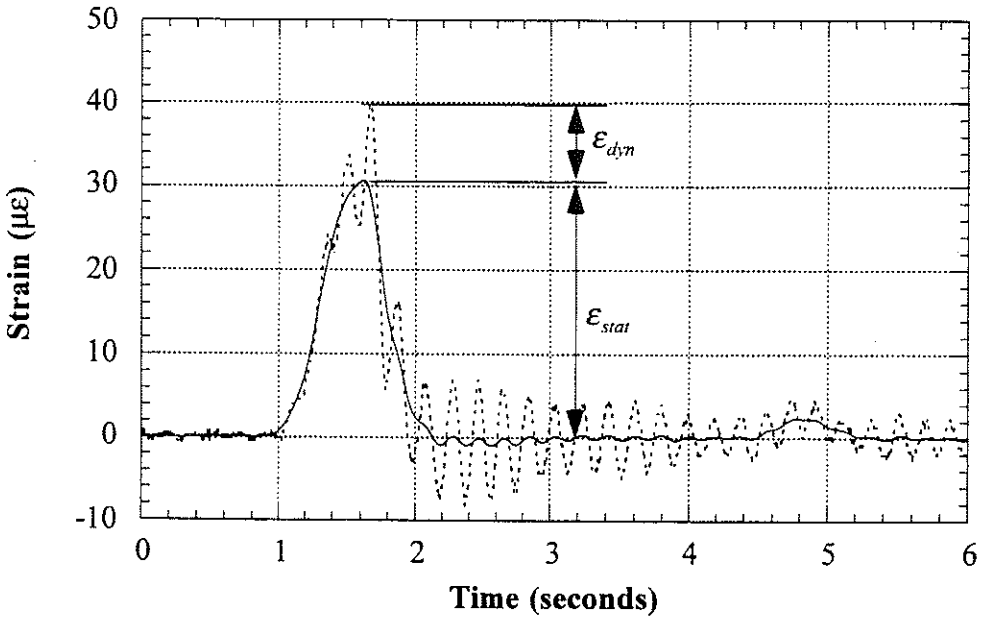

Figure 3.7 Dynamic and Static Strain under a Truck at Highway Speed.

Two additional considerations are associated with calculation of impact factors: strain magnitude and girder selection. First, the level of strain for each girder should be considered to calculate impact factors.

Impact factors corresponding to light vehicles, being relatively on the high side, tend to bias the data. It is, therefore, necessary that the data considered for developing the statistics of the impact factor correspond to the weight class of the design or evaluation vehicle. Strain data collected under passes of side-by-side trucks provided the reference strain value to obtain impact factors.

Second, impact factors should be calculated from the girder with maximum strain to be compatible with current design codes. Otherwise it will result in overestimated values. This is because the distribution factors in current design codes provide maximum static load effect in any girder from any possible static load combinations and the distribution factor is multiplied by an impact factor.

4. Specified Load Distribution Factors and Impact Factors

Measured girder distribution factors (GDF) and impact factors are compared in tables and figures with the values calculated according to the current design codes. Throughout the report, distribution factors are expressed in terms of axle load or full truck rather than a line of wheel loads or half truck. For moment in interior girders, the American Association of State Highway and Transportation Officials (AASHTO) standard specifications (1996) specifies GDF's as follows. For one lane steel girder and prestressed concrete girder bridges, GDF is:

$$GDF = \frac{S}{4.27} \tag{4-1}$$

and for multi lane steel and prestressed concrete girder bridges,

$$GDF = \frac{S}{3.36} \tag{4-2}$$

where S = girder spacing (m).

The AASHTO Load and Resistant Factor Design (LRFD) Code (1994) specifies GDF as a function of girder spacing, span length, stiffness parameters, and bridge skew. For moment in interior girders with one lane loading, GDF is:

$$GDF = \left\{0.075 + \left(\frac{S}{2900}\right)^{0.6}\left(\frac{S}{L}\right)^{0.2}\left(\frac{K_g}{Lt_s^3}\right)^{0.1}\right\}\left\{1 - c_1(\tan\theta)^{1.5}\right\} \tag{4-3}$$

and in multi lane loading:

$$GDF = \left\{0.06 + \left(\frac{S}{4300}\right)^{0.4}\left(\frac{S}{L}\right)^{0.3}\left(\frac{K_g}{Lt_s^3}\right)^{0.1}\right\}\left\{1 - c_1(\tan\theta)^{1.5}\right\} \tag{4-4}$$

$$c_1 = 0.25\left(\frac{K_g}{Lt_s^3}\right)^{0.25}\left(\frac{S}{L}\right)^{0.5} \qquad \text{for } 30° < \theta < 60° \tag{4-5}$$

$$c_1 = 0 \qquad \text{for } \theta < 30° \tag{4-6}$$

where S = girder spacing (mm); L = span length (mm); $K_g = n(I + Ae_g^2)$; t_s = depth of concrete slab (mm); n = modular ratio between girder and slab materials; I = moment of inertia of the girder (mm^4); A = area of the girder (mm^2); e_g = distance between the center of gravity of the girder and slab (mm); and θ = skew angle in degrees. Because the term $K_g / (Lt_s^3)$ implies more accuracy than exists for bridge evaluation, it is recommended that they be taken as 1.0. In this report, however, actual values of the term $K_g / (Lt_s^3)$ are used in calculation of girder distribution factors. The AASHTO LRFD (1994) formulas have been developed based on a National Cooperative Highway Research Program (NCHRP) Project 12-26 (Zokaie *et al.* 1991). This method includes the longitudinal stiffness parameter, K_g, and the span length, L, in addition to the girder spacing, S. AASHTO Guide for Load Distribution (1994) specifies similar load factors to those of AASHTO LRFD (1994).

Most bridge design codes specify the dynamic load as an additional static live load. In the current AASHTO (1996), impact factors are specified as a function of span length only:

$$I = \frac{50}{3.28L + 125} \qquad (4\text{-}7)$$

where I= impact factor (maximum 30 percent); and L= span length (m). This empirical equation has been in effect since 1944. In the AASHTO LRFD (1994), live load is specified as a combination of MS18 truck (AASHTO 1996) and a uniformly distributed load of 9.3 kN/m. The impact factor is equal to 0.33 of the truck effect, with no dynamic load applied to the uniform loading.

5. Bridge on M-156 over Silver Creek in Morenci (B02-46032, M156/SC)

5.1 Description

This bridge was built in 1935 and is located on state highway M-156 over Silver Creek in Morenci, Michigan. This bridge is designated as M156/SC, and can be identified by the road carried by the bridge and the creek under the bridge. It has one lane in each direction. As shown in Figure 5.1, the superstructure is composed of ten steel girders spaced at 1.32 m and a 190 mm thick concrete slab with a 76 mm asphalt overlay. It is a simply supported single span structure and was designed to be noncomposite. The total span length is 13.7 m with a skew of 30 degrees. The legal speed limit is 48 km/h. The deck slab and approach to the bridge were in good condition, and the bridge has a load rating of 792 kN.

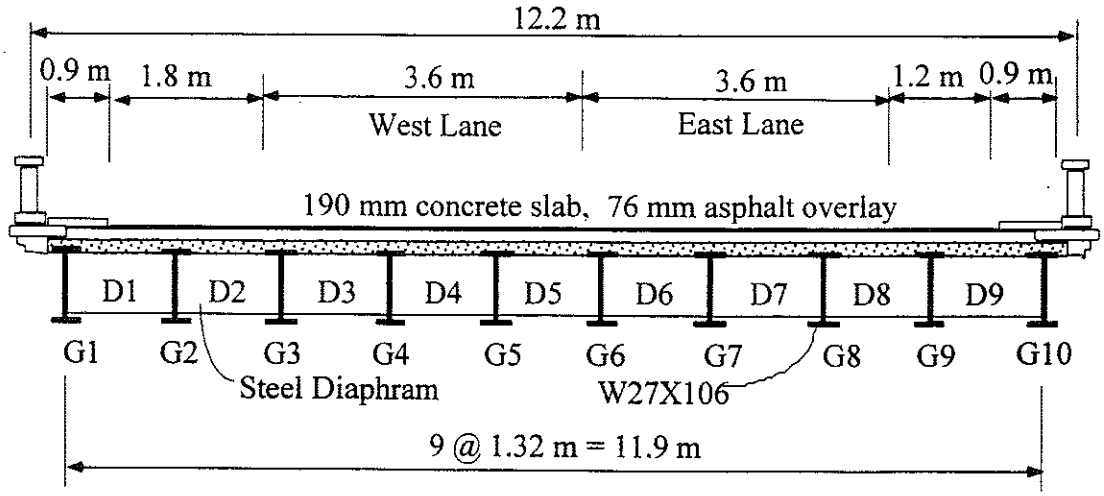

Figure 5.1 Cross-Section of Bridge M156/SC in Morenci.

5.2 Instrumentation

Strain transducers were installed on the bottom flanges of girders in the middle of the span and close to the support (Figure 5.2). The bridge test was performed on June 26, 1997.

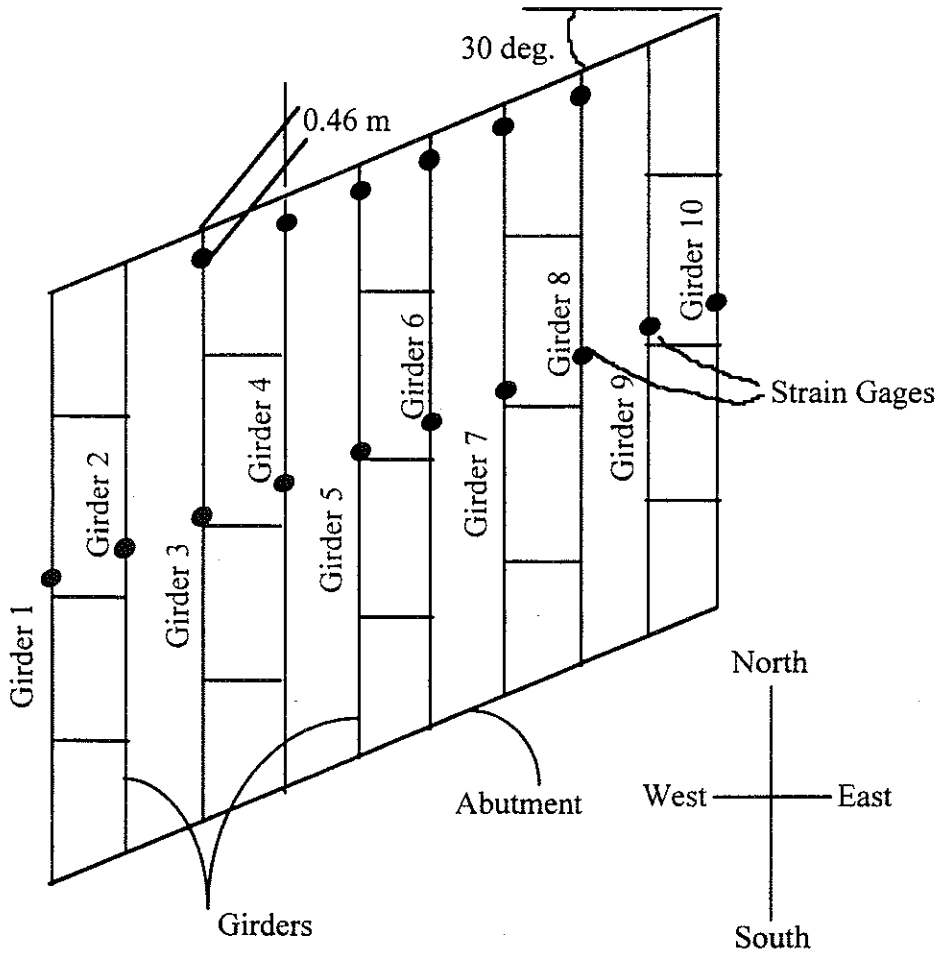

Figure 5.2 Strain Transducer Locations in Bridge M156/SC in Morenci.

5.3 Truck Loads

The strain data necessary to calculate girder distribution and impact factors were taken from the midspan transducers. The bridge was loaded with three-unit 10-axle and 11-axle trucks. The 10 and 11-axle trucks have gross weights of 582 kN and 637 kN, with wheelbases of 14.3 m and 15.6 m, respectively. Truck configurations are shown in Figures 5.3 and 5.4.

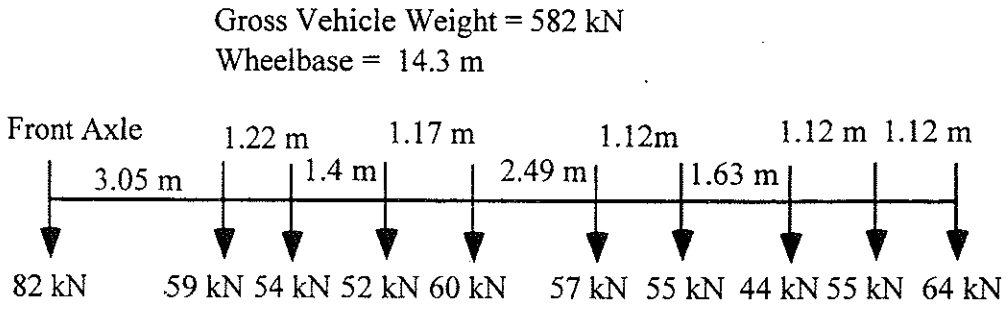

Figure 5.3 Ten-Axle Truck Configuration, Bridge M156/SC in Morenci.

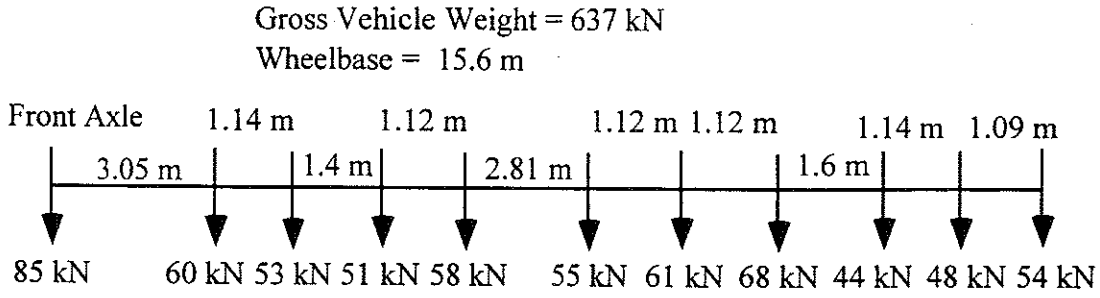

Figure 5.4 Eleven-Axle Truck Configuration, Bridge M156/SC in Morenci.

The following load cases were applied during the tests:

Static positions (trucks were stopped completely):

- 11-axle truck at near analytical maximum bending moment location in the center of west lane
- 11-axle truck at analytical maximum bending moment location in the center of west lane
- 11-axle truck at analytical maximum bending moment location contact with curb of west lane
- 11-axle truck at near analytical maximum bending moment location in the center of east lane
- 11-axle truck at analytical maximum bending moment location in the center of east lane
- 11-axle truck at analytical maximum bending moment location contact with the curb of east lane
- 10-axle truck at analytical maximum bending moment location in the center of east lane
- 10-axle truck at near analytical maximum bending moment location in the center of west lane
- 10-axle truck at analytical maximum bending moment location in the center of west lane

Crawling speed positions:

- 11-axle truck in the center of west lane
- 11-axle truck close to curb of west lane
- 11-axle truck in the center of east lane
- 10-axle truck in the center of west lane
- 10-axle truck in the center of east lane
- 10-axle truck in the center of west lane and 11-axle truck in the center of east lane

At high speed, the maximum speed obtained by the test trucks were:

- 11-axle truck in the center of east lane, 48 km/h
- 10-axle truck in the center of west lane, 64 km/h
- 10-axle truck in the center of east lane, 64 km/h
- 11-axle truck in the center of west lane, 56 km/h
- 11-axle truck in the center of west lane and 10-axle truck in the center of east lane, 48 km/h

5.4 Load Test Results

Strains resulting from both the static and crawling-speed tests are considered non-dynamic. For a given truck and lane position, the maximum strains from a non-dynamic test can be compared with its high-speed counterpart. By subtracting out non-dynamic strain, the strains caused by dynamic effects can then be determined. Girder distribution factors were determined from static strains using Eq. (3-4) and the impact factor was calculated using dynamic strains.

Figures 5.5 to 5.9 present all static load cases including static positioning and crawling-speed tests. Strains from a crawling-speed test were always greater than those from static positioning at the analytical maximum bending position. This likely indicates a combination of actual bridge behavior differing from simplified theory and a truck positioning error. Each figure presents all load cases of one truck type in the same lane for all longitudinal and lateral positions. Figure 5.13 shows dynamic strains from all high speed tests.

Figures 5.5 to 5.8 present static strains and girder distribution factors (GDF's) for one truck on the bridge. Figure 5.9 shows static strains and GDF's for a side-by-side static load test. GDF's are calculated from corresponding static strains using Eq. (3-4).

Figures 5.5 to 5.8 show the static strains and resulting GDF's on each girder for several different load cases, as described on the diagrams. Figure 5.10 shows the maximum effect from all cases in Figures 5.5 to 5.8. Because the AASHTO Code specifies GDF's for both lanes loaded, the results in Figure 5.10, which represent the effect of a single truck, are not directly comparable to code values. By superimposing the results of one loaded lane with the other, however, the GDF's for two loaded lanes can be determined. The results are shown in Figure 5.11, together with those of a side-by-side crawling-speed truck test. For the purpose of comparison, code specified distributions factors are also plotted. In calculation of AASHTO LRFD Girder distribution factors, actual value of the term $K_g / (Lt_s^3)$ is used.

Notice that in Figure 5.11, the results are taken as the maximum effect caused by the combination of two transverse truck positions in each lane (see Figs. 5.5 to 5.8); in the center of the lane, and near the curb. In contrast, Figure 5.9 shows the results when both trucks were in the same transverse position in their respective lanes.

As expected, as the trucks are placed closer to the curbs, the GDF increases on the outside girders. The interior girders still experience a higher load effect, however. The maximum value obtained from the tests is very close to AASHTO Standard (S/3.36) GDF. However, this does not indicate that the bridge behaves as assumed when designed. Comparing design stresses and stresses found from the tests, it was found that the bridge has a significant extra live load carrying capacity, despite the fact that the maximum GDF is close to design values.

Figure 5.12 compares static strains obtained by superposing strains under one truck loading with those from simultaneous side-by-side truck loading. They have practically the same values, verifying the superposition method used.

Figure 5.13 presents the dynamic strains obtained from high speed tests. The girder distribution factors calculated from those dynamic

strains are plotted in Figure 5.14 and 5.15 and compared with Code specified distribution factors.

Figure 5.16 presents the corresponding strains from static tests used to calculate impact factors. Only the static load cases in which the trucks have the same lateral positions as in the high-speed tests are shown in Figure 5.16. Impact factors are calculated from Eq. (3-5) and presented in Figure 5.17. Impact factors for exterior girders are high because the static strains in these girders are very low. Because of these low static strains, the addition of dynamic effects still results in a low overall value. Therefore, large impact factors in exterior girders are not of concern. It is clear in Figure 5.18, which shows the relationship between strain magnitude and impact factors, that large impact factors correspond to low static strains. Dynamic strains remain nearly constant, while static strains increase with truck loading. This results in large impact factors for low static strains. For side-by-side truck loading, the impact factor is approximately 10%.

Figures 5.19 to 5.23 show the strains taken from transducers installed close to the abutment. They correspond to Figures 5.5 to 5.9. It is not surprising that there are negative strains at the support, which indicates partial fixity of the joints. These values are significant when compared with those in the middle of span. Support strains vary from one third to one half of the strain values in the middle of the span.

The measured static strains were compared to static strains calculated using the design stiffness and GDF's determined by tests in this study. The maximum observed static strain for this bridge is 67.5 με for a single truck and 102.4 με for two trucks side-by-side. The corresponding calculated static strain for a single truck in a composite section is 180 με and for a non-composite section it is 260 με. For two trucks side-by-side, the calculated static strains are 262 με and 379 με for a composite section and a non-composite section, respectively.

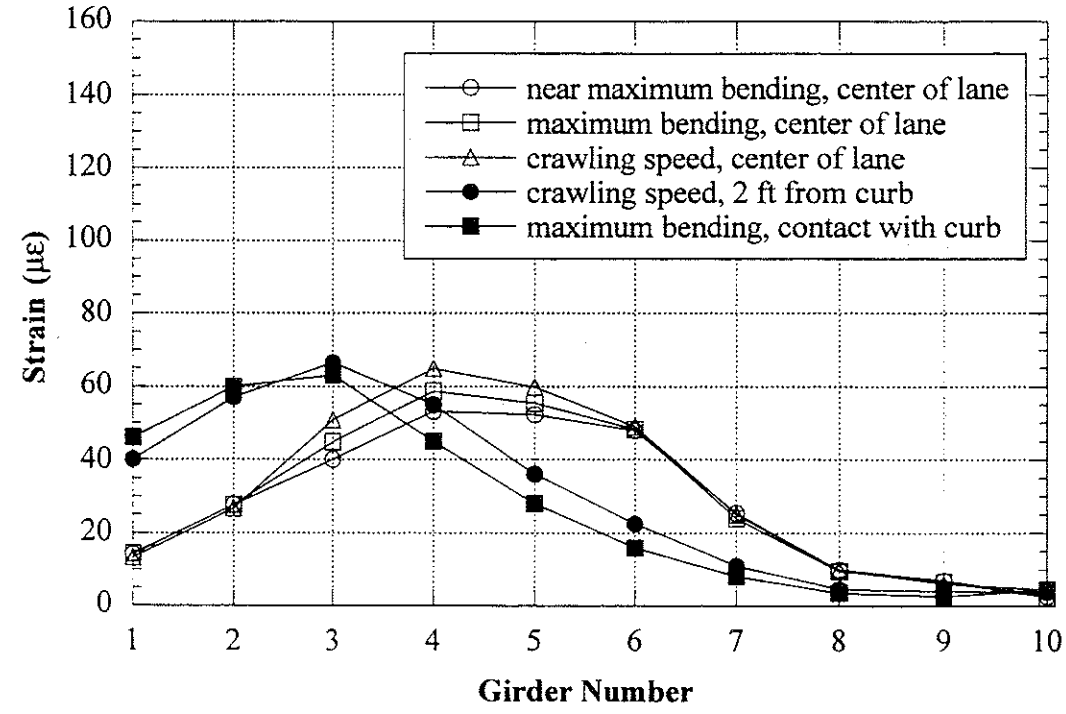

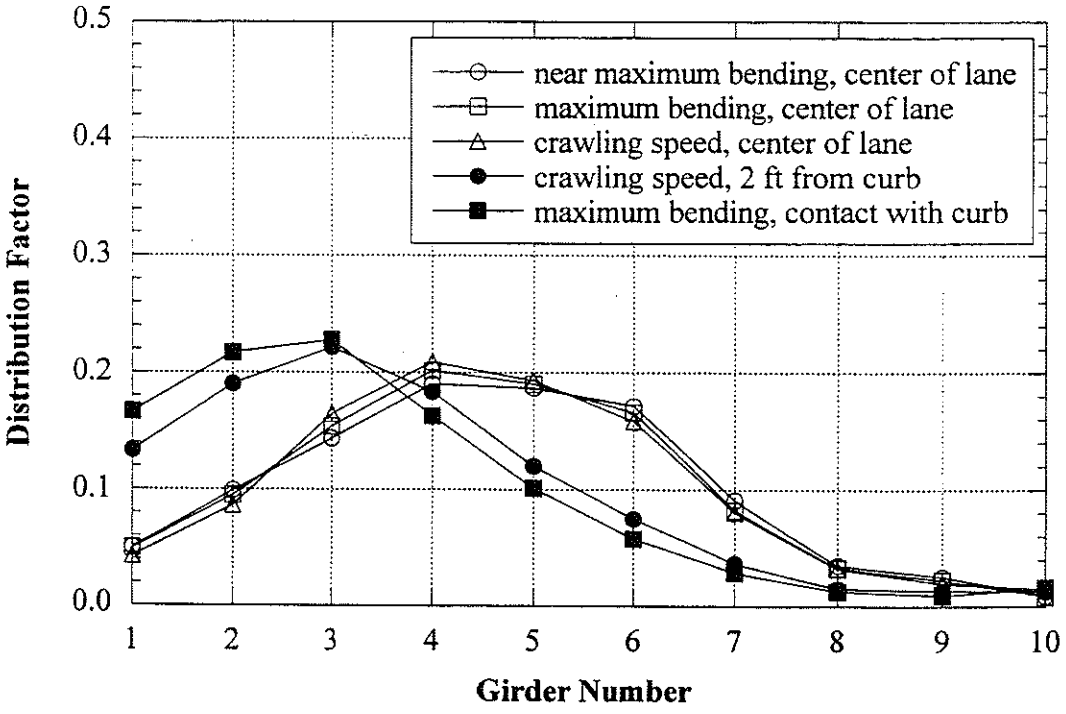

Figure 5.5 West Lane, 11-Axle Truck, Static Loading, Midspan.

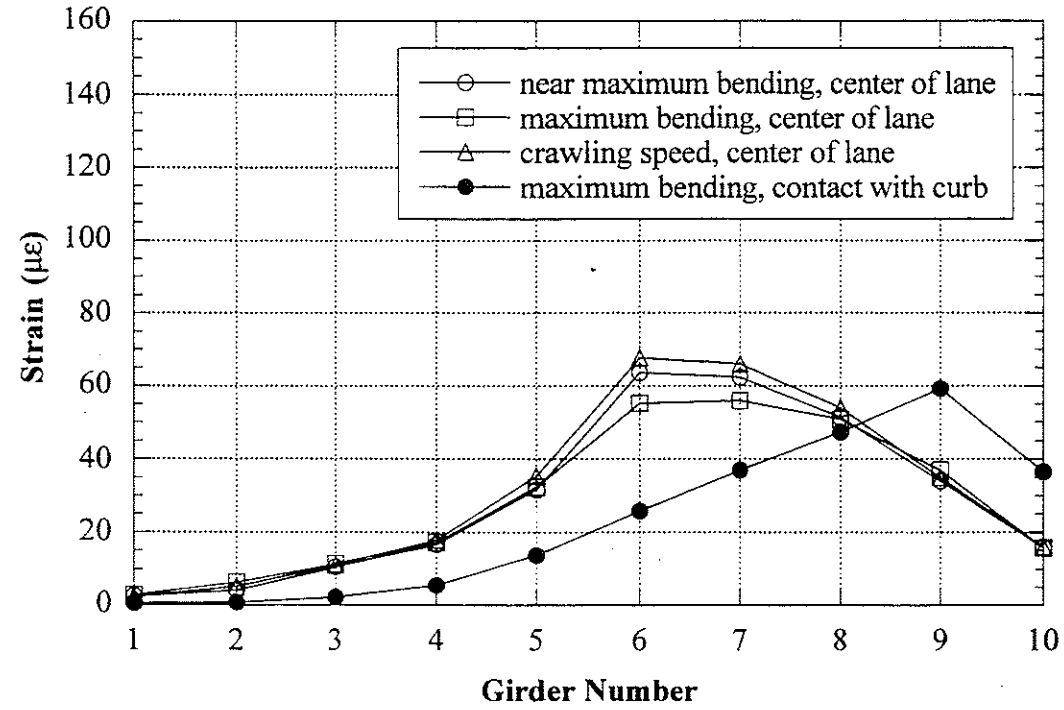

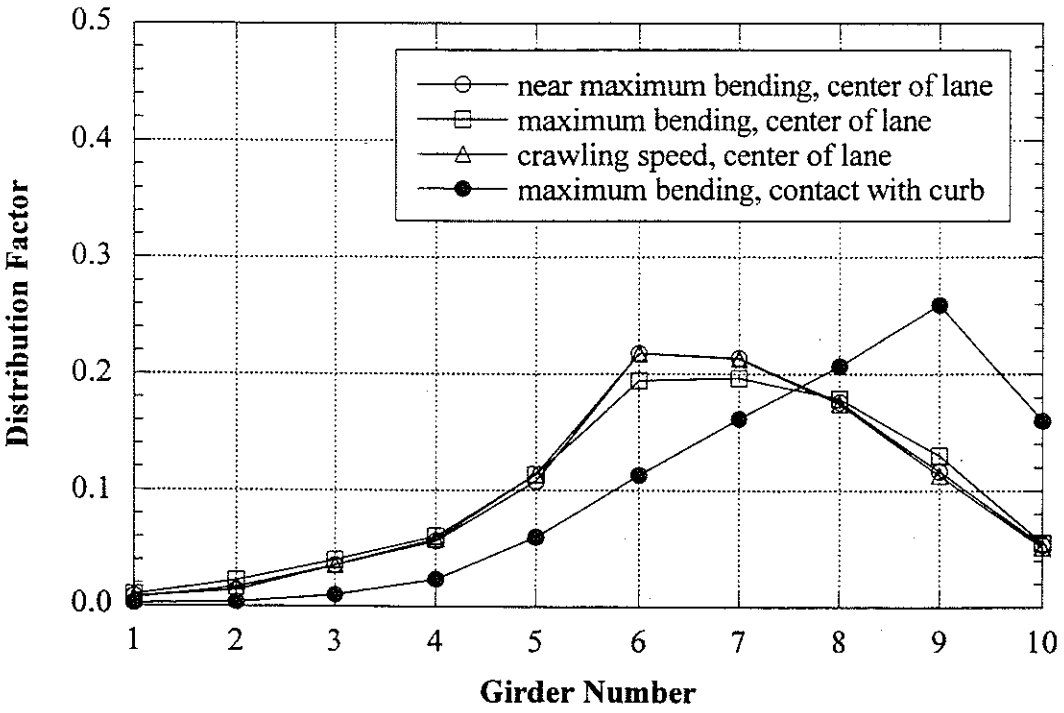

Figure 5.6 East Lane, 11-Axle Truck, Static Loading, Midspan.

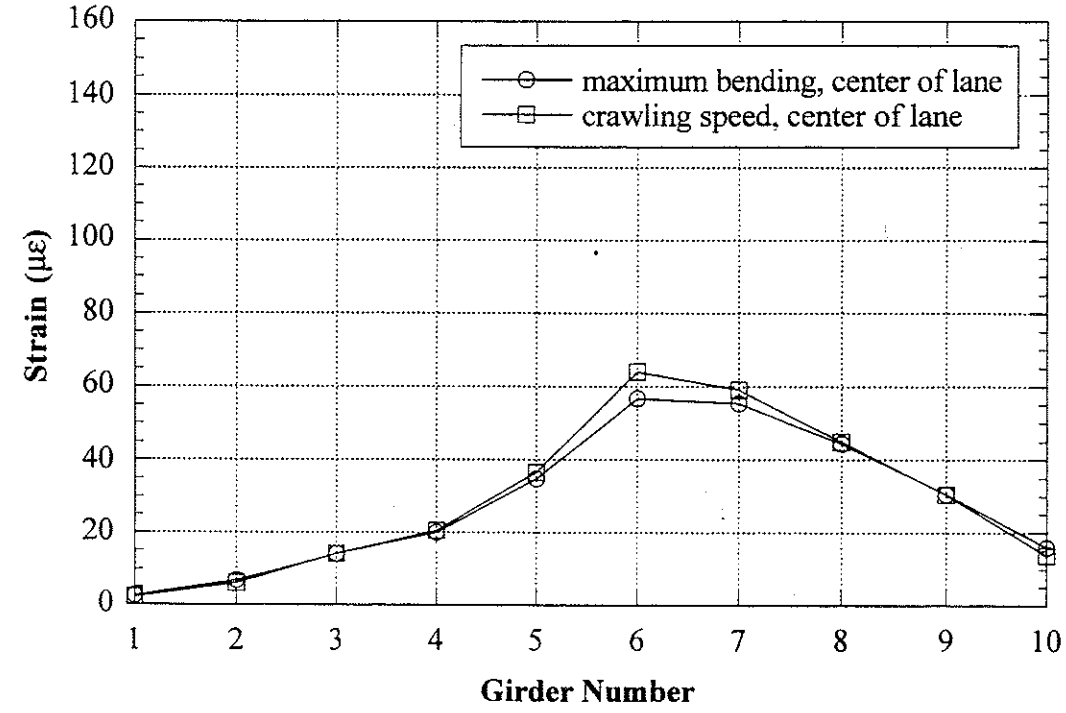

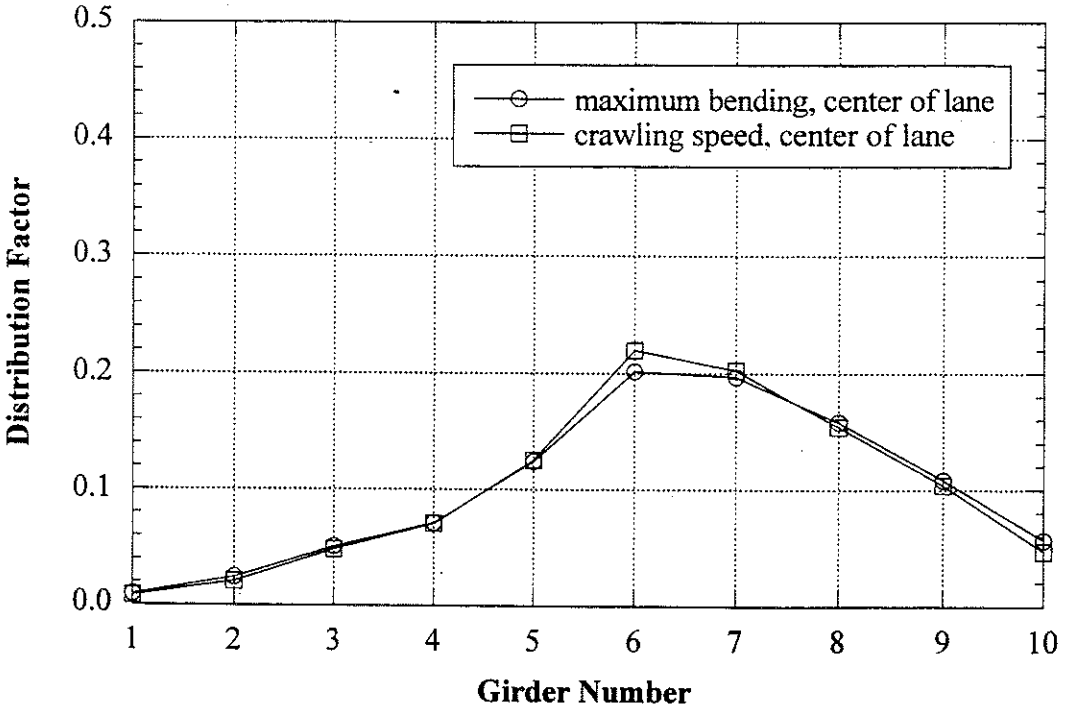

Figure 5.7 East Lane, 10-Axle Truck, Static Loading, Midspan.

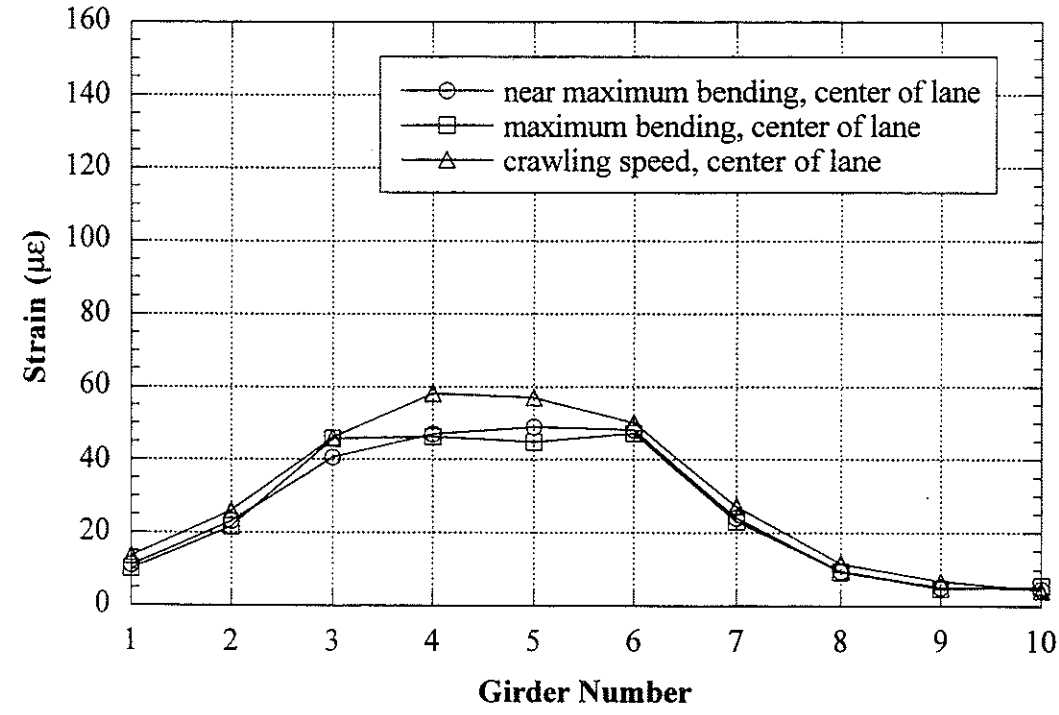

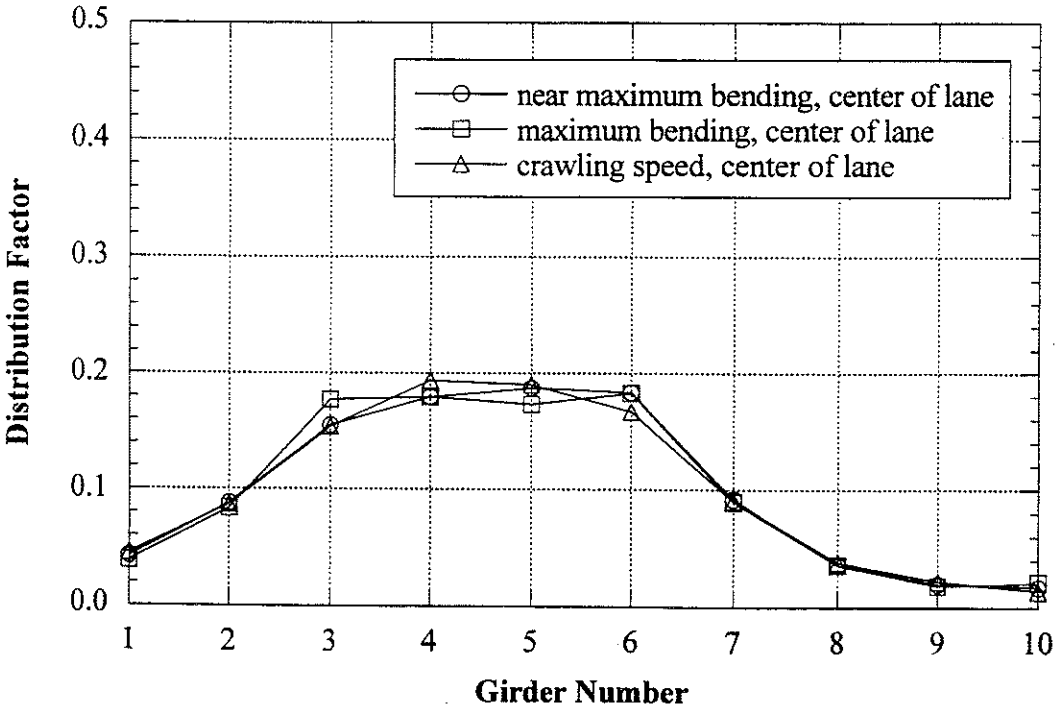

Figure 5.8 West Lane, 10-Axle Truck, Static Loading, Midspan.

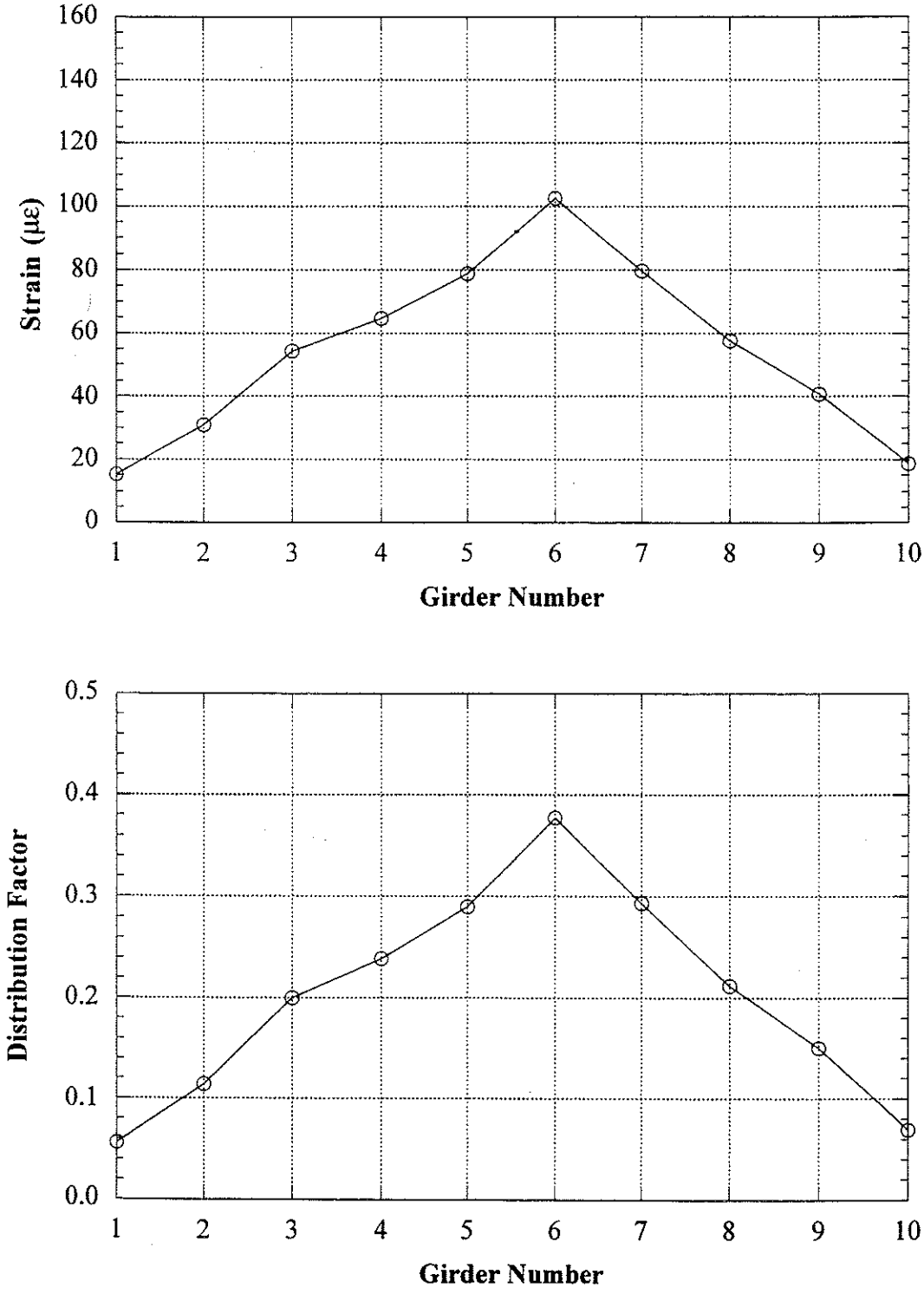

Figure 5.9 Side-by-Side Crawling Speed, Center of Lane, 10-Axle in West Lane, 11-Axle in East Lane, Midspan.

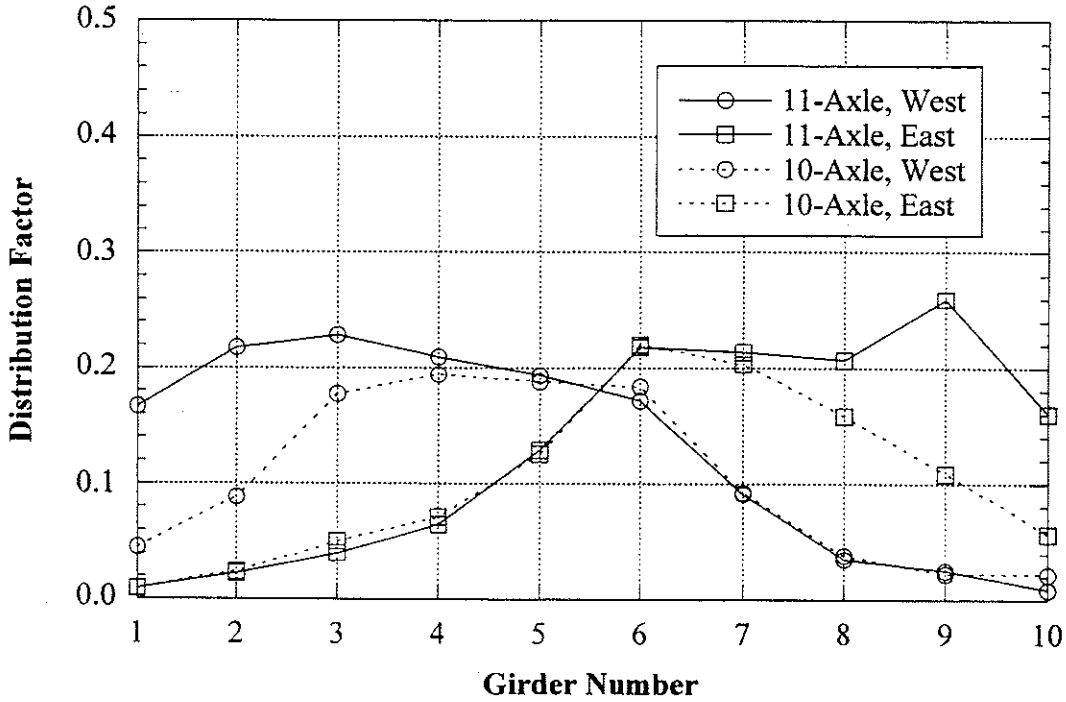

Figure 5.10 Maximum Girder Distribution Factor For One Truck at Crawling Speed.

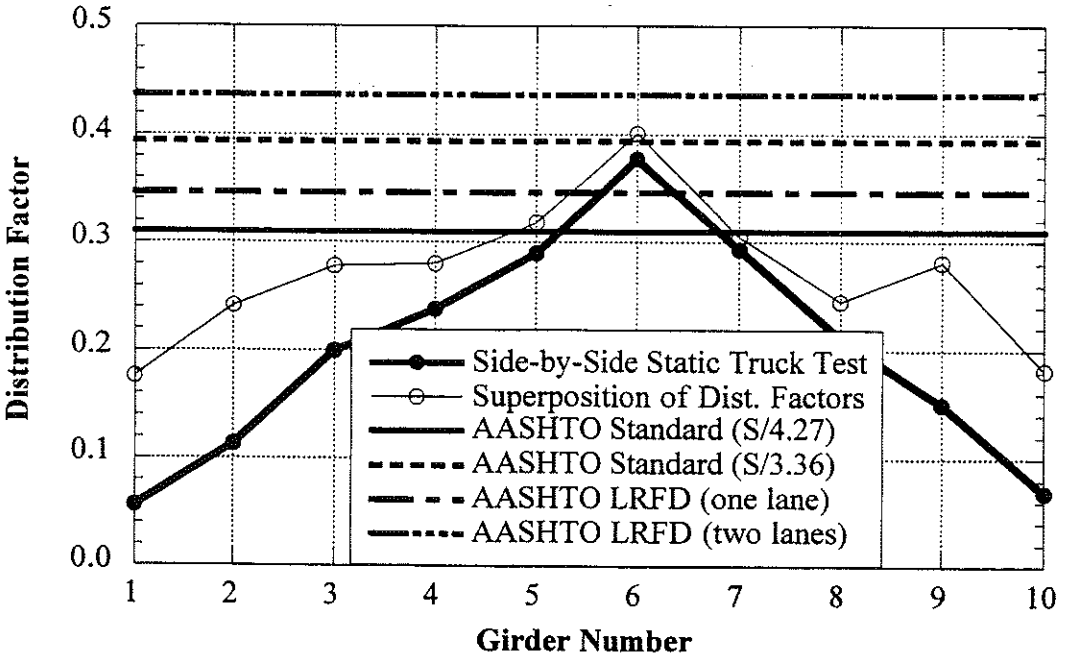

Figure 5.11 Comparison with Code Specified Distribution Factors at Crawling Speed

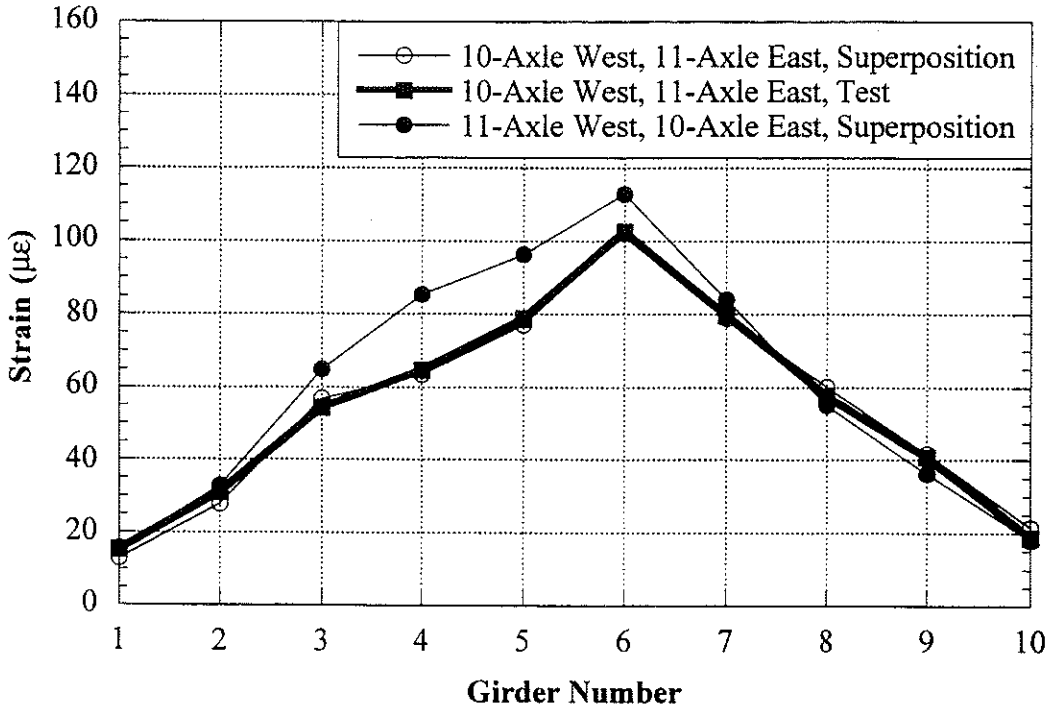

Figure 5.12 Strain Superposition and Comparison with Static Test.

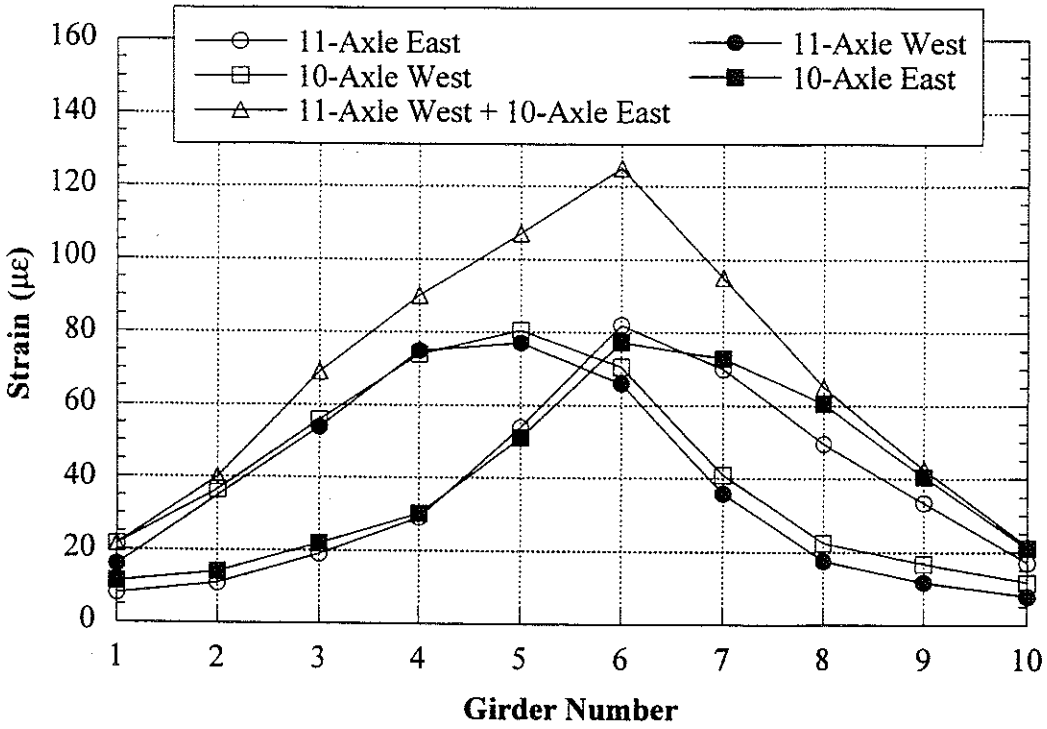

Figure 5.13 Strains under High Speed Trucks.

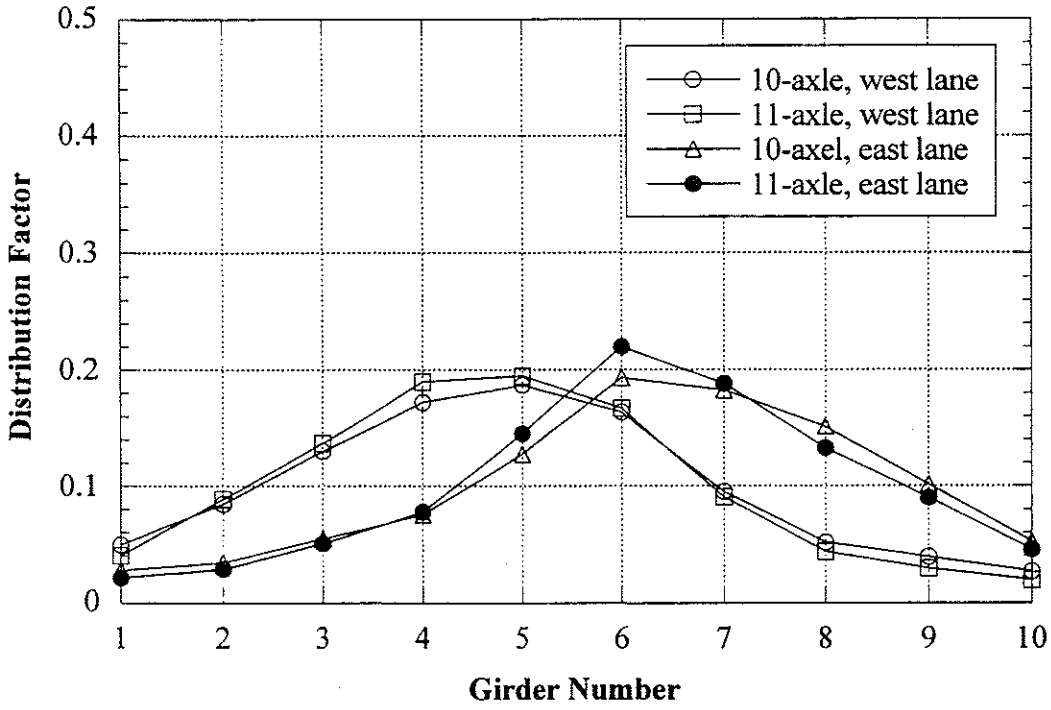

Figure 5.14 Distribution Factors for One Truck Loading at High Speed.

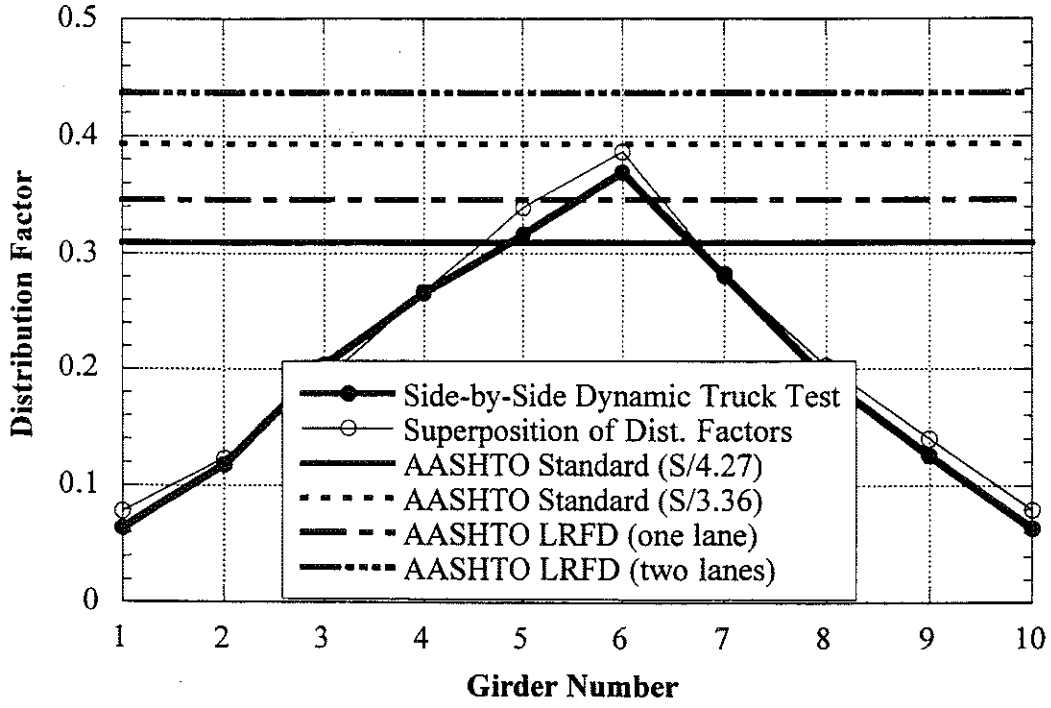

Figure 5.15 Comparison with Code Specified Distribution Factors at High Speed.

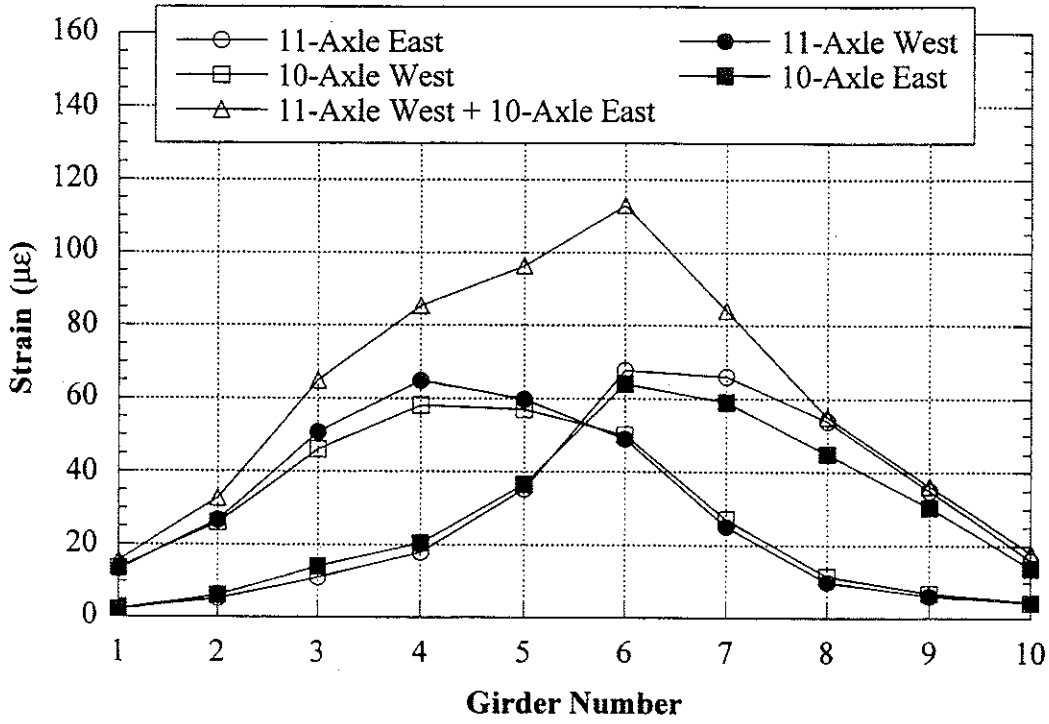

Figure 5.16 Static Strains for Impact Factors.

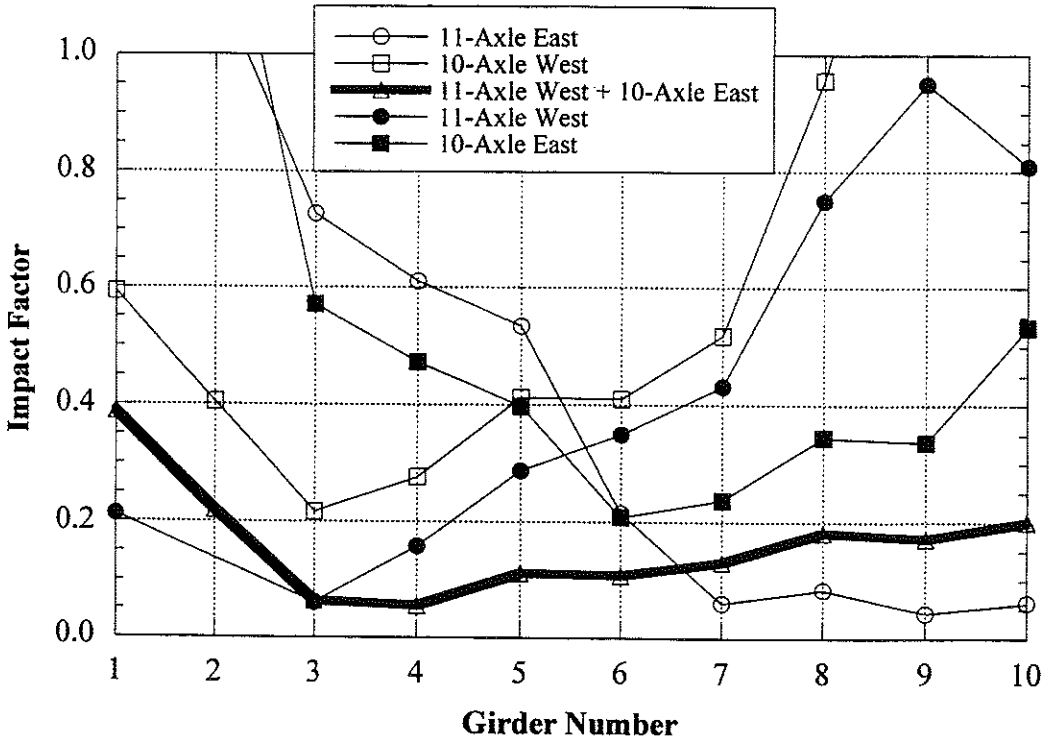

Figure 5.17 Impact Factors.

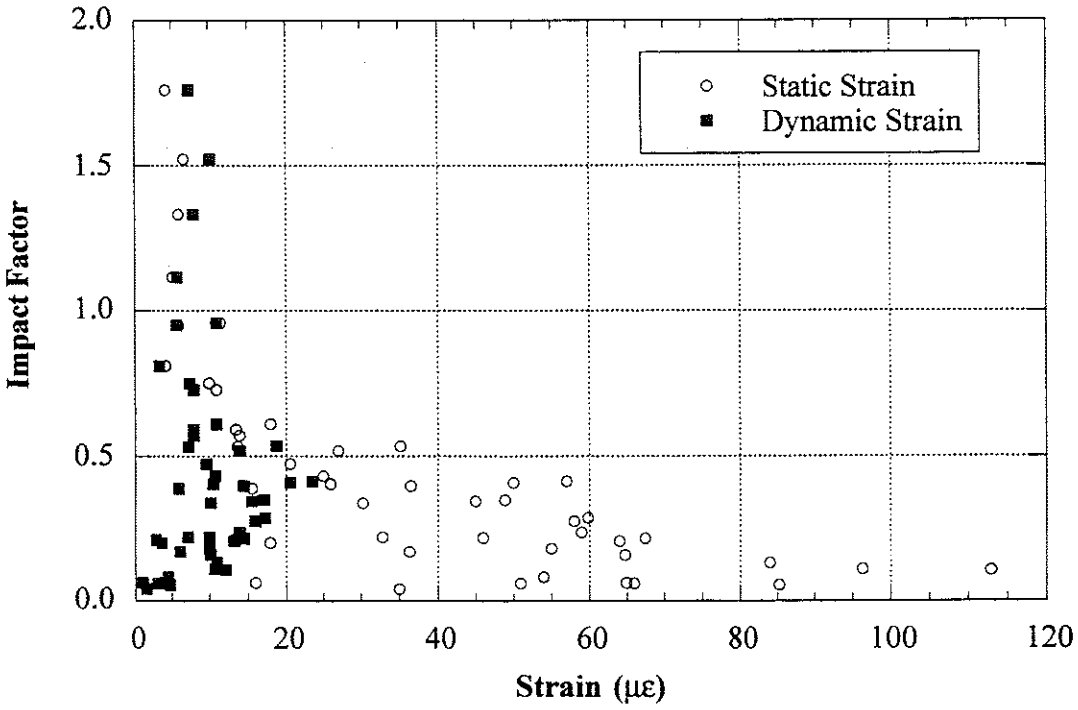

Figure 5.18 Strain versus Impact Factors.

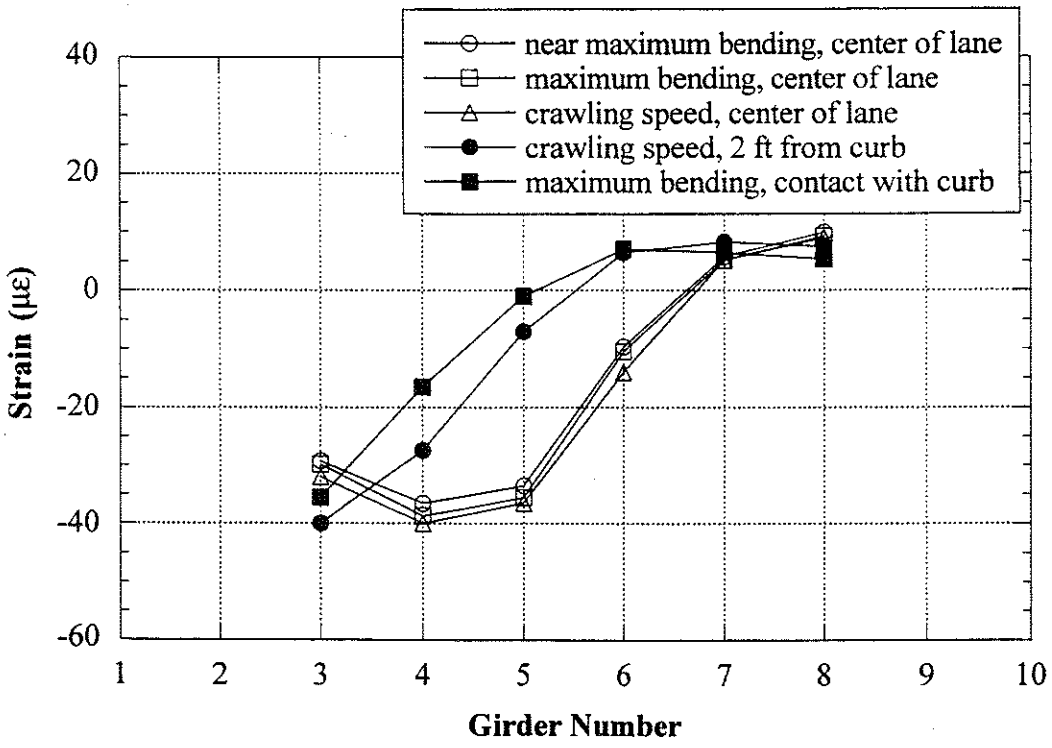

Figure 5.19 West Lane, 11-Axle Truck, Static Loading, Support.

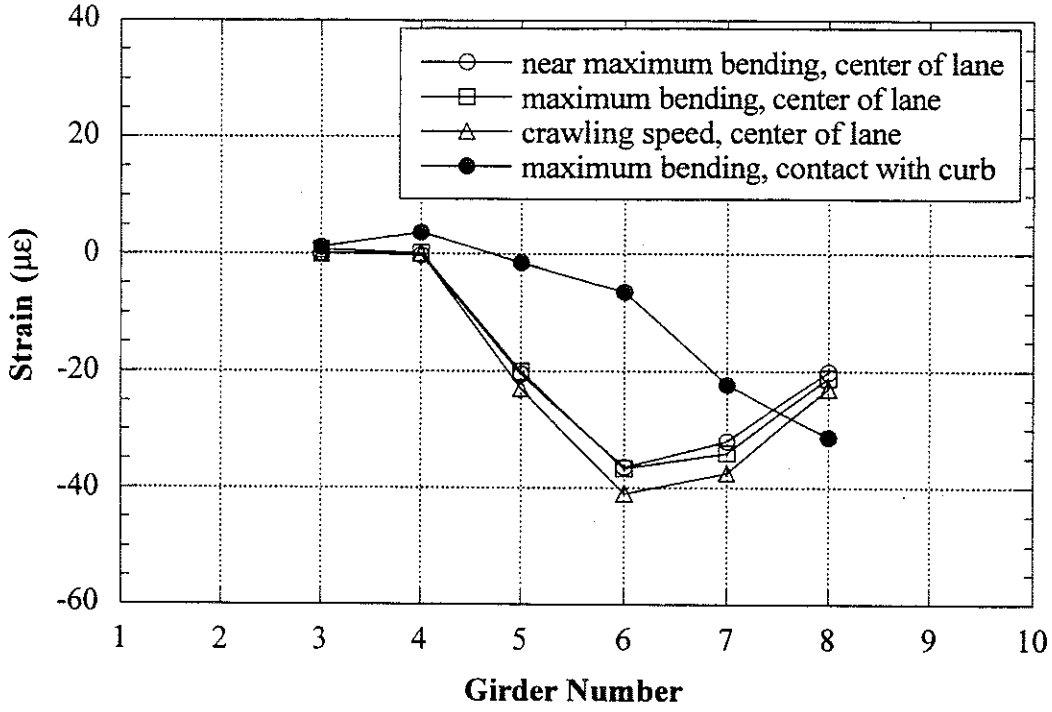

Figure 5.20 East Lane, 11-Axle Truck, Static Loading, Support.

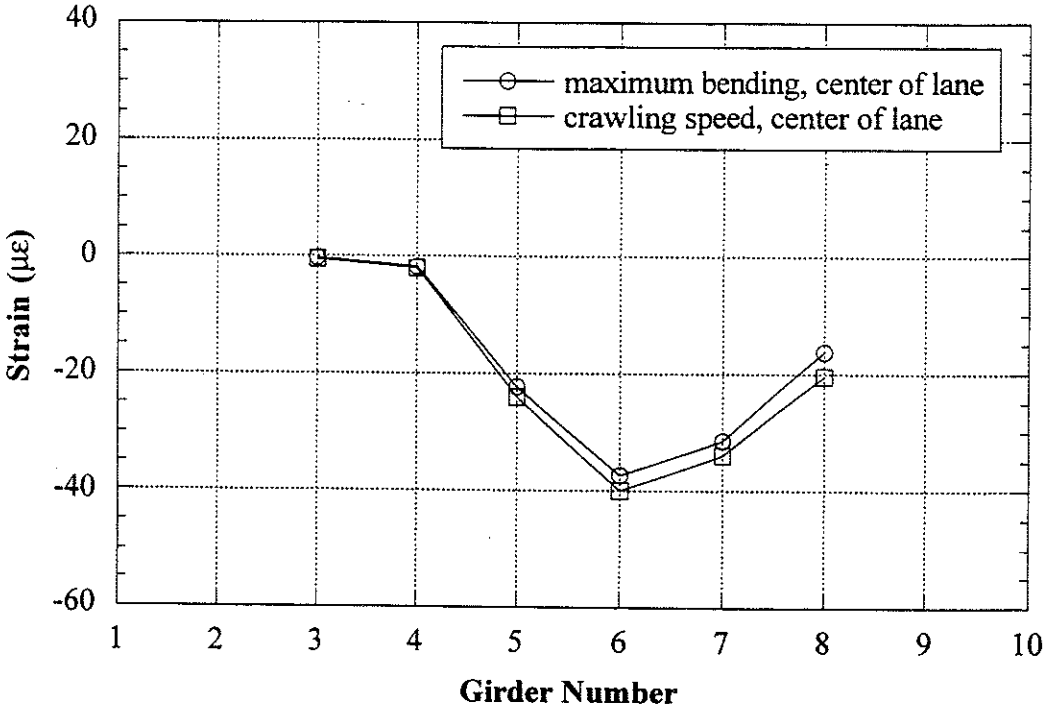

Figure 5.21 East Lane, 10-Axle Truck, Static Loading, Support.

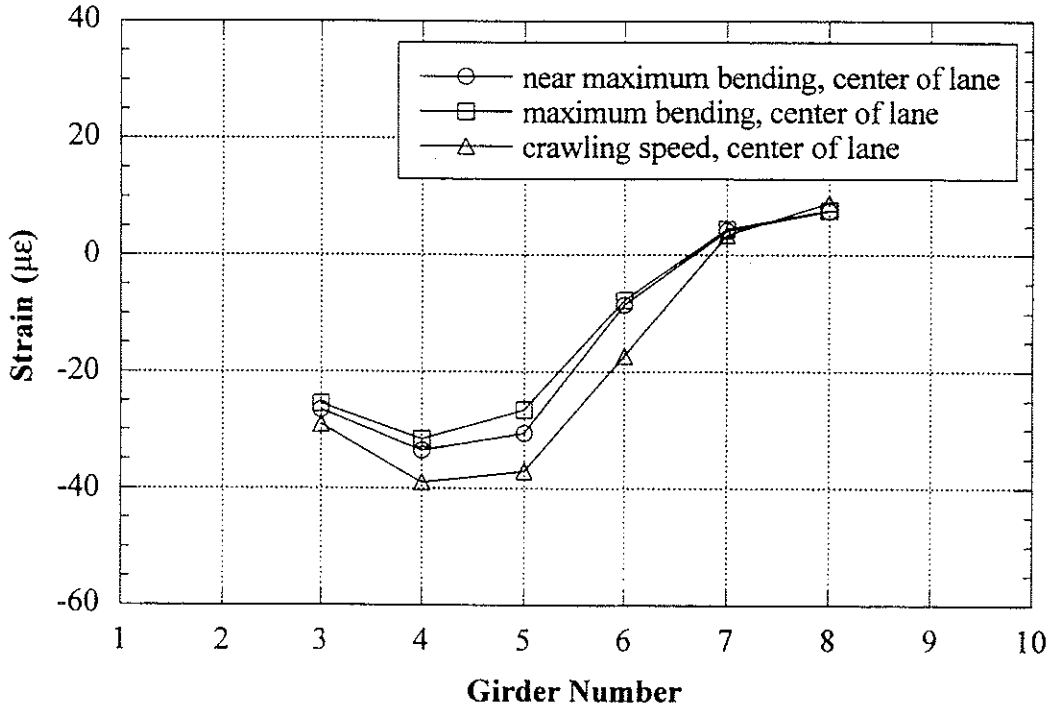

Figure 5.22 West Lane, 10-Axle Truck, Static Loading, Support.

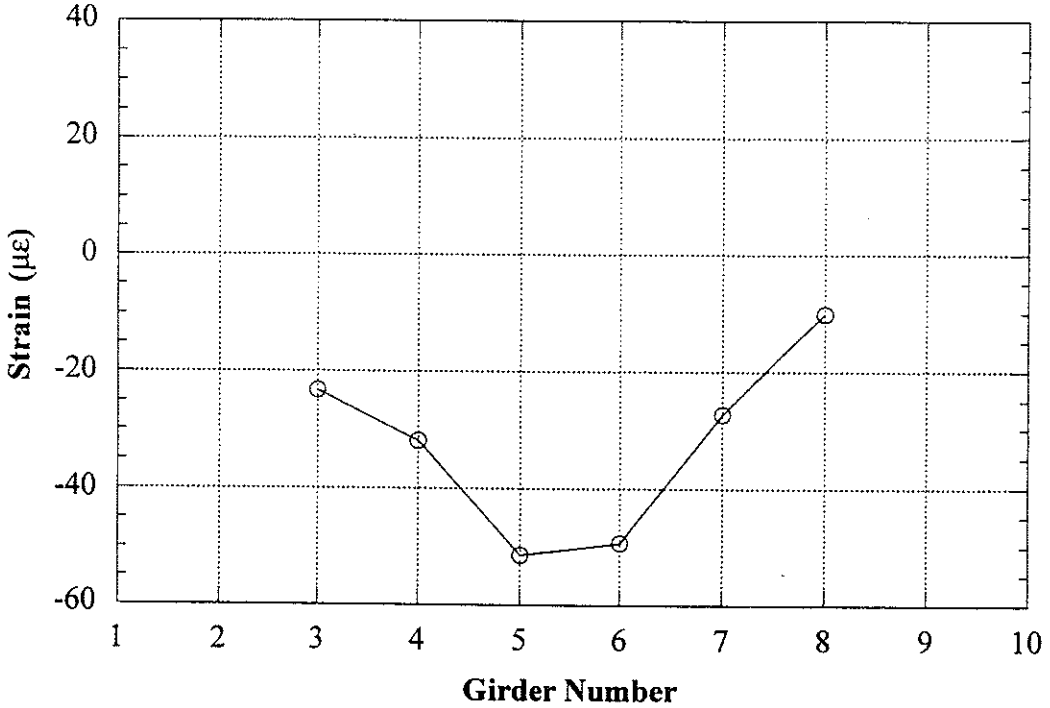

Figure 5.23 Side-by-Side Static Loading, Center of Lane, 10-Axle in West Lane, 11-Axle in East Lane, Support.

Note:

Intentionally left blank

6. Bridge on M-34 over South Branch of Raisin River in Adrian (B05-46041, M34/RR)

6.1 Description

This bridge was built in 1932 and is located over South Branch of Raisin River in Adrian, Michigan. This bridge is designated as M34/RR and was identified by the road over the bridge and the river under the bridge. It has one lane in each direction and carries state highway M-34. As shown in Figure 6.1, it has eleven steel girders spaced at 1.41 m to 1.46 m. It is a simply supported single span structure and was designed to be noncomposite. The total span length is 16.8 m without skew. The bridge is near traffic lights and the speed limit is 48 km/h. Although the approach to the bridge showed slight cracks, both the deck slab and the approach to the bridge were in good condition. The bridge has a load rating of 694 kN. The thickness of slab is 152 mm, with a 76 mm concrete wearing surface.

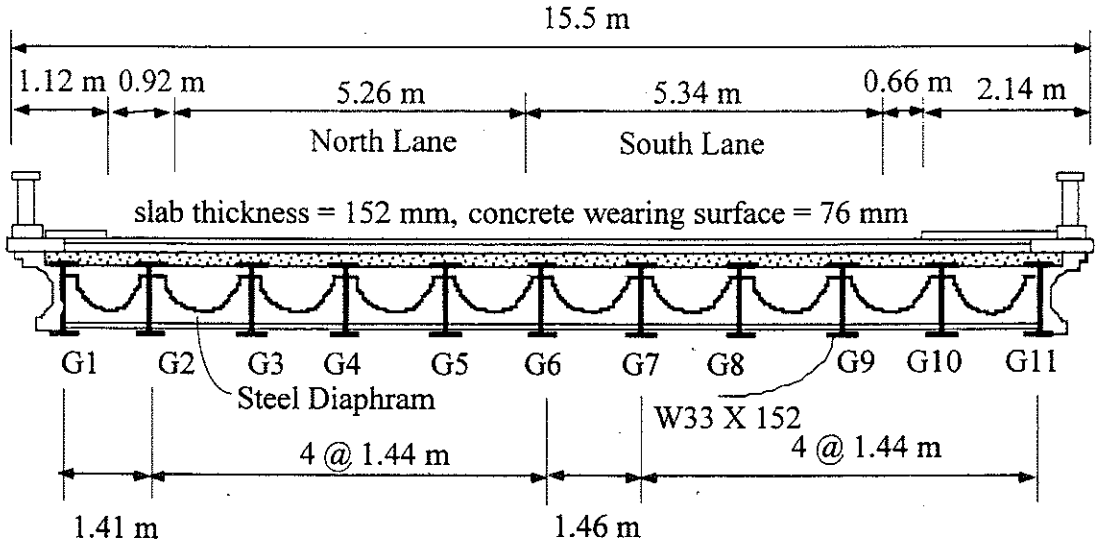

Figure 6.1 Cross-Section of Bridge M34/RR in Adrian.

6.2 Instrumentation

Strain transducers were installed on the bottom flanges of girders in the middle of the span and close to the support (Figure 6.2). The bridge test was performed on July 22, 1997.

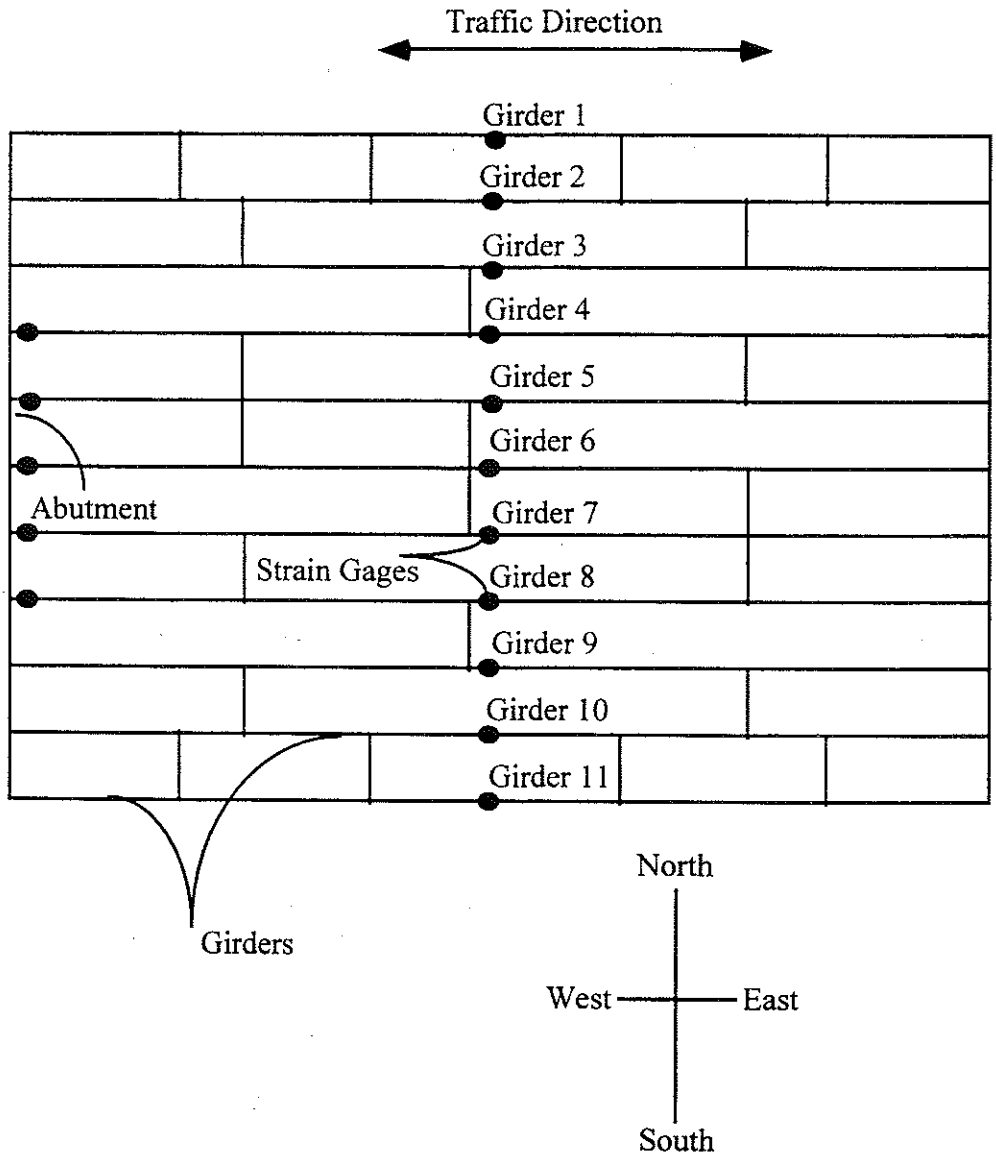

Figure 6.2 Strain Transducer Locations in Bridge M34/RR in Adrian.

6.3 Truck Loads

Strain data necessary to calculate girder distribution and impact factors were taken from the mid-span transducers. The data were obtained under passes of 10-axle and 11-axle three-unit trucks with known weights and configurations. The ten-axle and 11-axle trucks have gross weights of 580 kN and 637 kN, with wheelbases of 14.3 m and 15.6 m respectively. Truck configurations are shown in Figures 6.3 and 6.4.

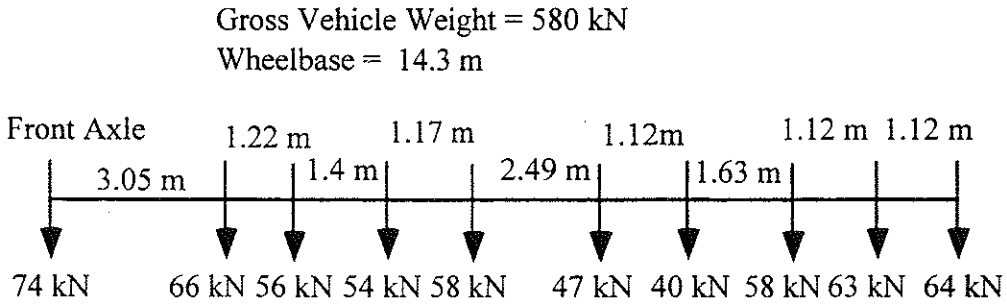

Figure 6.3 Ten-Axle Truck Configuration, Bridge M34/RR in Adrian.

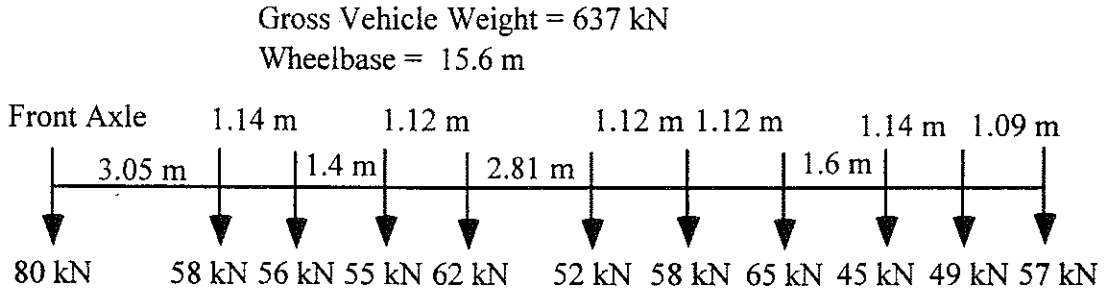

Figure 6.4 Eleven-Axle Truck Configuration, Bridge M34/RR in Adrian.

For the bridge carrying M-156 over Silver Creek in Morenci, the locations causing the analytical maximum bending moments were calculated and the trucks were statically placed at these positions. Because the strains obtained from the crawling speed tests were always greater than those which resulted from placing the trucks at the

calculated positions of maximum moment, bridge M34/RR was tested only under crawling speed and high speed. The following load combinations were performed during the tests:

at crawling speed,

- 11-axle truck along the center of north lane
- 11-axle truck close to the curb of north lane
- 10-axle truck along the center of north lane
- 10-axle truck close to the curb of north lane
- 11-axle truck along the center of south lane
- 11-axle truck close to the curb of south lane
- 10-axle truck along the center of south lane
- 10-axle truck close to the curb of south lane
- 10-axle truck along the center of south lane and 11-axle truck along the center of north lane
- 11-axle truck along the center of south lane and 10-axle truck along the center of north lane

at high speed, the maximum speed obtained by a test truck at a bridge site,

- 10-axle truck along the center of north lane, 48 km/h
- 11-axle truck along the center of north lane, 40 km/h
- 10-axle truck along the center of south lane, 56 km/h
- 11-axle truck along the center of south lane, 40 km/h
- 10-axle truck along the center of south lane and 11-axle truck along the center of north lane, 40 km/h
- 11-axle truck along the center of south lane and 10-axle truck along the center of north lane, 40 km/h

6.4 Load Test Results

As with the Morenci (M156/SC) bridge, strains from crawling-speed tests are considered static, and these were used to calculate girder distribution factors. Additional strains above the static values that were caused by high-speed tests are considered dynamic, and these were used to compute impact factors.

Figures 6.5 to 6.7 present the results of all crawling-speed (static) tests. Figures 6.5 to 6.6 present static strains and GDF's for one truck on the bridge. Figure 6.7 shows static strains and GDF's from side-by-side static load tests. GDF's are calculated from static strains using Eq. (3-4). Figure 6.7 also compares static strains obtained by superposing strains under one truck loading with those from side-by-side truck loading. They have practically the same values and again verify the superposition method used.

The maximum distribution factors from all cases in Figure 6.5 to 6.6 are presented in Figure 6.8, which represents the envelope of GDF's for one truck static loading. The maximum GDF's for one loaded lane were superimposed with the other to obtain GDF's for two-lane loading. The results are shown in Figure 6.9 together with the distribution factors from a side-by-side crawling-speed truck test.

In Figure 6.8, the results are taken as the maximum effect caused by the combination of two transverse truck positions in each lane; in the center of the lane, and near the curb. In contrast, Figure 6.9 shows the results when both trucks were in the same transverse position in their respective lanes. As expected, as the trucks are placed closer to the curbs, the GDF increases on the outside girders. The interior girders still experience a higher load effect, however. All measured GDF's are well below all AASHTO Code specified GDF's. Actual values of the term $K_g/(Lt_s^3)$ are used in calculation of Code specified GDF values.

Figures 6.10 and 6.11 present the dynamic strains obtained from high-speed tests. The distribution factors calculated from the dynamic strains using Eq. (3-4) are plotted and compared with Code specified GDF's in Figures 6.12 and 6.13.

From the corresponding static and dynamic strains from Figures 6.10 and 6.11, impact factors are calculated using Eq. (3-5) and presented in Figure 6.14. Similar to the Morenci bridge, the impact factors for exterior girders are large, due to a low static strain versus dynamic strain. But again, the absolute magnitude of dynamic strain at the exterior girders is low and is not significant. Figure 6.15 shows the relationship between strain magnitude and impact factors. For side-by-side truck loading, the impact factors do not exceed 10% at interior girders.

No significant strains at the supports were found, but a qualitative description of the results is as follows: At the beginning of the loading (when a truck begins to drive upon the span), small negative strains are induced, which indicates partial fixity of the supports. As the truck continues across the bridge, the negative strain values suddenly drop. This may indicate that the support fixity is released under heavy loads.

The measured static strains were compared to static strains calculated using the design stiffness and GDF's determined by tests in this study. The maximum observed static strain for this bridge is 64 με for a single truck and 87 με for two trucks side-by-side. The corresponding calculated strain for a single truck in a composite section is 148 με and for a non-composite section it is 242 με. For two trucks side-by-side loading, the calculated strains are 201 με and 328 με for a composite section and a non-composite section, respectively.

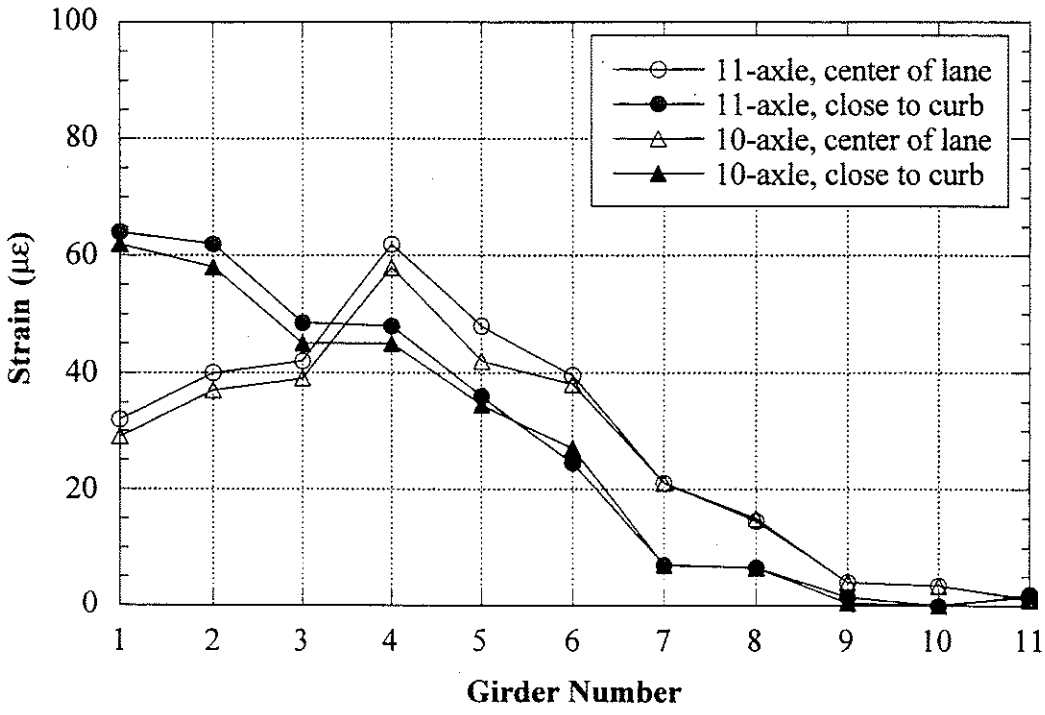

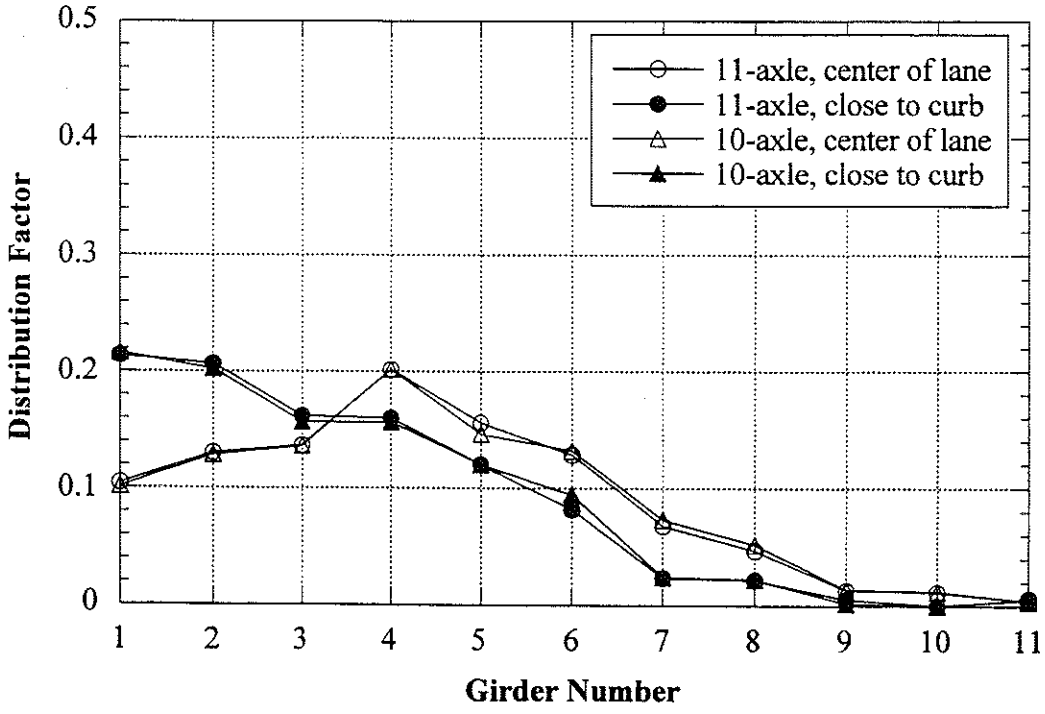

Figure 6.5 North Lane, Crawling Speed, Midspan.

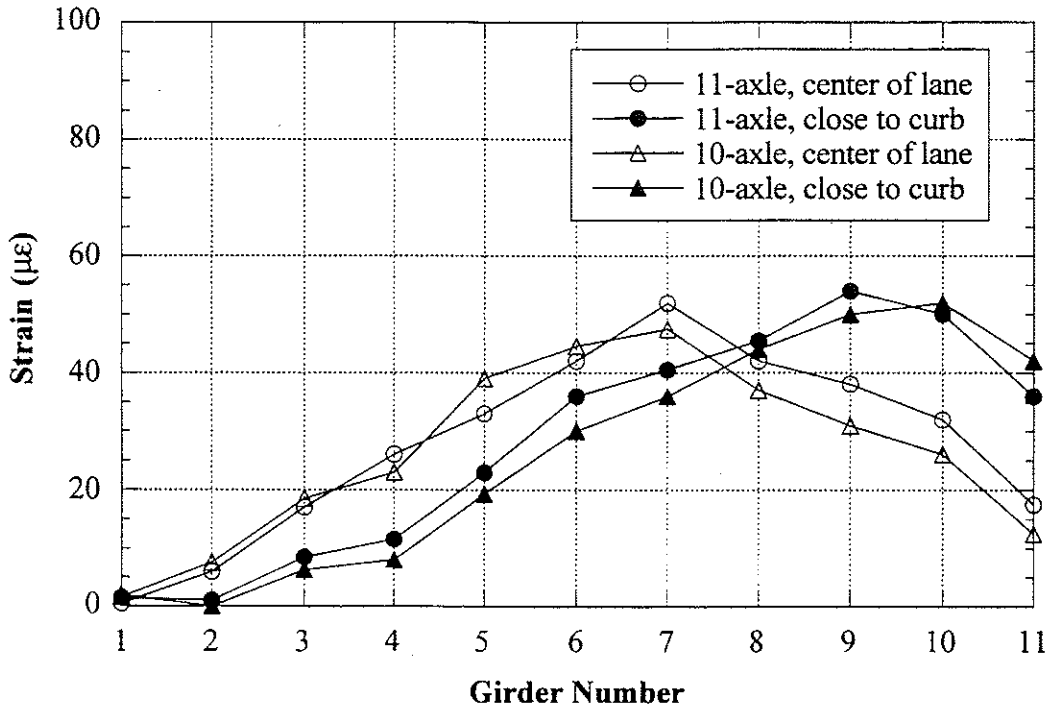

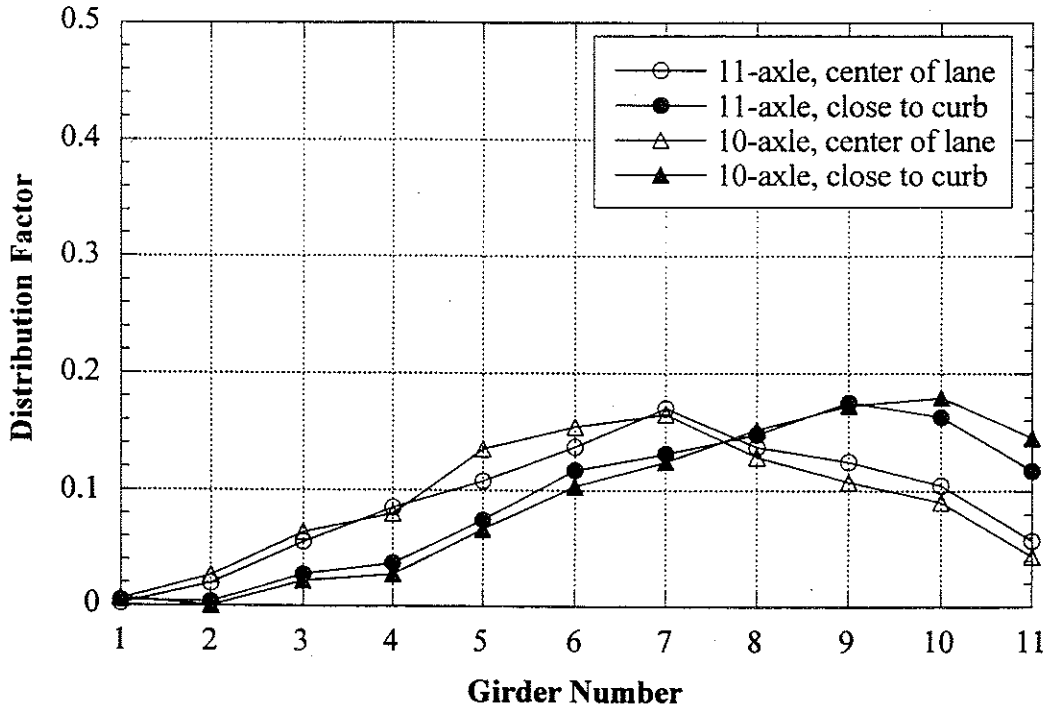

Figure 6.6 South Lane, Crawling Speed, Midspan.

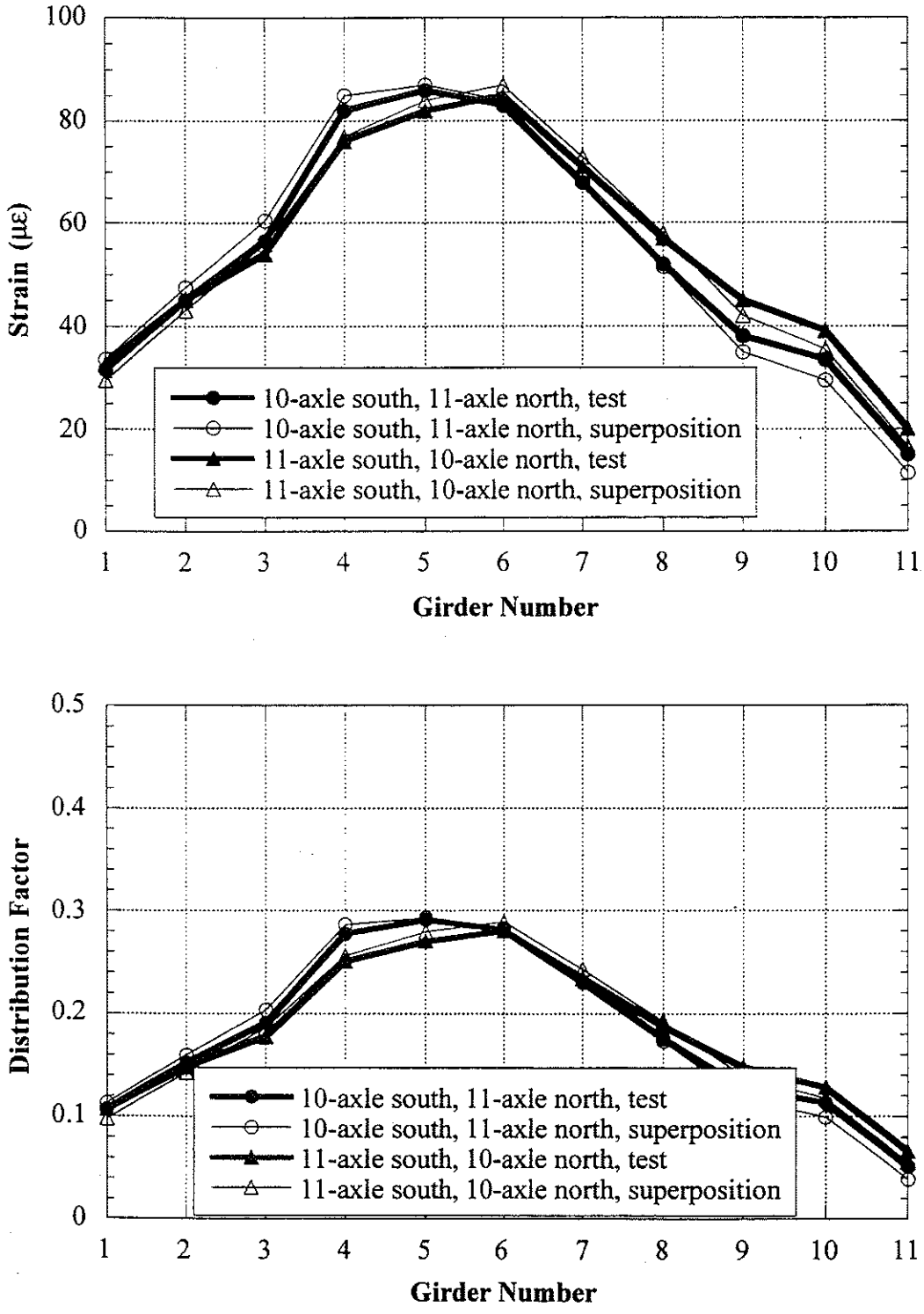

Figure 6.7 Side-by-Side Static Loading, Center of Lane, Midspan at Crawling Speed.

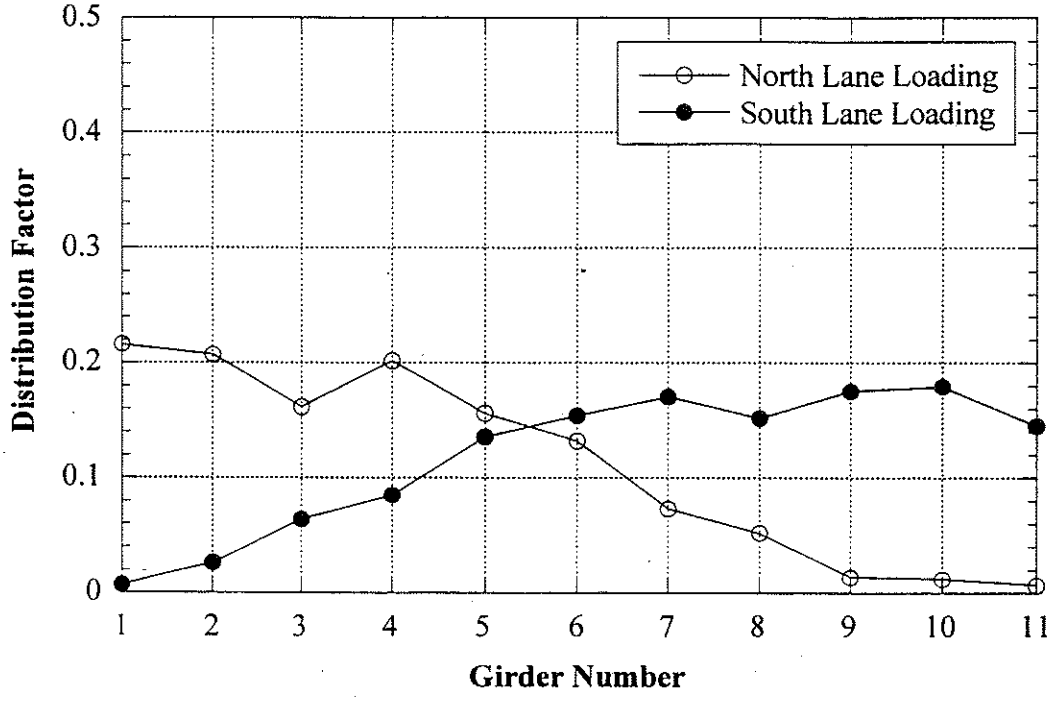

Figure 6.8 Envelope of Girder Distribution Factor
For One Truck Static Loading, Crawling Speed.

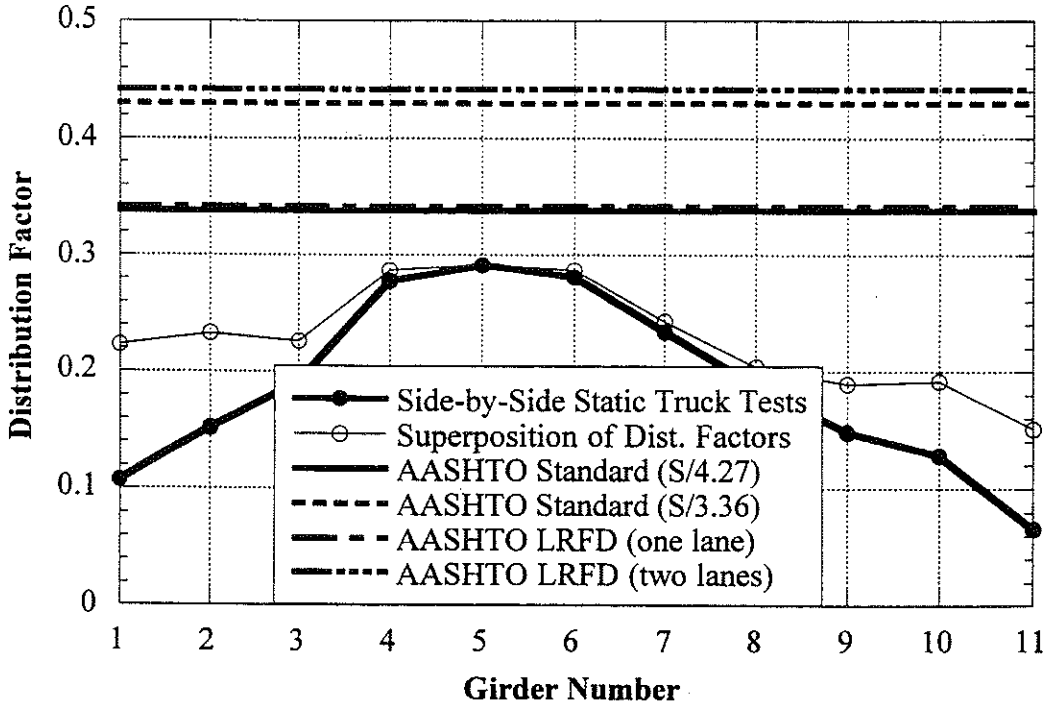

Figure 6.9 Comparison with Code Specified Distribution Factor
at Crawling Speed.

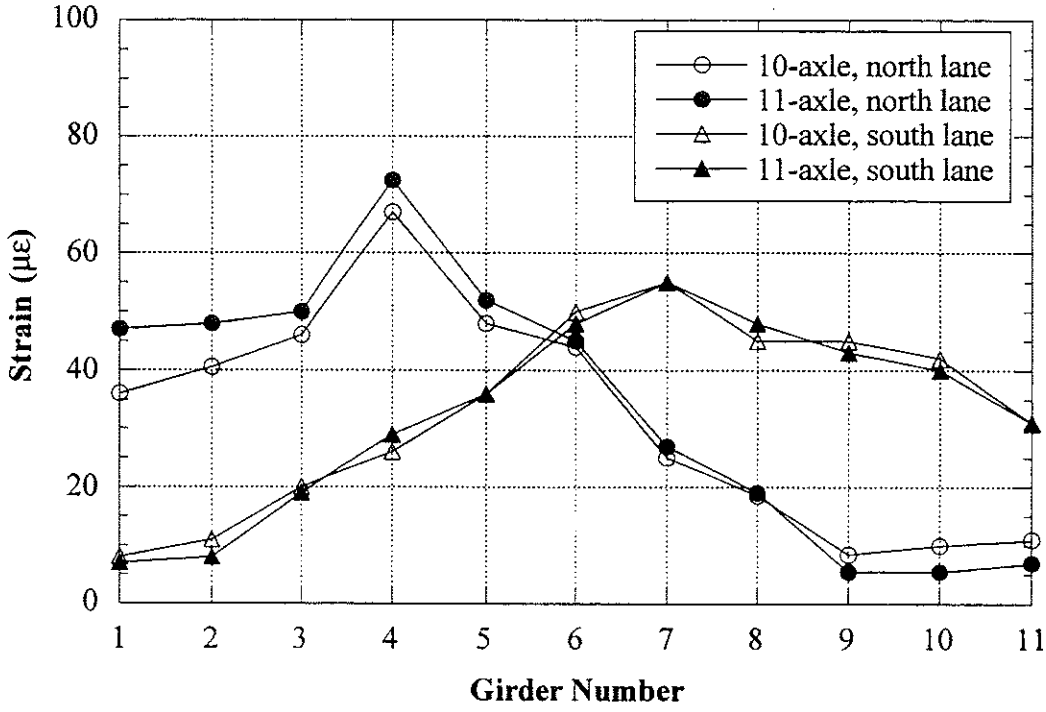

Figure 6.10 Strains under One Truck Loading at High Speed.

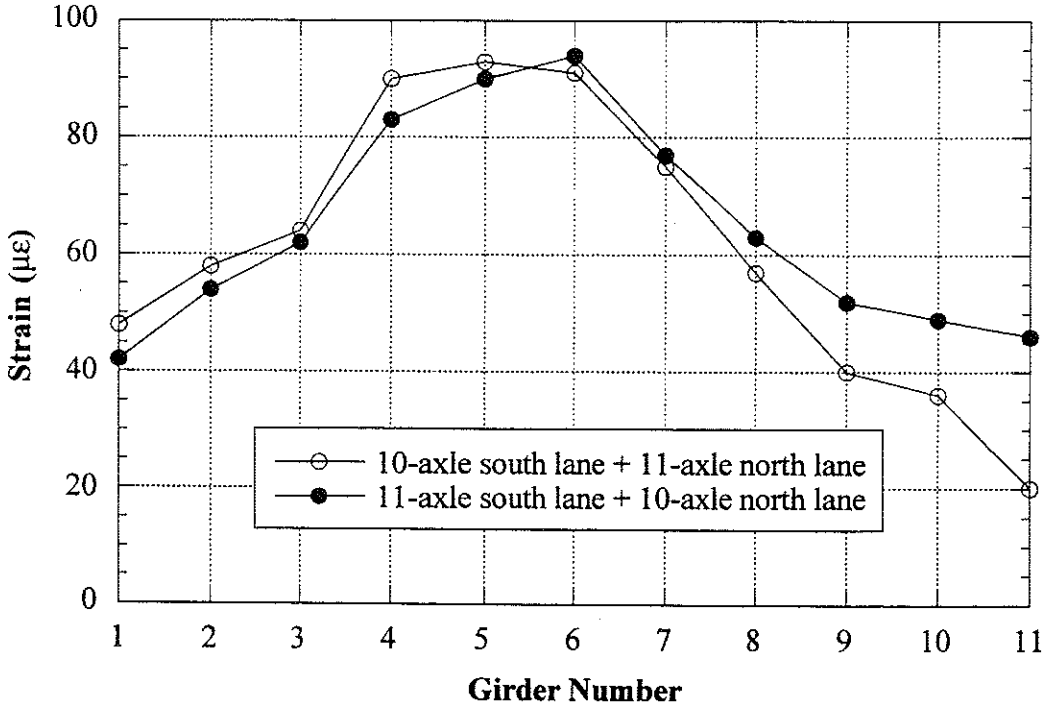

Figure 6.11 Strains under Side-by-Side Truck Loading at High Speed.

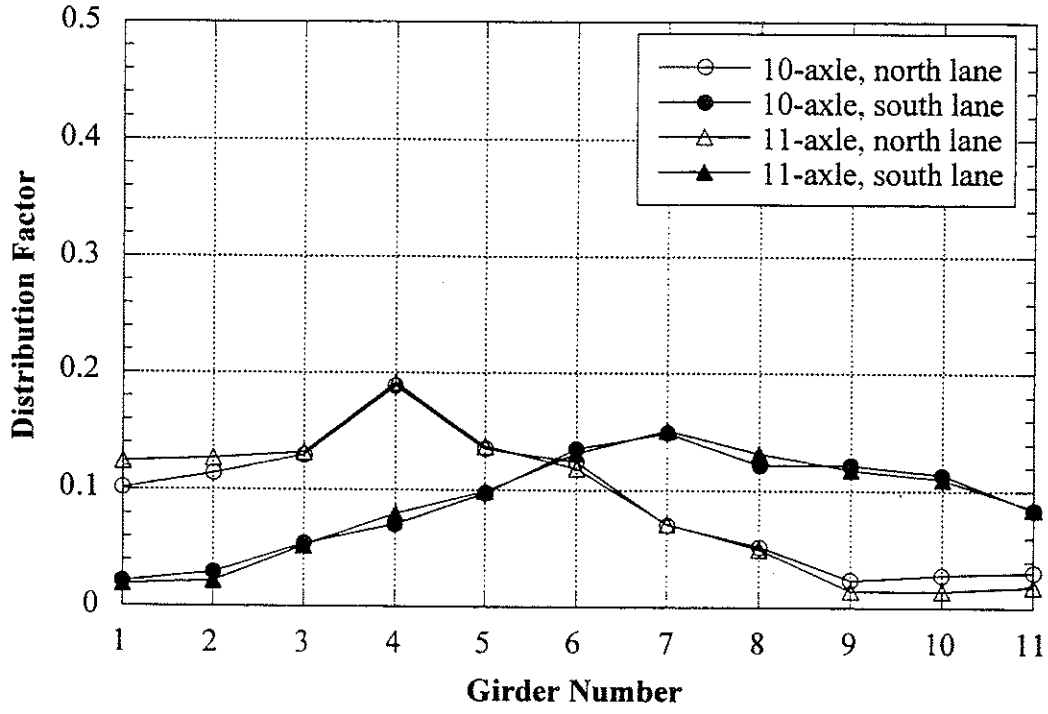

Figure 6.12 Distribution Factors for One Truck Loading at High Speed.

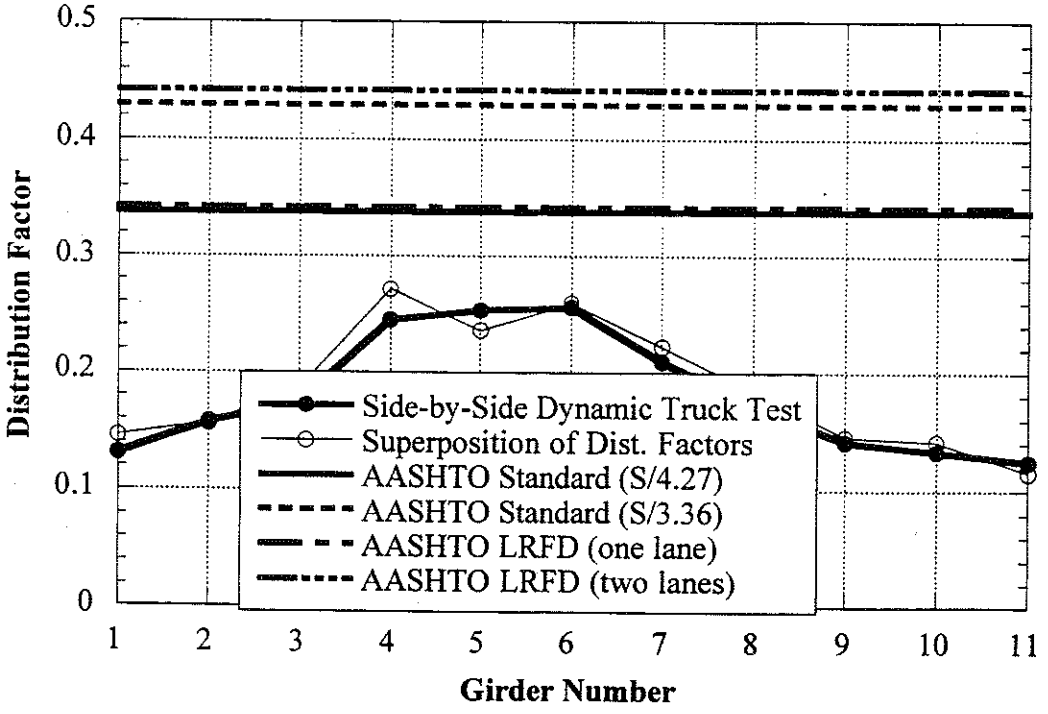

Figure 6.13 Comparison with Code Specified Distribution Factors at High Speed.

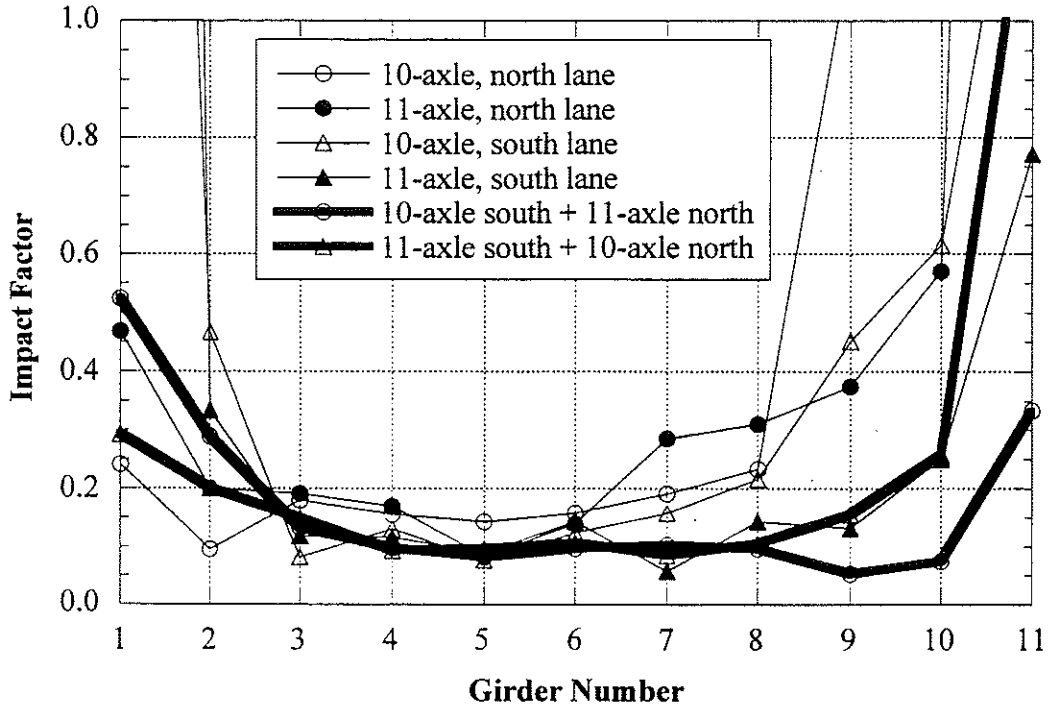

Figure 6.12 Impact Factors.

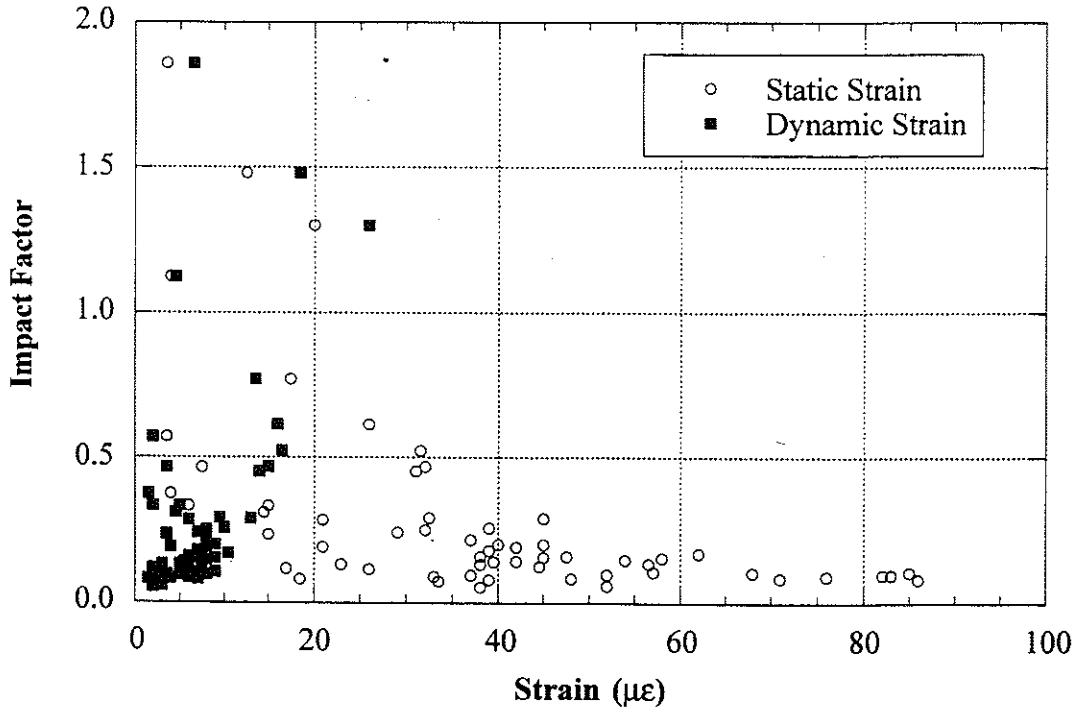

Figure 6.15 Strain versus Impact Factors.

Note:

Intentionally left blank

7. Bridge on US-12 over Swan Creek near Bronson (B02-12021, US12/SC)

7.1 Description

This bridge was built in 1922 and is located on US-12 over Swan Creek near Bronson, Branch County, Michigan. This bridge is designated as US12/SC and can be identified by the road carried by the bridge and the creek under the bridge. It has one lane in each direction. As shown in Figure 7.1, it has twelve steel girders spaced at 0.91 m to 1.39 m. The middle 6 girders were built in 1922. The remaining girders were added in 1932, along with additional abutments to support them. With these abutments, a large transverse beam was added that helps support the original girders near the bearings (see Figures. 7.1 and 7.2). The bridge is a simply supported single span structure and was designed to be noncomposite. The total span length is 11.7 m between the outside abutments (original abutments) with a skew of 10 degrees. The span length between the added abutments is 9.9 m. The supporting beam practically reduces the total span length from 11.7 m to 9.9 m. With the addition of the transverse beam, the middle six girders act as a three span continuous structure with a long main span (9.9 m) and very short end spans (see Figure 7.2). For structural calculations, a 9.9 m span length was used. The speed limit on the bridge is 72 km/h. Although the approach to the bridge showed slight cracks, both the deck slab and approach to the bridge were in good condition. The bridge has a load rating of 685 kN. The bridge has a 190 mm thick concrete slab, a 105 mm concrete wearing surface and a 50 mm asphalt overlay.

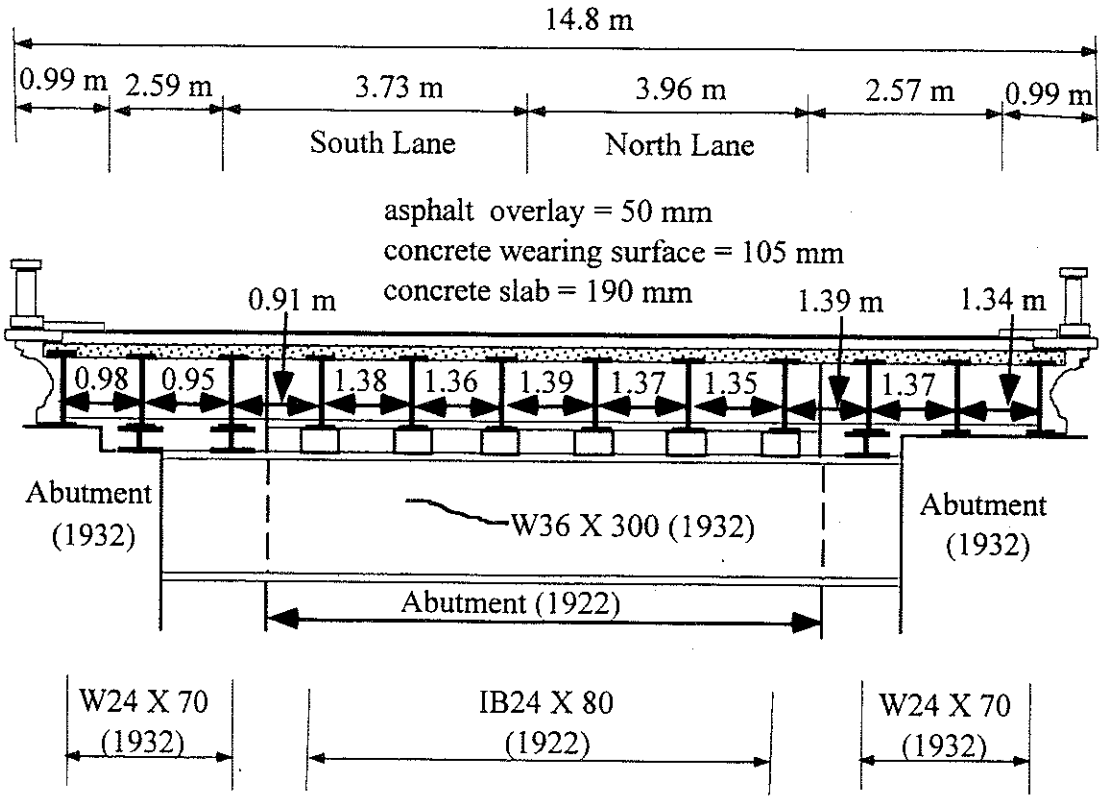

Figure 7.1 Cross-Section of Bridge US12/SC near Bronson, East Abutment View from West to East or West Abutment View from East to West.

7.2 Instrumentation

Strain transducers were installed on the bottom flanges of all girders in the middle of the span, and at the quarter points and close to the supports for girder 6 (Figure 7.2). LVDTs were installed on girders 2 to 11. The bridge test was performed on August 21, 1997.

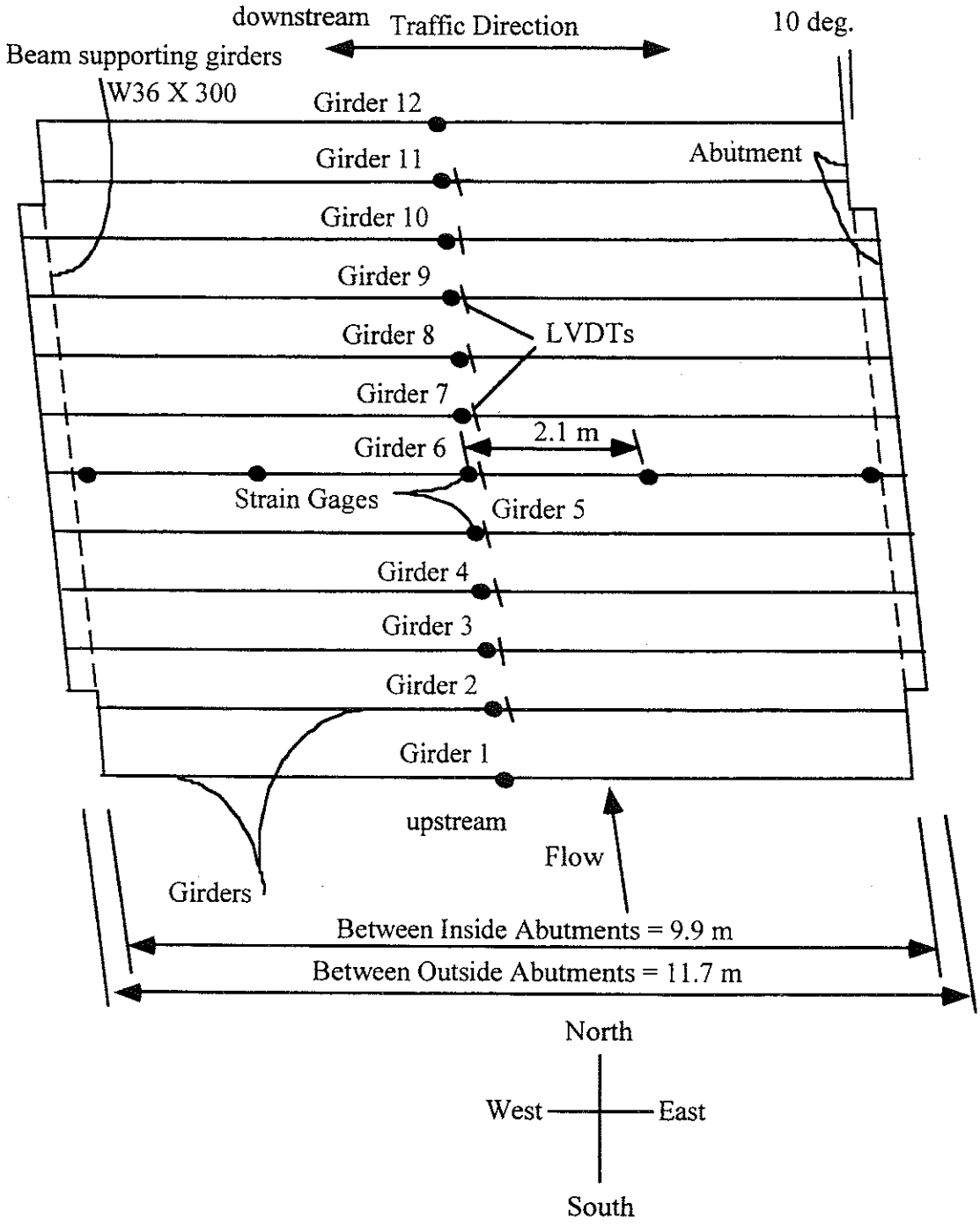

Figure 7.2 Strain and LVDT Transducer Locations in Bridge US12/SC near Bronson.

7.3 Truck Loads for Load Distribution Test

Both load distribution and proof load tests were performed on Bridge US12/SC. For the load distribution test, 10 and 11-axle trucks were used. For the proof load test, two M-60 military tanks were used.

Strain data necessary to calculate girder distribution and impact factors were taken from midspan transducers. The bridge was loaded with three-unit 10-axle and 11-axle trucks. The 10 and 11-axle trucks have gross weights of 573 kN and 640 kN, with wheelbases of 14.3 m and 15.6 m, respectively. Truck configurations are shown in Figures 7.3 and 7.4.

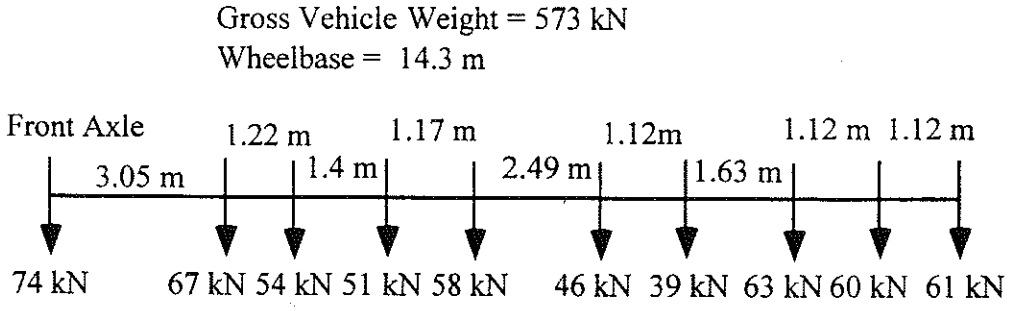

Figure 7.3 Ten-Axle Truck Configuration, Bridge US12/SC near Bronson

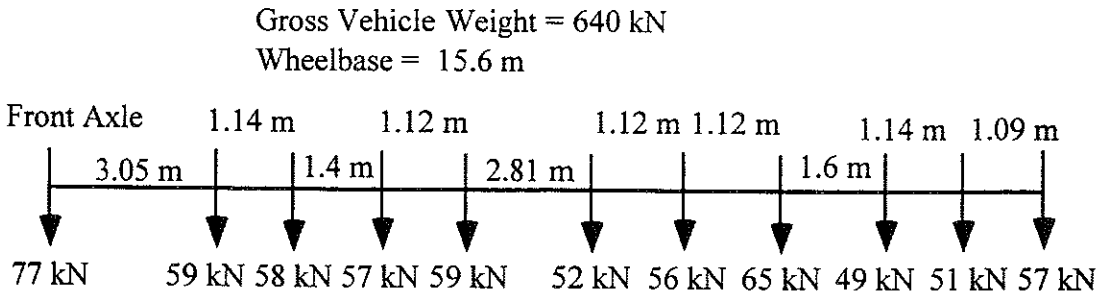

Figure 7.4 Eleven-Axle Truck Configuration, Bridge US12/SC near Bronson

This bridge was tested under crawling speed and full speed for the experimental derivation of load distribution and impact factors. The following load combinations were performed during the tests:

At crawling speed:

- 11-axle truck along the center of north lane
- 11-axle truck close to the curb of north lane
- 10-axle truck along the center of north lane
- 10-axle truck close to the curb of north lane
- 11-axle truck along the center of south lane
- 11-axle truck close to the curb of south lane
- 10-axle truck along the center of south lane
- 10-axle truck close to the curb of south lane
- 10-axle truck along the center of south lane and 11-axle truck along the center of north lane
- 11-axle truck along the center of south lane and 10-axle truck along the center of north lane

At high speed, the maximum speed obtained by the test trucks were:

- 10-axle truck along the center of north lane, 48 km/h
- 11-axle truck along the center of north lane, 48 km/h
- 10-axle truck along the center of south lane, 48 km/h
- 11-axle truck along the center of south lane, 45 km/h
- 10-axle truck along the center of south lane and 11-axle truck along the center of north lane, 42 km/h
- 11-axle truck along the center of south lane and 10-axle truck along the center of north lane, 42 km/h

7.4 Load Distribution Test Results

Strains from crawling-speed tests are considered static, and these were used to calculate girder distribution factors. Additional strains above the static values that were caused by high-speed tests are considered dynamic, and these were used to compute impact factors.

Figures 7.5 to 7.7 present the results of all crawling-speed (static) tests. Figures 7.5 to 7.6 present static strains and GDF's for one truck on the bridge. Figure 7.7 shows static strains and GDF's from side-by-side static load tests. GDF's are calculated from corresponding static strains using Eq. (3-4). Figure 7.7 also compares static strains obtained by superposing strains under one truck loading with those from side-by-side truck loading. They have practically the same values and again verify the superposition method used.

The maximum distribution factors from all cases in Figure 7.5 to 7.6 are presented in Figure 7.8, which represents the envelope of GDF's for one truck static loading. The maximum GDF's for one loaded lane were superimposed with the other to obtain GDF's for two-lane loading. The results are shown in Figure 7.9 together with the distribution factors from a side-by-side crawling-speed truck test.

In Figure 7.8, the results are taken as the maximum effect caused by the combination of two transverse truck positions in each lane; in the center of the lane, and near the curb. In contrast, Figure 7.9 shows the results when both trucks were in the same transverse position in their respective lanes. As expected, as the trucks are placed closer to the curbs, the GDF increases on the outside girders. The interior girders still experience a higher load effect, however. All measured GDF's are well below the AASHTO Code specified values. Actual value of the term $K_g / (Lt_s^3)$ is used in calculation of AASHTO LRFD GDF values.

Figures 7.10 to 7.12 show the static strain profile of girder 6 along the bridge length. Not all gages were working during the test, however,

so some data points are missing. Readings at the west supports show small negative strains, indicating partial support fixity in the case of north lane and side-by-side truck loading. For south lane loading, strain at the support is practically zero. In addition, the east supports seem to have less fixity than the west supports.

Figures 7.13 and 7.14 present the strains obtained from high-speed tests. The distribution factors calculated from the dynamic strains are plotted and compared with Code specified GDF's in Figures 7.15 and 7.16.

From the corresponding static and dynamic strains, impact factors are calculated using Eq. (3-5) and presented in Figure 7.17. As in previous tests, this bridge also shows large impact factors for exterior girders, due to a low static strain versus dynamic strain. And again, the absolute magnitude of dynamic strain at the exterior girders is low and is not significant. Figure 7.18 shows the relationship between strain magnitude and impact factors. For side-by-side truck loading, the impact factors do not exceed 10% at interior girders.

The measured static strains were compared to static strains calculated using the design stiffness and GDF's determined by tests in this study. The maximum observed static strain for this bridge is 42 με for a single truck and 71 με for two trucks side-by-side. The corresponding calculated strain for a single truck in a composite section is 94 με and for a non-composite section it is 181 με. For two trucks side-by-side loading, the calculated strains are 124 με and 240 με for a composite section and a non-composite section, respectively.

For truck loading, only strains were measured during the test. However, deflections caused by the proof load tests were measured by LVDT's.

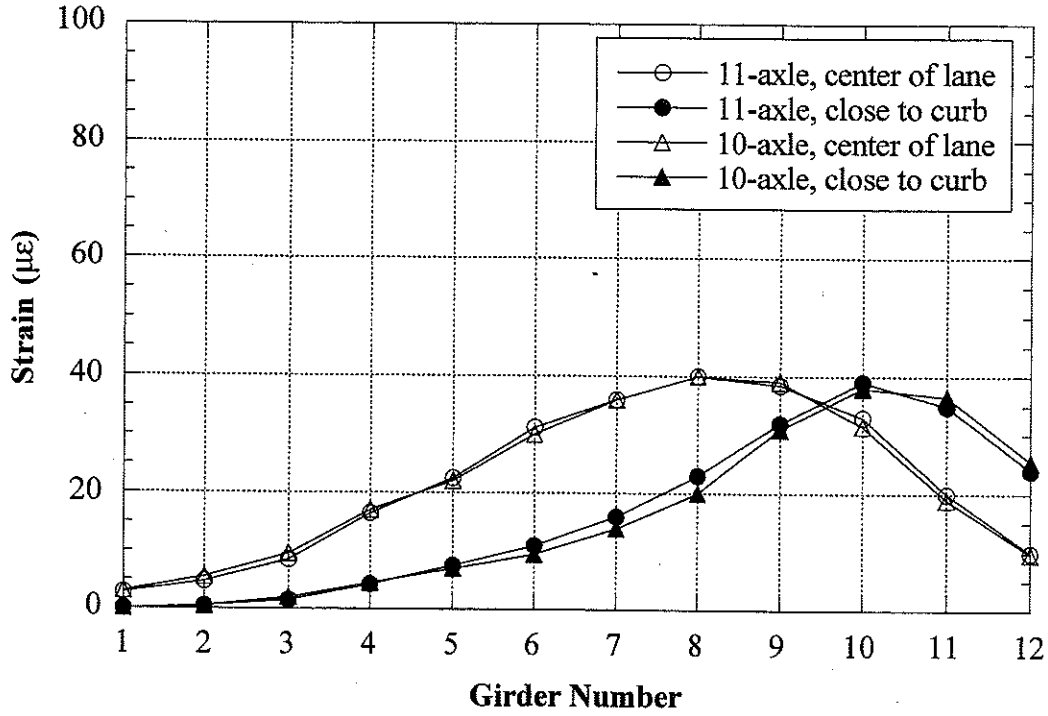

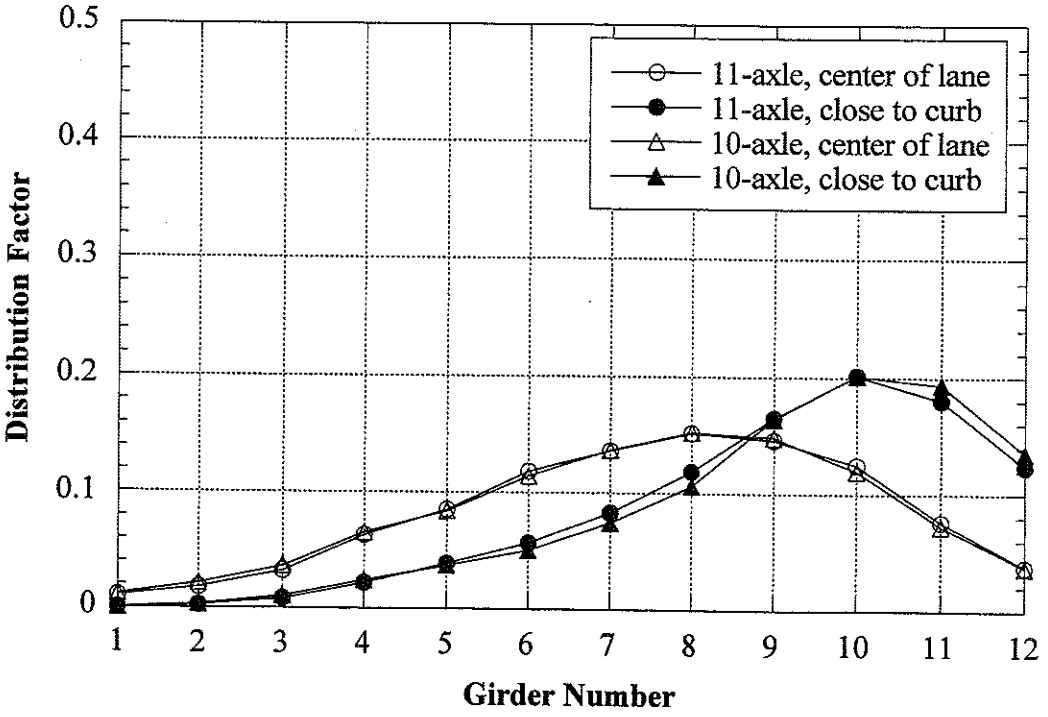

Figure 7.5 North Lane, Crawling Speed, Midspan.

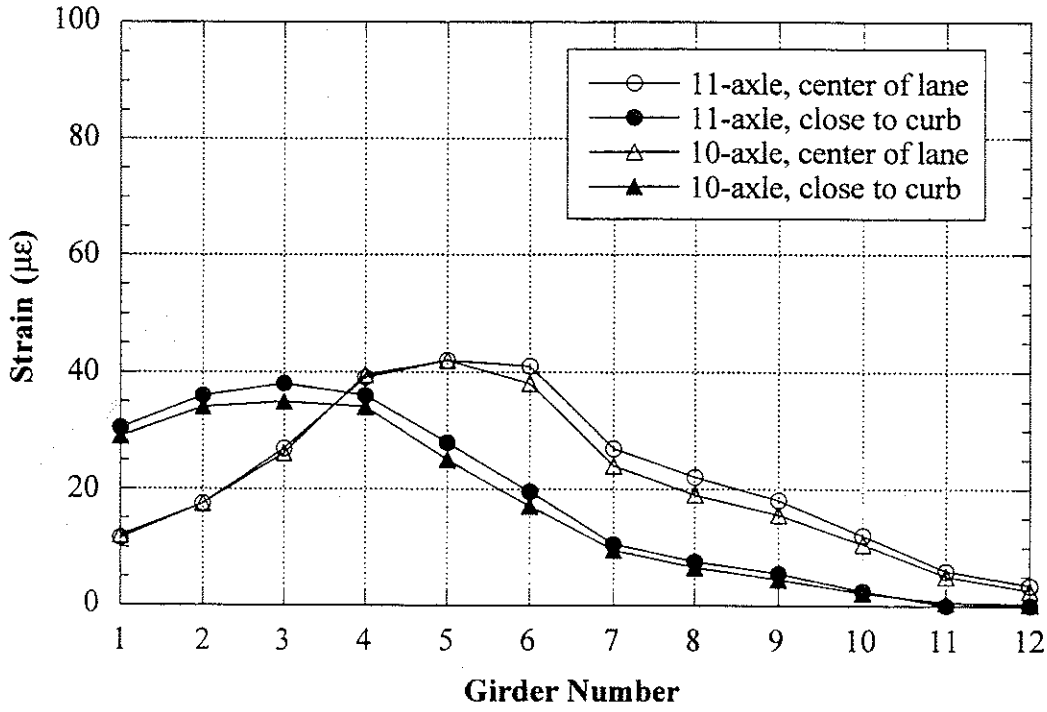

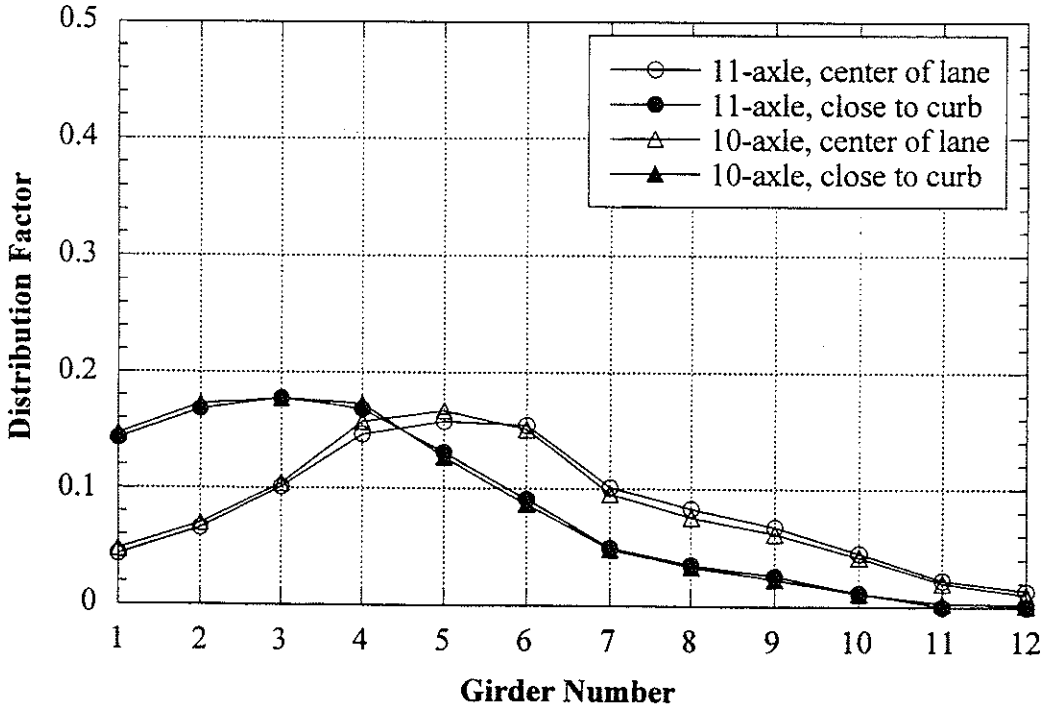

Figure 7.6 South Lane, Crawling Speed, Midspan.

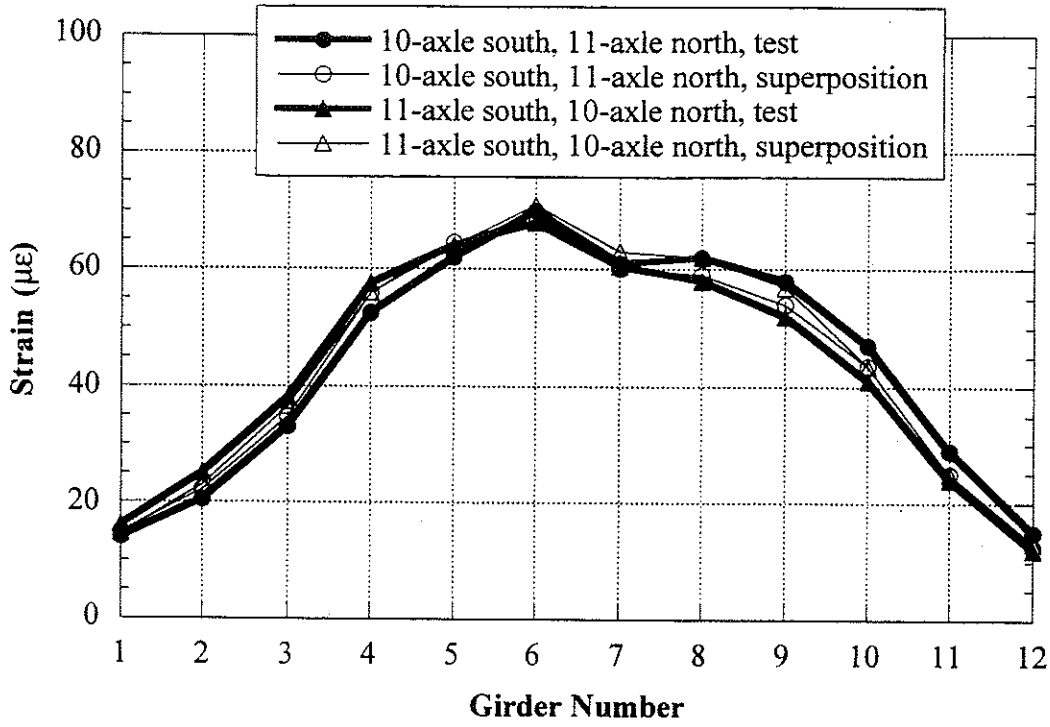

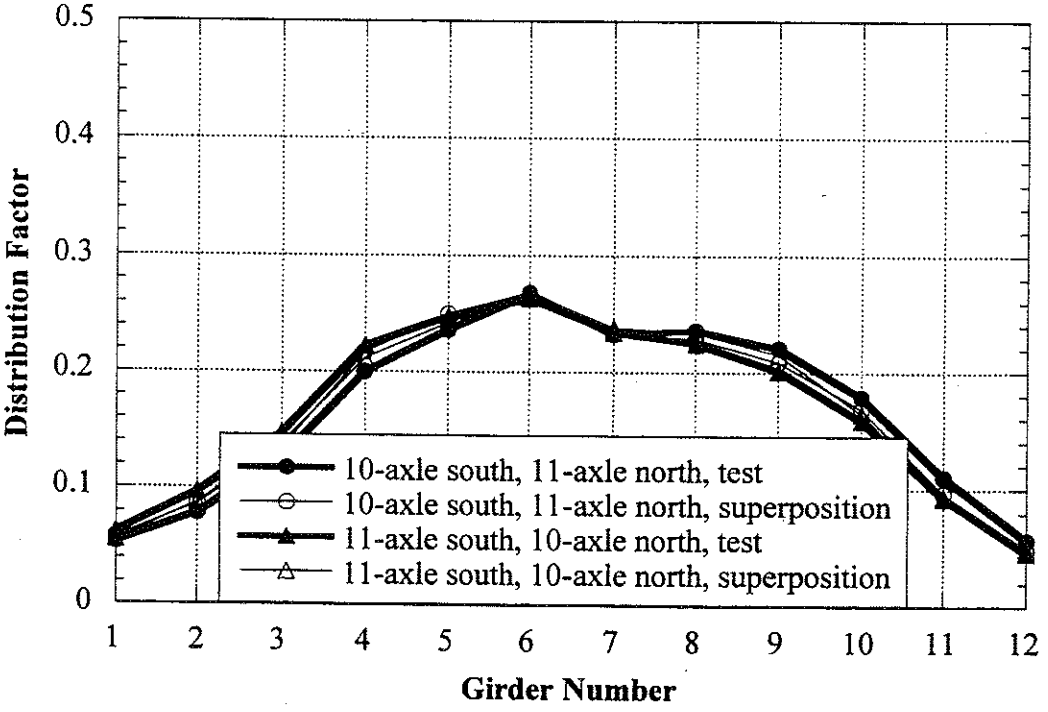

Figure 7.7 Side-by-Side Loading, Center of Lane, Crawling Speed Midspan.

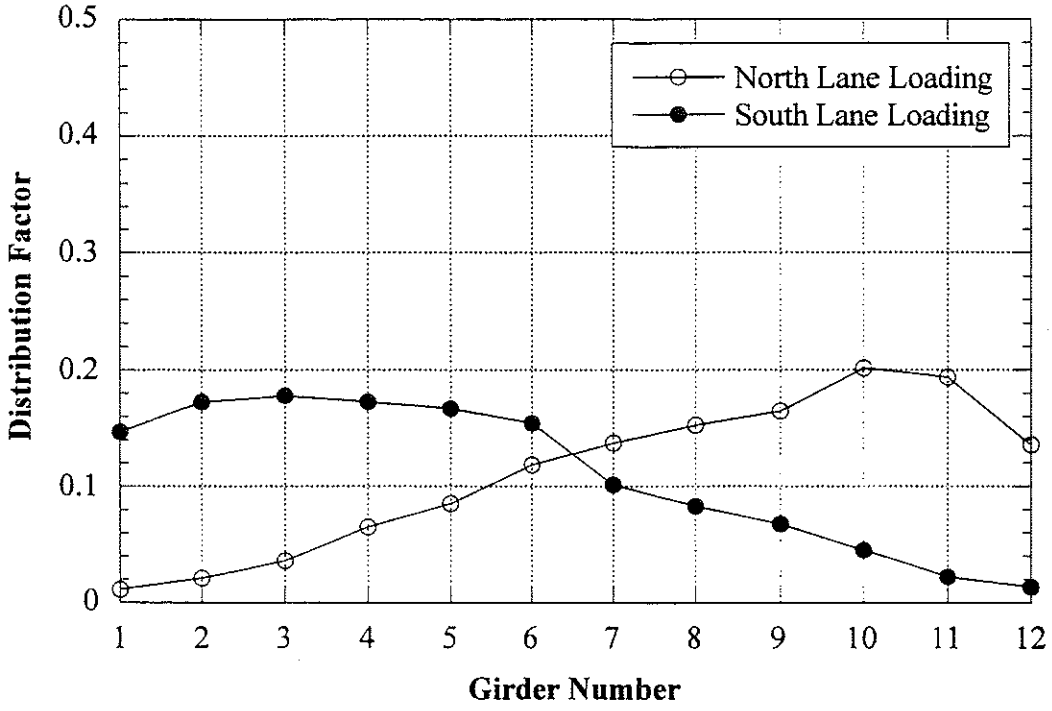

Figure 7.8 Envelope of Girder Distribution Factor
For One Truck Static Loading, Crawling Speed.

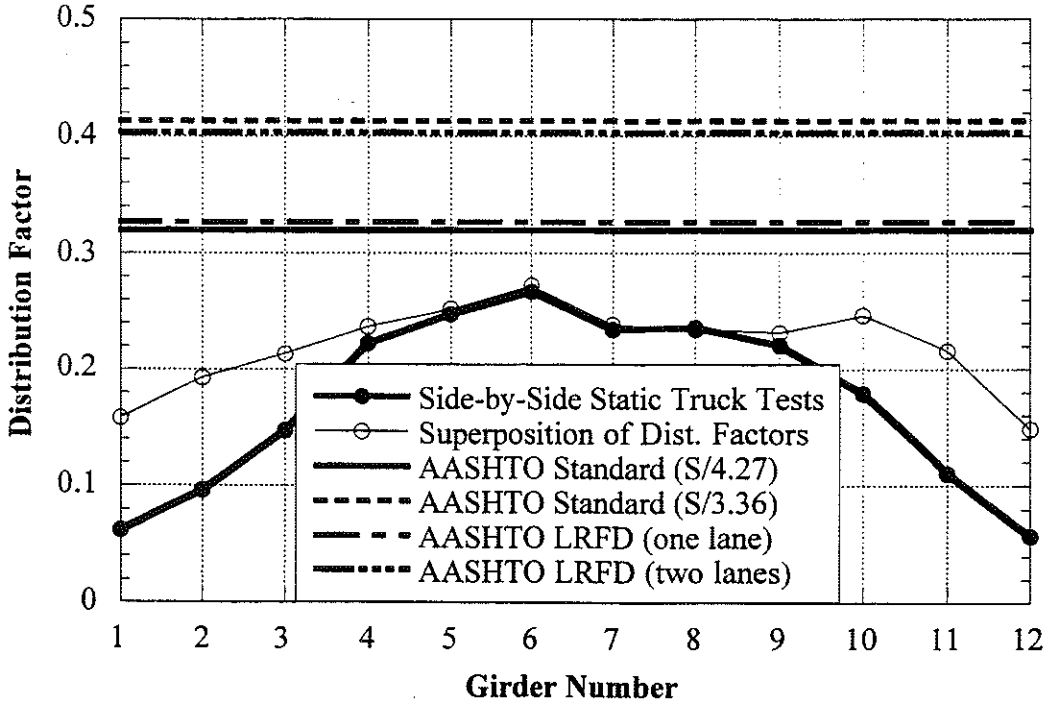

Figure 7.9 Comparison with Code Specified Distribution Factors,
Crawling Speed

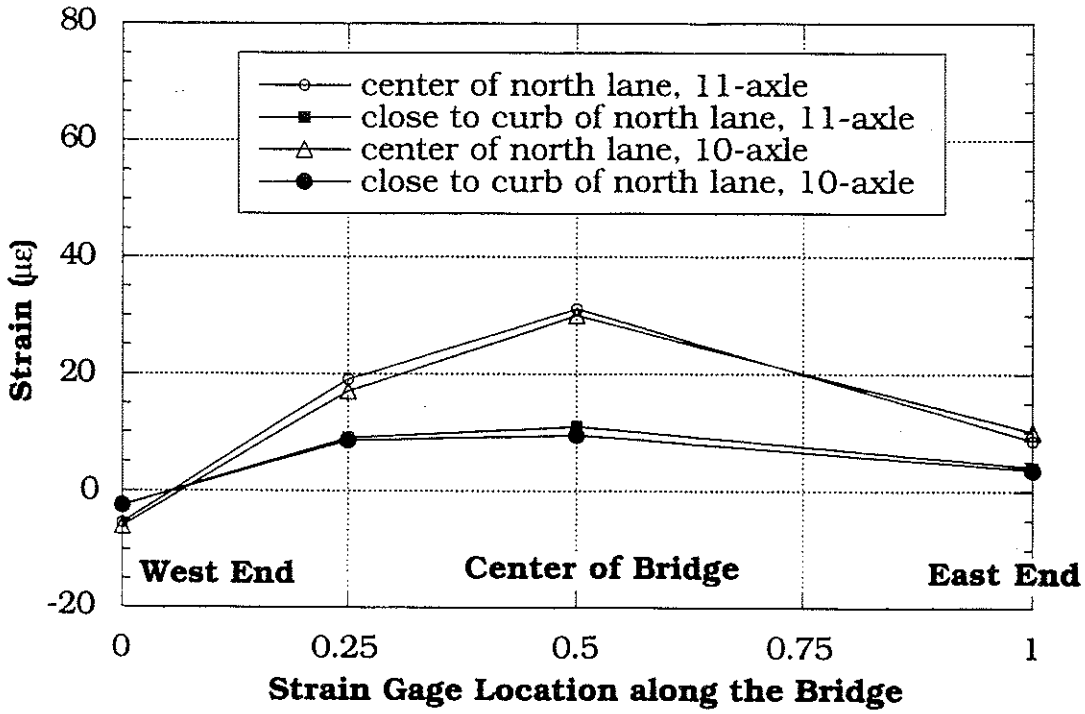

Figure 7.10 Strain Profile on Girder 6 along the Bridge, North Lane, Crawling Speed.

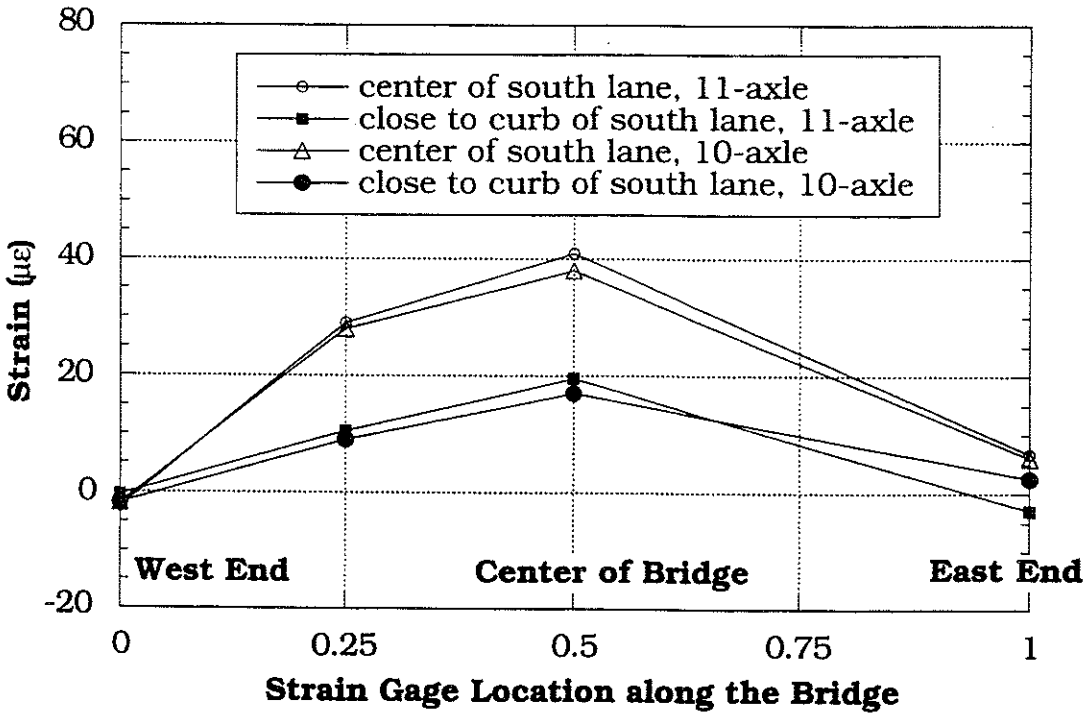

Figure 7.11 Strain Profile on Girder 6 along the Bridge, South Lane, Crawling Speed.

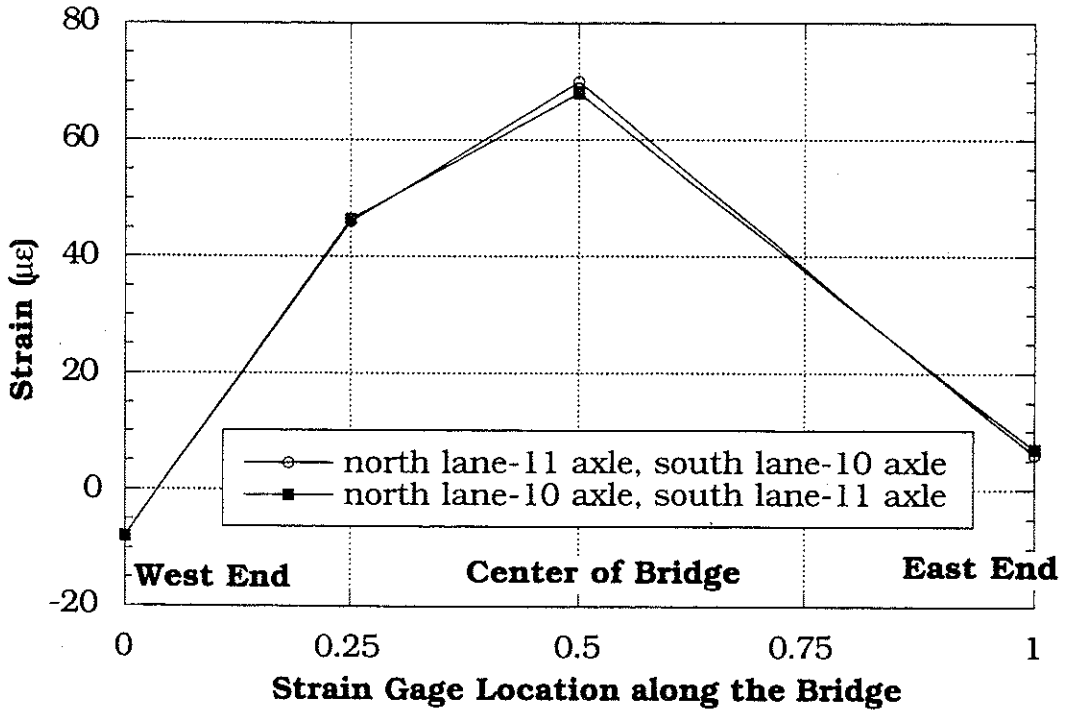

Figure 7.12 Strain Profile on Girder 6 along the Bridge, Side-by-Side, Crawling Speed.

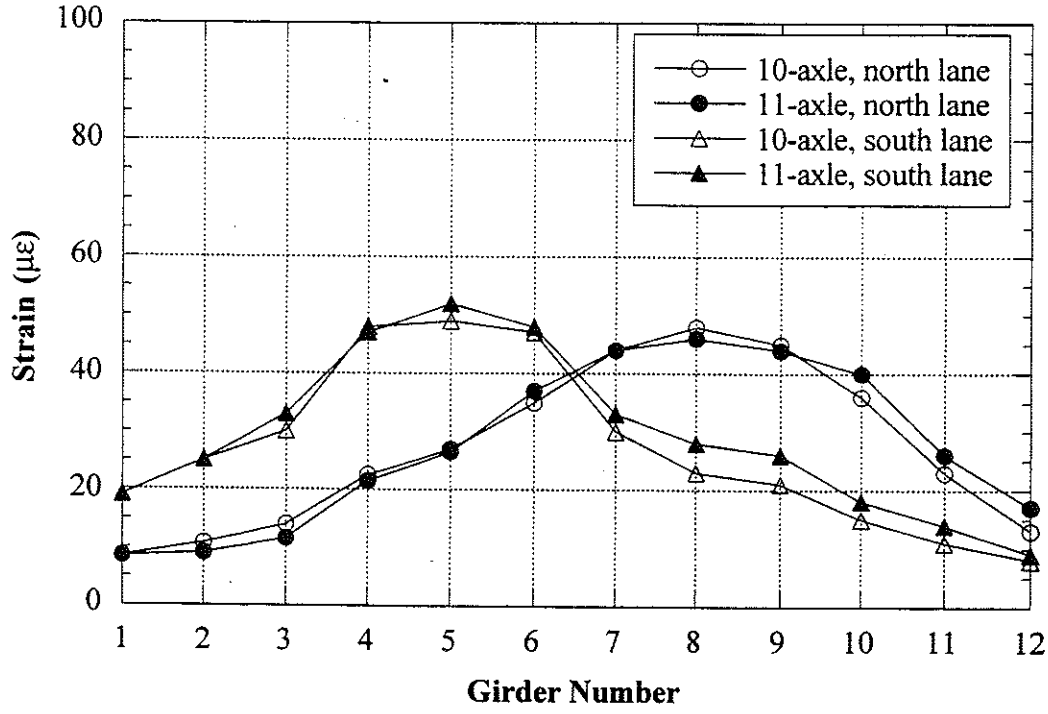

Figure 7.13 Strains under One Truck Loading at High Speed.

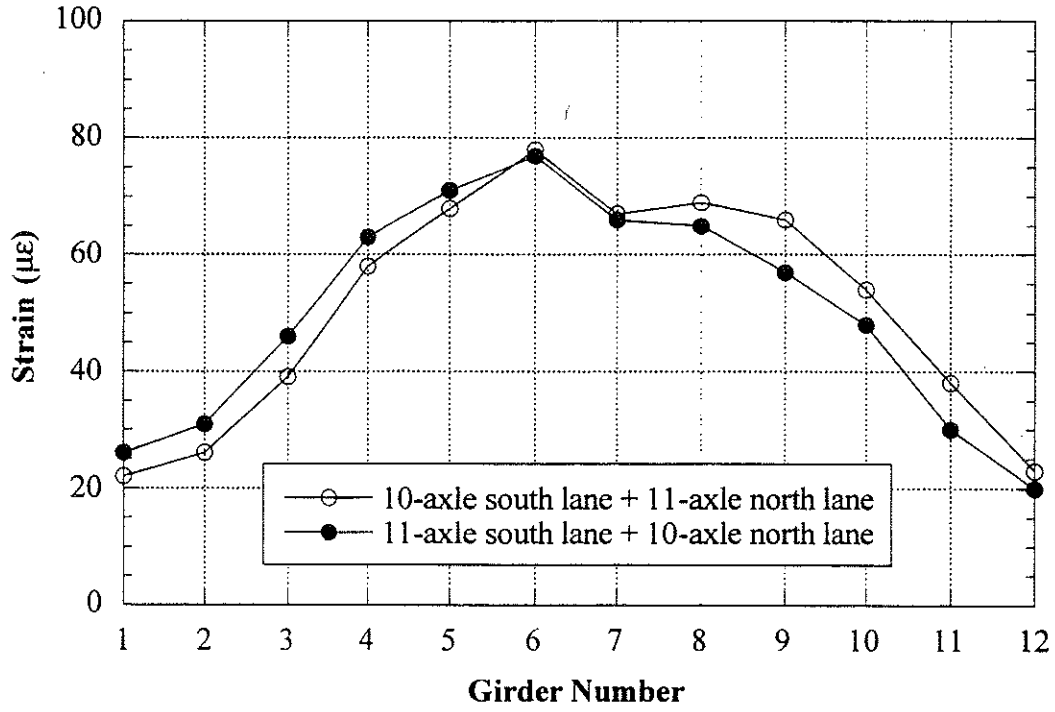

Figure 7.14 Strains under Side-by-Side Truck Loading at High Speed.

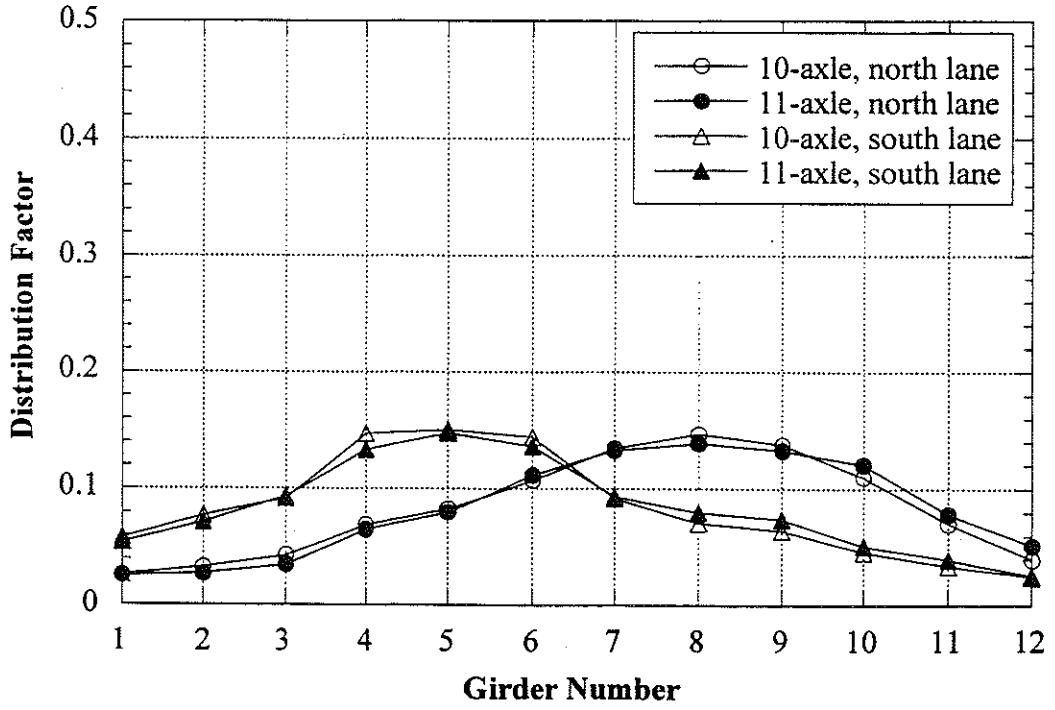

Figure 7.15 Distribution Factors under One Truck Loading at High Speed

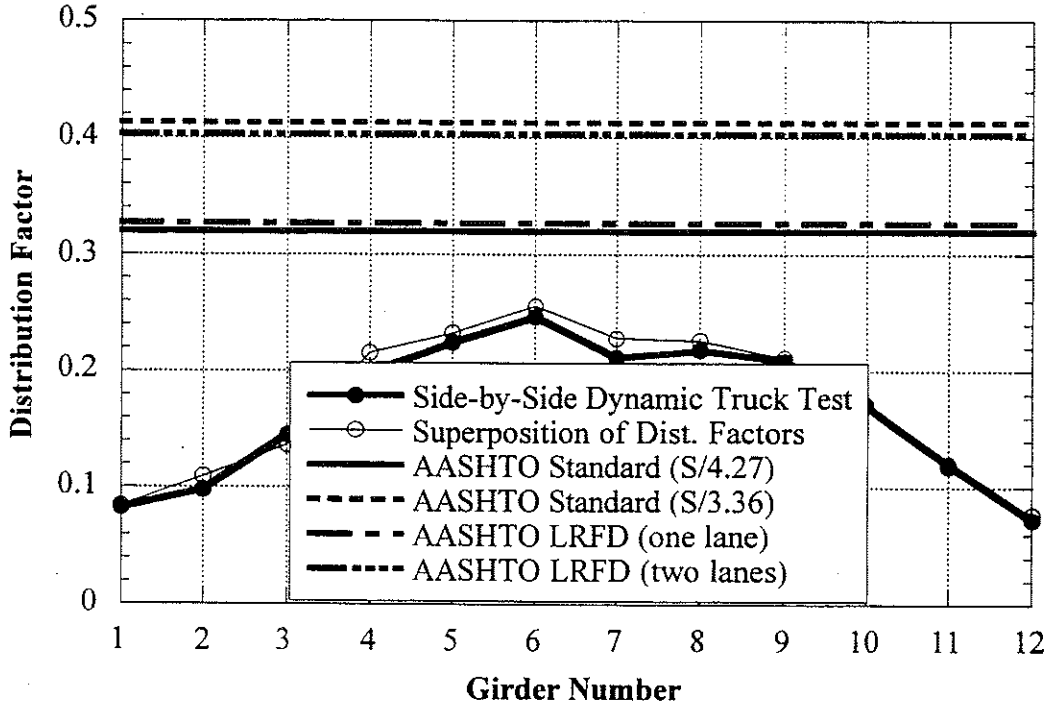

Figure 7.16 Comparison with Code Specified Distribution Factors at High Speed

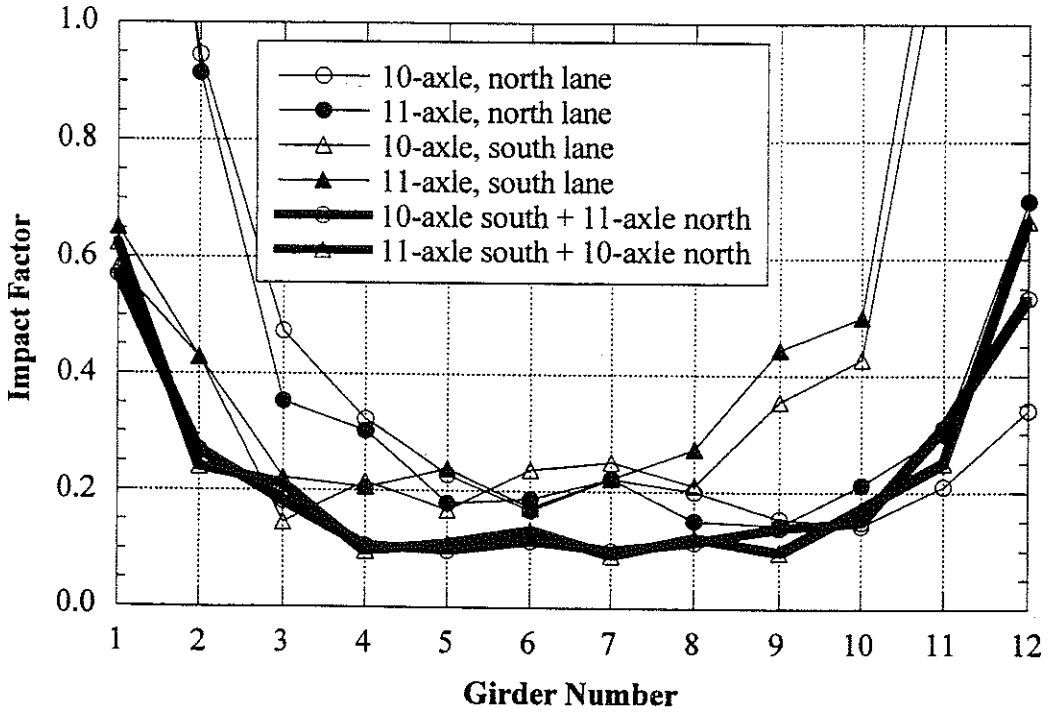

Figure 7.17 Impact Factors.

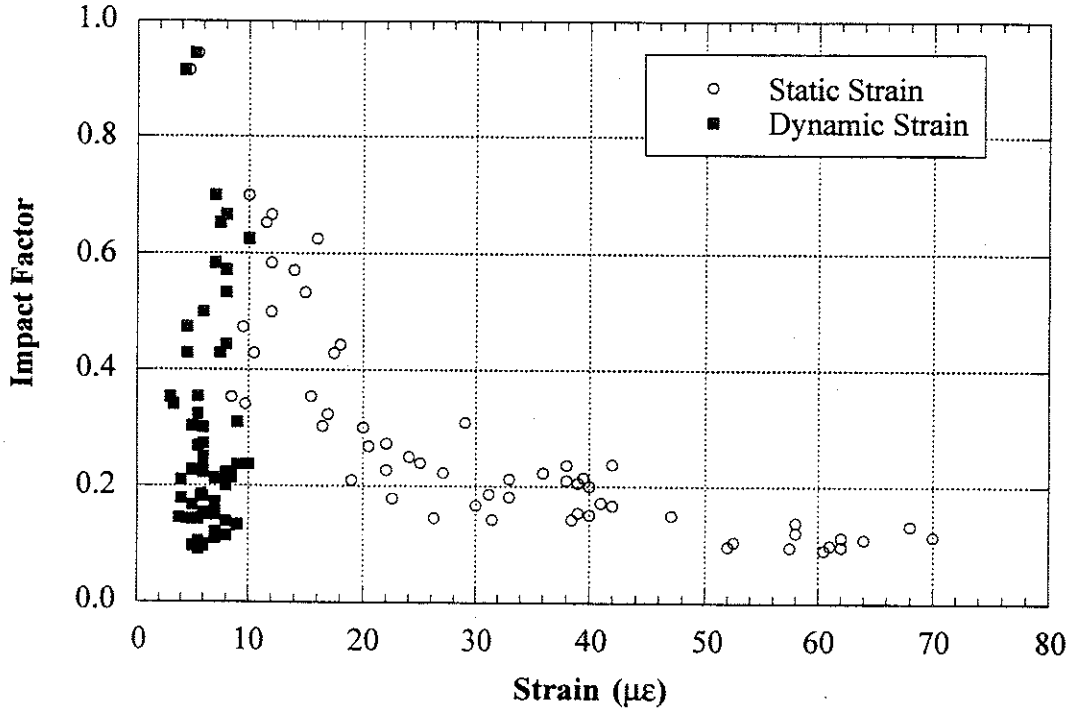

Figure 7.18 Strain versus Impact Factors.

7.5 Loads for Proof Load Test

Two M-60 tanks were used for the proof load test. The tanks were placed adjacent to each other in three different longitudinal and three different transverse positions, and rested directly on the pavement. Traffic was allowed over a partial width of the bridge during the test, and it was fully stopped only at critical times of maximum load placement.

Maximum lane moment on the 9.9m span due to the legal load is 638 kN-m. The target proof load lane moment was obtained from Section 3.3.1. The bridge is ratable and has no hidden details. Therefore, the target proof load was reduced by 5 percent. No other adjustment was applicable to the bridge. The required proof load level of 933 kN was determined as follows:

$X_p = 1.4$ basic target load factor

$\Sigma = -5\ \%$ because the bridge is ratable and has no hidden details

$X_{Pa} = 1.4(1+(\Sigma/100) = 1.33$ from Eq. (3-1)

Above X_{Pa} satisfies Eq. (3-3).

The target proof load (L_t) is

$$L_t = 1.33 \times 1.10\ L_r = 1.46\ L_r \quad \text{from Eq. (3-2)}$$

$L_r = 638$ kN from Michigan Bridge Analysis Guide

$L_t = 1.46 \times 638 = 933$ kN

Table 7.1 shows the maximum lane moments caused by the trucks and tanks. The applied proof load lane moment was 964 kN-m.

Table 7.1 Moment due to Trucks and Tanks.

Load Type	Maximum Lane Moment
Ten-axle test truck	469 kN-m
Eleven-axle test truck	514 kN-m
Tank at 0.61 m from middle of span	943 kN-m
Tank in the middle of span	964 kN-m

The testing sequence was as follows: First, one tank per lane was applied to the bridge with two different lateral positions: center of lane and close to the curb. Then, side-by-side tanks were placed in the middle of the bridge width to obtain the maximum proof load level. When placed side-by-side, the tanks are nearly in contact with each other. The following proof load cases were applied for Bridge US12/SC:

- one tank close to the curb of north lane in the middle of span
- one tank close to the curb of north lane 0.61 m east from the middle of span
- one tank close to the curb of north lane 0.61 m west from the middle of span
- one tank at the center of north lane in the middle of span
- one tank at the center of north lane 0.61 m east from the middle of span
- one tank at the center of north lane 0.61 m west from the middle of span
- one tank close to the curb of south lane in the middle of span
- one tank close to the curb of south lane 0.61 m east from the middle of span

- one tank close to the curb of south lane 0.61 m west from the middle of span
- one tank at the center of south lane in the middle of span
- one tank at the center of south lane 0.61 m east from the middle of span
- one tank at the center of south lane 0.61 m west from the middle of span
- two side-by-side tanks at the center of bridge width, both tanks 0.61 m east from the middle of span
- two side-by-side tanks at the center of bridge width, one tank 0.61 m east from the middle of span, the other tank in the middle of span
- two side-by-side tanks at the center of bridge width, both tanks in the middle of span
- two side-by-side tanks at the center of bridge width, one tank 0.61 m west from the middle of span, the other tank in the middle of span
- two side-by-side tanks at the center of bridge width, both tanks 0.61 m west from the middle of span

Detailed proof load positions are shown in Figures 7.19 to 7.23.

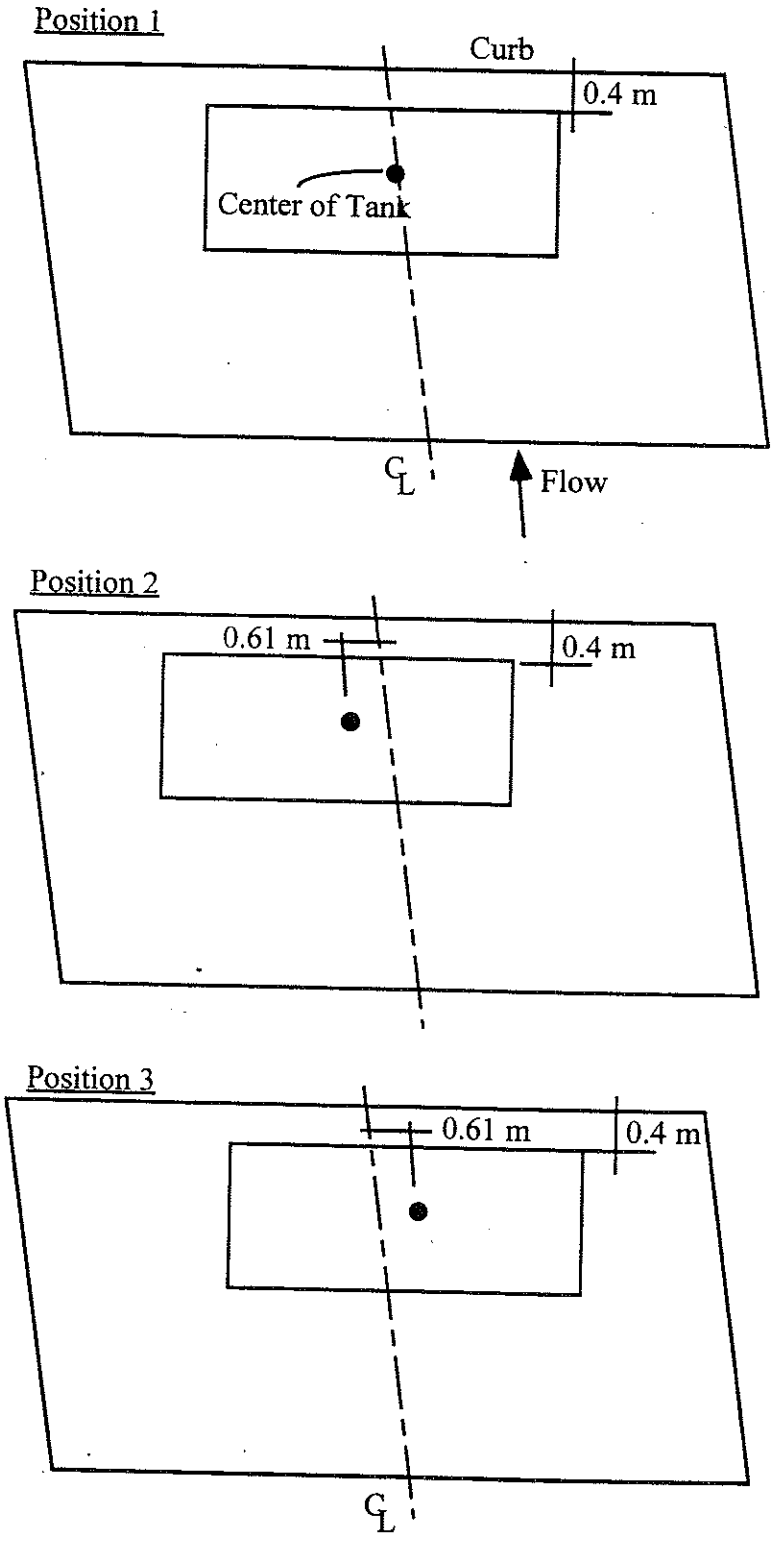

Figure 7.19 Proof Load, North Lane Loading, Close to Curb.

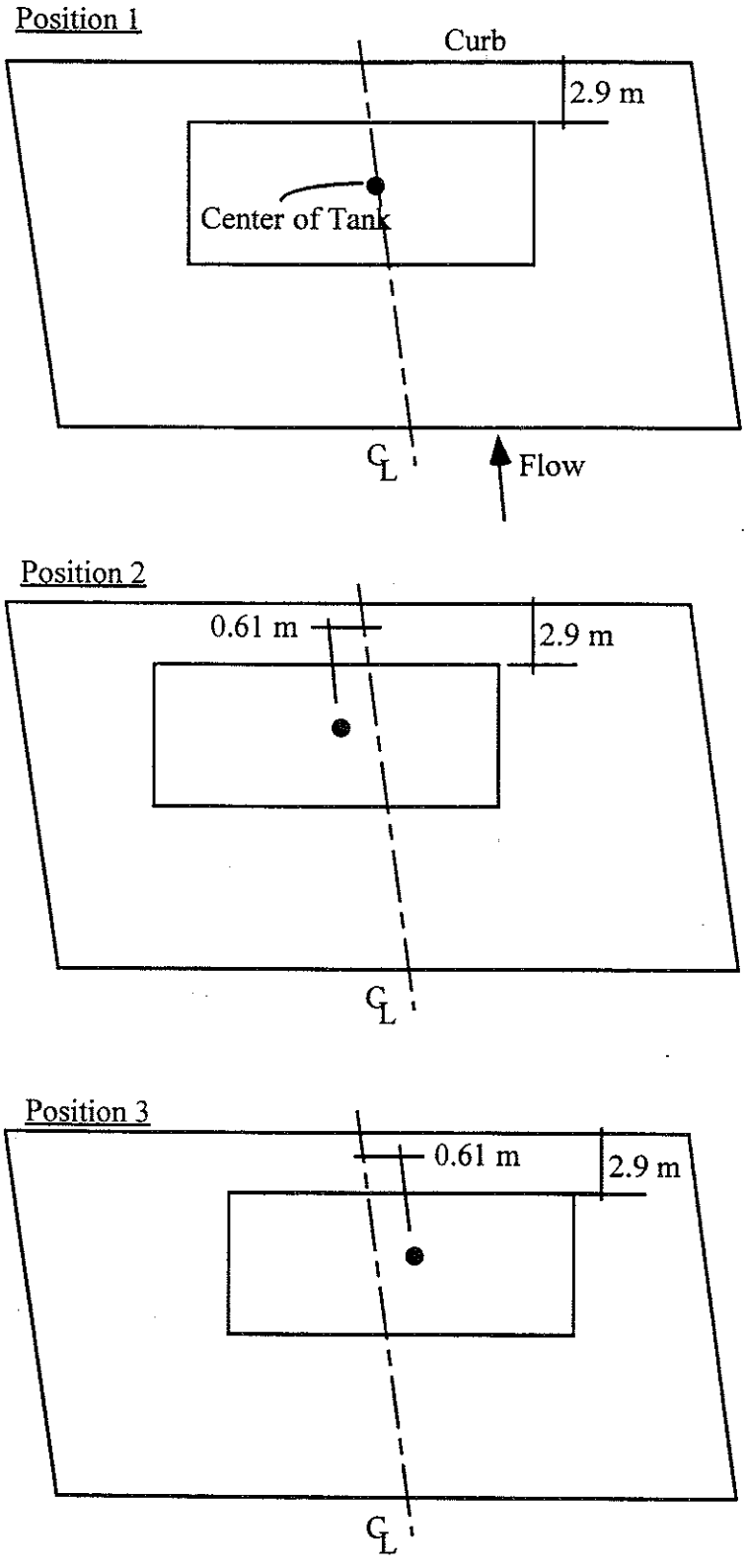

Figure 7.20 Proof Load, North Lane Loading, Center of Lane.

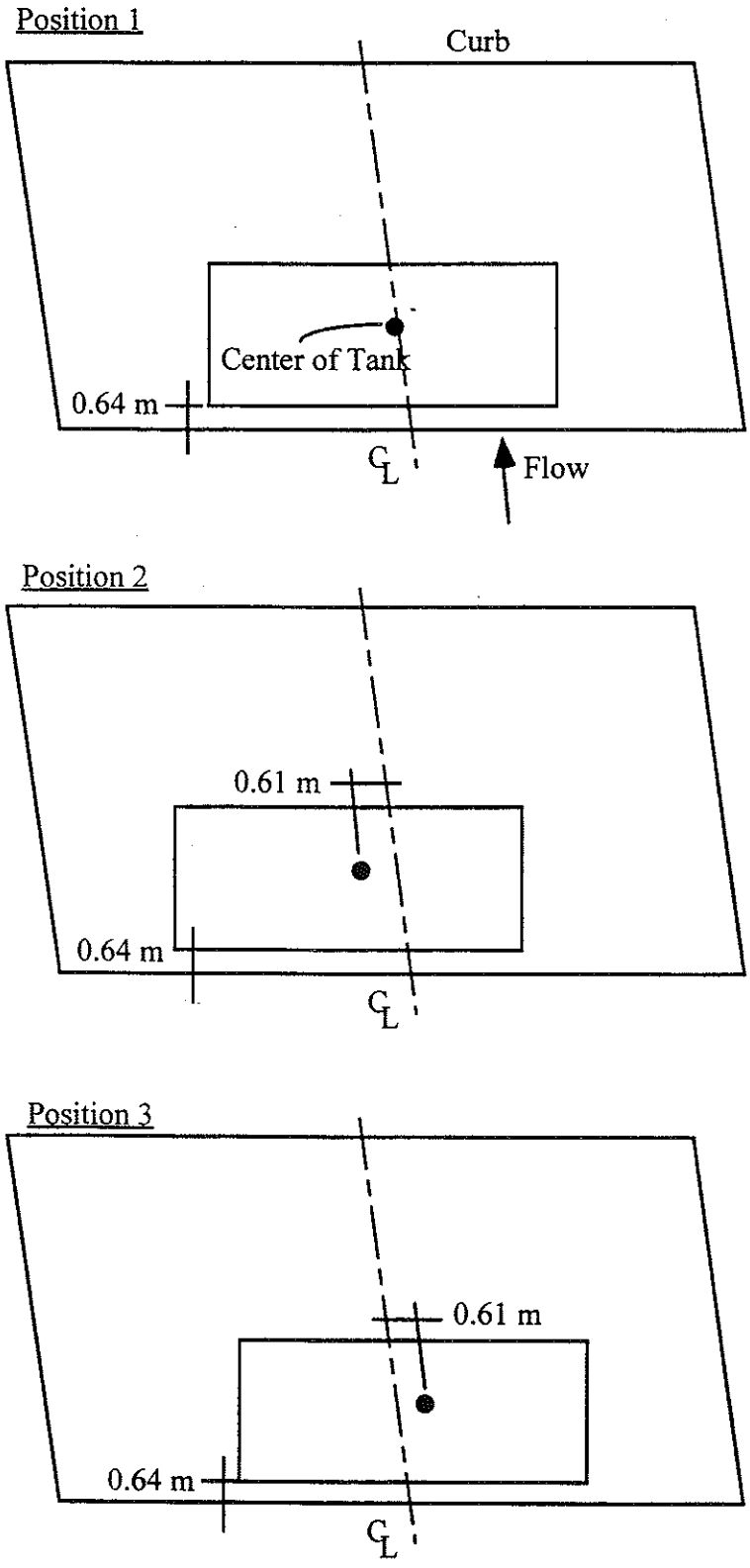

Figure 7.21 Proof Load, South Lane Loading, Close to Curb.

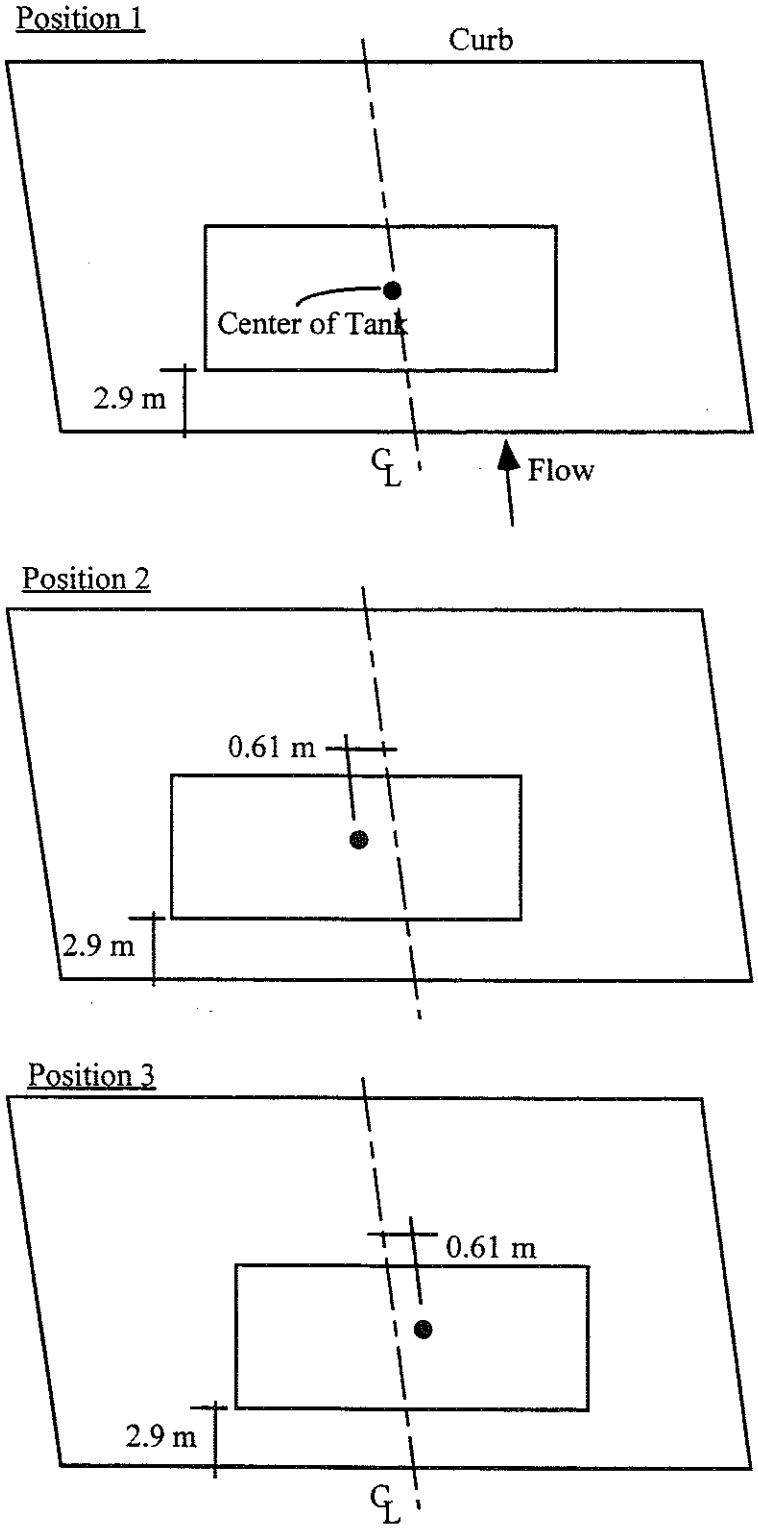

Figure 7.22 Proof Load, South Lane Loading, Center of Lane.

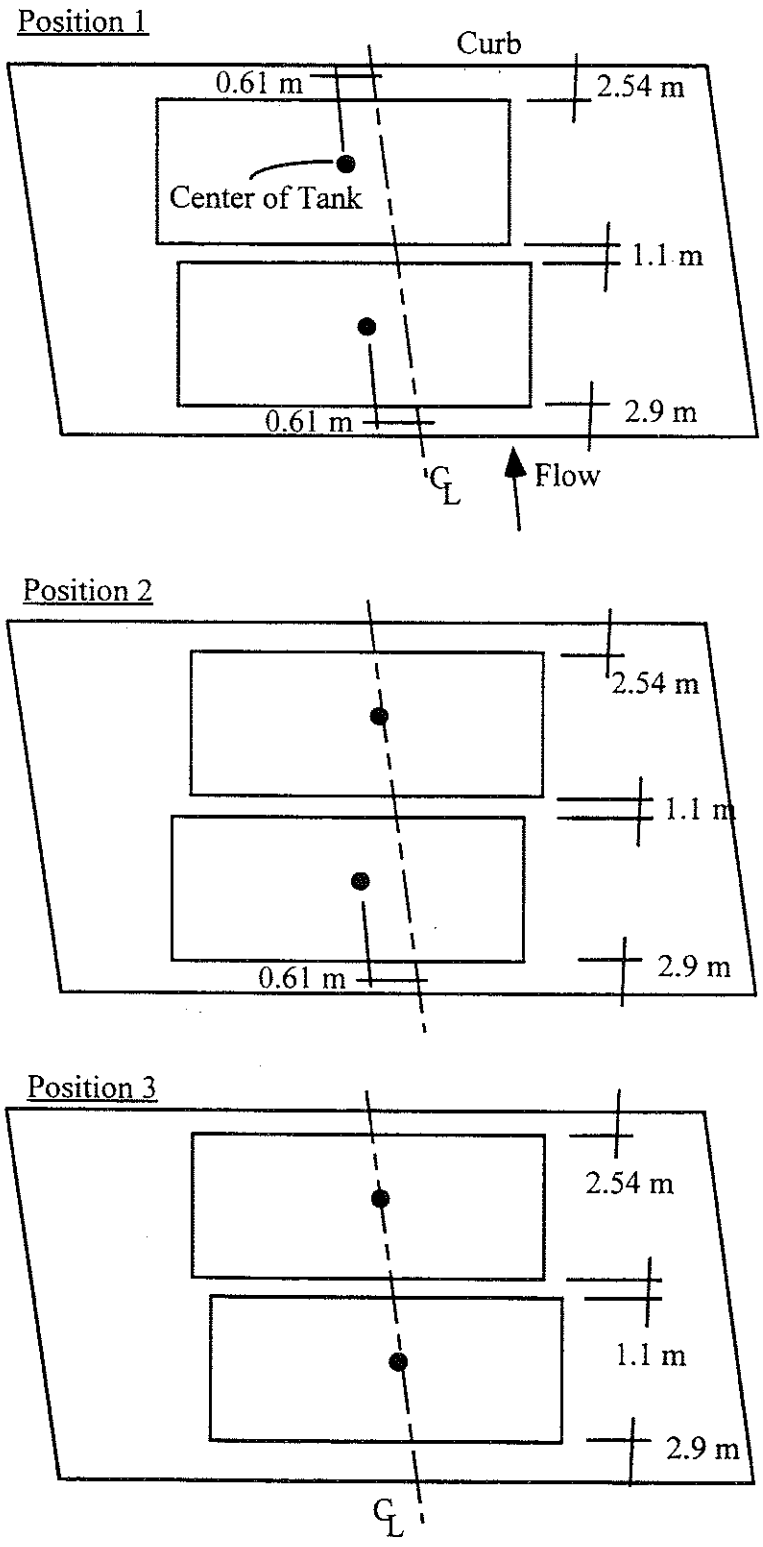

Figure 7.23 Proof Load, Side-by-Side Loading, Center of Bridge Width.

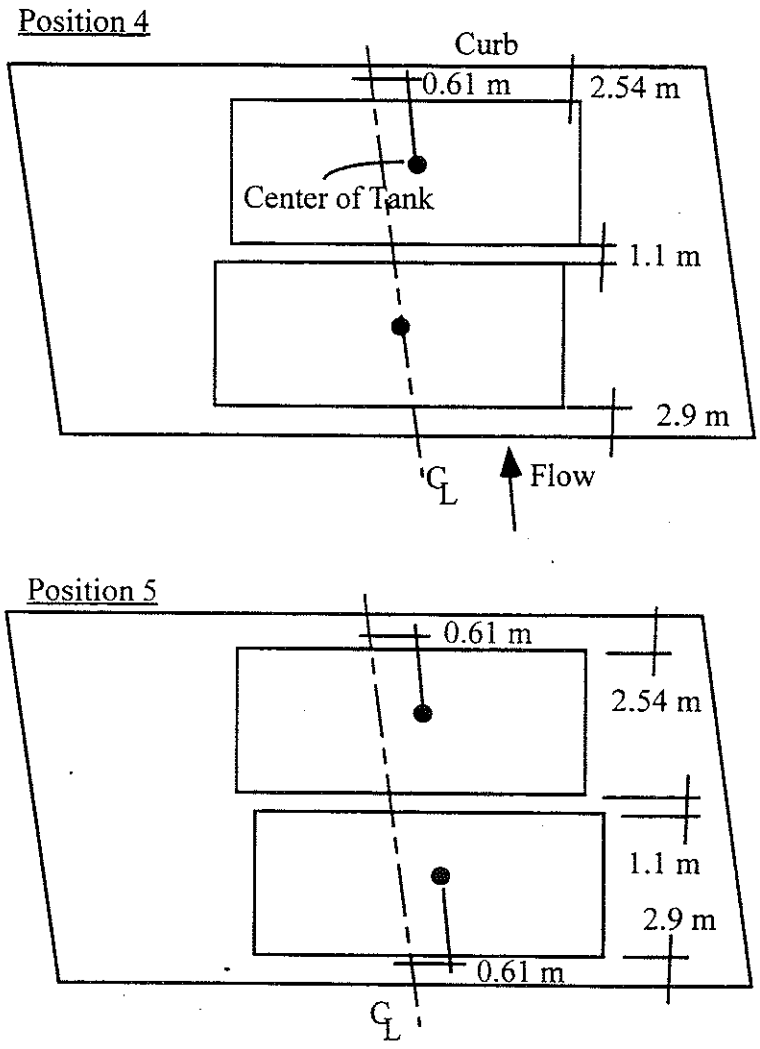

Figure 7.23 Proof Load, Side-by-Side Loading, Center of Road, Continued.

7.6 Results for Proof Load Test

The proof load test was successfully completed without any sign of distress to the structure. The maximum deflection due to the applied load was only 2.4 mm. The maximum strain was about 130 micro-strain, which is approximately a stress of 26 MPa. The load versus response curve indicated that the structure behaved linearly.

Figure 7.24 shows strains and girder distribution factors for a tank in the north lane. The load positions for Figure 7.24 are shown in Figures 7.19 and 7.20. Figure 7.25 shows strains and GDF's for a tank in the south lane. The load positions for Figure 7.25 are shown in Figures 7.21 and 7.22. The results from one tank (Figure 7.24 and 7.25) indicate a slightly more uniform load distribution than that of one truck (Figures 7.5 and 7.6). The better distribution may be caused by the tank's larger width. Figure 7.26 shows strains and GDF's for side-by-side tanks. The load positions for Figure 7.26 are shown in Figure 7.23. The load distribution factors for side-by-side tanks (Figure 7.26) are slightly larger than those for side-by-side trucks (Figure 7.7). This was probably caused by the closer adjacent positioning of the tanks compared with that of the trucks. Figure 7.27 shows the envelope of GDF's for one tank loading. It is very similar to that for a single truck (Figure 7.8). Figure 7.28 shows load distribution comparison with AASHTO Code specified values. Actual value of the term $K_g/(Lt_s^3)$ is used in calculation of Code specified GDF values.

Figures 7.29 to 7.31 show strain profiles on girder 6 along the bridge length. Because some strain gages were not working, not all expected data values could be plotted on the figures. The strain reading at the west supports shows small negative values. However, the readings at the east end show less fixity than at the west end.

Figure 7.32 shows deflections for a tank in the north lane. The load positions are shown in Figures 7.19 and 7.20. A total of 10 LVDTs were installed, one each on girders 2 to 11. LVDTs on girders 5 and 6

were not working and thus these data values are missing. Figure 7.33 shows deflections for a tank in the south lane. The load positions are shown in Figures 7.21 and 7.22. Figure 7.34 shows deflections for side-by-side tanks on the bridge. The load positions are shown in Figure 7.23.

Figures 7.35 to 7.46 plot applied moment per girder versus measured strain, for girders 1 to 12. The applied moment per girder was obtained by multiplying, for each load case, the total applied moment due to the load by the GDF measured for that load case. Included in the figures are not only the measured strains from tanks but also those from trucks. All girders showed reasonably linear behavior.

Figures 7.47 to 7.54 present the applied moment per girder versus measured deflection, for girders 2, 3, 4, 7, 8, 9, 10, and 11, respectively. Again, all girders showed reasonably linear behavior.

The measured static strains were compared to static strains calculated using the design stiffness and GDF's determined by tests in this study. The maximum observed static strain for this bridge is 72 με for a single tank and 137 με for two tanks side-by-side. The corresponding calculated strain for a single tank in a composite section is 156 με and for a non-composite section it is 302 με. For two tanks side-by-side loading, the calculated strains are 260 με and 504 με for a composite section and a non-composite section, respectively.

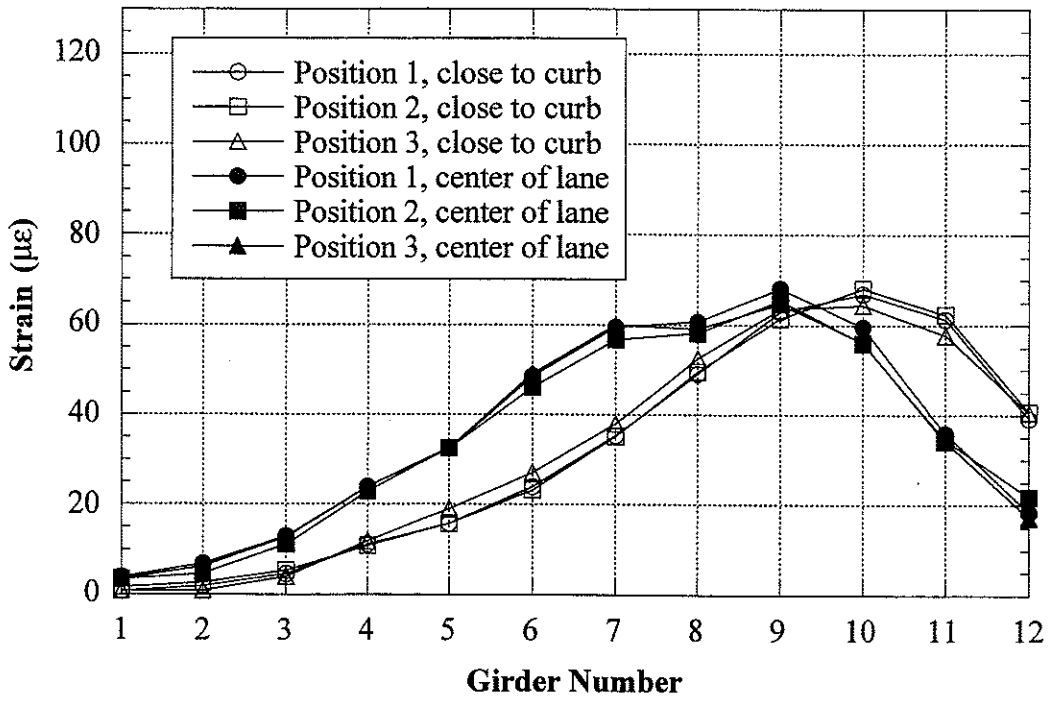

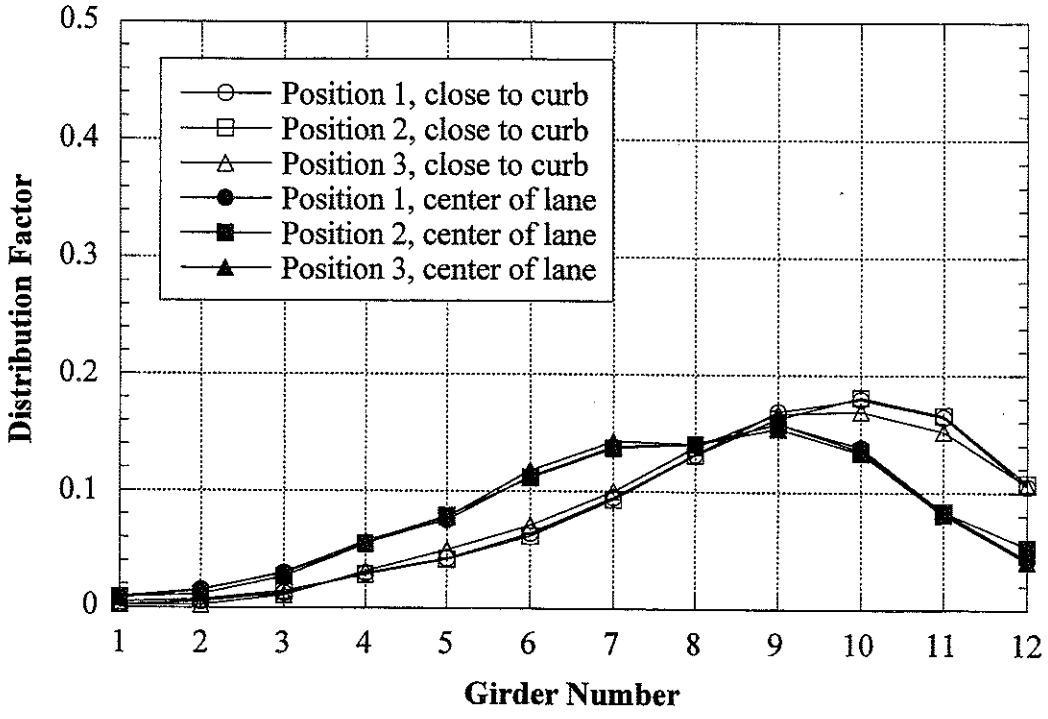

Figure 7.24 Proof Load, North Lane Loading.

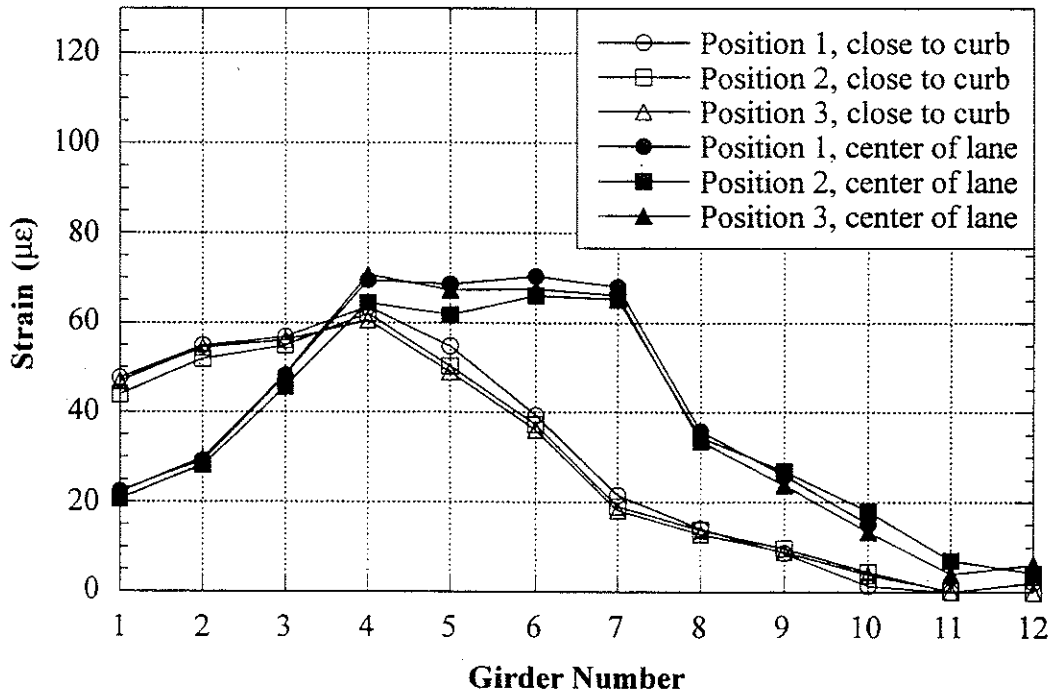

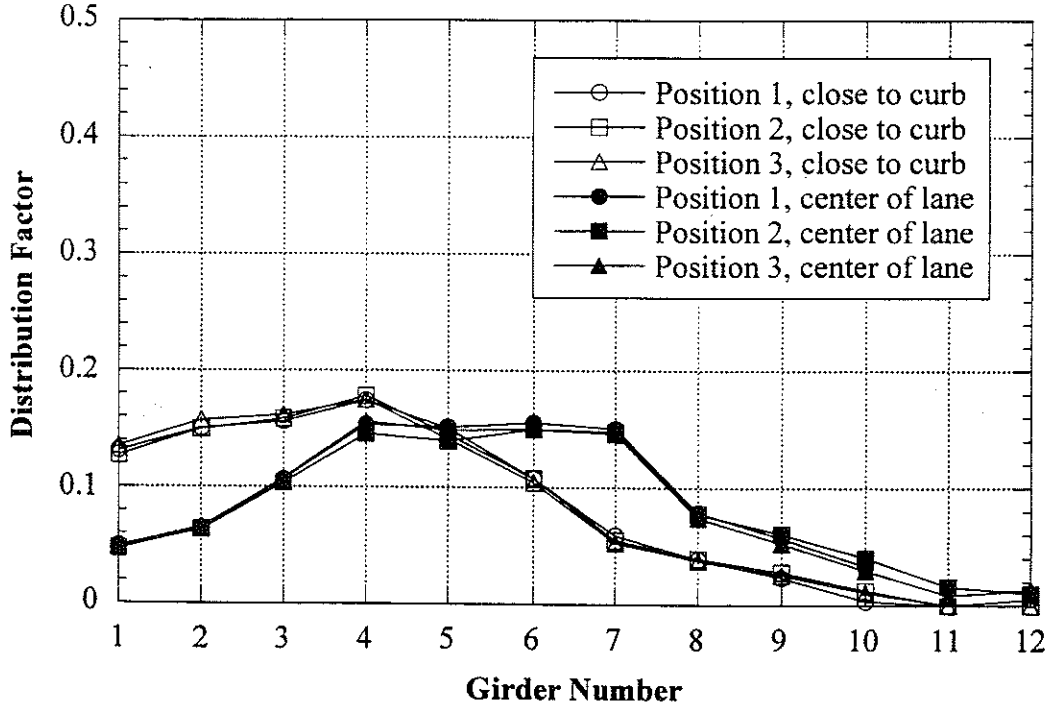

Figure 7.25 Proof Load, South Lane Loading.

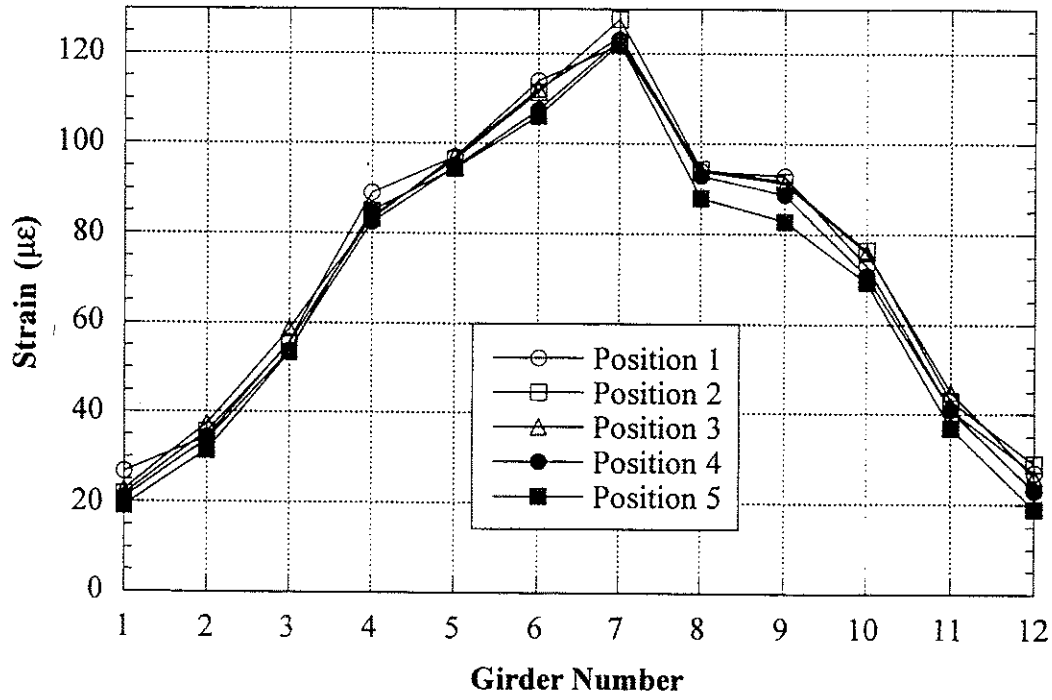

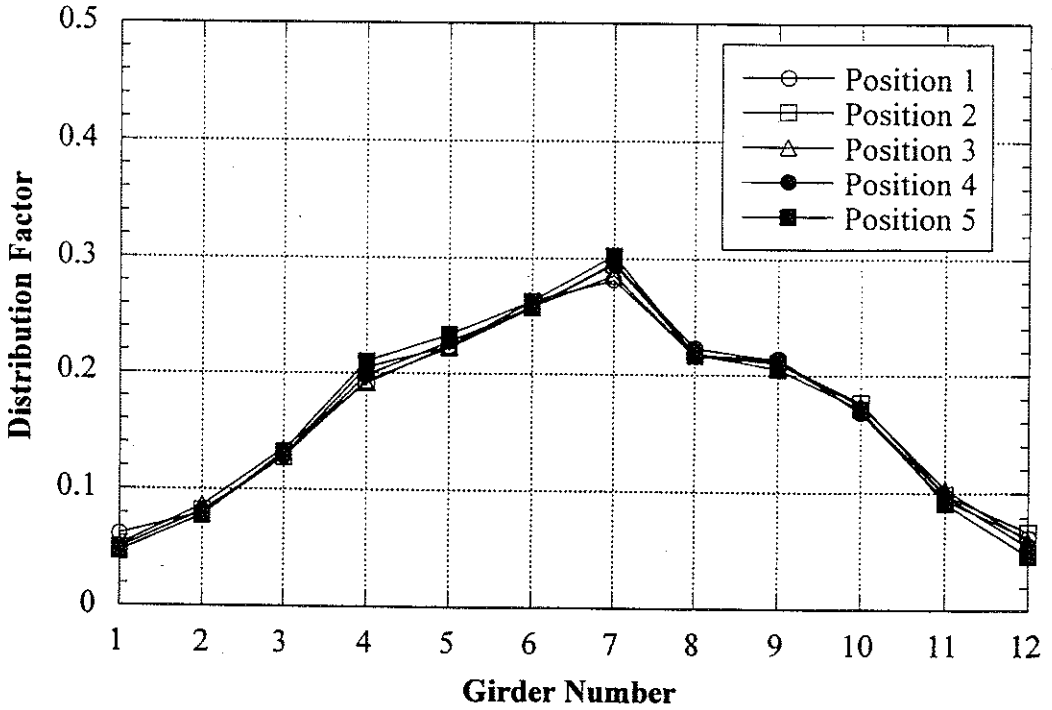

Figure 7.26 Proof Load, Side-by-Side Loading.

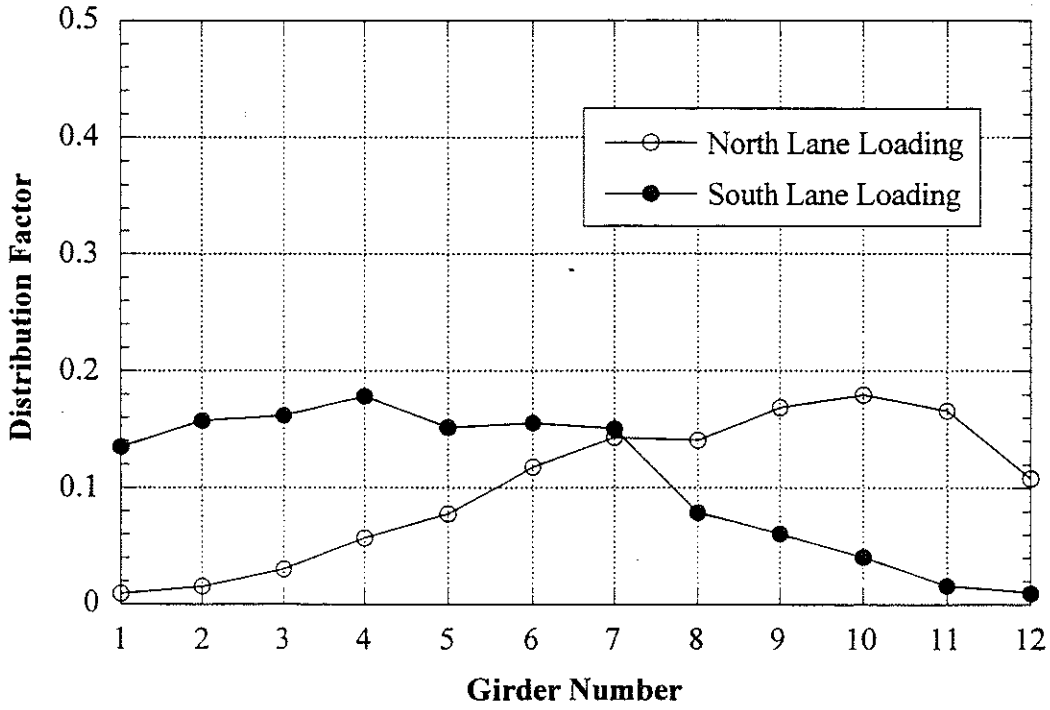

Figure 7.27 Envelope of Girder Distribution Factors For One Tank Loading.

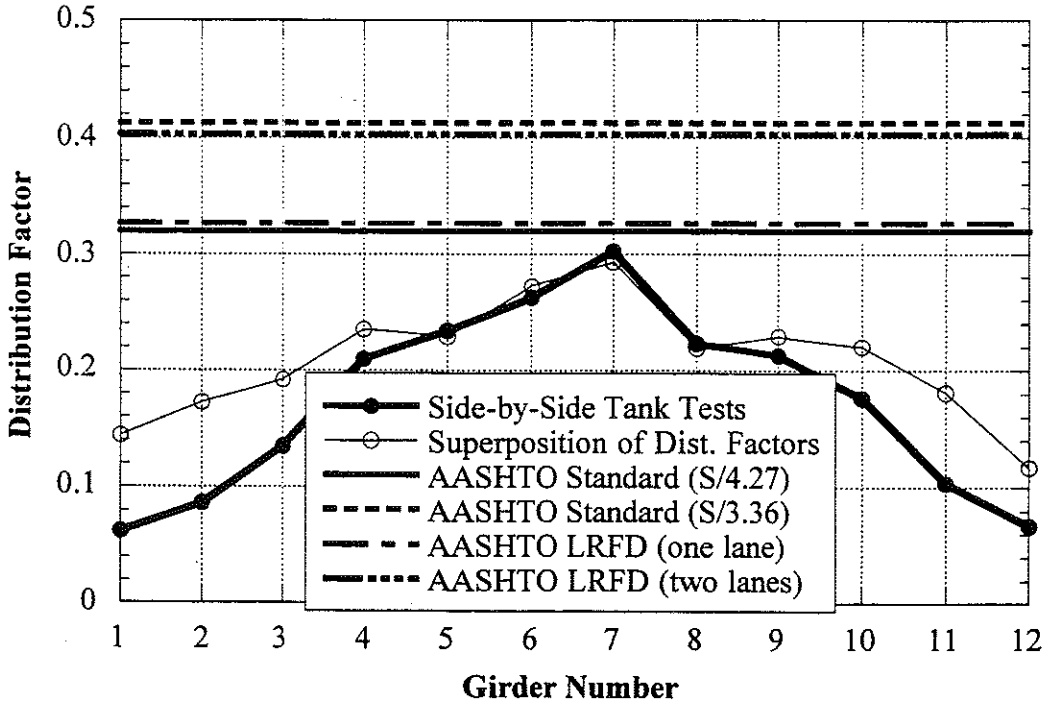

Figure 7.28 Proof Load Test, Comparison with Code Specified Distribution Factor.

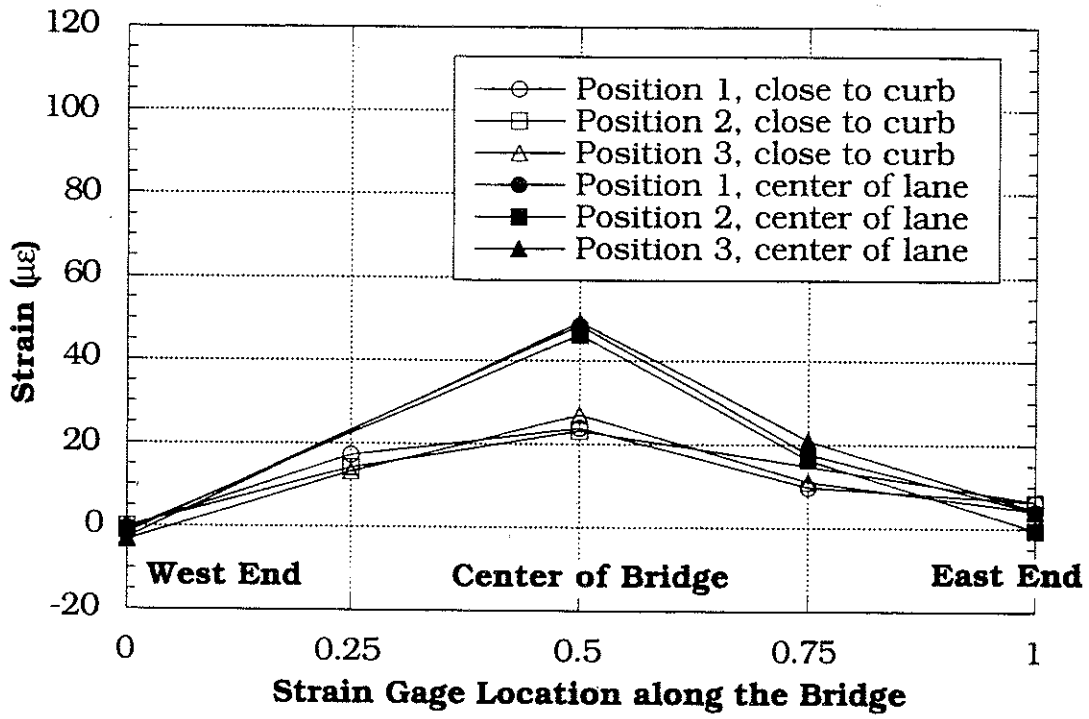

Figure 7.29 Proof Load Test, Strain Profile on Girder 6 along the Bridge, North Lane Loading.

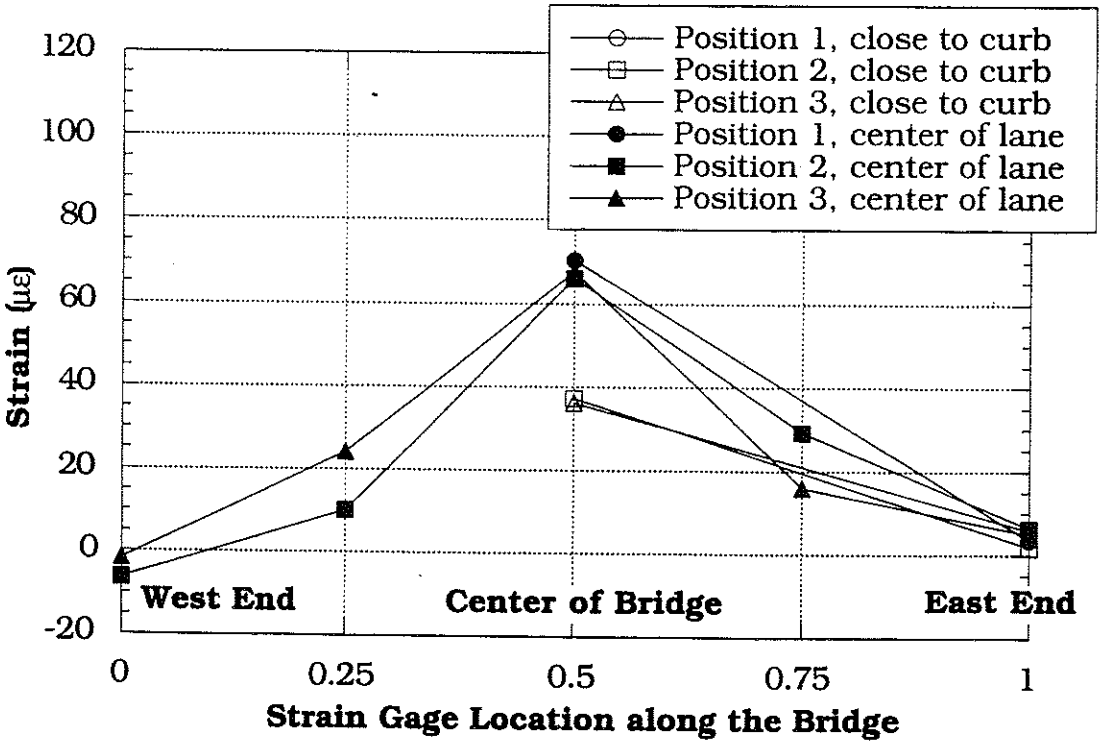

Figure 7.30 Proof Load Test, Strain Profile on Girder 6 along the Bridge, South Lane Loading.

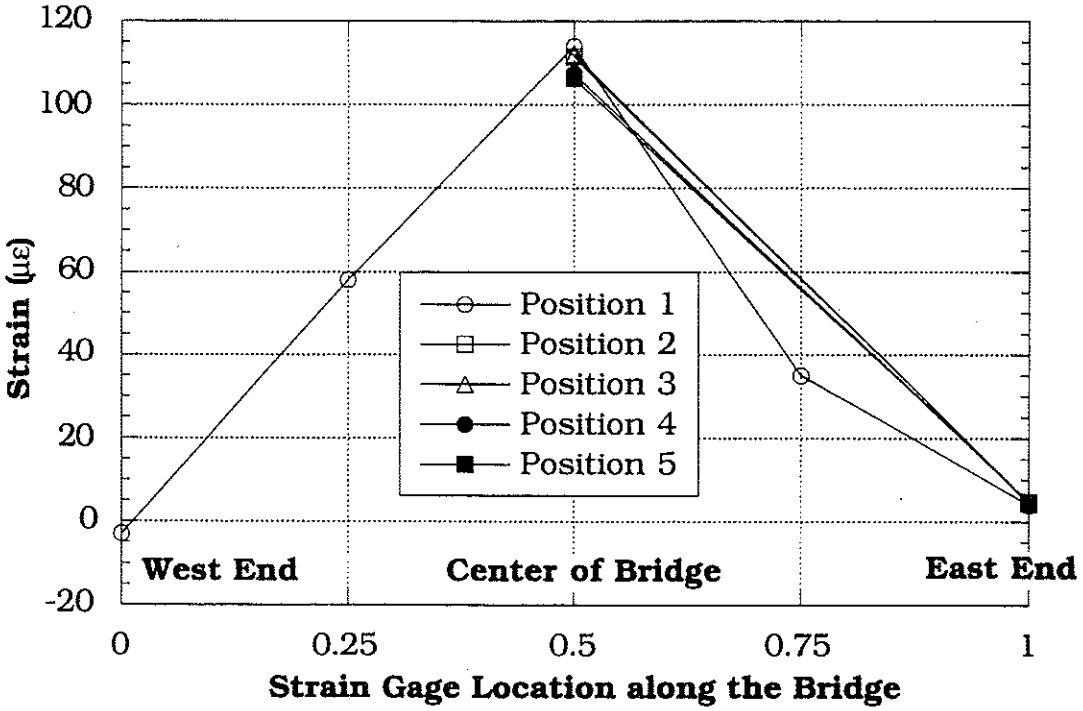

Figure 7.31 Strain Profile on Girder 6 along the Bridge, Side-by-Side Proof Load Test.

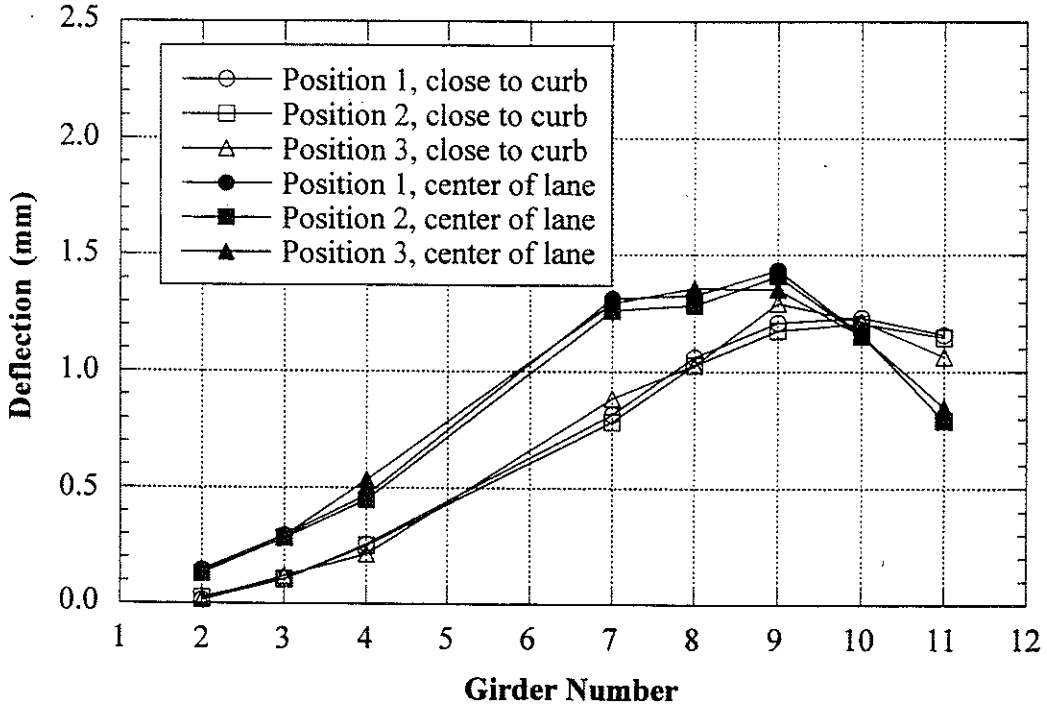

Figure 7.32 Deflections due to Proof Load, North Lane Loading.

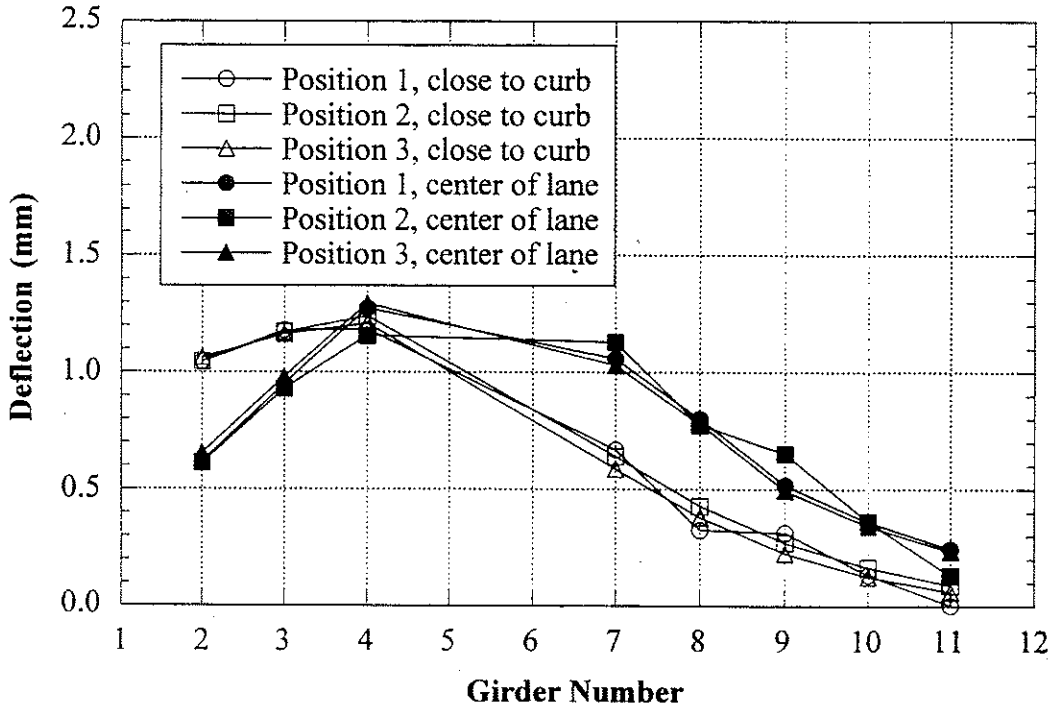

Figure 7.33 Deflections due to Proof Load, South Lane Loading.

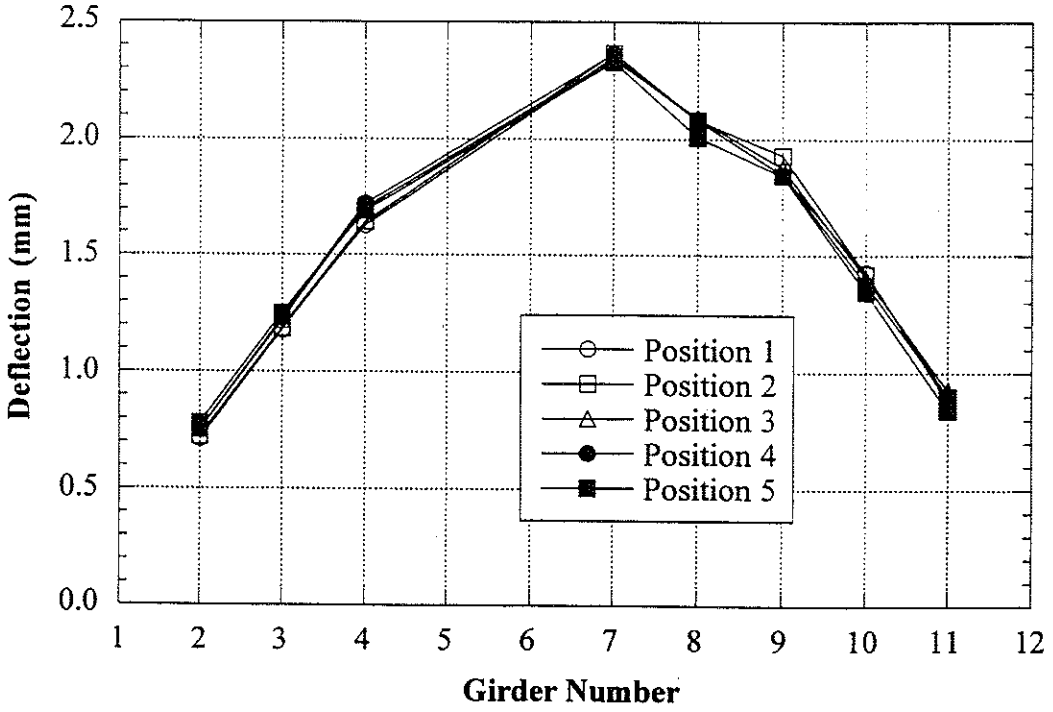

Figure 7.34 Deflections due to Proof Load, Side-by-Side Loading.

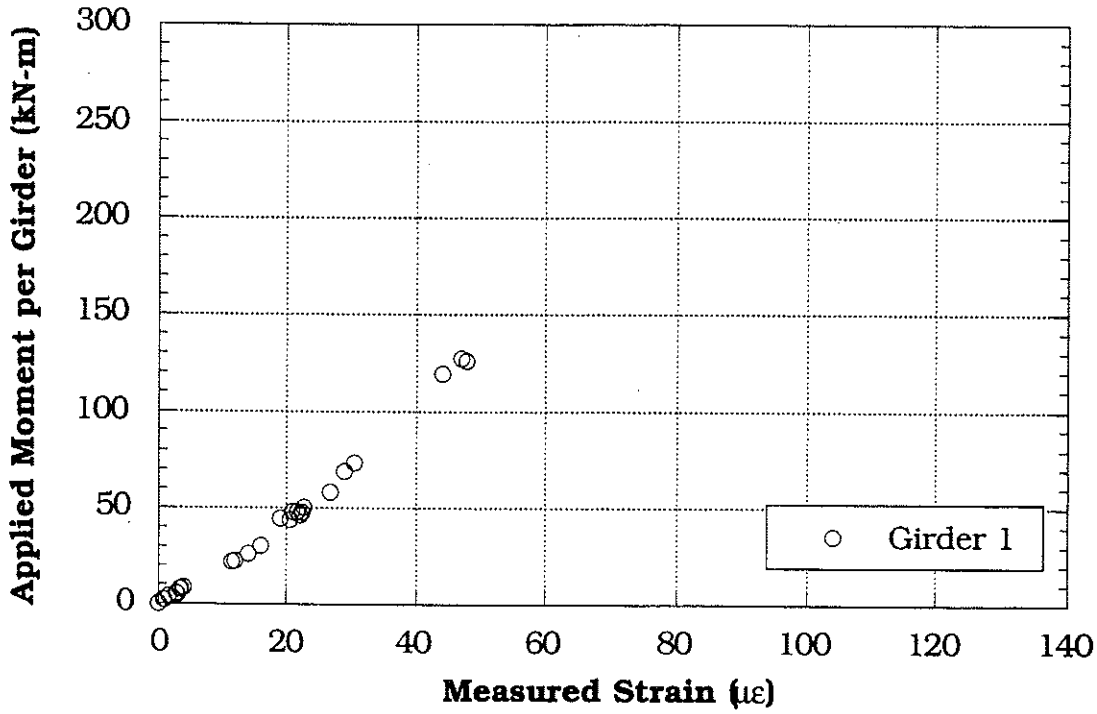

Figure 7.35 Moment per Girder vs Measured Strain, Girder 1.

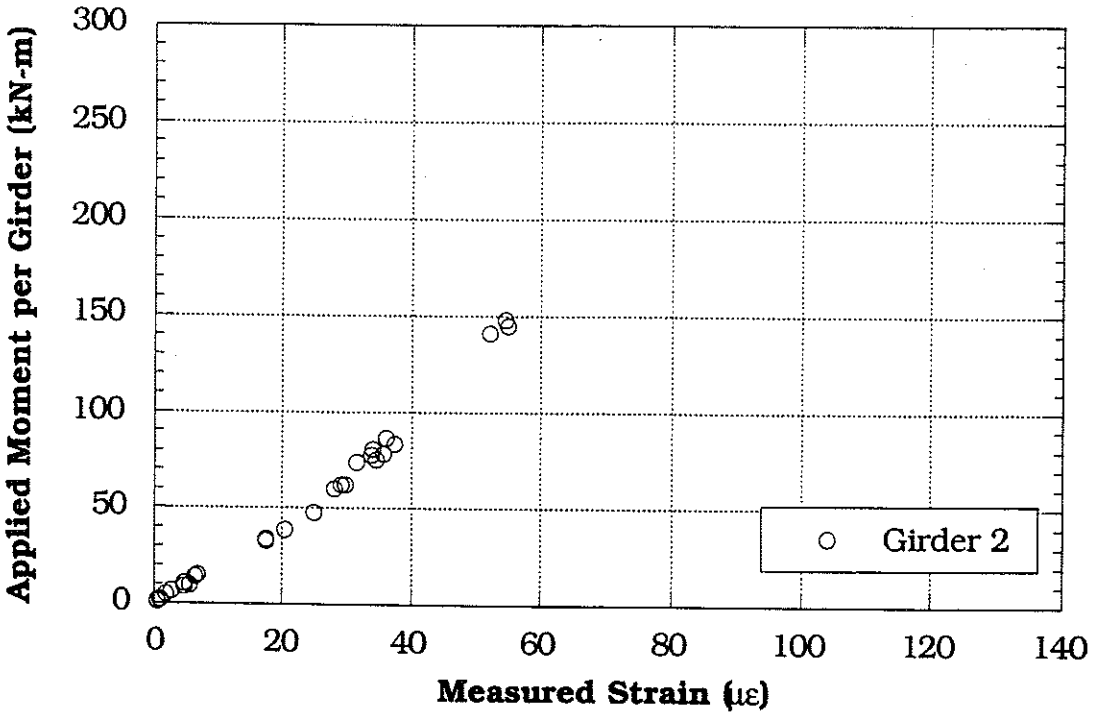

Figure 7.36 Moment per Girder vs Measured Strain, Girder 2.

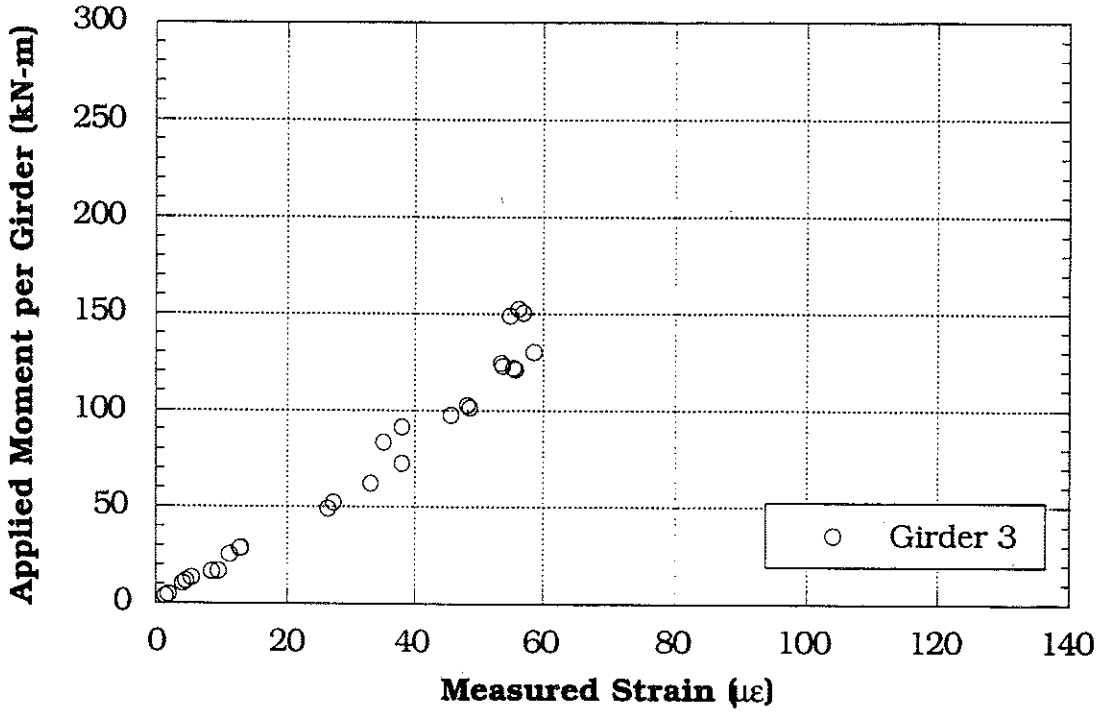

Figure 7.37 Moment per Girder vs Measured Strain, Girder 3.

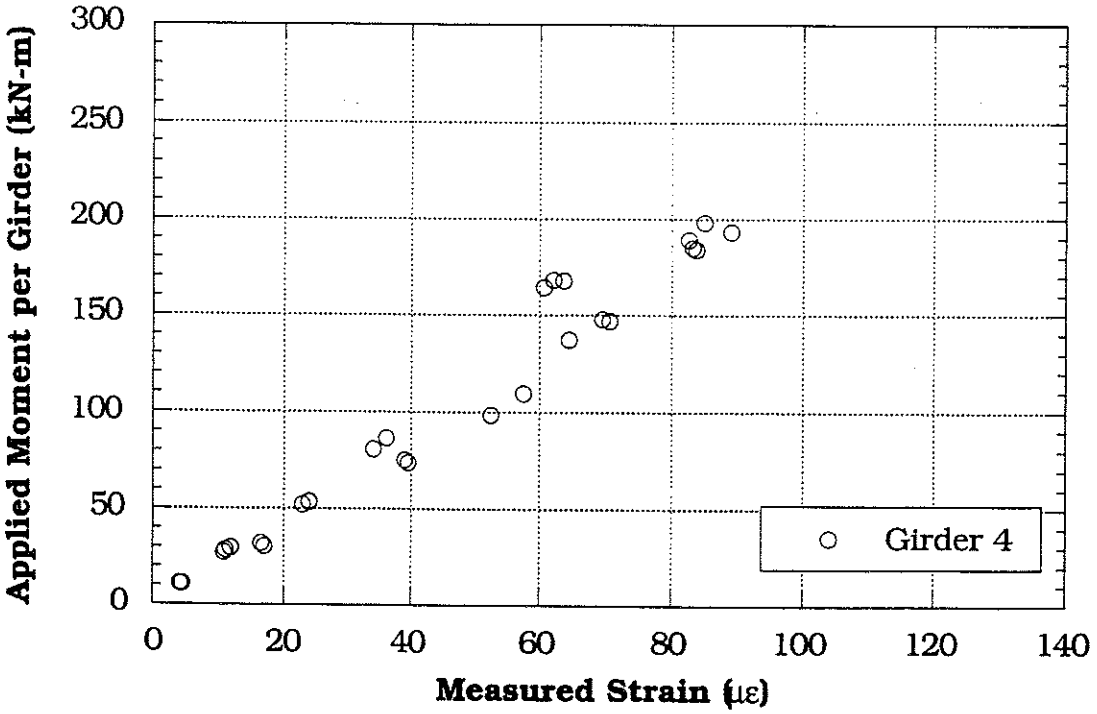

Figure 7.38 Moment per Girder vs Measured Strain, Girder 4.

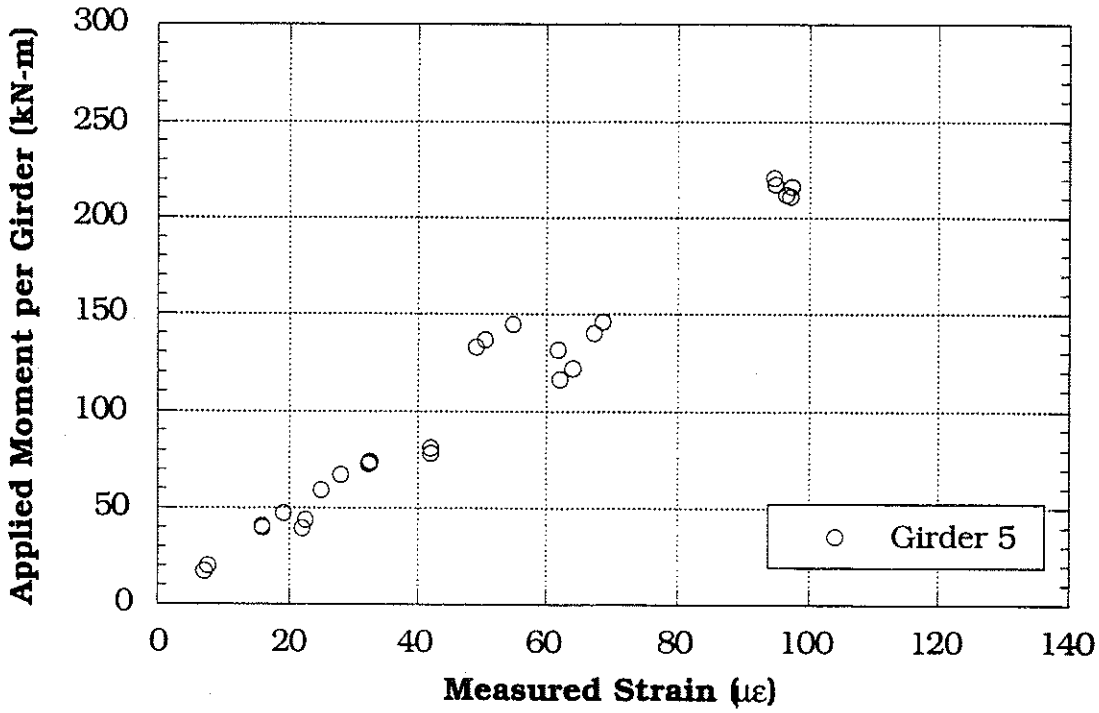

Figure 7.39 Moment per Girder vs Measured Strain, Girder 5.

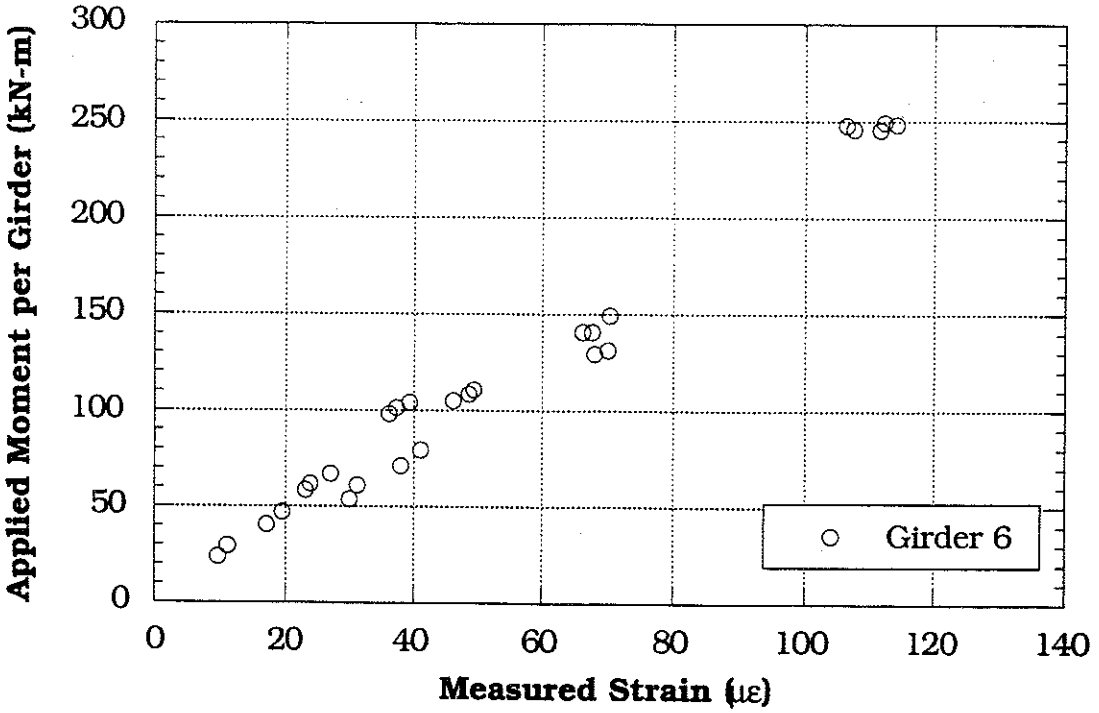

Figure 7.40 Moment per Girder vs Measured Strain, Girder 6.

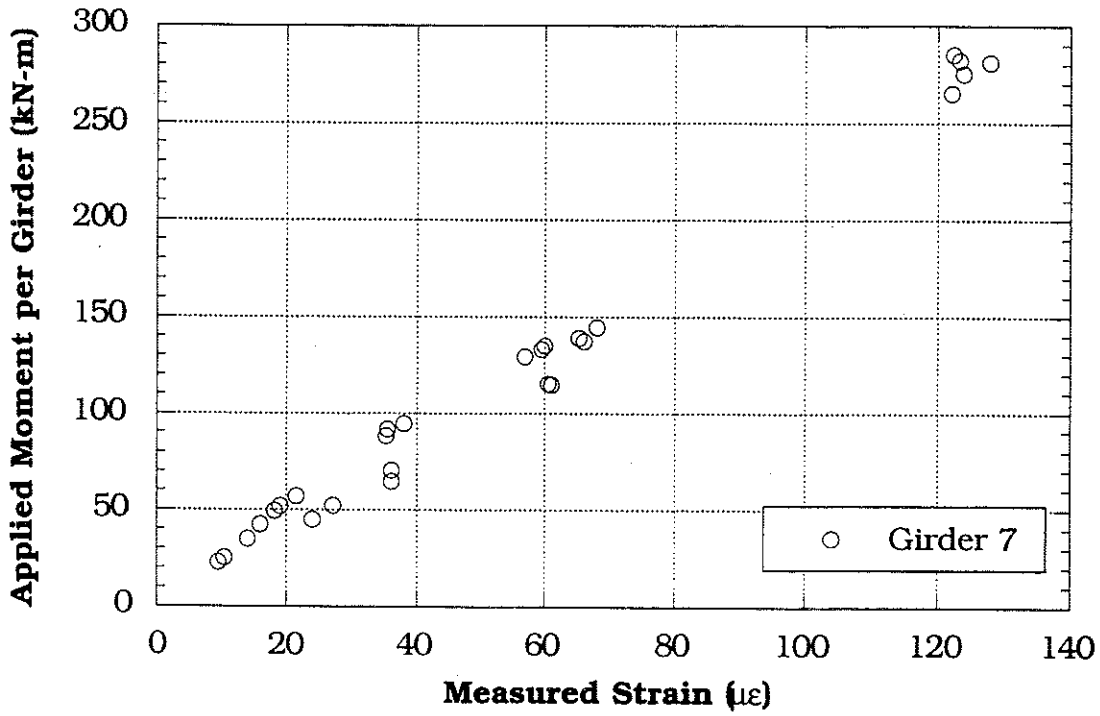

Figure 7.41 Moment per Girder vs Measured Strain, Girder 7.

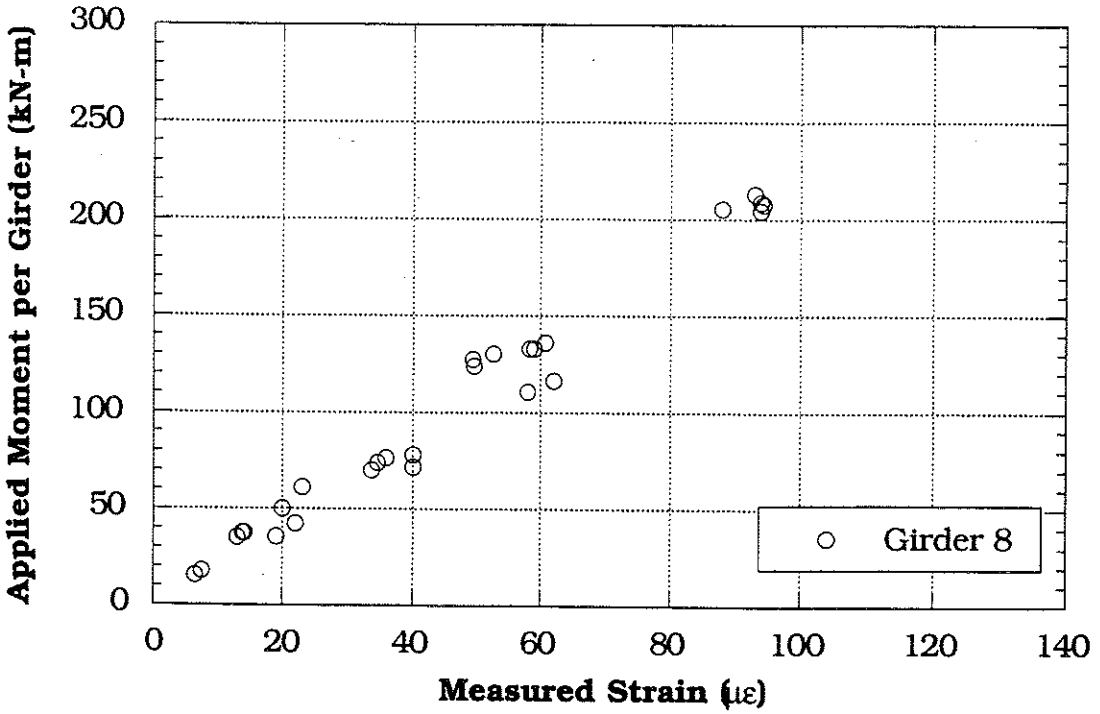

Figure 7.42 Moment per Girder vs Measured Strain, Girder 8.

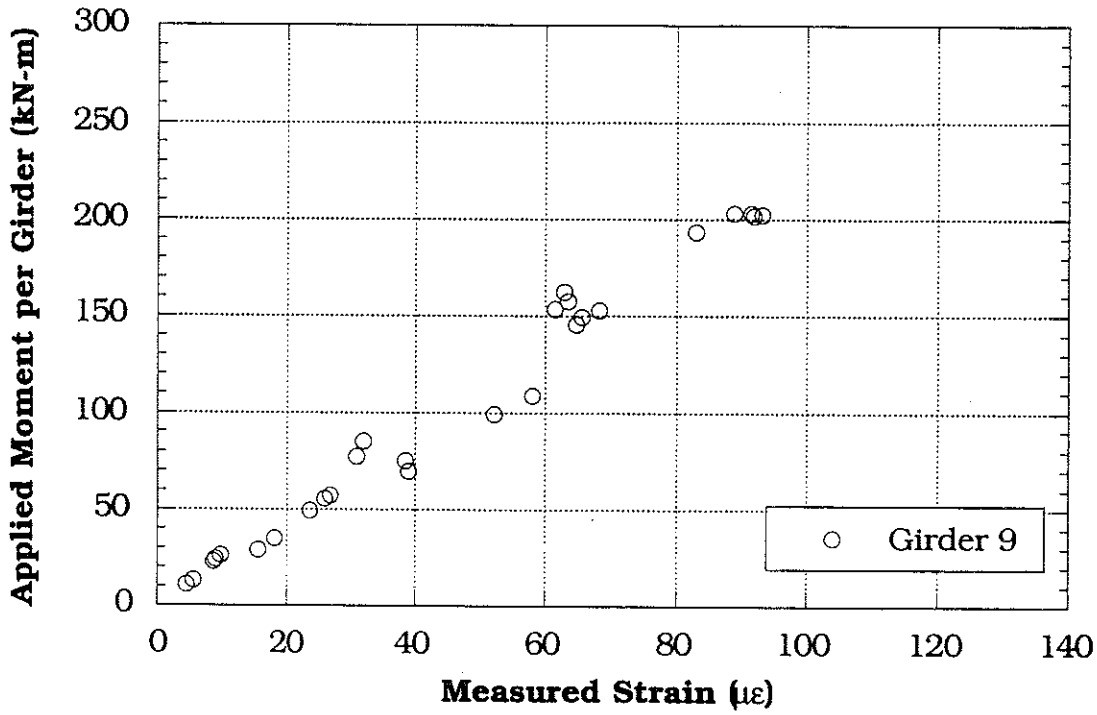

Figure 7.43 Moment per Girder vs Measured Strain, Girder 9.

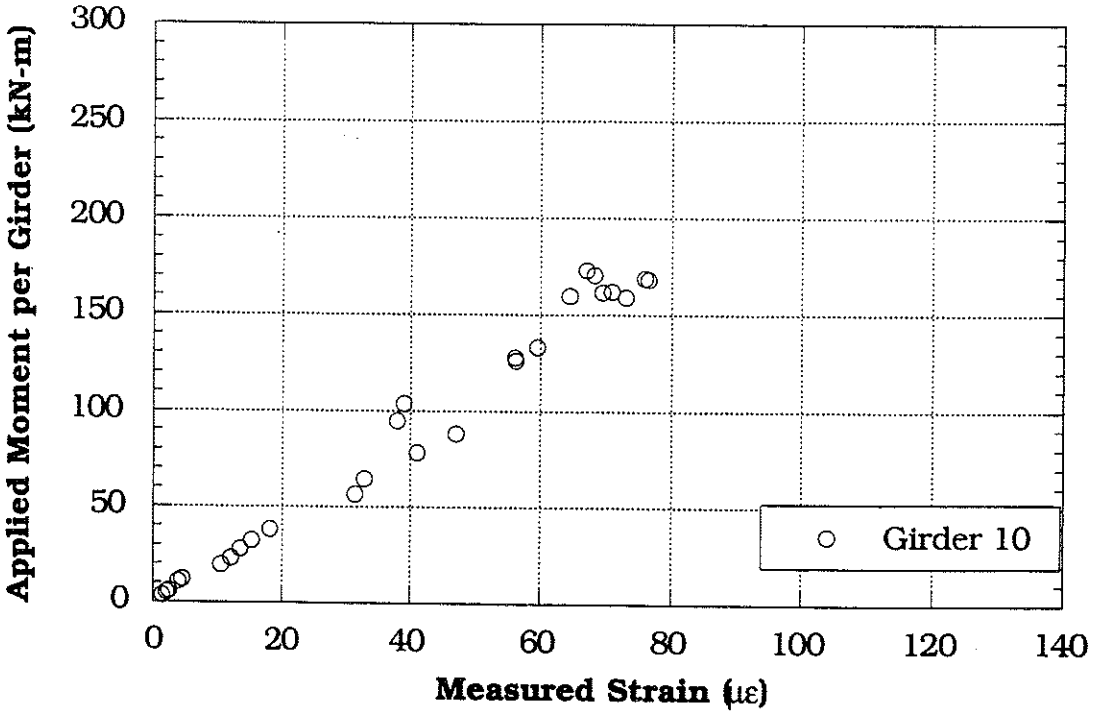

Figure 7.44 Moment per Girder vs Measured Strain, Girder 10.

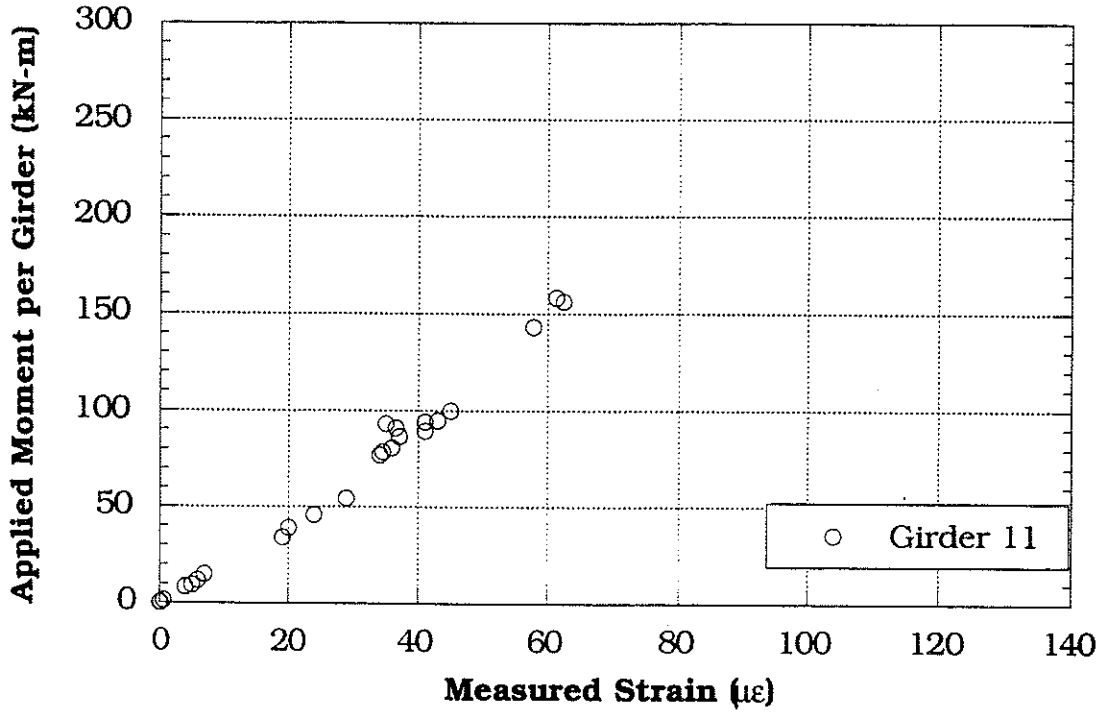

Figure 7.45 Moment per Girder vs Measured Strain, Girder 11.

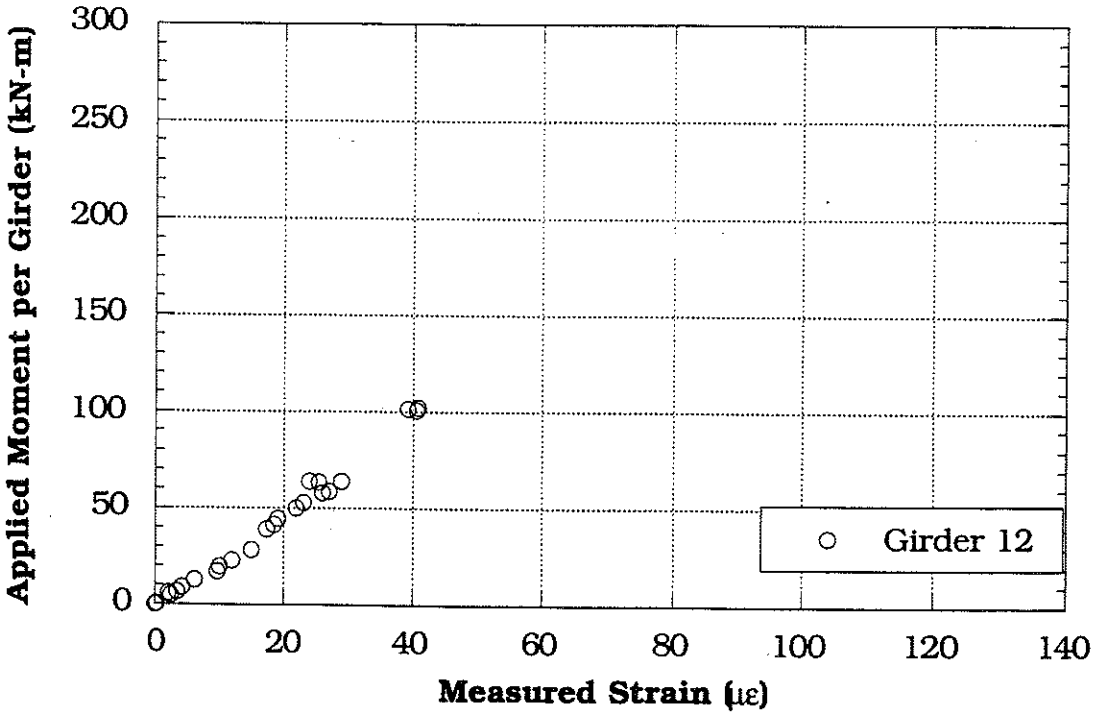

Figure 7.46 Moment per Girder vs Measured Strain, Girder 12.

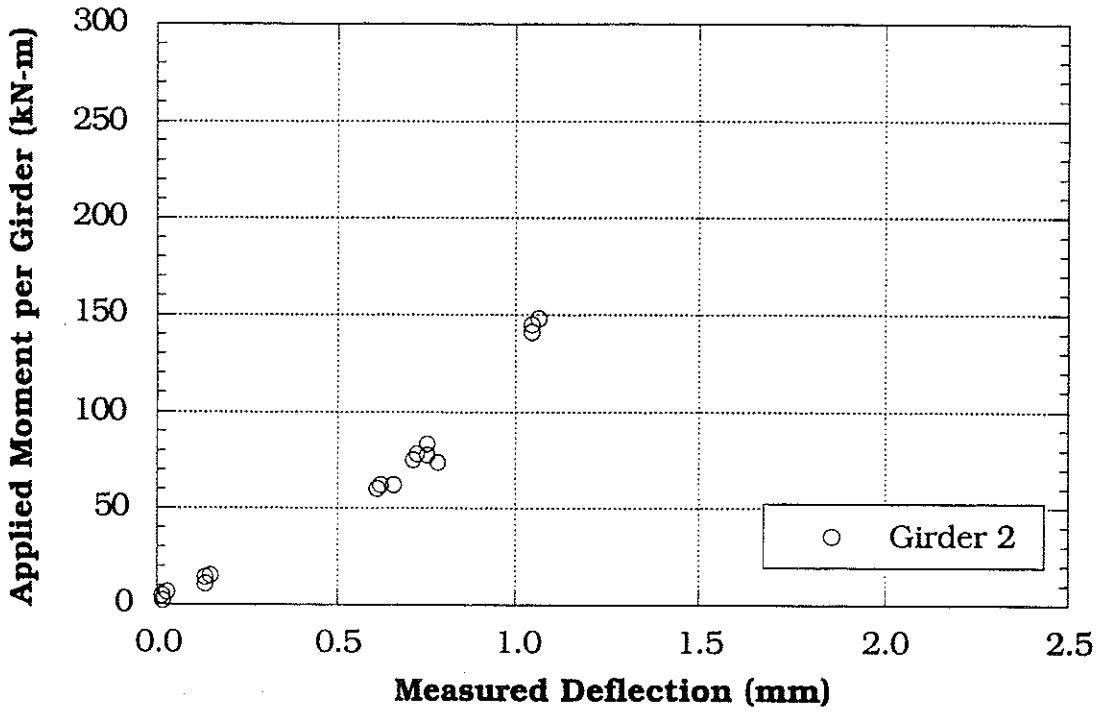

Figure 7.47 Moment per Girder vs Measured Deflection, Girder 2.

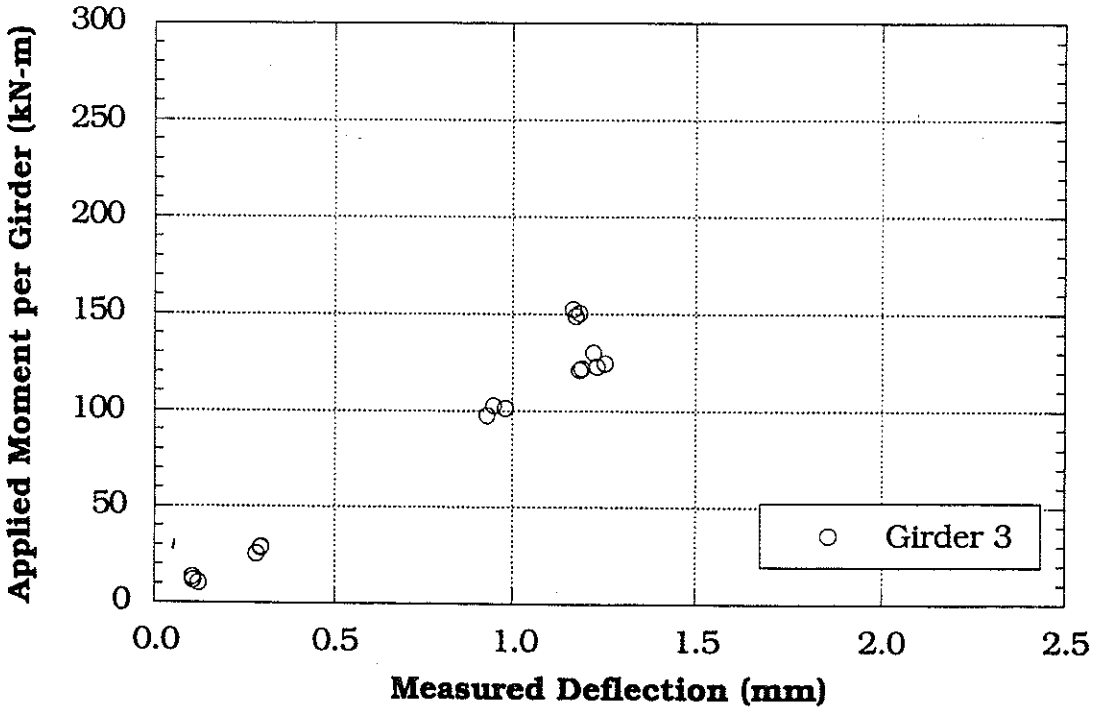

Figure 7.48 Moment per Girder vs Measured Deflection, Girder 3.

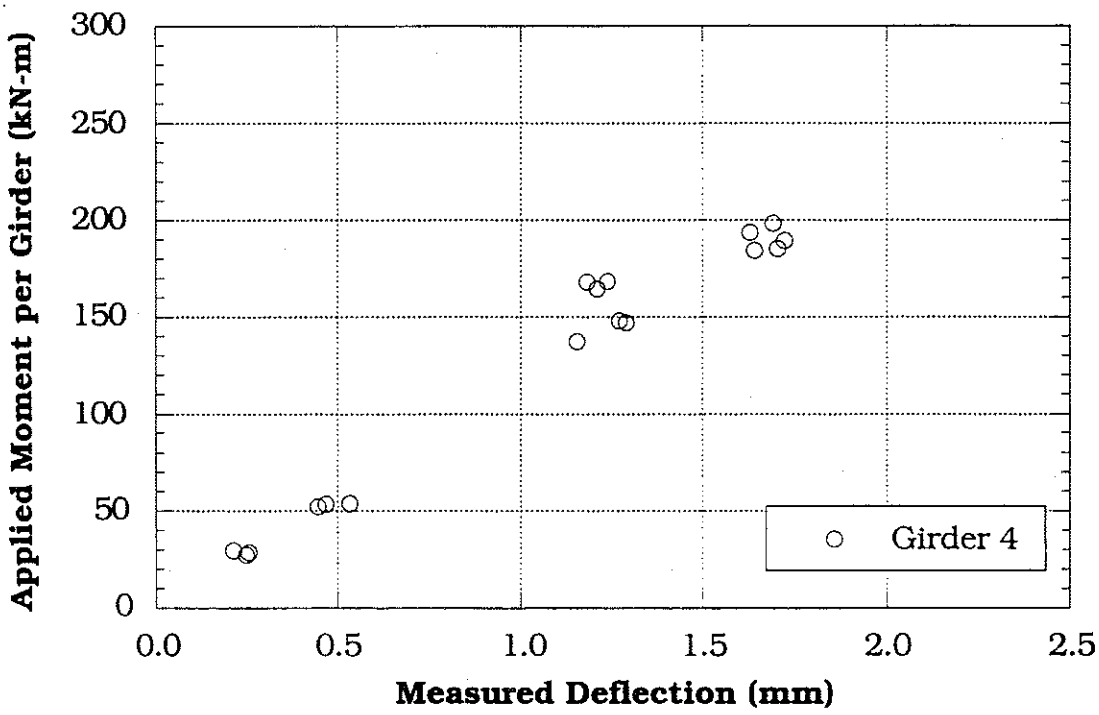

Figure 7.49 Moment per Girder vs Measured Deflection, Girder 4.

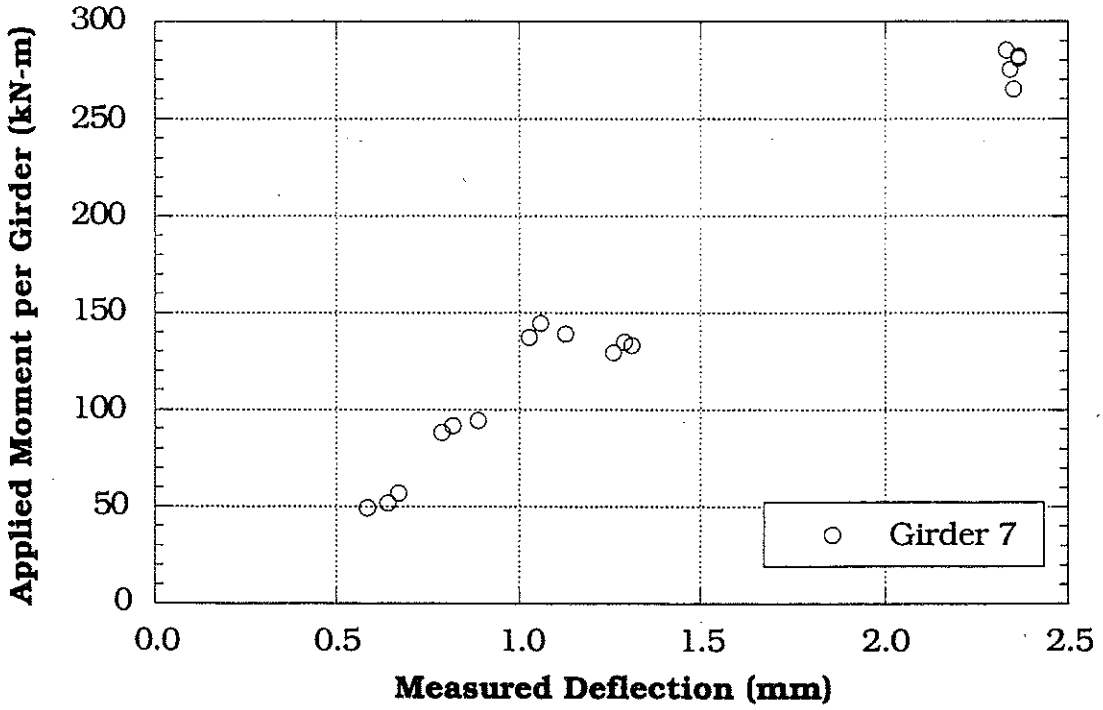

Figure 7.50 Moment per Girder vs Measured Deflection, Girder 7.

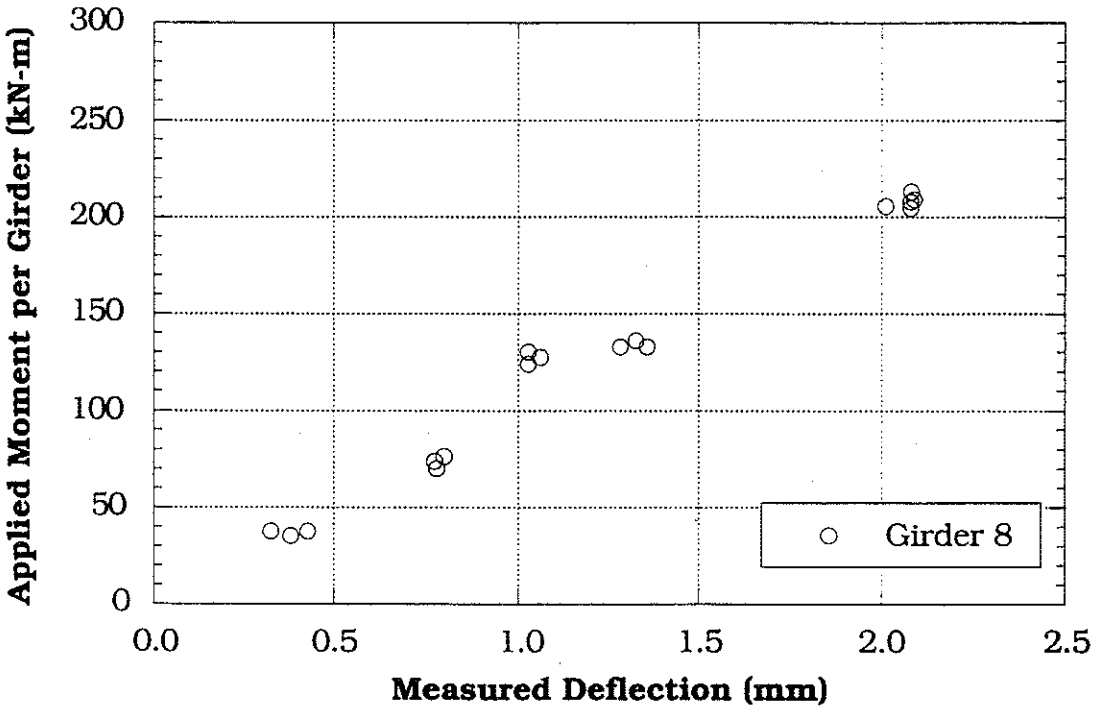

Figure 7.51 Moment per Girder vs Measured Deflection, Girder 8.

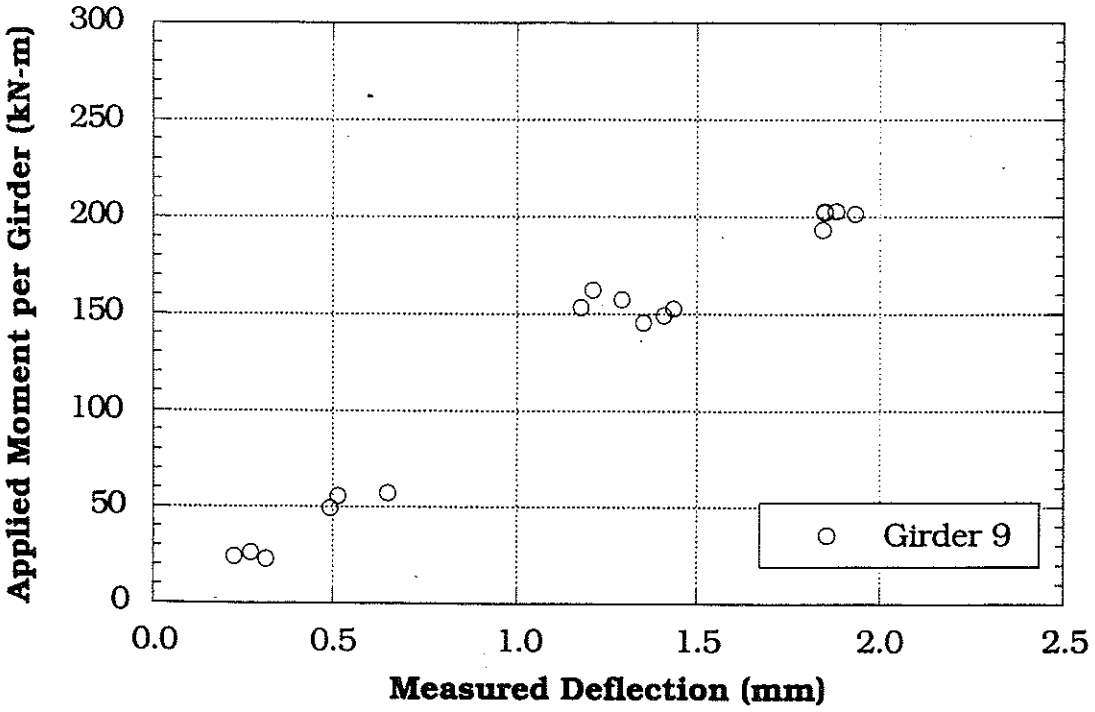

Figure 7.52 Moment per Girder vs Measured Deflection, Girder 9.

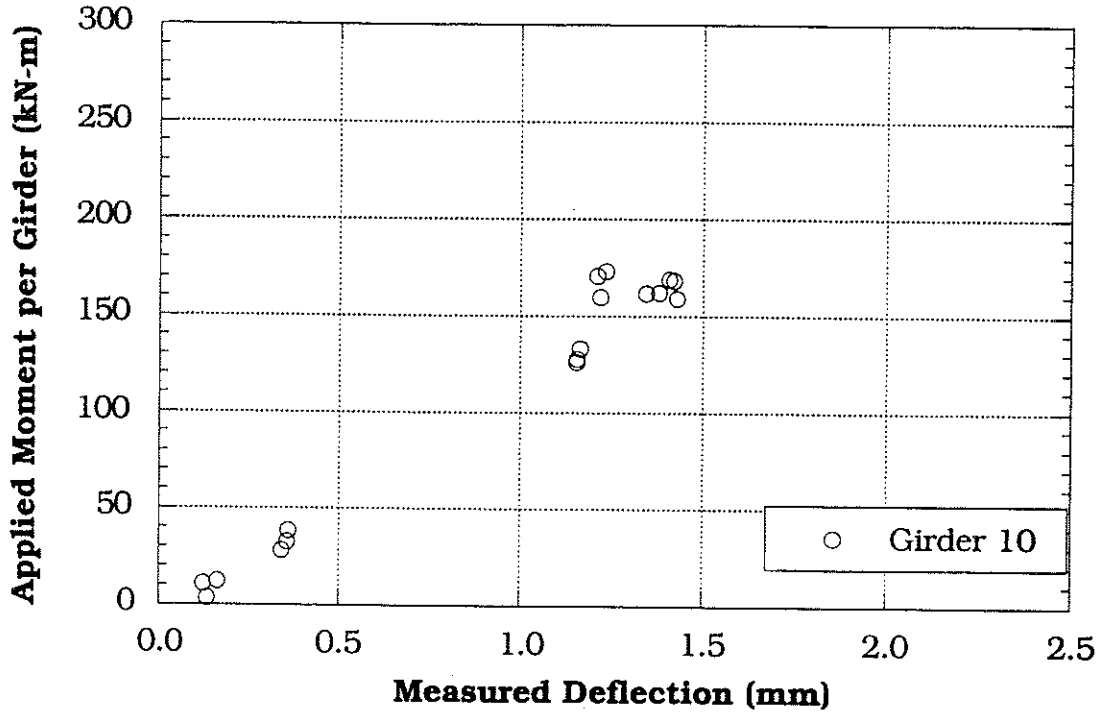

Figure 7.53 Moment per Girder vs Measured Deflection, Girder 10.

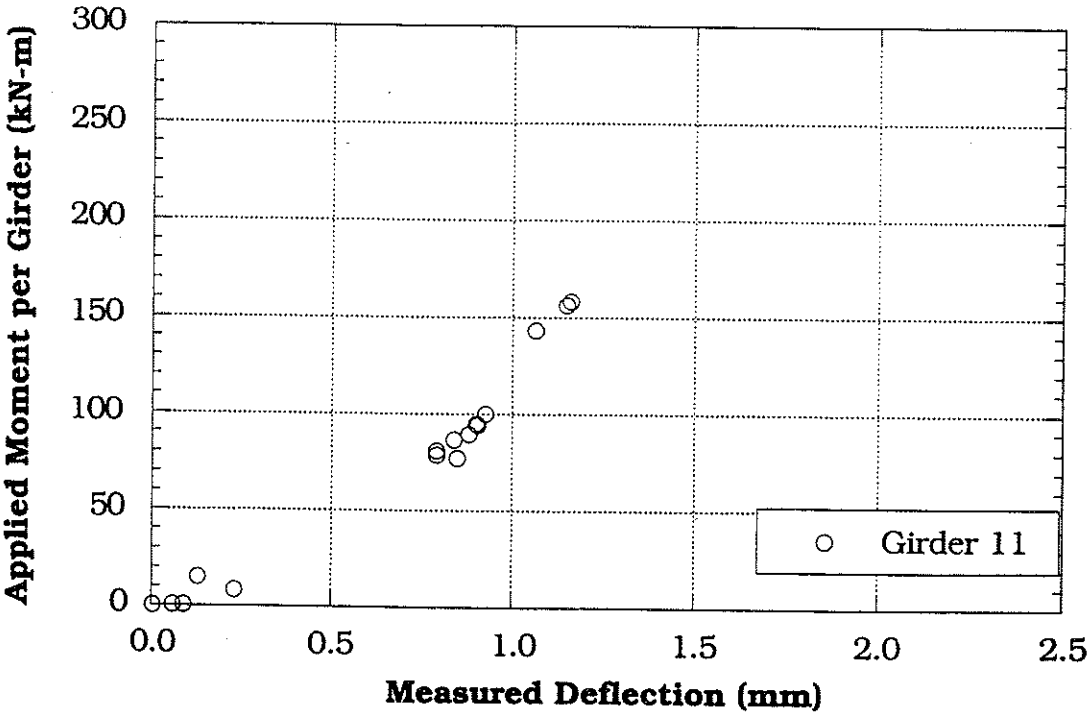

Figure 7.54 Moment per Girder vs Measured Deflection, Girder 11.

8. Bridge on M-106 over Portage River Drain near Munith (B02-38051, M106/PRD)

8.1 Description

This bridge was built in 1939 and is located on M-106 over Portage River Drain near Munith, Michigan. This bridge is designated as M106/PRD and can be identified by the road carried by the bridge and the river under the bridge. It has one lane in each direction. As shown in Figure 8.1, it has nine steel girders spaced at 1.46 m. It is a simply supported single span structure, designed as a noncomposite section. The total span length is 13.7 m with a skew of 20 degrees. The speed limit on this bridge is 89 km/h. Both the deck slab and the approach of the bridge were in good condition. The bridge has a load rating of 792 kN. The thickness of slab is 235 mm, with 61 mm of asphalt overlay.

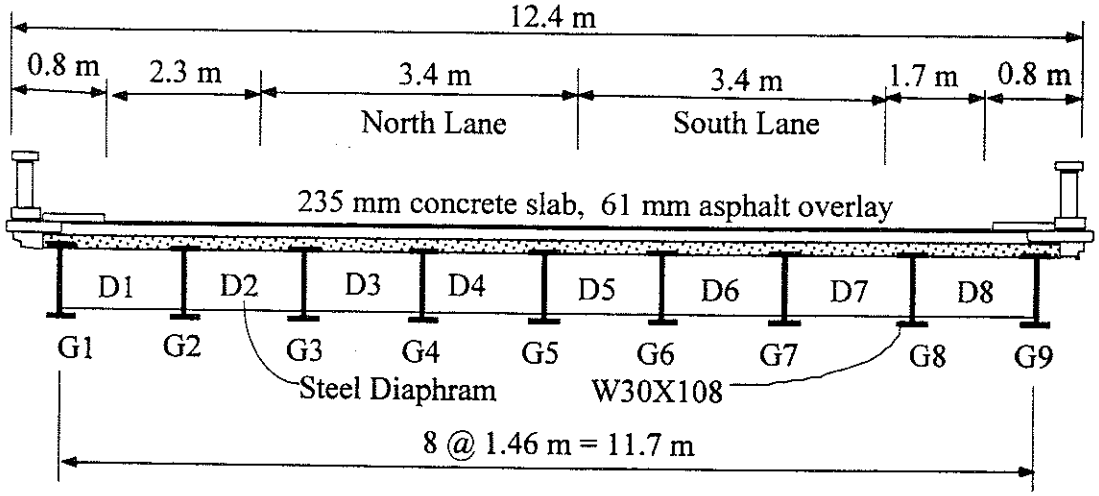

Figure 8.1 Cross-Section of Bridge M106/PRD near Munith.

8.2 Instrumentation

Strain transducers were installed on the bottom flanges of girders at mid-span (Figure 8.2). The bridge test was performed on September 25, 1997.

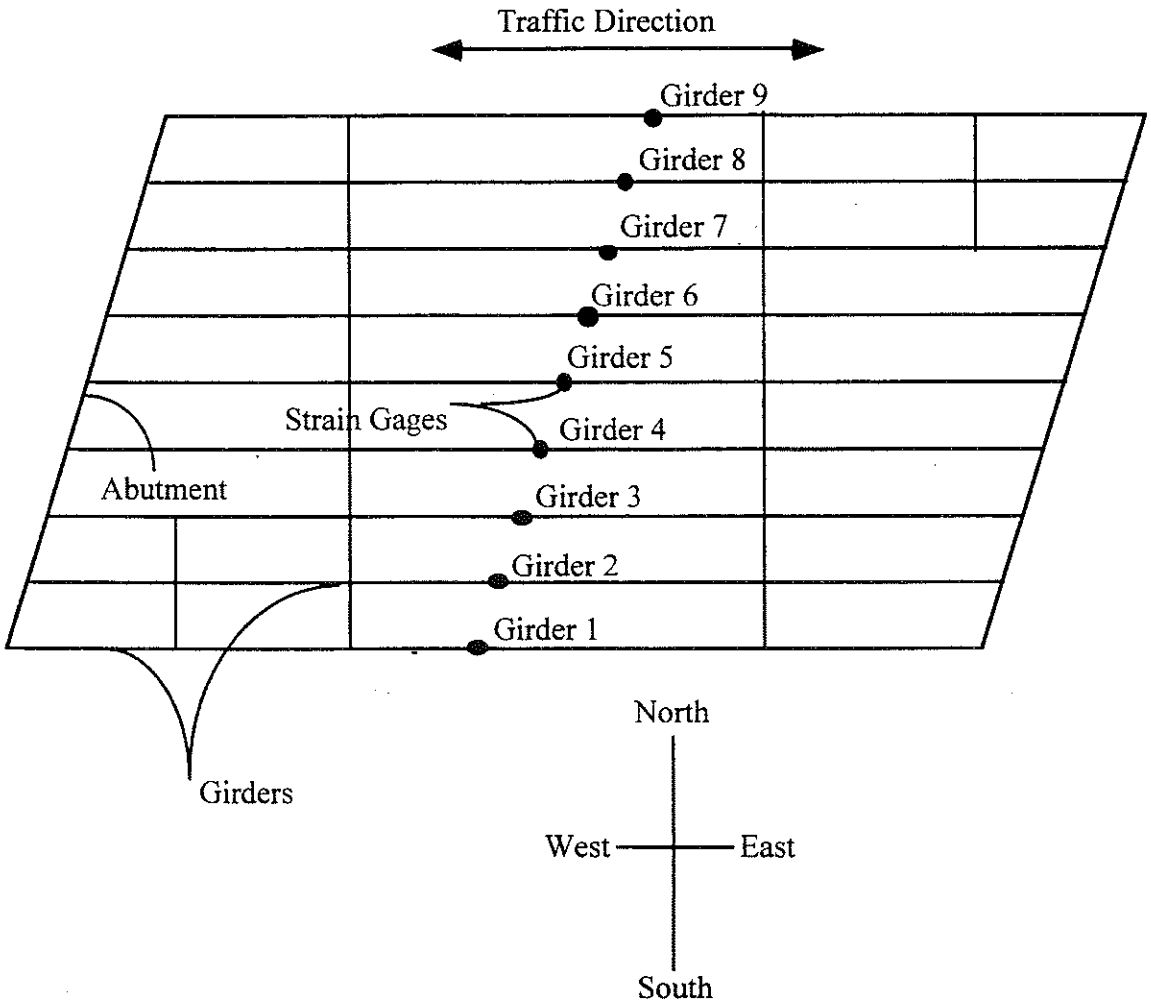

Figure 8.2 Strain Transducer Locations in Bridge M106/PRD near Bronson.

8.3 Truck Loads

Strain data necessary to calculate girder distribution and impact factors were taken from the mid-span transducers. The bridge was loaded with three-unit 10-axle and 11-axle trucks. The 10 and 11-axle trucks have gross weights of 585 kN and 644 kN, with wheelbases of 14.3 m and 15.6 m, respectively. Truck configurations are shown in Figures 8.3 and 8.4.

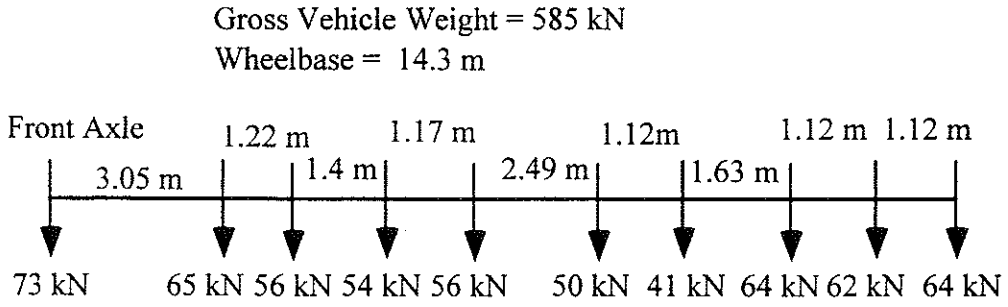

Figure 8.3 Ten-Axle Truck Configuration, Bridge M106/PRD near Munith.

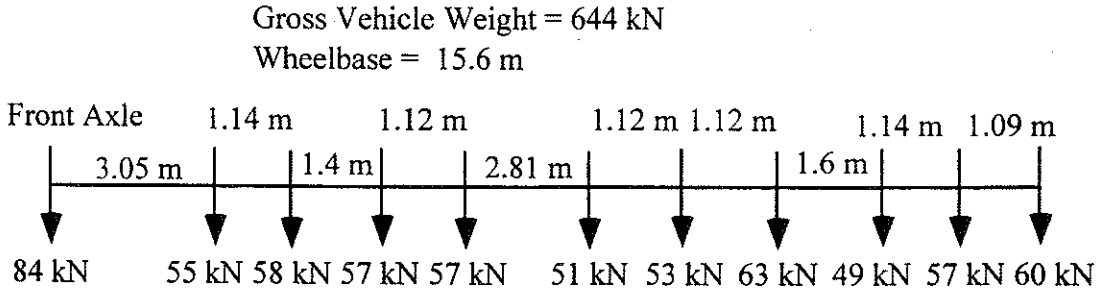

Figure 8.4 Eleven-Axle Truck Configuration, Bridge M106/PRD near Munith.

This bridge was tested only under crawling speed and full speed for the experimental derivation of load distribution and impact factors. The following load combinations were performed during the tests:

At crawling speed:

- 11-axle truck along the center of north lane
- 11-axle truck close to the curb of north lane
- 10-axle truck along the center of north lane
- 10-axle truck close to the curb of north lane
- 11-axle truck along the center of south lane
- 11-axle truck close to the curb of south lane
- 10-axle truck along the center of south lane
- 10-axle truck close to the curb of south lane
- 10-axle truck along the center of south lane and 11-axle truck along the center of north lane
- 11-axle truck along the center of south lane and 10-axle truck along the center of north lane

At high speed, the maximum speed obtained by the test trucks were:

- 10-axle truck along the center of north lane, 48 km/h
- 11-axle truck along the center of north lane, 40 km/h
- 10-axle truck along the center of south lane, 56 km/h
- 11-axle truck along the center of south lane, 40 km/h
- 10-axle truck along the center of south lane and 11-axle truck along the center of north lane, 40 km/h
- 11-axle truck along the center of south lane and 10-axle truck along the center of north lane, 40 km/h

8.4 Load Test Results

Strains from crawling-speed tests are considered static, and these were used to calculate girder distribution factors. Additional strains above the static values that were caused by high-speed tests are considered dynamic, and these were used to compute impact factors.

Figures 8.5 to 8.7 present the results of all crawling-speed (static) tests. Figures 8.5 to 8.6 present static strains and GDF's for one truck on the bridge. Figure 8.7 shows static strains and GDF's from side-by-side static load tests. GDF's are calculated from static strains using Eq. (3-4). Figure 8.7 also compares static strains obtained by superposing strains under one truck loading with those from side-by-side truck loading. They have practically the same values and again verify the superposition method used.

The maximum distribution factors from all cases in Figure 8.5 to 8.6 are presented in Figure 8.8, which represents the envelope of GDF's for one truck static loading. The maximum GDF's for one loaded lane were superimposed with the other to obtain GDF's for two-lane loading. The results are shown in Figure 8.9 together with the distribution factors from a side-by-side crawling-speed truck test.

In Figure 8.8, the results are taken as the maximum effect caused by the combination of two transverse truck positions in each lane; in the center of the lane, and near the curb. In contrast, Figure 8.9 shows the results when both trucks were in the same transverse position in their respective lanes. As expected, as the trucks are placed closer to the curbs, the GDF increases on the outside girders. The interior girders still experience a higher load effect, however. All measured GDF's are below the AASHTO Standard (S/3.36) and LRFD (two lanes) distribution factors. Actual value of the term $K_g / (Lt_s^3)$ is used in calculation of Code specified GDF values.

Figures 8.10 and 8.11 present the dynamic strains obtained from high-speed tests. The distribution factors calculated from the dynamic

strains are plotted in Figures 8.12 and 8.13 and compared to Code specified values.

From the corresponding static and dynamic strains, impact factors are calculated using Eq. (3-5) and presented in Figure 8.14. As in previous tests, this bridge also shows large impact factors for exterior girders, due to a low static strain versus dynamic strain. And again, the absolute magnitude of dynamic strain at the exterior girders is low and is not significant. Figure 8.15 shows the relationship between strain magnitude and impact factors. For side-by-side truck loading, the impact factors do not exceed 10% at interior girders.

The measured static strains were compared to static strains calculated using the design stiffness and GDF's determined by tests in this study. The maximum observed strain for this bridge is 78 με for a single truck and 112 με for two trucks side-by-side. The corresponding calculated static strain for a single truck in a composite section is 151 με and for a non-composite section it is 235 με. For two trucks side-by-side loading, the calculated strains are 236 με and 369 με for a composite section and a non-composite section, respectively.

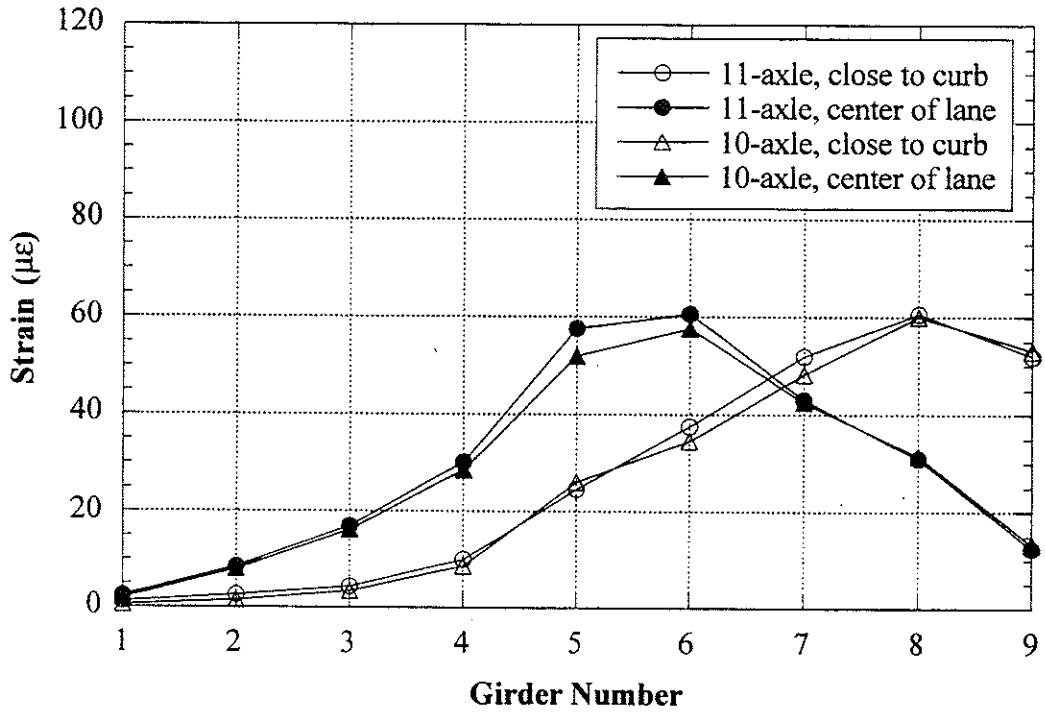

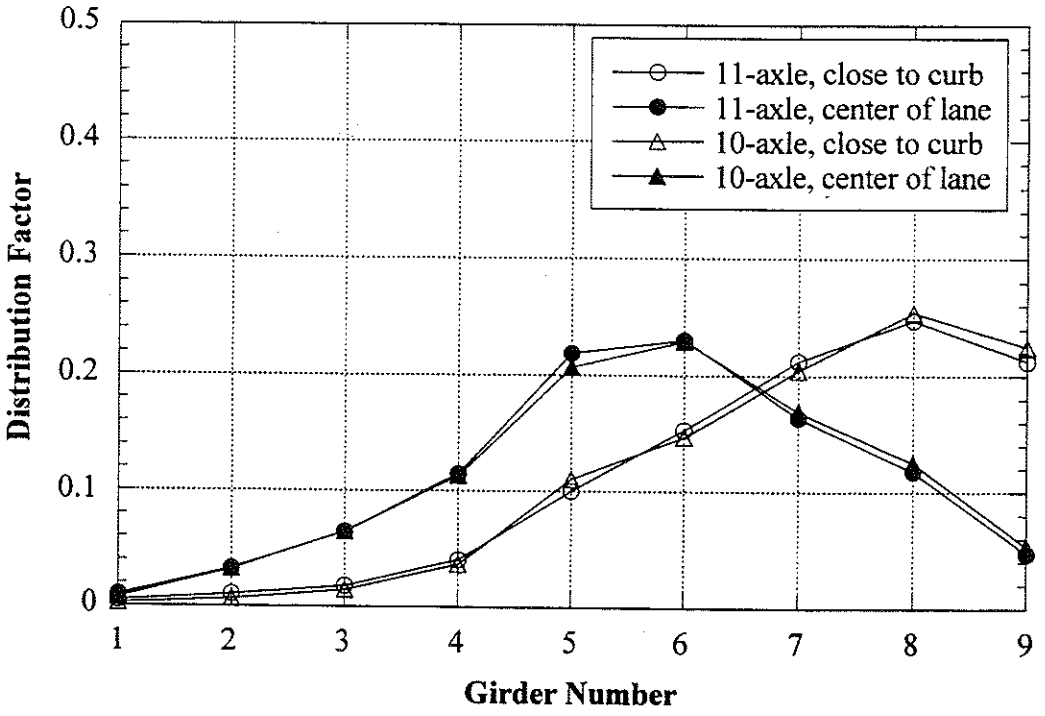

Figure 8.5 North Lane, Crawling Speed, Midspan.

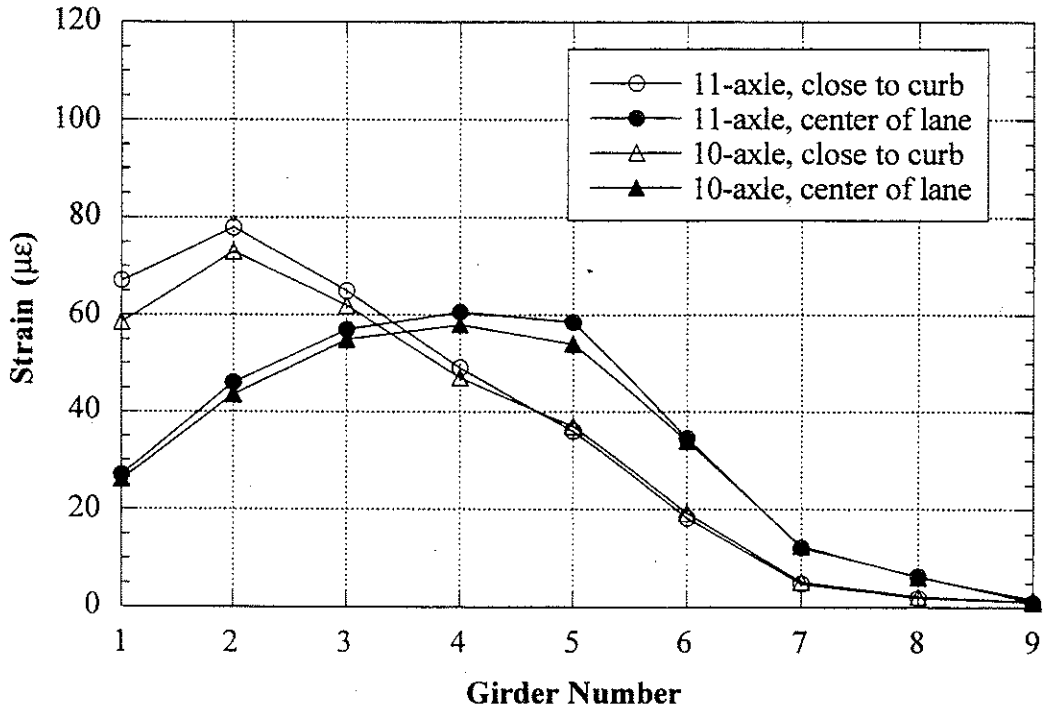

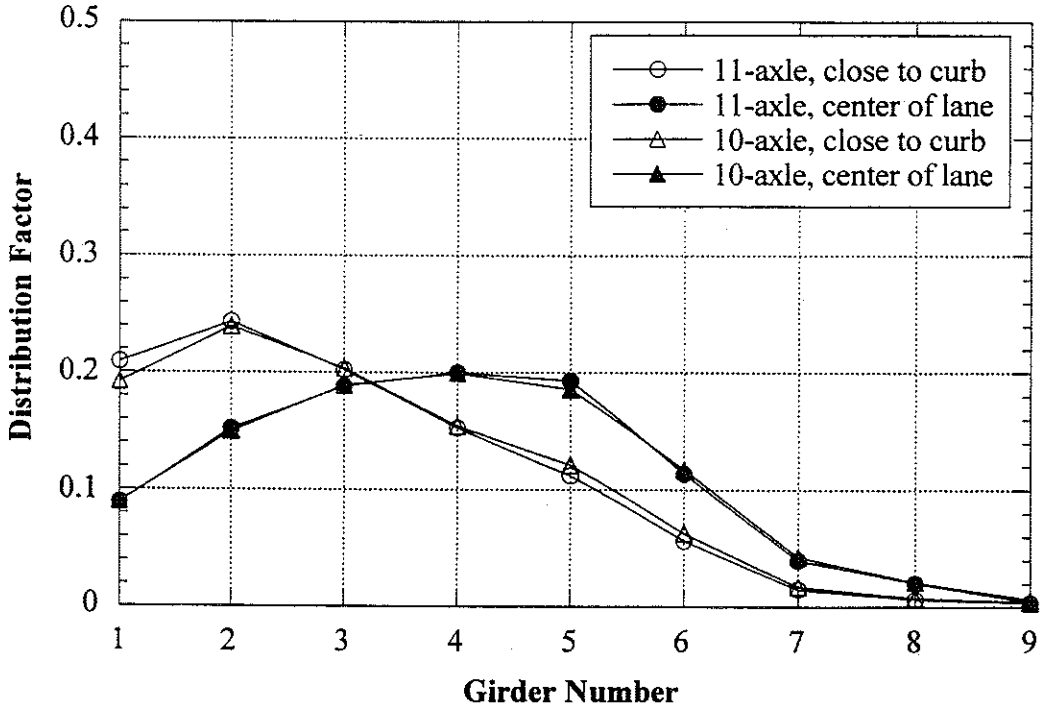

Figure 8.6 South Lane, Crawling Speed, Midspan.

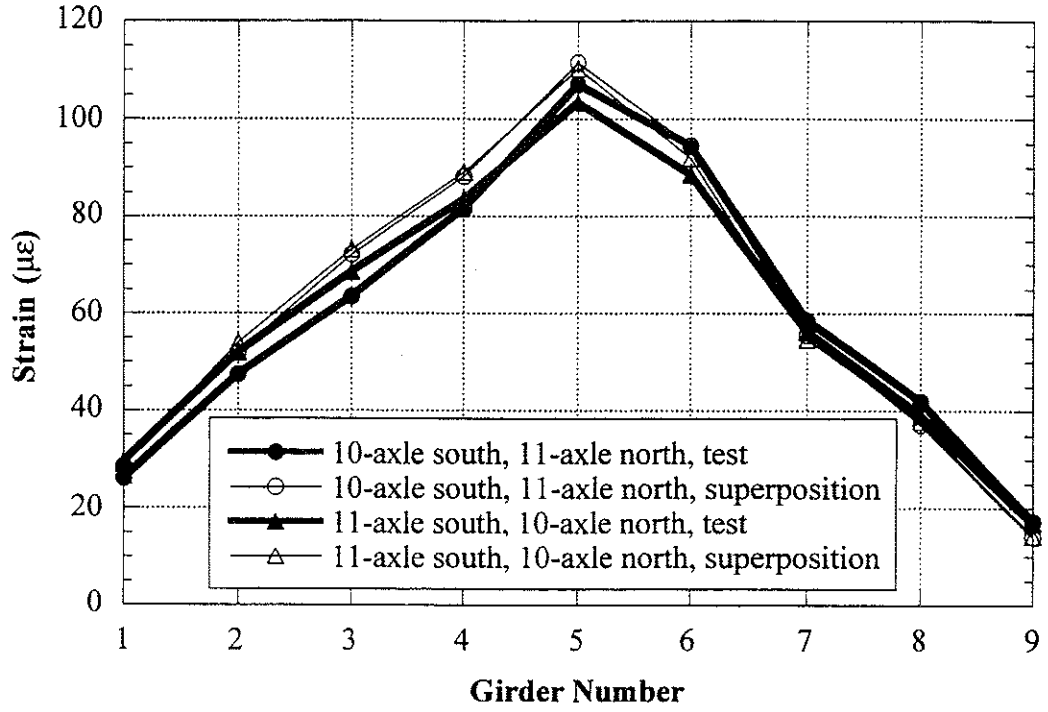

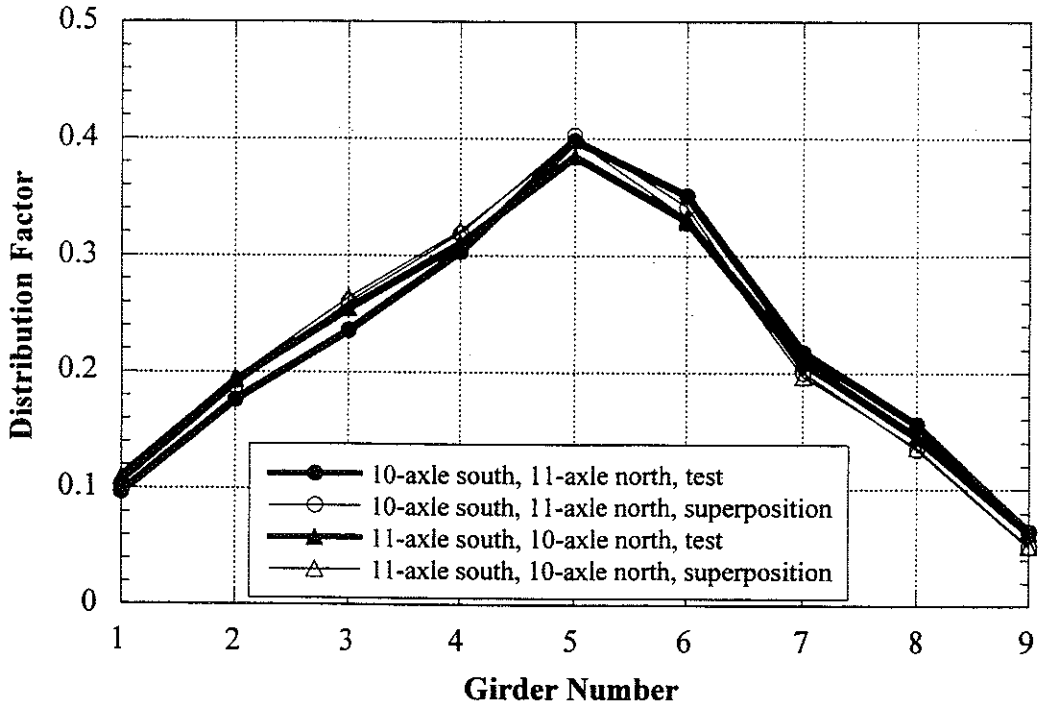

Figure 8.7 Side-by-Side Static Loading, Center of Lane, Midspan, Crawling Speed.

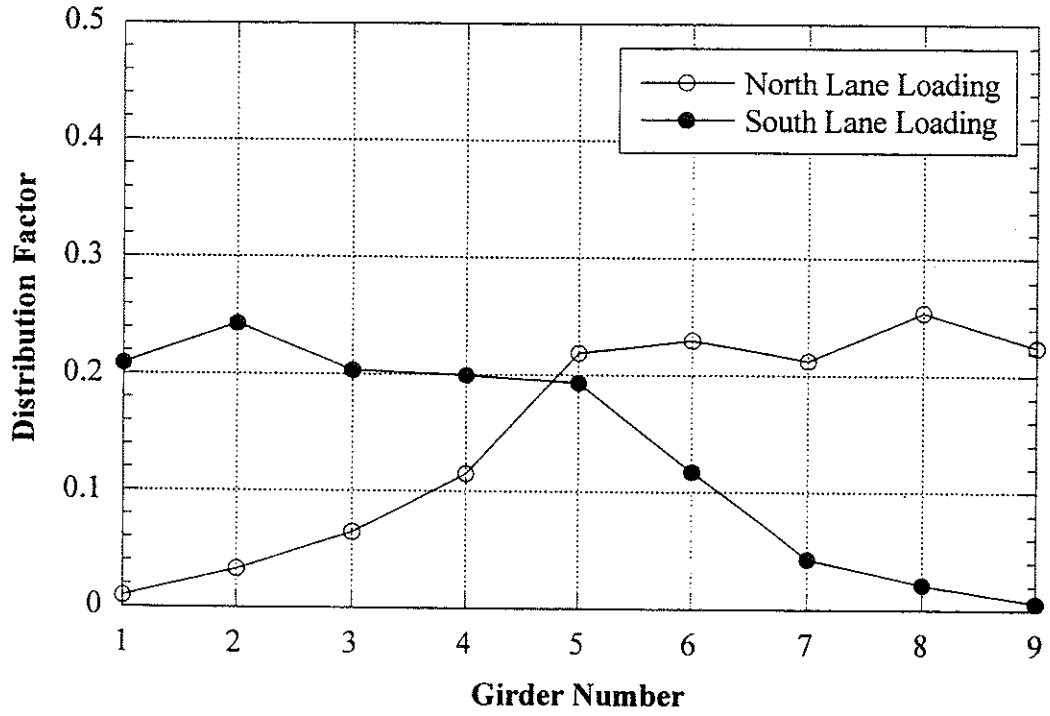

Figure 8.8 Envelope of Girder Distribution Factor
For One Truck Static Loading, Crawling Speed.

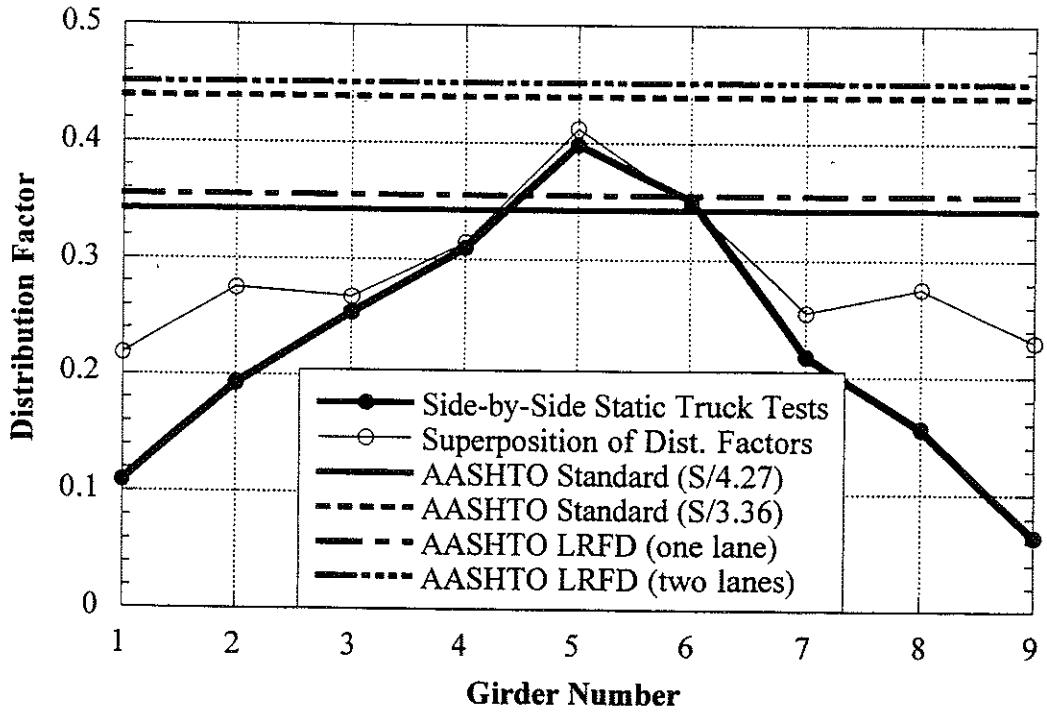

Figure 8.9 Comparison with Code Specified Distribution Factor,
Crawling Speed.

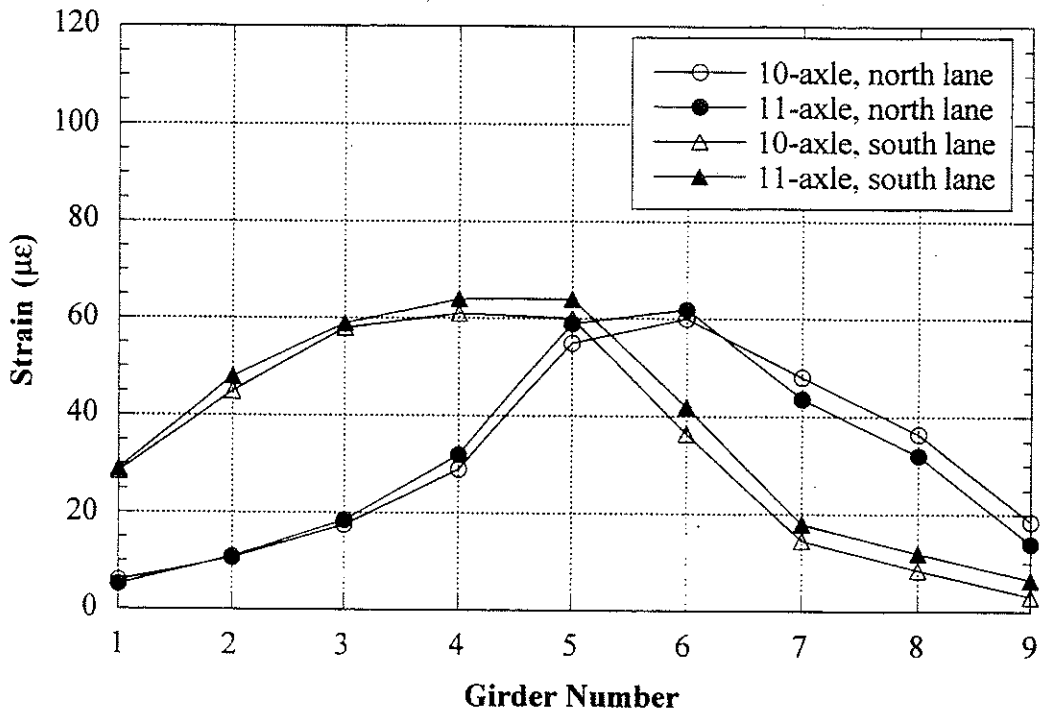

Figure 8.10 Strains under One Truck Loading at High Speed.

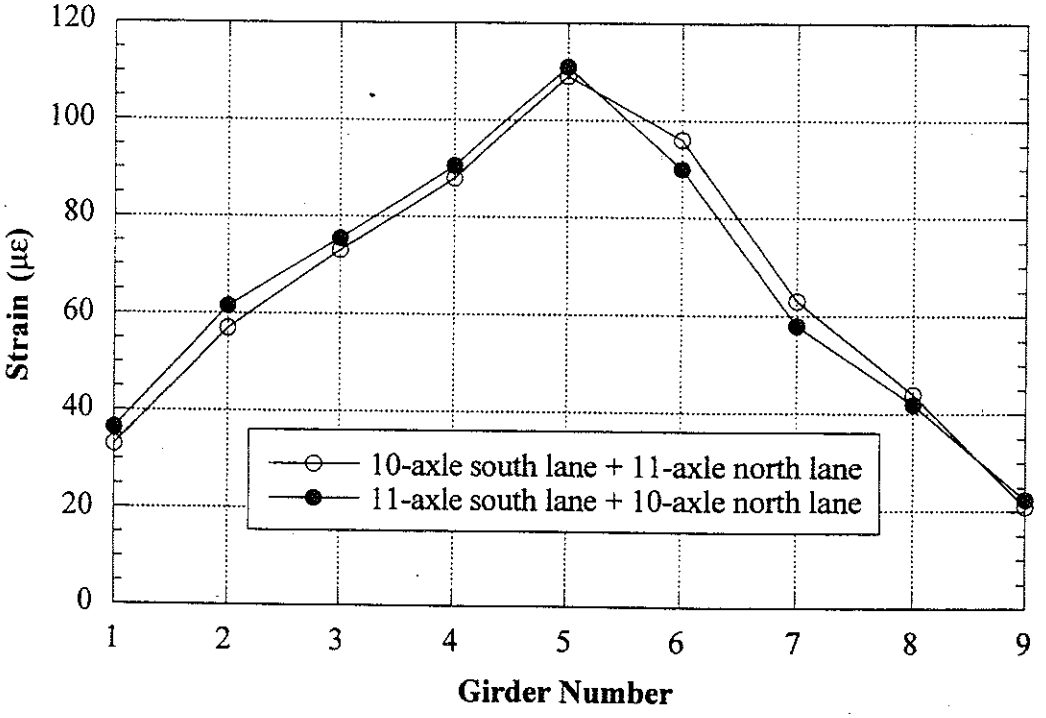

Figure 8.11 Strains under Side-by-Side Truck Loading at High Speed.

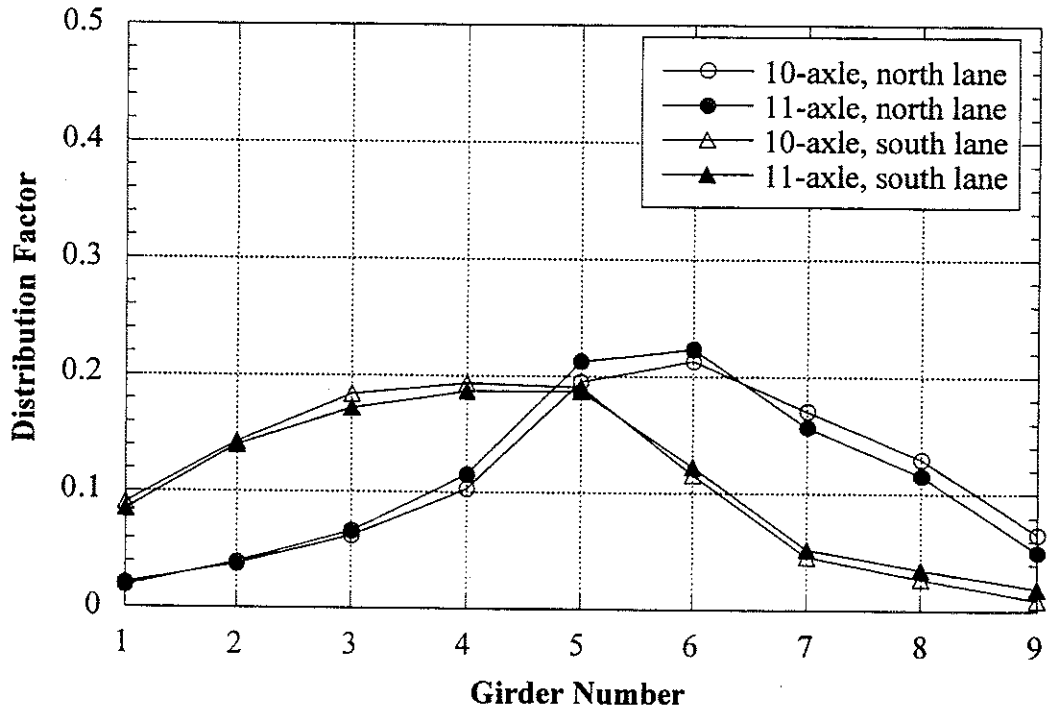

Figure 8.12 Distribution Factors for One Truck Loading at High Speed

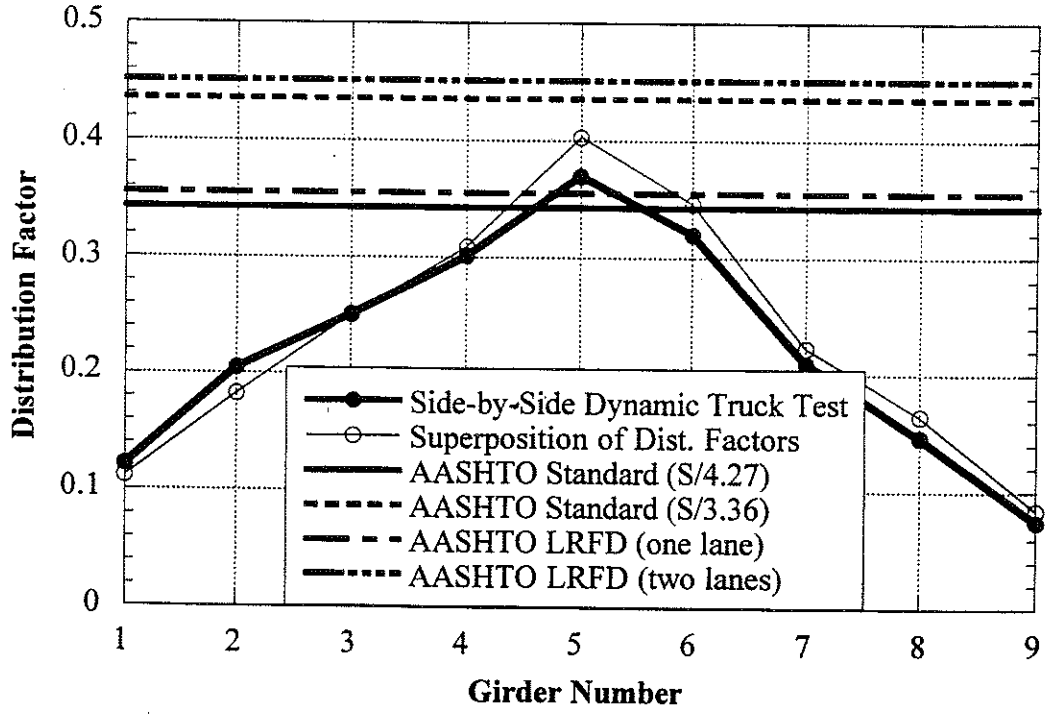

Figure 8.13 Comparison with Code Specified Distribution Factors at High Speed

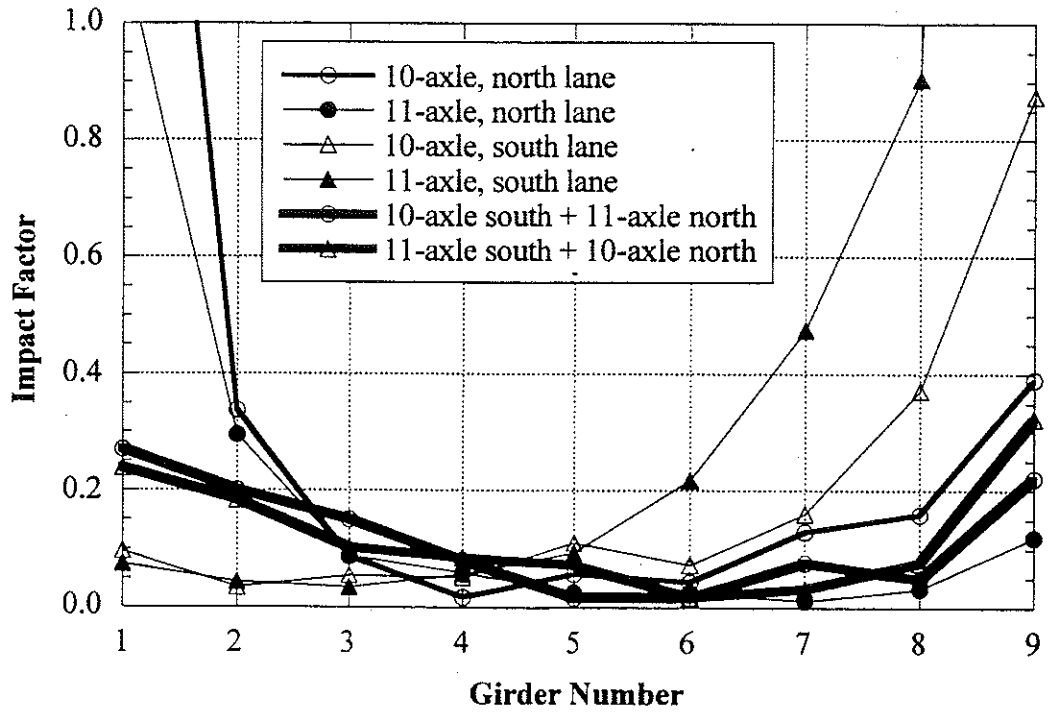

Figure 8.14 Impact Factors.

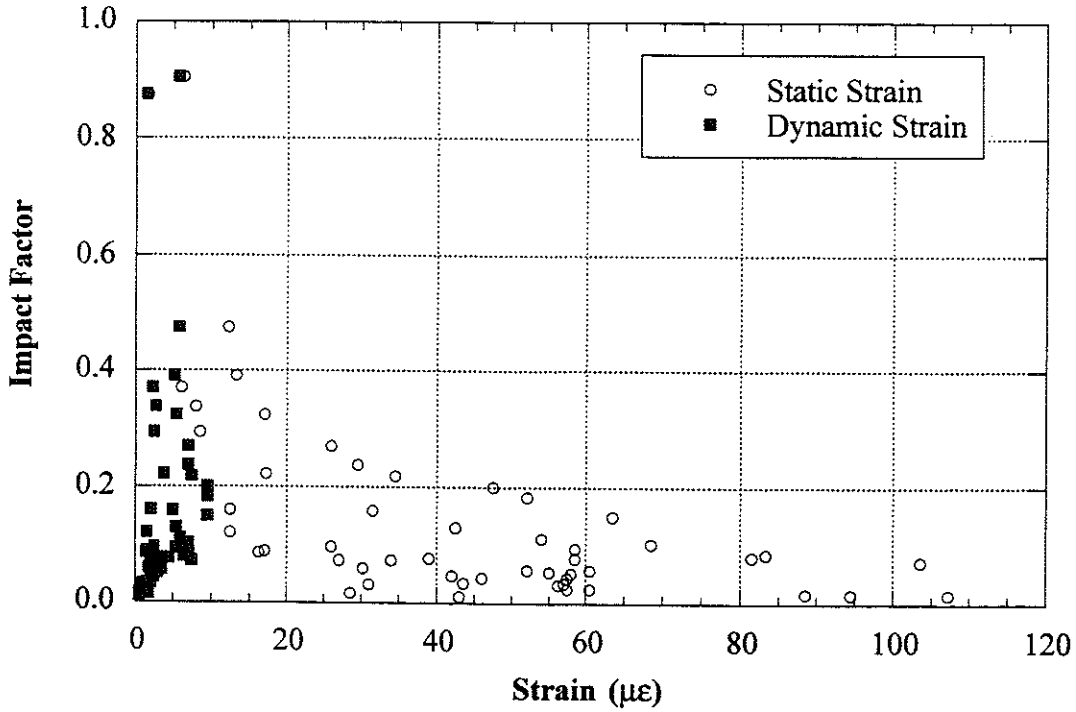

Figure 8.15 Strain versus Impact Factors.

Note:

Intentionally left blank

9. Bridge on M-45 over Bass River, West of Grand Rapids (B01-70041, M45/BR)

9.1 Description

This bridge was built in 1929 and is located on M-45 over Bass River west of Grand Rapids, Michigan. This bridge is designated as M45/BR and can be identified by the road carried by the bridge and the river under the bridge. It has one lane in each direction. As shown in Figure 9.1, it has ten steel girders spaced at 1.42 m. The total span length is 11.7 m without skew. The bridge has a slightly wider south lane than north lane. It is a simply supported single span structure and was designed to be noncomposite. The speed limit on this bridge is 88 km/h. Both the deck slab and the approach slab of the bridge were in good condition. The bridge has a load rating of 738 kN. The thickness of the slab is 317 mm, with a 38 mm asphalt overlay. The slab thickness and asphalt overlay depth were obtained from MDOT's rating sheet of the bridge.

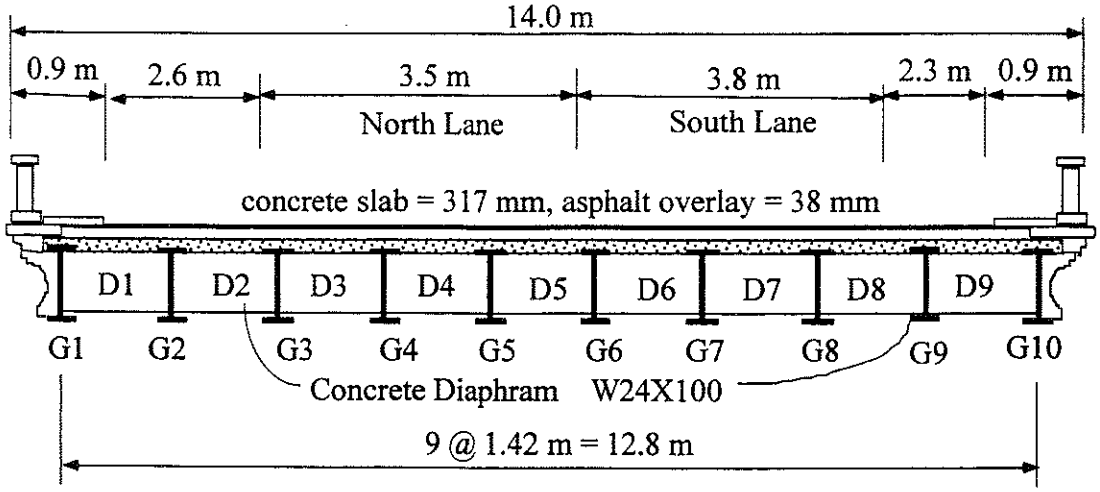

Figure 9.1 Cross-Section of Bridge M45/BR, West of Grand Rapids.

9.2 Instrumentation

Strain transducers were installed on the bottom flanges of girders at midspan (Figure 9.2). The bridge test was performed on October 30, 1997.

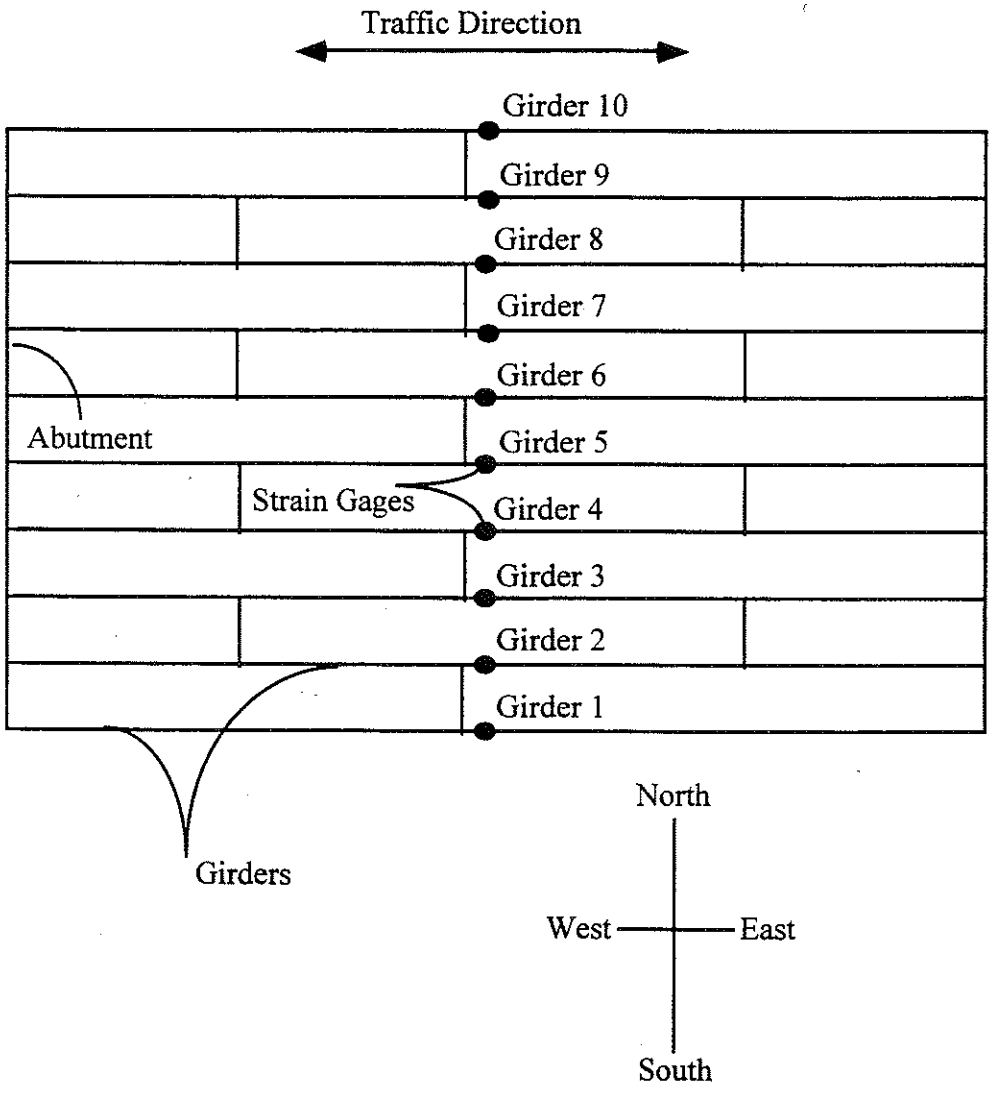

Figure 9.2 Strain Transducer Locations in Bridge M45/BR, West of Grand Rapids.

9.3 Truck Loads

Strain data necessary to calculate girder distribution and impact factors were taken from midspan transducers. The bridge was loaded with 2 three-unit 11-axle trucks. The trucks have gross weights of 696 kN and 682 kN, and both have a wheelbase of 18.2 m. Truck configurations are shown in Figures 9.3 and 9.4.

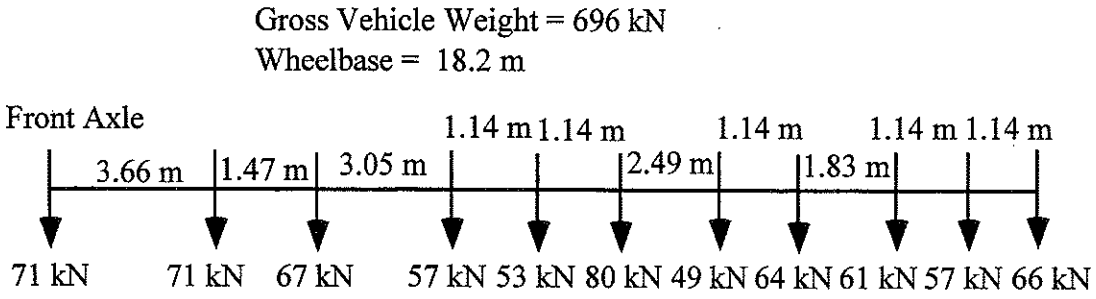

Figure 9.3 Configuration of Truck A, Bridge M45/BR, West of Grand Rapids.

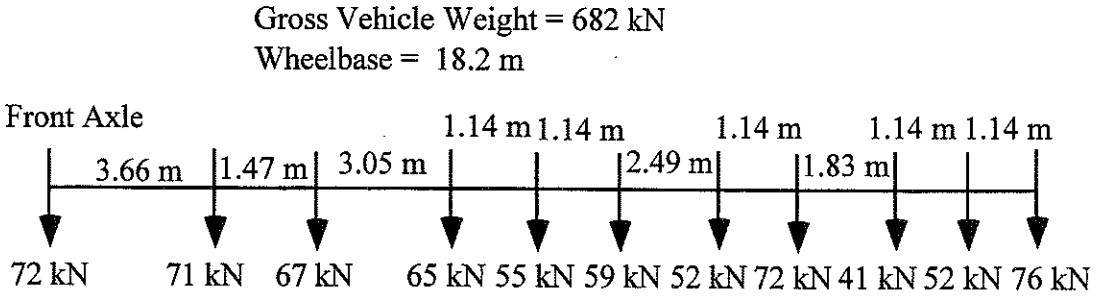

Figure 9.4 Configuration of Truck B, Bridge M45/BR, West of Grand Rapids.

This bridge was tested under crawling speed and full speed for the experimental derivation of load distribution and impact factors. The following load combinations were performed during the tests:

At crawling speed:

- truck A along the center of north lane
- truck A close to the curb of north lane

- truck B along the center of north lane
- truck B close to the curb of north lane
- truck A along the center of south lane
- truck A close to the curb of south lane
- truck B along the center of south lane
- truck B close to the curb of south lane
- truck A along the center of south lane and truck B along the center of north lane

At high speed, the maximum speed obtained by the test trucks were:

- truck A along the center of north lane, 48 km/h
- truck B along the center of north lane, 56 km/h
- truck A along the center of south lane, 56 km/h
- truck B along the center of south lane, 56km/h
- truck A along the center of south lane and truck B along the center of north lane, 58km/h

9.4 Load Test Results

Strains from crawling-speed tests were used to obtain static strains to calculate girder distribution factors and to calculate impact factors by comparing with strains from high-speed tests. In other words, strains from crawling-speed tests are considered as static strain, while strains from high speed tests provide dynamic strains.

Figures 9.5 to 9.7 present the results of all crawling-speed (static) tests. Figures 9.5 to 9.6 present static strains and GDF's for one truck on the bridge. Figure 9.7 shows static strains and GDF's from side-by-side static load tests. GDF's are calculated from static strains using Eq. (3-4). Figure 9.7 also compares static strains obtained by superposing

strains under one truck loading with those from side-by-side truck loading. They have practically the same values and again verify the superposition method used.

The maximum distribution factors from all cases in Figure 9.5 to 9.6 are presented in Figure 9.8, which represents the envelope of GDF's for one truck static loading. The maximum GDF's for one loaded lane were superimposed with the other to obtain GDF's for two-lane loading. The results are shown in Figure 9.9 together with the distribution factors from a side-by-side crawling-speed truck test.

In Figure 9.8, the results are taken as the maximum effect caused by the combination of two transverse truck positions in each lane; in the center of the lane, and near the curb. In contrast, Figure 9.9 shows the results when both trucks were in the same transverse position in their respective lanes. As expected, as the trucks are placed closer to the curbs, the GDF increases on the outside girders. The interior girders still experience a higher load effect. Measured GDF's are close to the specified AASHTO LRFD Code GDF (two lanes) but less than Standard GDF (S/3.36). AASHTO Standard (S/4.27) and LRFD (one lane) GDF's are also plotted in Figure 9.9. Actual value of the term $K_g / (Lt_s^3)$ is used in calculation of Code specified GDF values.

Figures 9.10 and 9.11 present the dynamic strains obtained from high-speed tests. Girder distribution factors calculated from dynamic strains are plotted and compared with Code specified GDF's in Figure 9.13.

From the corresponding static and dynamic strains, impact factors are calculated using Eq. (3-5) and presented in Figure 9.14. As in previous tests, this bridge also shows large impact factors for exterior girders, due to a low static strain versus dynamic strain. And again, the absolute magnitude of dynamic strain at the exterior girders is low and is not significant. Figure 9.15 shows the relationship between strain magnitude and impact factors. For side-by-side truck loading, the impact factors do not exceed 10% at interior girders.

The measured static strains were compared to static strains calculated using the design stiffness and GDF's determined by tests in this study. The maximum observed static strain for this bridge is 64 με for a single truck and 96 με for two trucks side-by-side. The corresponding calculated strain for a single truck in a composite section is 139 με and for a non-composite section it is 249 με. For two trucks side-by-side loading, the calculated strains are 172 με and 308 με for a composite section and non-composite section, respectively.

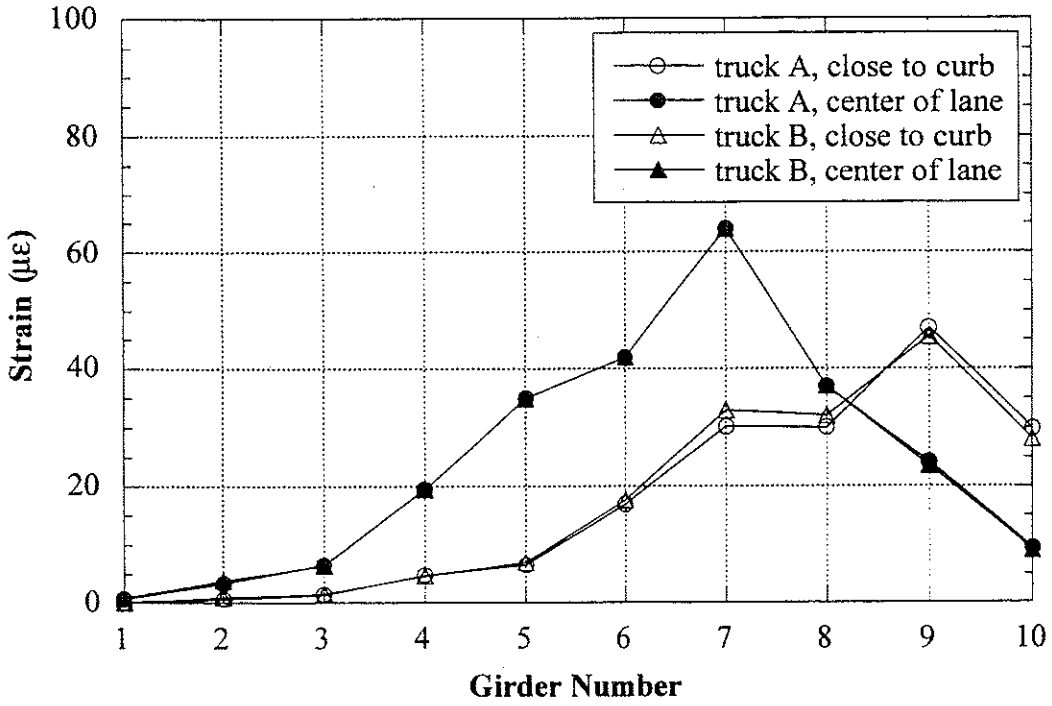

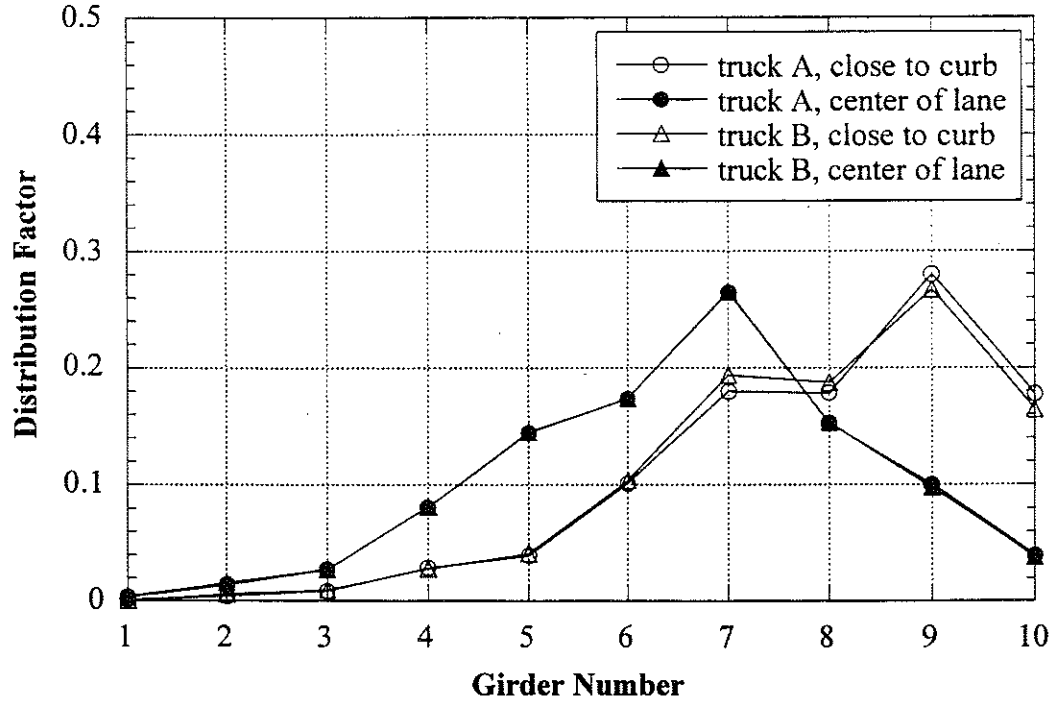

Figure 9.5 North Lane, Crawling Speed.

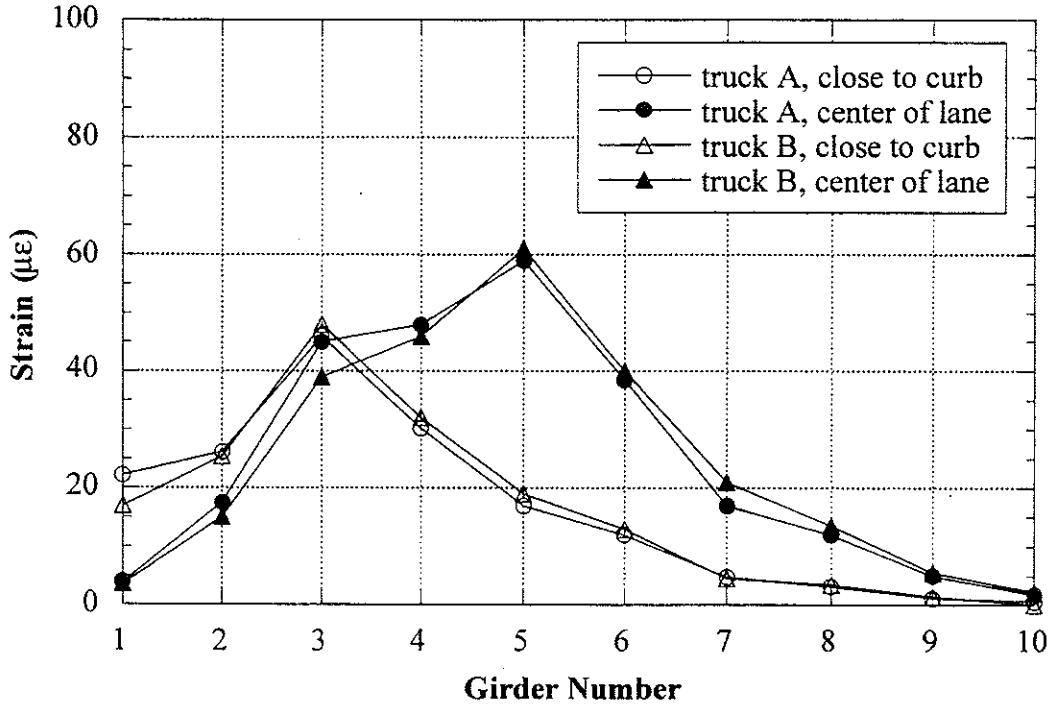

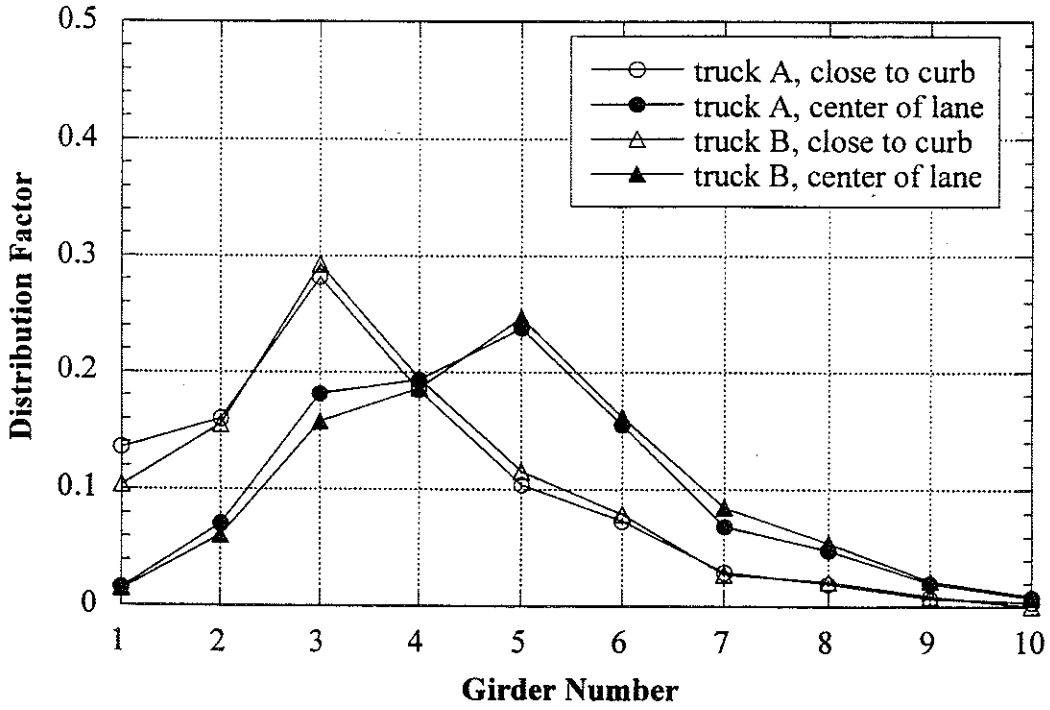

Figure 9.6 South Lane, Crawling Speed.

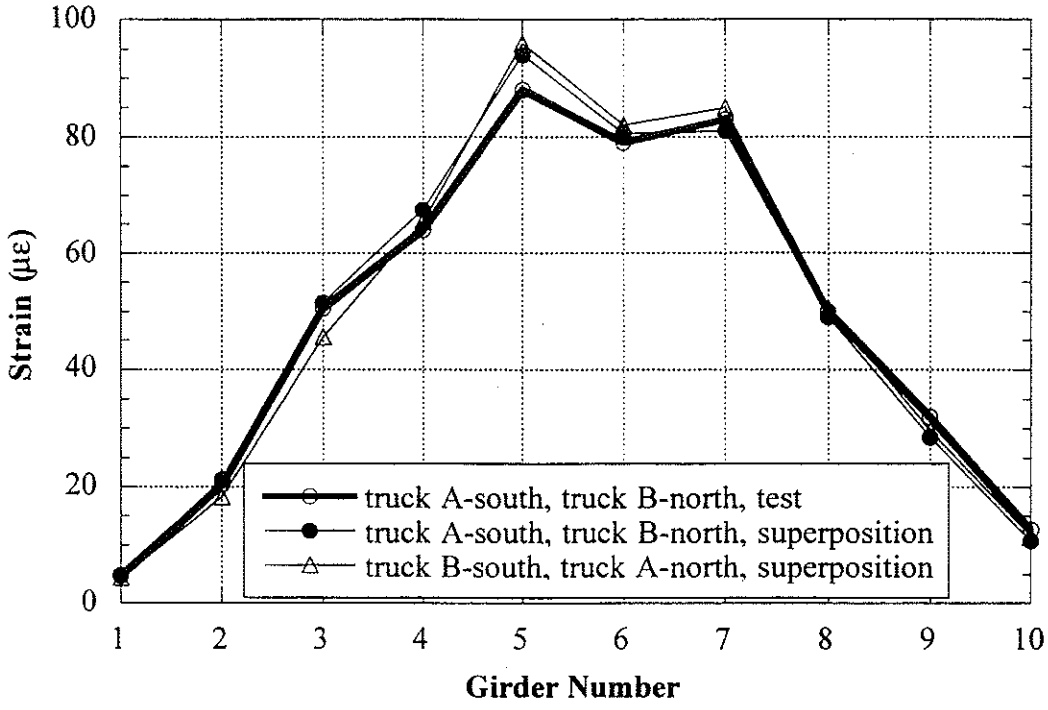

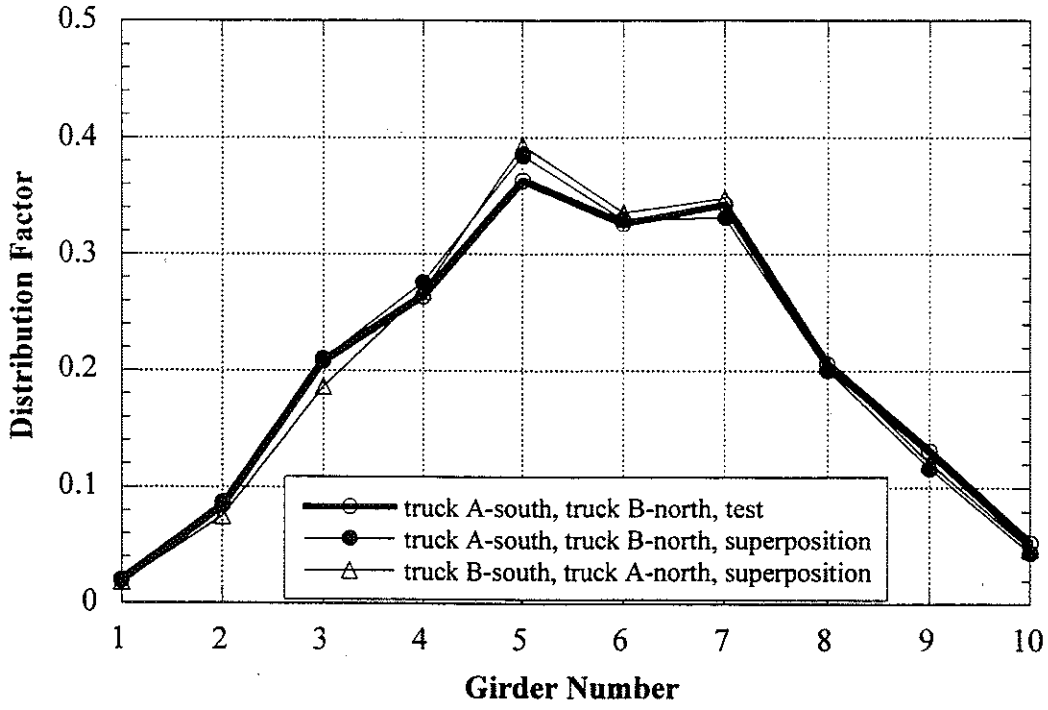

Figure 9.7 Side-by-Side Static Loading, Center of Lane.

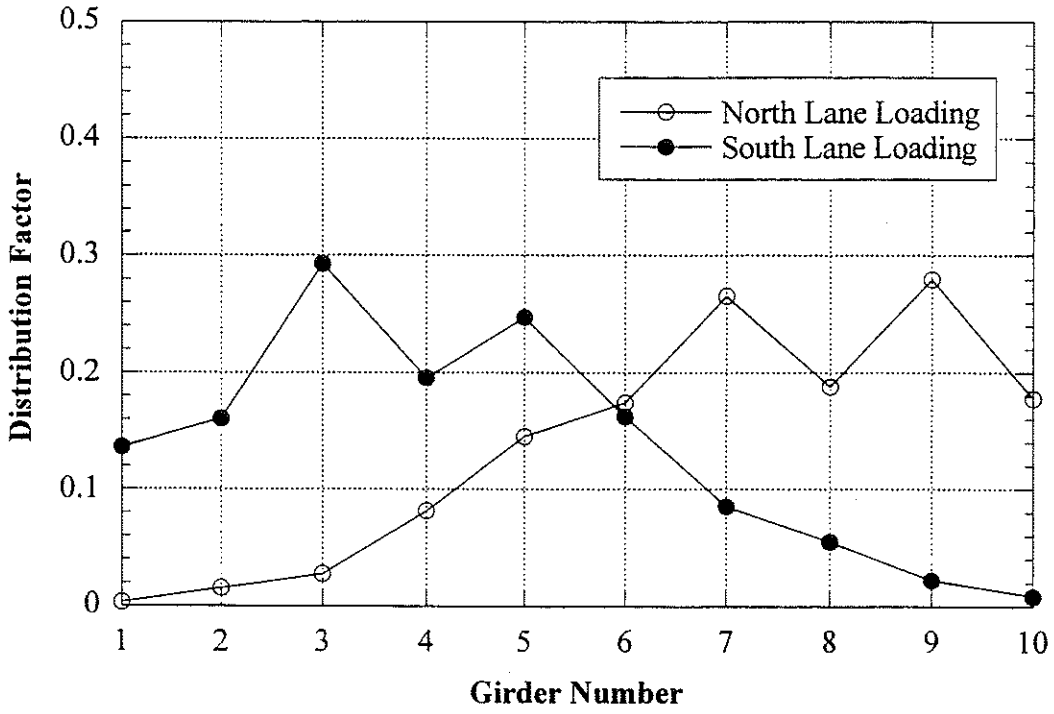

Figure 9.8 Envelope of Girder Distribution Factor
For One Truck Static Loading, Crawling Speed.

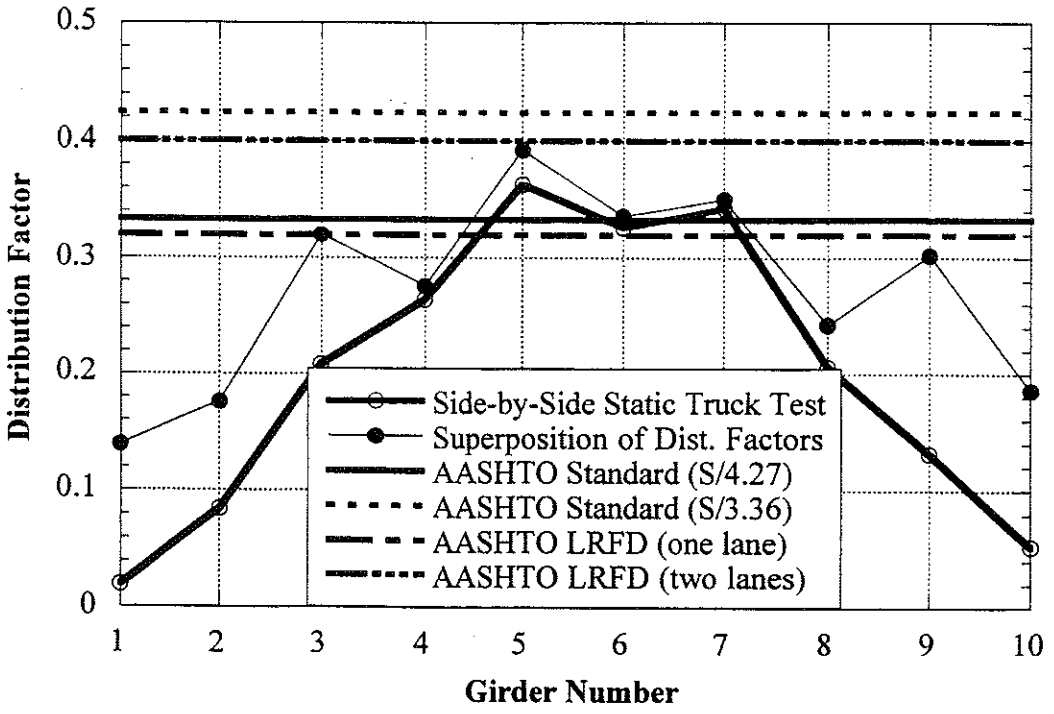

Figure 9.9 Comparison with Code Specified Distribution Factor,
Crawling Speed.

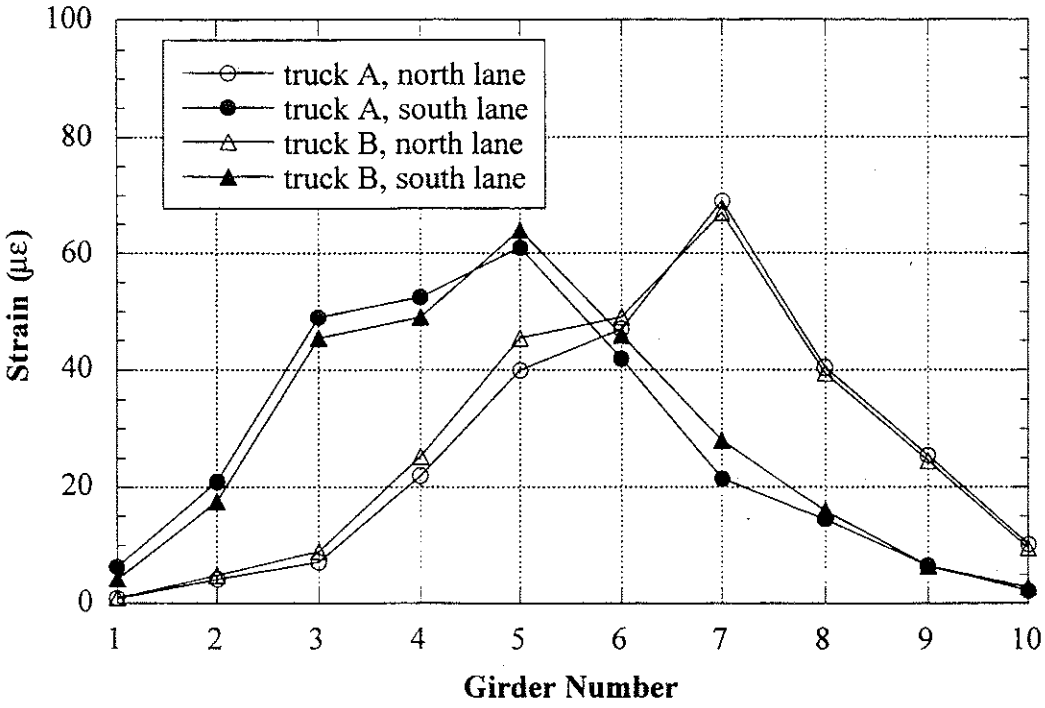

Figure 9.10 Strains under One Truck Loading at High Speed.

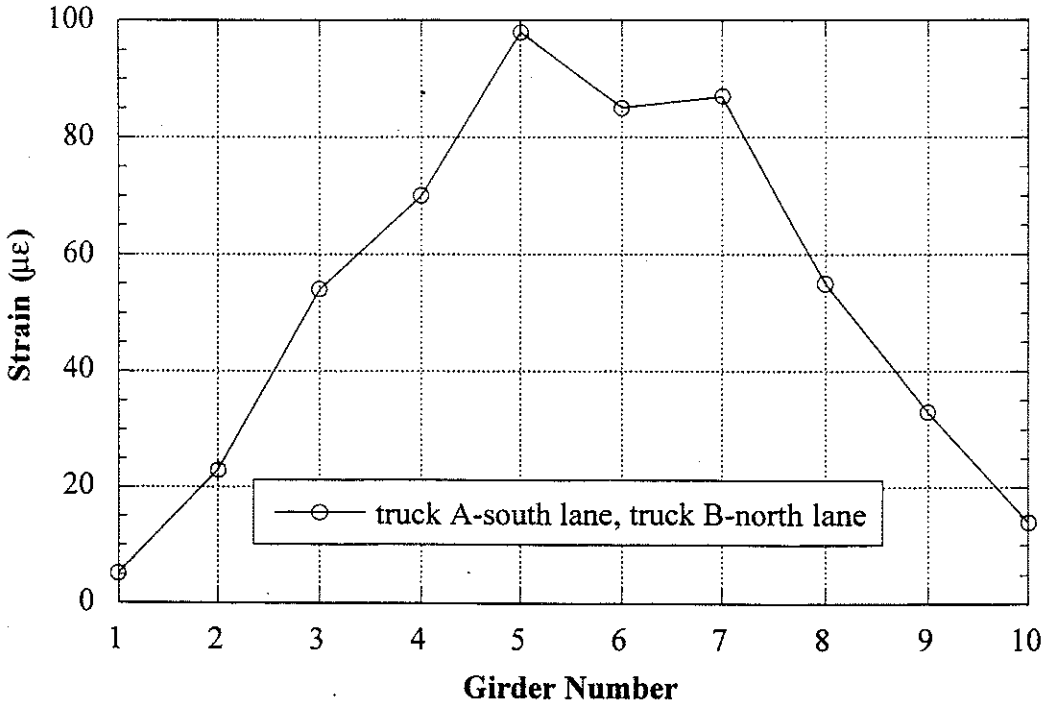

Figure 9.11 Strains under Side-by-Side Truck Loading at High Speed.

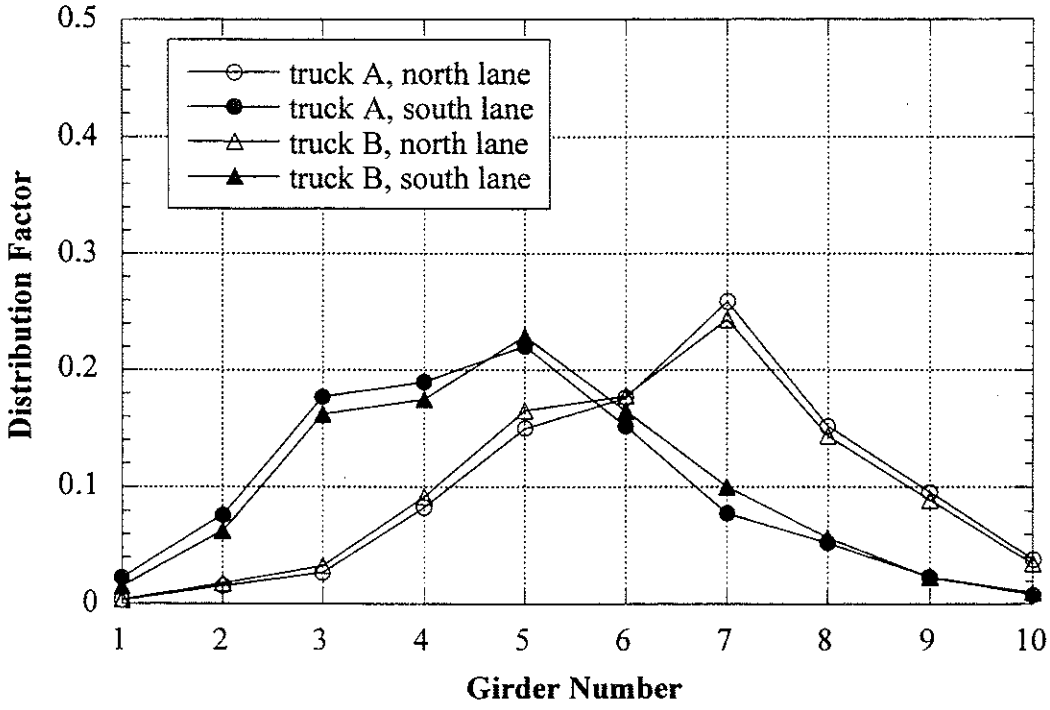

Figure 9.12 Distribution Factors for One Truck Loading at High Speed

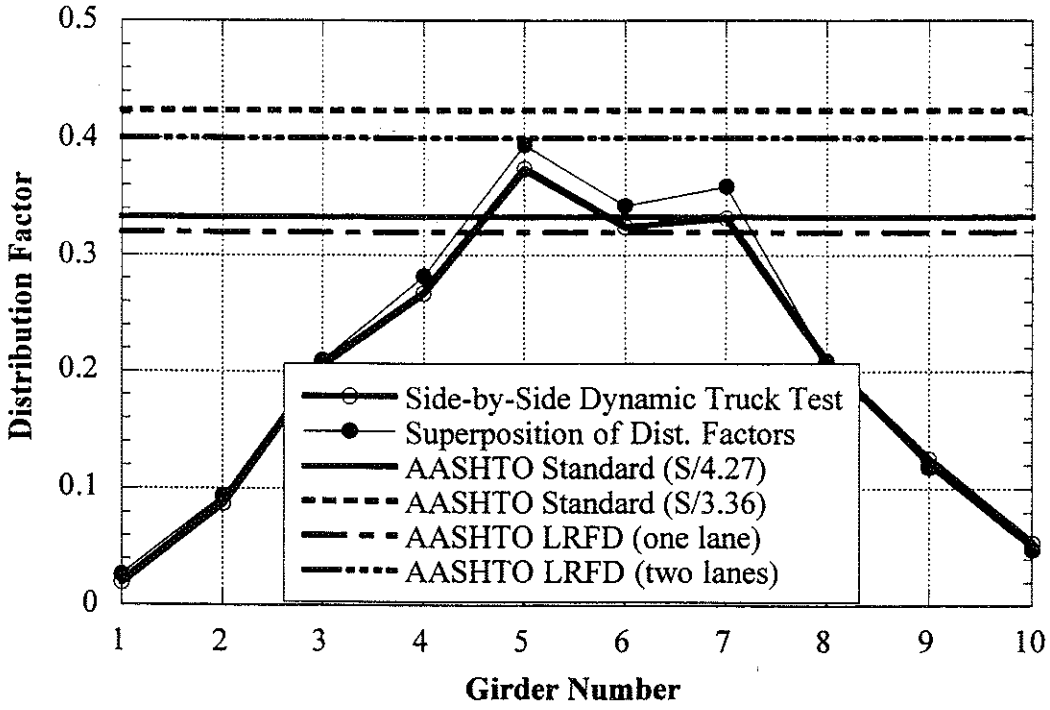

Figure 9.13 Comparison with Code Specified Distribution Factors at High Speed

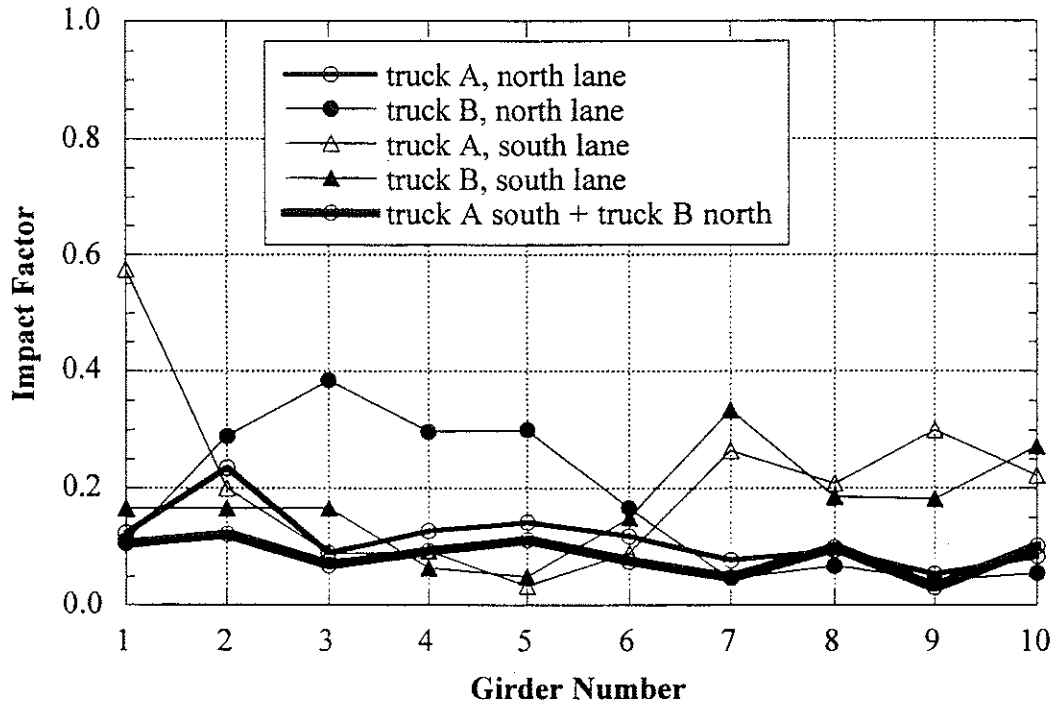

Figure 9.14 Impact Factors.

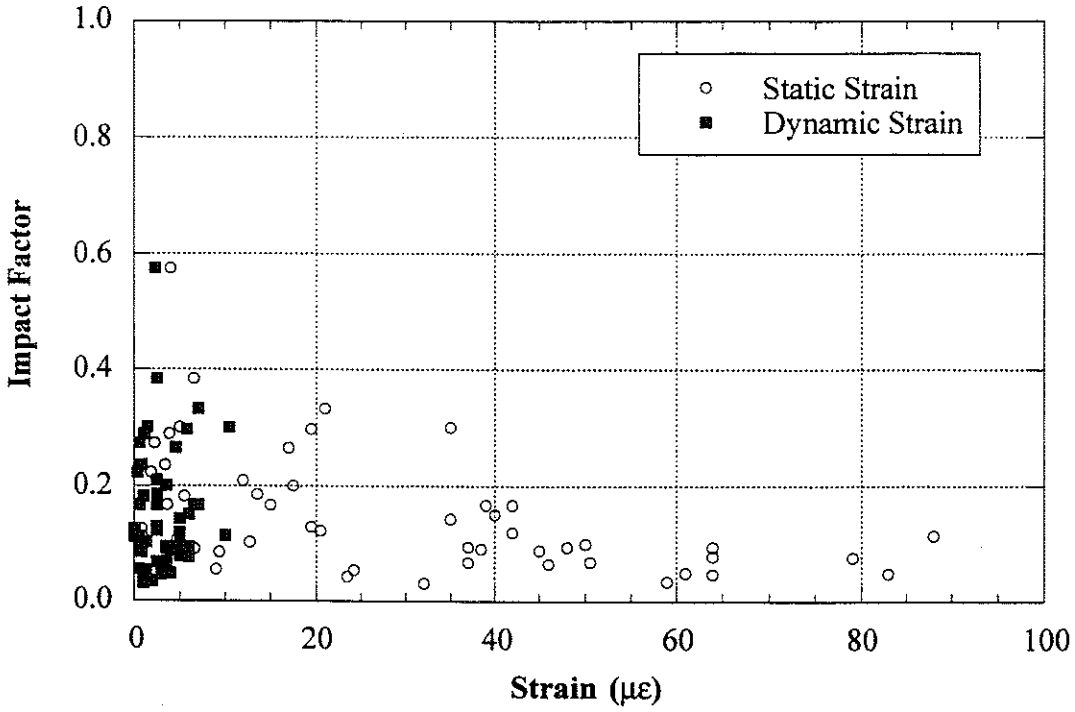

Figure 9.15 Strain versus Impact Factors.

Note:

Intentionally left blank

10. Summary and Conclusions

Five bridges were tested and the results are summarized as follows. Because all of the bridges tested are two lane bridges, traffic lanes are expressed in terms of left lane and right lane in figures 10.1-4. Specific lane orientations are shown in the figures.

Strains under a single truck are shown in Fig. 10.1 for vehicles moving at crawling speed in left lane, and in Fig. 10.2 for the right lane. The corresponding distribution factors are presented in Fig. 10.3 and 10.4. Strains caused by a single truck moving at high speed (40-60 km/h), are shown in Fig. 10.5. The corresponding distribution factors are plotted in Fig. 10.6. The envelopes of the distribution factors corresponding to a single truck are shown in Fig. 10.7.

For two trucks side-by-side at high speed (40-60 km/h), the strains are presented in Fig. 10.8. The measured strains due to two trucks at crawling speed are compared with the results of superposition of the effects of single trucks in Fig. 10.9. The distribution factors for two trucks are plotted in Fig. 10.10 for crawling speed and Fig. 10.11 for high speed. For comparison, the code specified distribution factors are also shown. The girder distribution factors for AASHTO (1996) are calculated as follows. In one lane steel girder and prestressed concrete girder bridges, GDF is:

$$GDF = \frac{S}{4.27} \tag{10-1}$$

and for multi lane steel and prestressed concrete girder bridges,

$$GDF = \frac{S}{3.36} \tag{10-2}$$

where S = girder spacing (m).

And for AASHTO LRFD (1994), the girder distribution factors are as follows. For moment in interior girders with multi-lane loading:

$$GDF = \left\{ 0.075 + \left(\frac{S}{2900} \right)^{0.6} \left(\frac{S}{L} \right)^{0.2} \left(\frac{K_g}{Lt_s^3} \right)^{0.1} \right\} \qquad (10\text{-}3)$$

and with one lane loading:

$$GDF = \left\{ 0.06 + \left(\frac{S}{4300} \right)^{0.4} \left(\frac{S}{L} \right)^{0.3} \left(\frac{K_g}{Lt_s^3} \right)^{0.1} \right\} \qquad (10\text{-}4)$$

where S = girder spacing (mm); L = span length (mm); $K_g = n(I + Ae_g^2)$; t_s = depth of concrete slab (mm); n = modular ratio between girder and slab materials; I = moment of inertia of the girder (mm^4); A = area of the girder (mm^2); e_g = distance between the center of gravity of the girder and slab (mm). Because the term $K_g/(Lt_s^3)$ implies more accuracy than exists for bridge evaluation, it is recommended that they be taken as 1.0. However, actual values of term $K_g/(Lt_s^3)$ are used to calculate girder distribution factors throughout this report.

Dynamic loads are also compared in Fig. 10.12. For two trucks side-by-side the dynamic load factor is shown as a thicker line. For exterior girders, the dynamic load factor is high, but it corresponds to a very low static load effect.

For comparison, the dynamic load factors are plotted vs. static strain in Fig. 10.13. It is clear that dynamic load factor decreases with increasing static load effect.

The measured maximum static strains are compared to calculated static strains in Table 10.1 for a single truck and in Table 10.2 for two trucks side-by-side. The calculated values are obtained using the maximum bending moment and the maximum GDF from the test results. Two cases are considered: (a) non-composite section, (b) composite section. Even assuming a composite action, the calculated strains are about twice larger than the maximum measured values. "Truck 1" indicates 11-axle truck or truck A for bridge B01-70041 and "Truck 2" indicates 10-axle truck or truck B for bridge B01-70041, respectively.

Table 10.1 Strains due to One Lane Loading

MDOT ID #	Maximum Strains from Test (10^{-6})	Calculated Maximum Strains (10^{-6})			
		Non-Composite Section		Composite Section	
		Truck 1	Truck 2	Truck 1	Truck 2
B02-46032	67.5	260.0	246.0	179.6	169.9
B05-46041	64.0	241.7	226.6	147.9	138.7
B02-12021	42.0	181.2	167.6	93.5	86.5
B02-38051	78.0	235.4	223.6	150.8	143.2
B01-70041	64.0	248.6	237.1	138.7	132.3
B02-12021(Proof Load)	72.0	302.5		156.2	

Table 10.2 Strains due to Two Lane Loading

MDOT ID #	Maximum Strains from Test (10^{-6})	Calculated Maximum Strains (10^{-6})					
		Non-Composite Section			Composite Section		
		Truck 1 & Truck 1	Truck 2 & Truck 2	Truck 1 & Truck 2	Truck1 & Truck 1	Truck 2 & Truck 2	Truck 1 & Truck 2
B02-46032	102.4	378.8	358.4	368.6	261.7	247.6	254.6
B05-46041	87.0	328.2	307.7	317.9	200.9	188.3	194.6
B02-12021	71.0	240.0	220.0	230.0	123.9	114.6	119.3
B02-38051	111.5	369.1	350.6	359.9	236.4	224.6	230.5
B01-70041	96.0	308.6	294.3	301.5	172.2	164.2	168.2
B02-12021 (Proof Load)	137.0	504.2			260.3		

The most important conclusions are:

(a) The observed response is linear, which is confirmed by superposition of truck effects. The comparison of strain values for a single truck indicates that for two trucks side-by-side tests, the results are equal to superposition of single truck results.

(b) The absolute value of measured strains is lower than expected. For a single truck, the maximum observed strain is less than 80 microstrains. This corresponds to 16 Mpa. For two trucks side-by-side, the maximum strain is 111 microstrains, which corresponds to 23 Mpa. The main reasons for low strains are: unintended composite action, partial fixity of supports and increased actual stiffness due to sidewalks, parapets and railings.

(c) Girder distribution factors observed in the tests are lower than AASHTO Standard (S/3.36) and LRFD (two lanes) GDF's. The maximum measured values for two trucks side-by-side tests were close to the specified values (S/3.36) in two bridges, and conservative for three bridges. However, the absolute values of stresses were rather low (less than 23 MPa).

(d) Dynamic load is lower than specified value by AASHTO (1996). For two trucks side-by-side it is about 0.10. Dynamic load decreases with increasing static load effect.

(e) Proof load test performed on Bridge US12/SC (B02-12021) confirmed that the bridge is adequate to carry the normal truck traffic. The measured deflections and strains were relatively low, and considerably lower than expected.

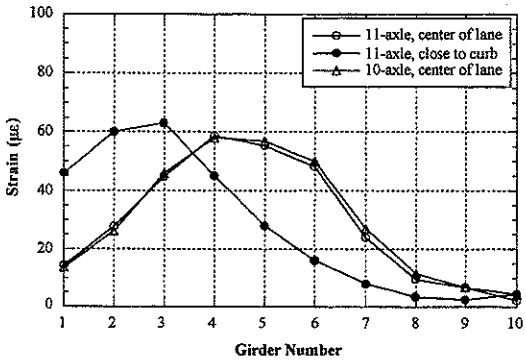

M156/SC, Morenci (B02-46032)

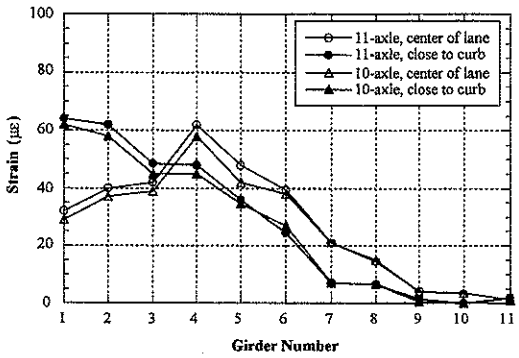

M34/RR, Adrian (B05-46041)

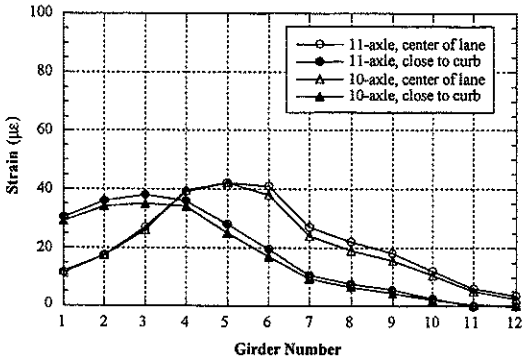

US12/SC, Bronson (B02-12021)

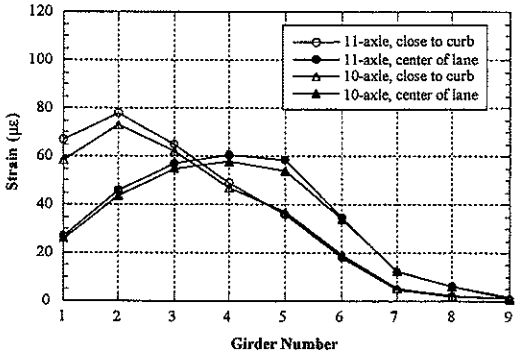

M106/PRD, Munith (B02-38051)

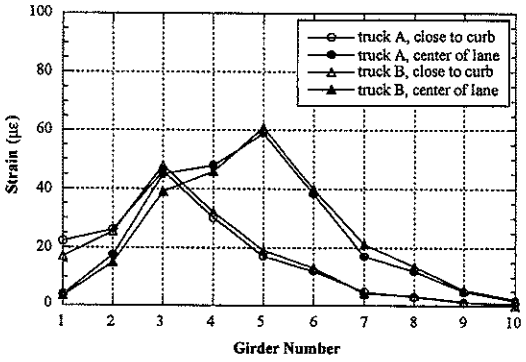

M45/BR, Grand Rapids (B01-70041)

Lane Orientations for Figure 10.1	
B02-46032	West Lane
B05-46041	North Lane
B02-12021	South Lane
B02-38051	South Lane
B01-70041	South Lane

Figure 10.1 Strains under Left Lane Loading at Crawling Speed

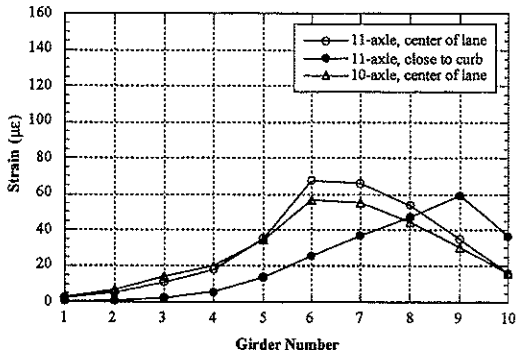

M156/SC, Morenci (B02-46032)

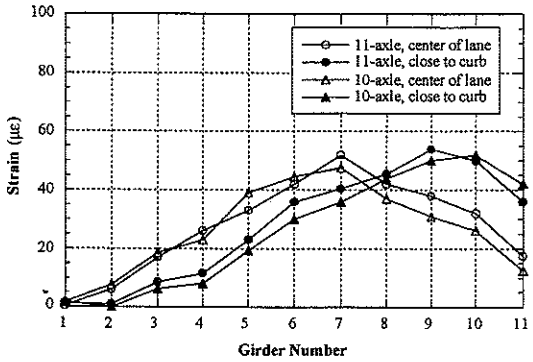

M34/RR, Adrian (B05-46041)

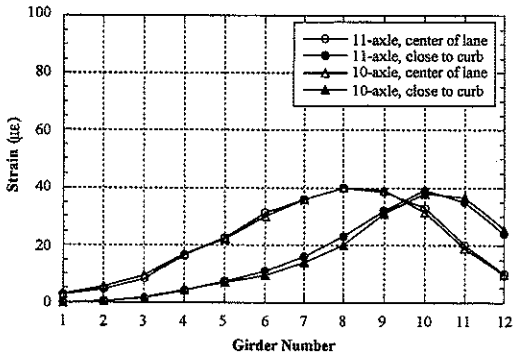

US12/SC, Bronson (B02-12021)

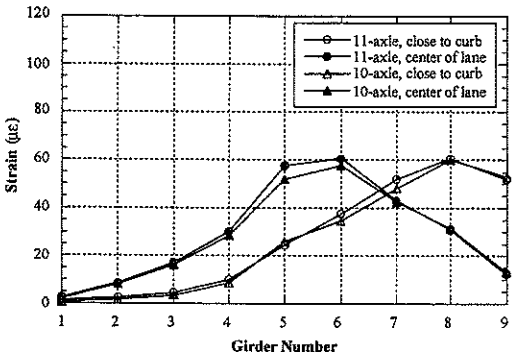

M106/PRD, Munith (B02-38051)

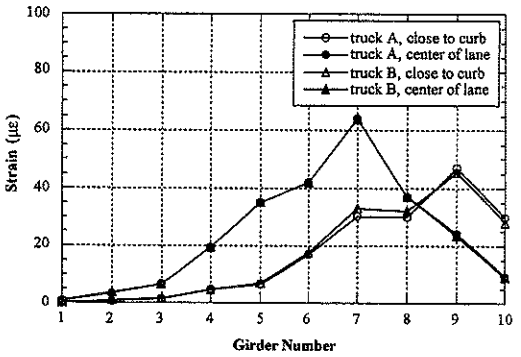

M45/BR, Grand Rapids (B01-70041)

Lane Orientations for Figure 10.2	
B02-46032	East Lane
B05-46041	South Lane
B02-12021	North Lane
B02-38051	North Lane
B01-70041	North Lane

Figure 10.2 Strains under Right Lane Loading at Crawling Speed

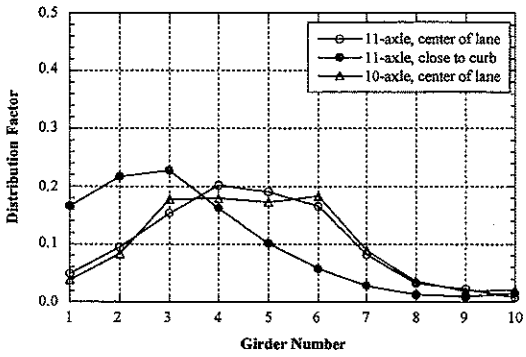

M156/SC, Morenci (B02-46032)

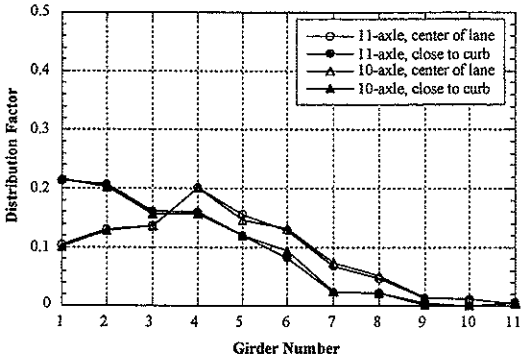

M34/RR, Adrian (B05-46041)

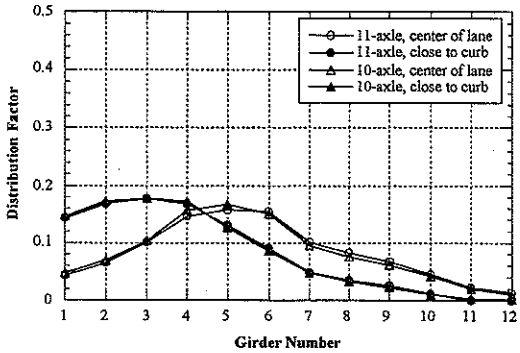

US12/SC, Bronson (B02-12021)

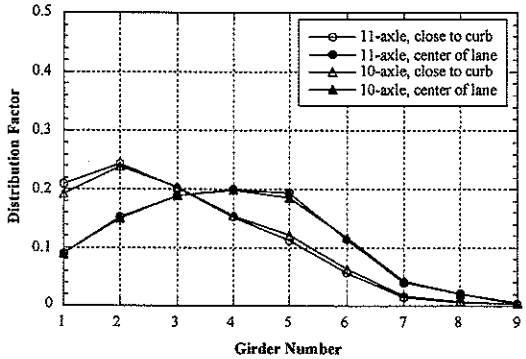

M106/PRD, Munith (B02-38051)

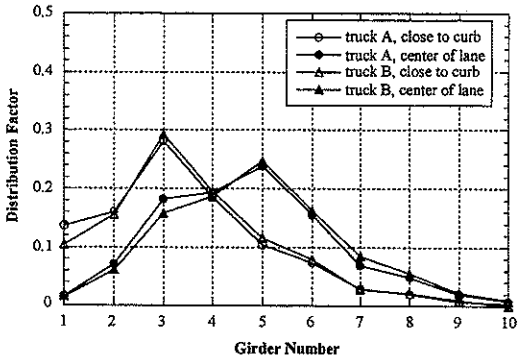

M45/BR, Grand Rapids (B01-70041)

Lane Orientations for Figure 10.3	
B02-46032	West Lane
B05-46041	North Lane
B02-12021	South Lane
B02-38051	South Lane
B01-70041	South Lane

Figure 10.3 Distribution Factors under Left Lane Loading at Crawling Speed

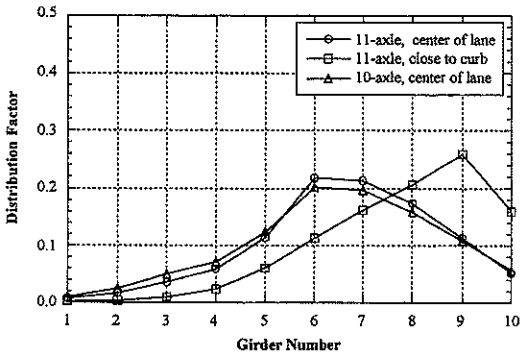

M156/SC, Morenci (B02-46032)

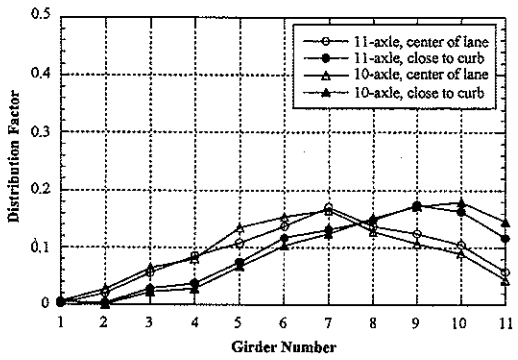

M34/RR, Adrian (B05-46041)

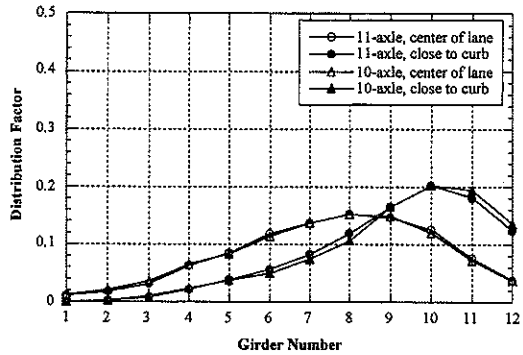

US12/SC, Bronson (B02-12021)

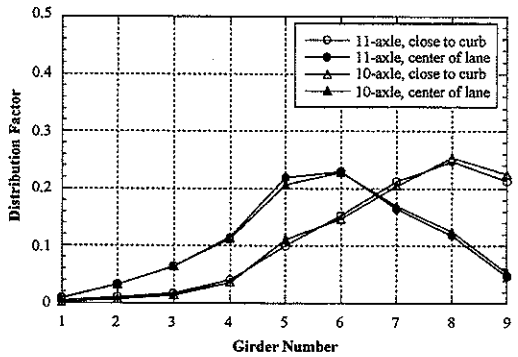

M106/PRD, Munith (B02-38051)

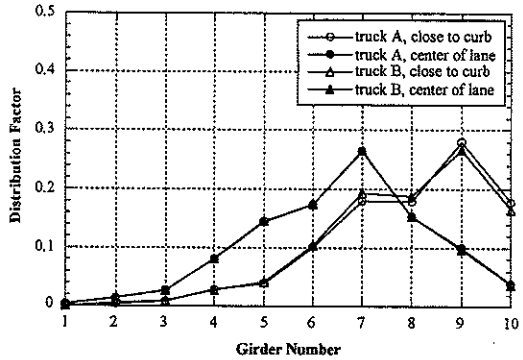

M45/BR, Grand Rapids (B01-70041)

Lane Orientations for Figure 10.4	
B02-46032	East Lane
B05-46041	South Lane
B02-12021	North Lane
B02-38051	North Lane
B01-70041	North Lane

Figure 10.4 Distribution Factors under Right Lane Loading at Crawling Speed

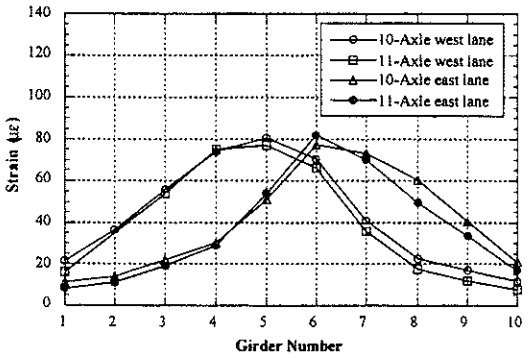

M156/SC, Morenci (B02-46032)

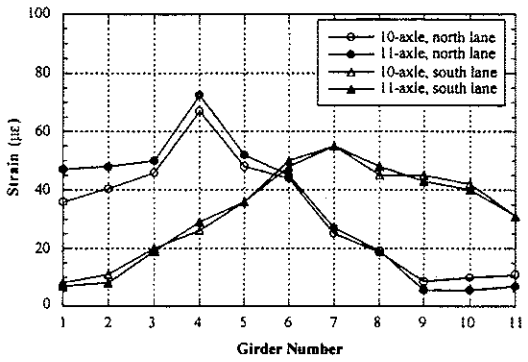

M34/RR, Adrian (B05-46041)

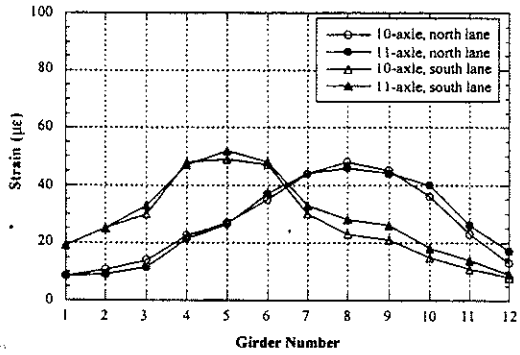

US12/SC, Bronson (B02-12021)

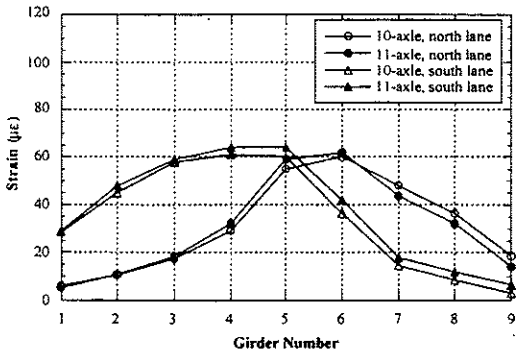

M106/PRD, Munith (B02-38051)

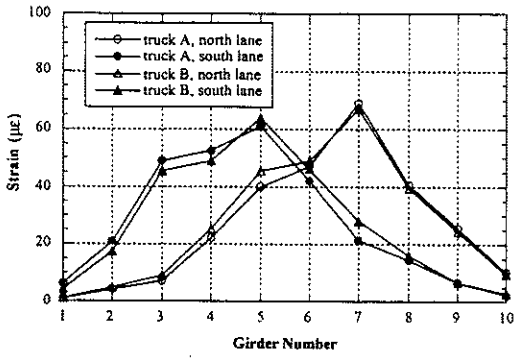

M45/BR, Grand Rapids (B01-70041)

Figure 10.5 Strains under One Truck Loading at High Speed

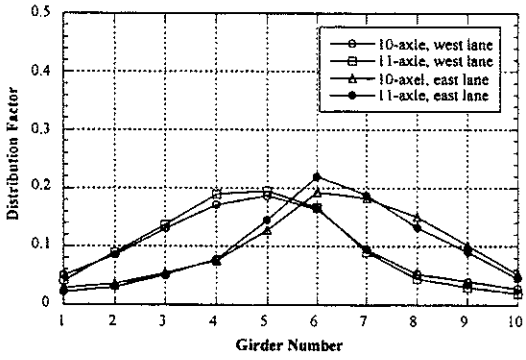

M156/SC, Morenci (B02-46032)

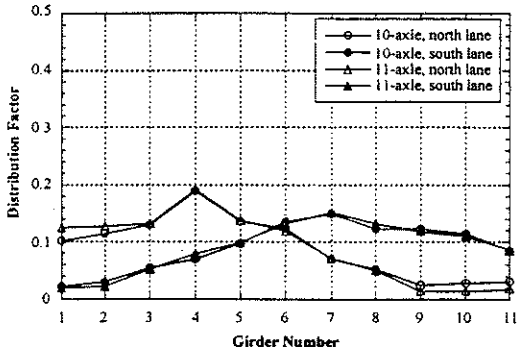

M34/RR, Adrian (B05-46041)

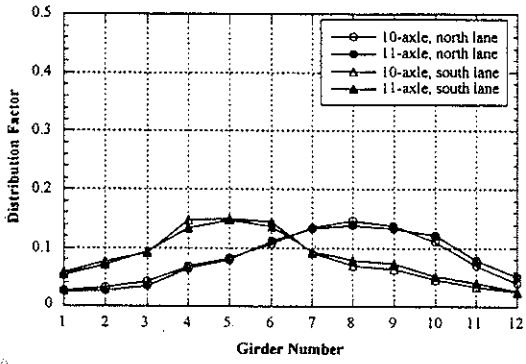

US12/SC, Bronson (B02-12021)

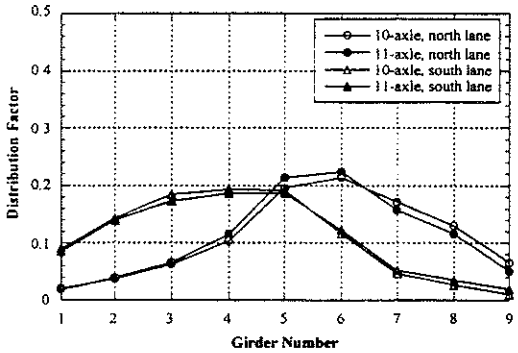

M106/PRD, Munith (B02-38051)

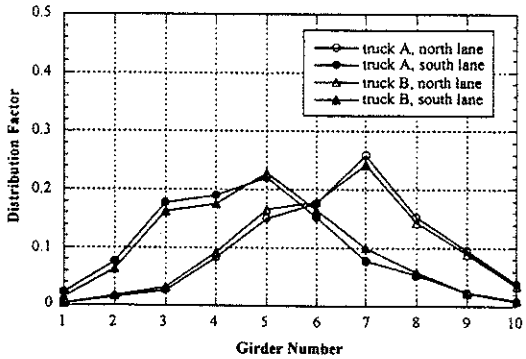

M45/BR, Grand Rapids (B01-70041)

Figure 10.6 Distribution Factors under One Truck Loading at High Speed

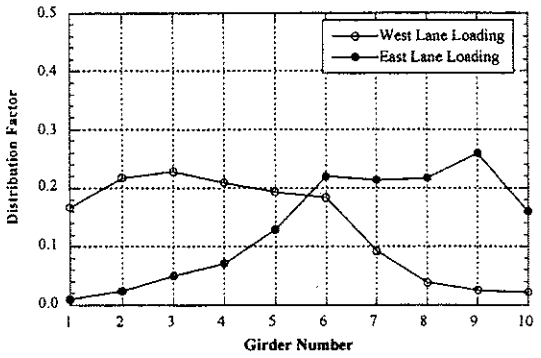

M156/SC, Morenci (B02-46032)

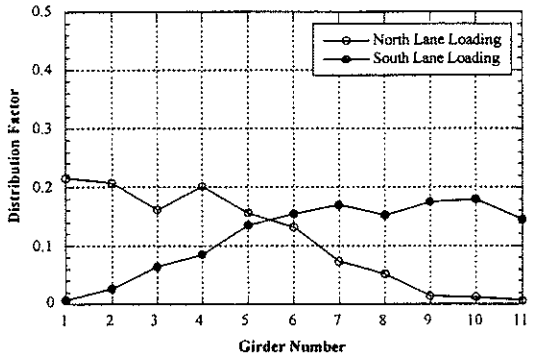

M34/RR, Adrian (B05-46041)

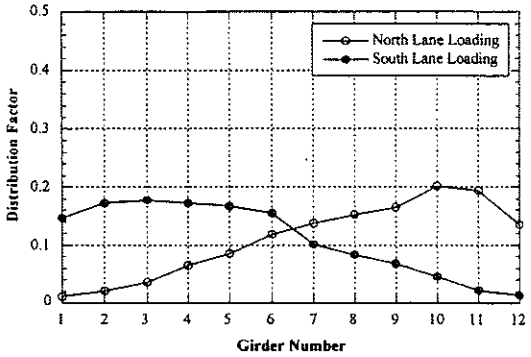

US12/SC, Bronson (B02-12021)

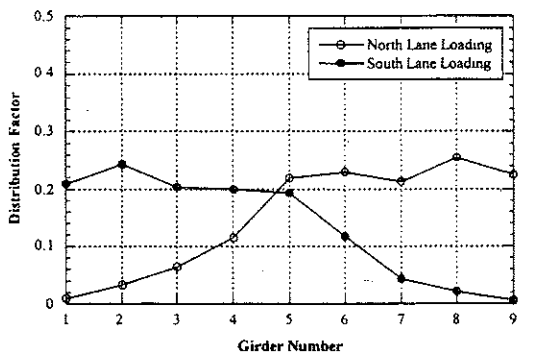

M106/PRD, Munith (B02-38051)

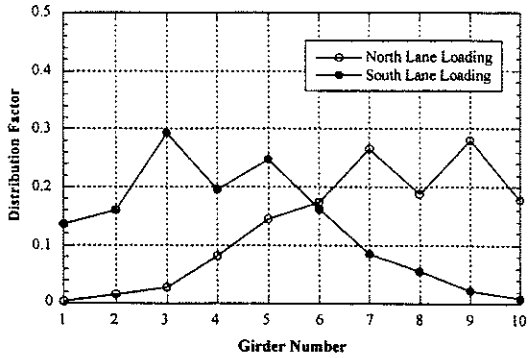

M45/BR, Grand Rapids (B01-70041)

Figure 10.7 Envelopes of Girder Distribution Factors For One Truck Loading at Crawling Speed

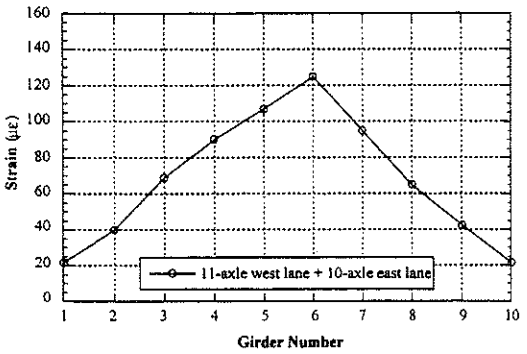

M156/SC, Morenci (B02-46032)

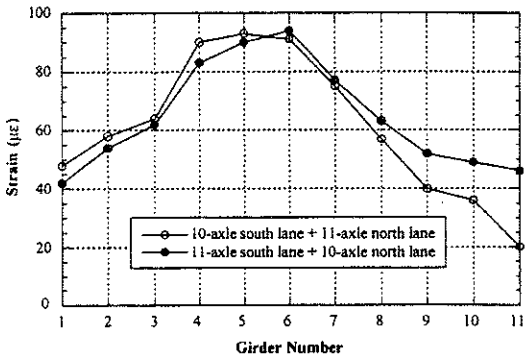

M34/RR, Adrian (B05-46041)

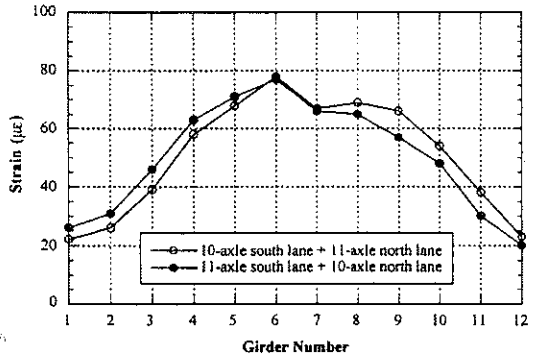

US12/SC, Bronson (B02-12021)

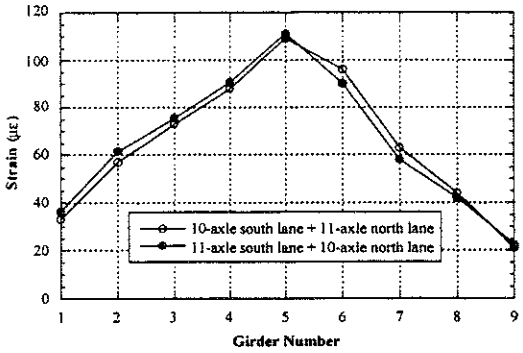

M106/PRD, Munith (B02-38051)

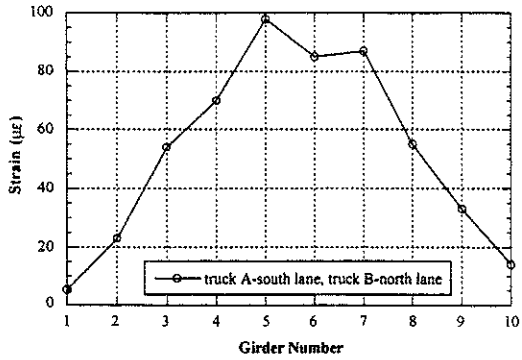

M45/BR, Grand Rapids (B01-70041)

Figure 10.8 Strains under Side-by-Side Truck Loading at High Speed

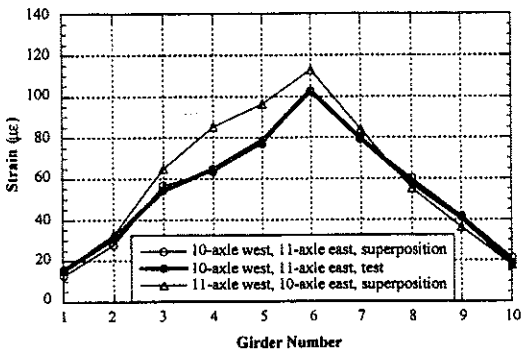

M156/SC, Morenci (B02-46032)

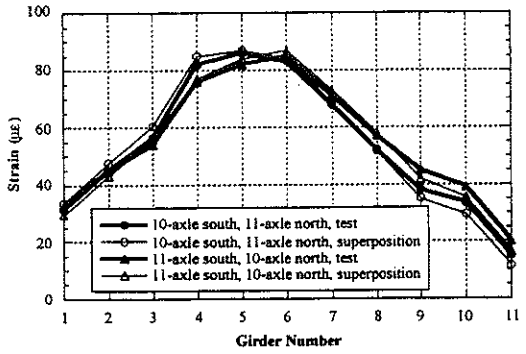

M34/RR, Adrian (B05-46041)

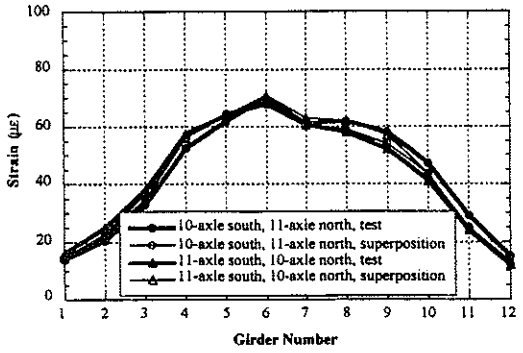

US12/SC, Bronson (B02-12021)

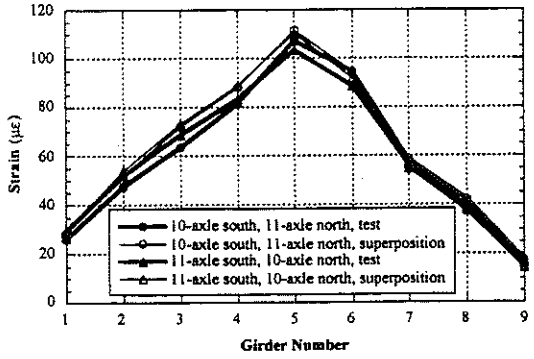

M106/PRD, Munith (B02-38051)

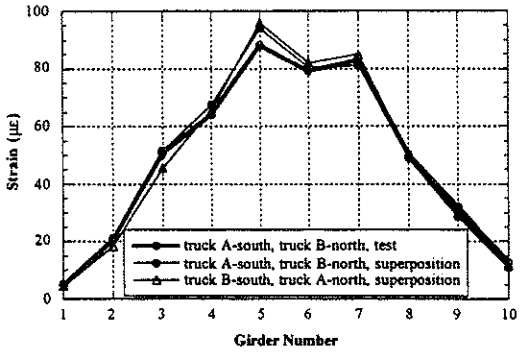

M45/BR, Grand Rapids (B01-70041)

Figure 10.9 Strains under Side-by-Side Truck Loading at Crawling Speed

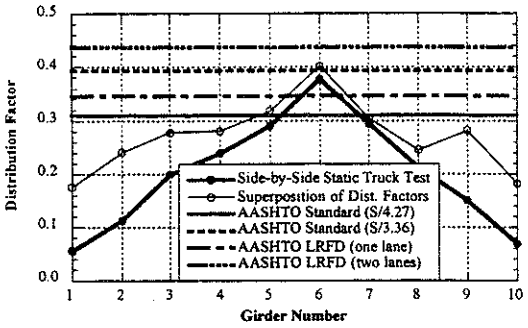

M156/SC, Morenci (B02-46032)

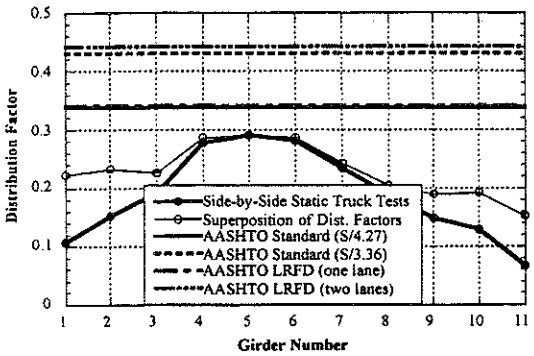

M34/RR, Adrian (B05-46041)

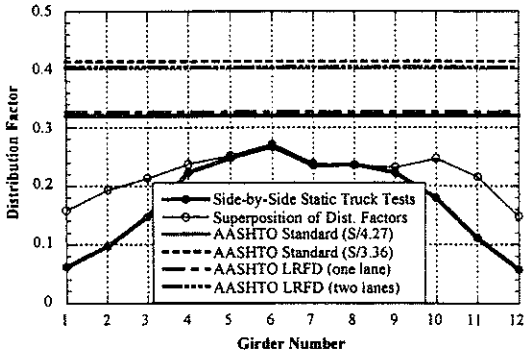

US12/SC, Bronson (B02-12021)

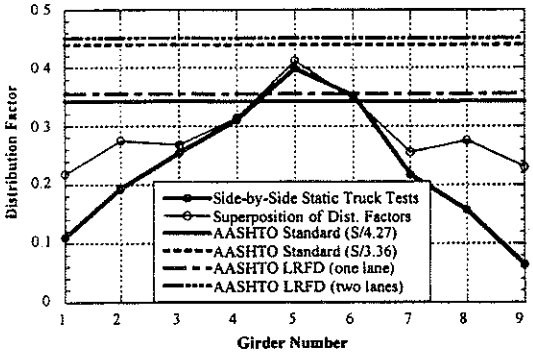

M106/PRD, Munith (B02-38051)

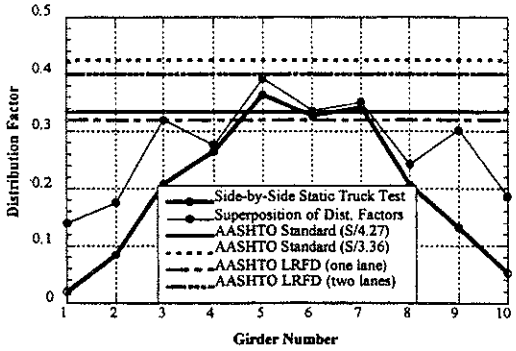

M45/BR, Grand Rapids (B01-70041)

Figure 10.10 Comparison with Code Specified Distribution Factors at Crawling Speed

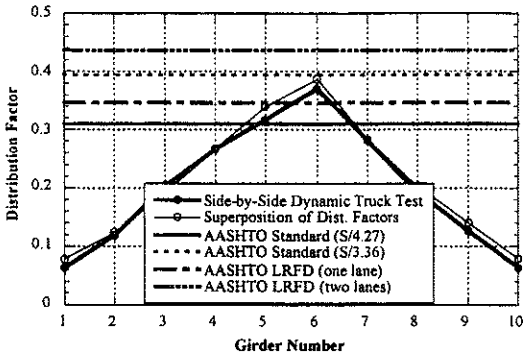

M156/SC, Morenci (B02-46032)

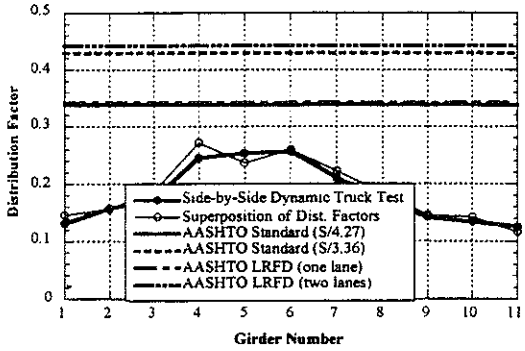

M34/RR, Adrian (B05-46041)

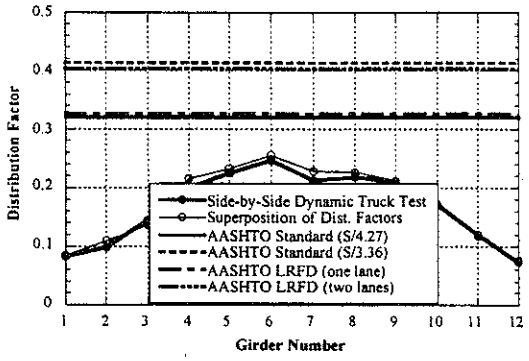

US12/SC, Bronson (B02-12021)

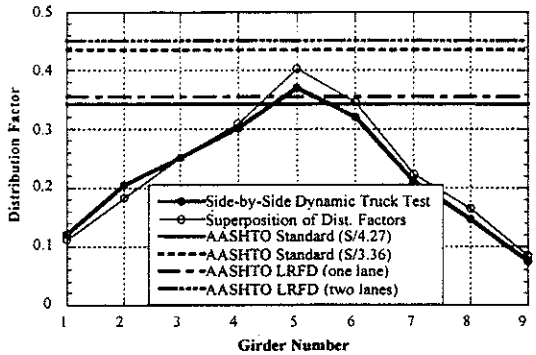

M106/PRD, Munith (B02-38051)

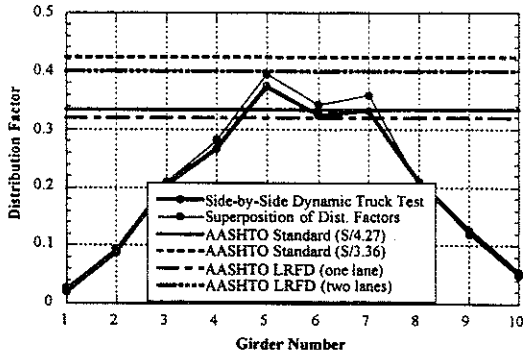

M45/BR, Grand Rapids (B01-70041)

Figure 10.11 Comparison with Code Specified Distribution Factors at High Speed

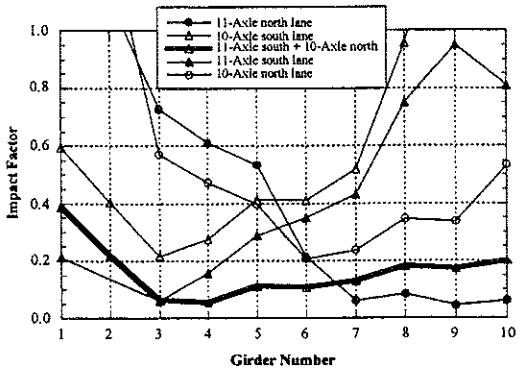

M156/SC, Morenci (B02-46032)

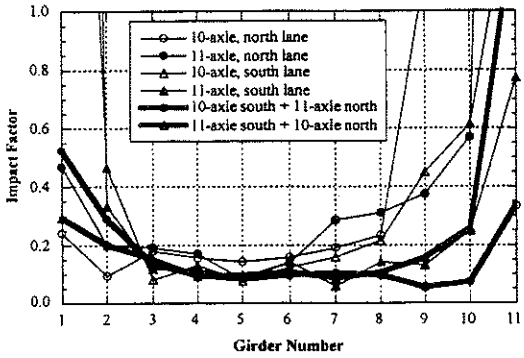

M34/RR, Adrian (B05-46041)

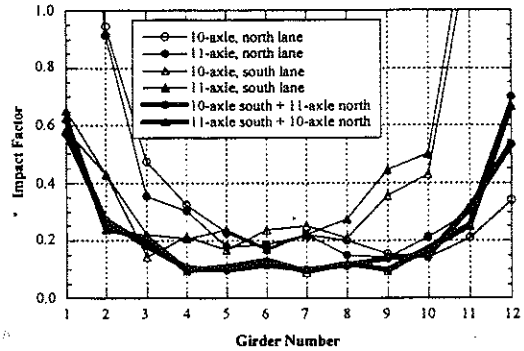

US12/SC, Bronson (B02-12021)

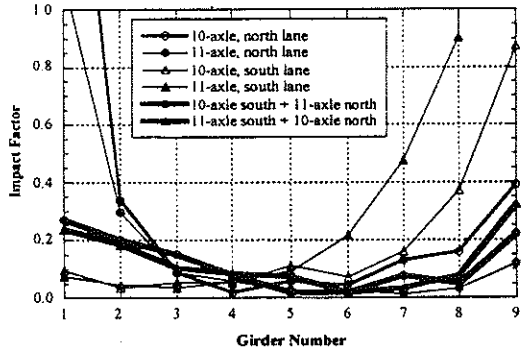

M106/PRD, Munith (B02-38051)

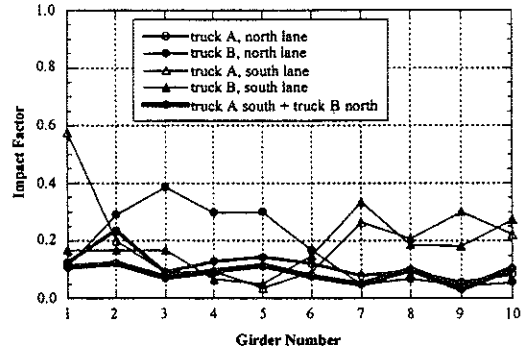

M45/BR, Grand Rapids (B01-70041)

Figure 10.12 Impact Factors

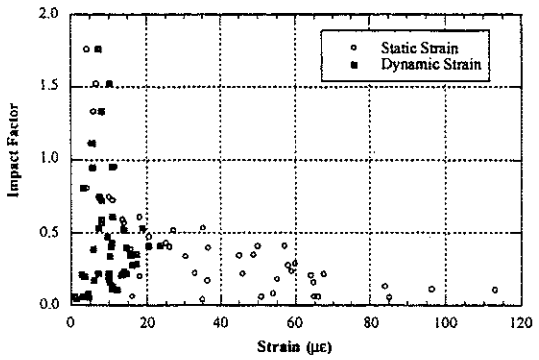

M156/SC, Morenci (B02-46032)

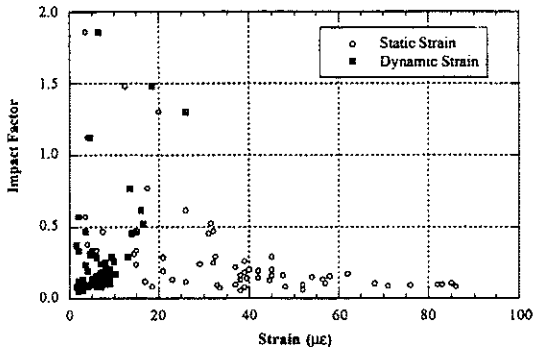

M34/RR, Adrian (B05-46041)

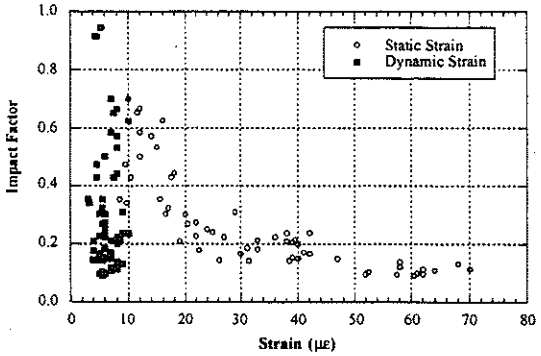

US12/SC, Bronson (B02-12021)

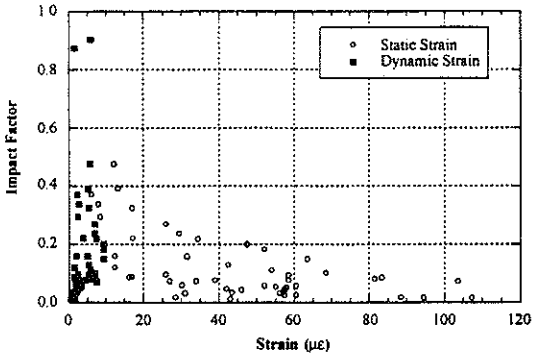

M106/PRD, Munith (B02-38051)

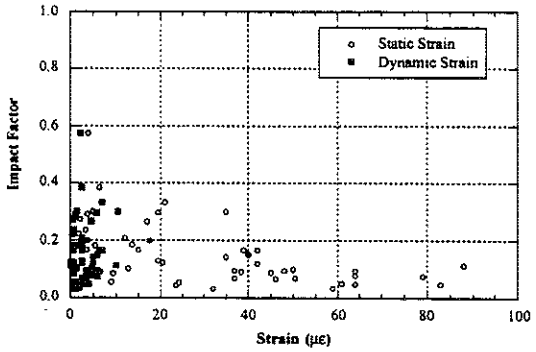

M45/BR, Grand Rapids (B01-70041)

Figure 10.13 Strains Versus Impact Factors

Note:

Intentionally left blank

11. References

1. *AASHTO Standard Specifications for Highway Bridges*, American Association of State and Transportation Officials, Washington, DC, 1996.

2. *AASHTO LRFD Bridge Design Specifications*. American Association of State Highway and Transportation Officials, Washington, D.C., 1994.

3. *AASHTO Guide Specifications for Distribution of Loads for Highway Bridges*, American Association of State Highway and Transportation Officials, Washington, D.C., 1994.

4. Bakht, B., and Pinjarkar, S.G., "Dynamic Testing of Highway Bridges-A Review." Transportation Research Record 1223, Transportation Research Board, National Research Council, Washington, D.C., pp. 93-100, 1989.

5. Ghosn, M., Moses, F., and Gobieski, J., "Evaluation of Steel Bridges Using In-Service Testing." Transportation Research Record 1072, Transportation Research Board, National Research Council, Washington, D.C., pp. 71-78, 1986.

6. Hwang, E.S., and Nowak, A.S., "Simulation of Dynamic Load for Bridges." Journal of Structural Engineering, ASCE, Vol. 117, No.5, pp.1413-1434, July, 1991.

7. Lichtenstein, A. G., *Bridge Rating Through Nondestructive Load Testing*, NCHRP Report 12-28(13) A, June 1993.

8. Nassif, H.H. and Nowak, A.S., "Dynamic Load Spectra for Girder Bridges." Transportation Research Record 1476, Transportation Research Board, National Research Council, Washington, D.C., pp. 69-83, 1995.

9. Nowak, A.S., Laman, J.A., and Nassif H., "Effect of Truck Loading on Bridges." Report UMCE 94-22. Department of Civil and Environmental Engineering, University of Michigan, Ann Arbor, 1994

10. Paultre, P., Chaallal, O., and Proulx, J., "Bridge Dynamics and Dynamic Amplification Factors-A Review of Analytical and Experimental Findings." Canadian Journal of Civil Engineering, Vol. 19, pp. 260-278, 1992.

11. Stallings, J.M., and Yoo, C.H., "Tests and Ratings of Short-Span Steel Bridges." Journal of Structural Engineering, ASCE, Vol. 119, No. 7, pp. 2150-2168, July, 1993.

12. Zokaie, T., Osterkamp, T.A., and Imbsen, R.A., *Distribution of Wheel Loads on Highway Bridges*, National Cooperative Highway Research Program Report 12-26, Transportation Research Board, Washington, D.C., 1991

UMCEE 98-13 June 1998

DEVELOPMENT OF A GUIDE FOR EVALUATION OF EXISTING BRIDGES PART II

PROJECT 97-0245 DIR

Report submitted to the Michigan Department of Transportation

Andrzej S. Nowak, Ahmet K. Sanli, Sangjin Kim, Chris Eamon and Junsik Eom

Department of Civil and Environmental Engineering
University of Michigan
Ann Arbor, Michigan 48109-2125

Testing and Research Section
Construction and Technology Division
Research Project No. RC-1362
Part II

This report, authorized by the transportation director, has been prepared to provide technical information and guidance for personnel in the Michigan Department of Transportation, the FHWA, and other reciprocating agencies. The cost of publishing 40 copies of this report at $5.96 per copy is $238.26 and it is printed in accordance with Executive Directive 1991-6.

Technical Report Documentation Page

1. Report No. Research Report RC-1362	2. Government Accession No.	3. Recipient's Catalog No.
4. Title and Subtitle Development of a Guide for Evaluation of Existing Bridges, Part II		5. Report Date May 1998
7. Author(s) Andrzej S. Nowak, Ahmet Sanli, Sangjin Kim and Chris Eamon		6. Performing Organization Code
9. Performing Organization Name and Address University of Michigan 2340 G. G. Brown Bldg. Ann Arbor, MI 48109-2125		8. Performing Org Report No. RC-1362
12. Sponsoring Agency Name and Address Michigan Department of Transportation Construction and Technology Division P.O. Box 30049 Lansing, MI 48909		10. Work Unit No. (TRAIS)
		11. Contract/Grant No. 97-0245 DIR
15. Supplementary Notes		13. Type of Report & Period Covered Final Report, 5-97/5-98
		14. Sponsoring Agency Code

16. Abstract

The objective of this report is to describe the procedures for evaluation of existing bridges using field testing. The procedures are based on test program performed by the research team at the University of Michigan in 1989-98, sponsored by the Michigan Department of Transportation (MDOT). Diagnostic and proof load tests are considered, including: (a) weigh-in-motion of truck loads and axle loads on bridges; (b) measurement of dynamic loads due to traffic; (c) measurement of fatigue load spectra; (d) verification of girder distribution factors (for live load); (e) verification of the minimum resistance by proof loading. The report can serve as a guide for field testing procedures. It includes the description of equipment, installation procedures, calibration of equipment, operation of equipment, measurement, and processing and interpretation of results. Diagnostic tests can be performed to verify the distribution of load, identify the critical components and sections, and explain inadequate performance (e.g. excessive vibration). The objective of the proof load tests is to determine the lower bound (minimum) of capacity of the tested structure. The procedures were verified on selected bridges. Field testing equipment include the data acquisition systems available at the University of Michigan and some new remote sensing devices.

17. Key Words Bridges, evaluation, field testing, proof load, weigh-in-motion, load distribution	18. Distribution Statement No restrictions. This document is available to the public through the Michigan Department of Transportation.		
19. Security Classification (report) Unclassified	20. Security Classification (Page) Unclassified	21. No of Pages	22. Price

Form DOT F 1700.7 (8-72)

DISCLAIMER

The contents of this report reflect the views of the authors, who are responsible for the facts and the accuracy of the information presented herein. This document is disseminated under the sponsorship of the Michigan Department of Transportation and Great Lakes Center for Truck Transportation Research at the University of Michigan Transportation Research Institute, in the interest of information exchange. The Michigan Department of Transportation assumes no liability for the contents or use thereof.

TABLE OF CONTENTS

Acknowledgments

The presented research has been sponsored by the Michigan Department of Transportation, and the Great Lakes Center for Truck and Transit Research (GLCTTR) at the University of Michigan which is gratefully acknowledged. The authors thank the technical staff of the Michigan DOT, Roger Till, Sonny Jadun, Sudhakar Kulkarni, and David Juntunen, for their useful comments, discussions and support, and Thomas Gillespie, of the University of Michigan Transportation Research Institute (UMTRI) for his support.

The project team received help from other researchers, current and former students and staff of the University of Michigan. In particular, thanks are due to Dr. Vijay Saraf and Chan-Hee Park.

Note:

Intentionally left blank

1. Introduction

The research work carried out as a part of this project is documented in two reports: Part I and Part II. The objective Part I is to present the results of the field tests carried out in 1997. The objective of this report, Part II, is to describe the procedures for evaluation of existing bridges using analytical methods and field testing. The procedures are based on test program performed by the research team at the University of Michigan in 1989-98, sponsored by the Michigan Department of Transportation (MDOT). Diagnostic and proof load tests are considered, including:

- Weigh-in-motion of truck loads and axle loads on bridges
- Measurement of dynamic loads due to traffic
- Measurement of fatigue load spectra
- Verification of girder distribution factors (for live load)
- Verification of the minimum resistance by proof loading.

A rational bridge management requires a good knowledge of the actual loads, load distribution, load effects and structural condition (load carrying capacity). Therefore, evaluation of existing structures is very important. Furthermore, MDOT is introducing the new bridge management system, PONTIS. Efficient management will depend even more on reliable data on loads and resistance. Yet, there is a considerable number of bridges which are very difficult, if not impossible, to evaluate using traditional inspection methods and analysis. For example, this applies to many deteriorated structures (severe corrosion, cracking), and those for which the documentation is missing. It also may apply to structures showing difficult to explain behavior (excessive vibration, deflection, accelerated deterioration, and so on).

Field testing is an increasingly important topic in the effort to deal with the deteriorating infrastructure, in particular bridges and pavements. There is a need for accurate and inexpensive methods for diagnostics, verification of load distribution and determination of the actual load carrying capacity. There is a growing need for developing efficient procedures for evaluation of the actual load spectra, load distribution, actual strength and predict the remaining life of the structure. Therefore, this project is focused on the development of efficient procedures for bridge evaluation and diagnostics, including both analytical methods and field testing.

Accuracy of bridge evaluation can be improved by using the recent developments in bridge diagnostics, structural tests, material tests, and structural analysis. Advanced diagnostic procedures can be applied to evaluation of the current capacity of the structure, monitoring of load and resistance history and evaluation of the accumulated damage. Full scale bridge tests provide very useful information about the structural behavior. There is a need for significantly more test data, covering various bridge types. However, extensive test programs are very costly. Therefore, a considerable effort should be directed towards evaluation and improvement of the current analytical methods, on the basis of available test data.

A considerable number of Michigan bridges were constructed in 1950's and 1960's. Many of them showed signs of deterioration. In particular, there is a severe corrosion on many steel and concrete structures. By analytical methods, many of these bridges are not adequate to carry the normal highway traffic. However, the actual load carrying capacity is often much higher than what can be determined by analysis, due to more favorable load sharing, effect of non-structural components (parapets, railing, sidewalks), and other difficult to quantify factors. Field testing, in particular proof load testing can

reveal the hidden strength reserve and thus verify the adequacy of the bridge.

Field testing must be proceeded by analytical evaluation of the bridge. The basic steps are summarized for calculation of the actual load carrying capacity of steel girder bridges, reinforced concrete T-beams, and prestressed concrete girders (AASHTO type). Load components are also evaluated using the current Michigan Guide for Bridge Analysis.

Selection of bridges for field testing is based on several considerations including accessibility for equipment, possible interruption for traffic flow, span length, material, degree of deterioration, and MDOT repair schedule. The study utilizes the available knowledge and data regarding the methodology, structural behavior (material properties, member resistance) and bridge loads. An important consideration in field testing is traffic control. There is a need for testing methods which do not require closure of the bridge or even a lane. However, it may not be feasible in all anticipated situations.

For each type of test, the Guide for Evaluation of Existing Bridges provides the description of the testing procedure, required equipment, installation of equipment, measurement procedures, and processing and presentation of the results.

Note:
Intentionally left blank

2. Analytical Evaluation

2.1. Required Input Data

Prior to field testing, the considered bridge must be evaluated analytically using the available design drawings and calculations. This evaluation is also required for a rating analysis. If the documentation is lost or incomplete, then there is a need for a visual inspection and some field measurements.

The field investigation is absolutely necessary to determine the current condition of the bridge, even if the design drawings and calculations are available. The needed information to get either from the plans or a field investigation is as follows:

- structural system of the bridge and geometry, including:
  - number of spans and span lengths
  - skew
  - deck type, thickness, and amount of reinforcement
  - structural system (simple spans, continuous)
  - wearing surface (type and thickness)
  - girder properties (spacing, dimensions, reinforcement, composite action, haunch depth)
  - transverse member properties (types, locations)
  - sidewalk, curb, and railing presence
- material properties - of the wearing surface, deck, and girders
- supports - type (simple, fixed, others) and bearing material (steel, elastomeric)
- deterioration
  - deck (cracks, holes, spalling)
  - girders; cracks (location, lengths, and widths), and corrosion (location, patterns)

misalignment and movement at joints and bearings
condition of expansion joints
unusual thermal movements
condition of approaches

- other factors which may effect load testing

Data obtained from the field investigation and review of available records can be used to calculate the load capacity of the bridge; to identify critical structural elements, including connection details, and their load capacities; and to evaluate the presence of conditions which may enhance the response of the bridge to applied loads.

2.2. Loads

The basic load combination for highway bridges is a simultaneous occurrence of dead load, live load and dynamic load. This combination is used for the evaluation of existing bridges.

2.2.1. Dead Load

Dead load, D, is the gravity load due to the self weight of the structural and non structural elements permanently connected to the bridge. D can be described as:

$$D = D_1 + D_2 + D_3 + D_4 \qquad (2\text{-}1)$$

where:

D_1 = weight of factory made elements (steel, precast concrete members),

D_2 = weight of cast-in-place concrete members,

D_3 = weight of the wearing surface (e.g. asphalt),

D_4 = miscellaneous weight (e.g. railing, luminaries).

If it is not possible to find exact value of the asphalt thickness, its average value may be taken as 80 mm. The weight of components which are not continuously distributed on the bridge, such as the sidewalk, parapet, railing, and diaphragms, can be assumed uniformly distributed on the bridge surface.

2.2.2. Live Loads

Live load (L) covers a range of forces produced by vehicles moving on the bridge. Traditionally, the static and dynamic effects are considered separately. Therefore, in this section, L covers only the static component.

Generally, the number of design lanes should be determined by taking the integer part of the ratio w/3600, where w is the clear roadway width in mm between curbs and/or barriers.

Three live load models can be considered:

- MS18 or MS23 specified by the Michigan Design Manual: Bridge Design
- HL-93 specified by AASHTO LRFD Code (1994)
- Michigan Legal Loads

The MS18 loading consists of a tractor truck with semi-trailer or the corresponding lane load as illustrated in Fig 2-1. The variable axle spacing should be adjusted to get the maximum moment. MS23 loading is 125% of MS18 loading.

The HL-93 loading consists of a combination of the design truck or design tandem, and design lane load, as shown in Fig. 2-2. The midspan moment due to HL-93 is about 1.25 MS18 for 10 m span, 1.5 MS18 for 25 m span, and 1.75 MS18 for 50 m span. For continuous

bridges, the negative moment is calculated using a uniform load and two trucks. The resulting moment is reduced by 10%. Note, however, that this live load is not currently used by MDOT.

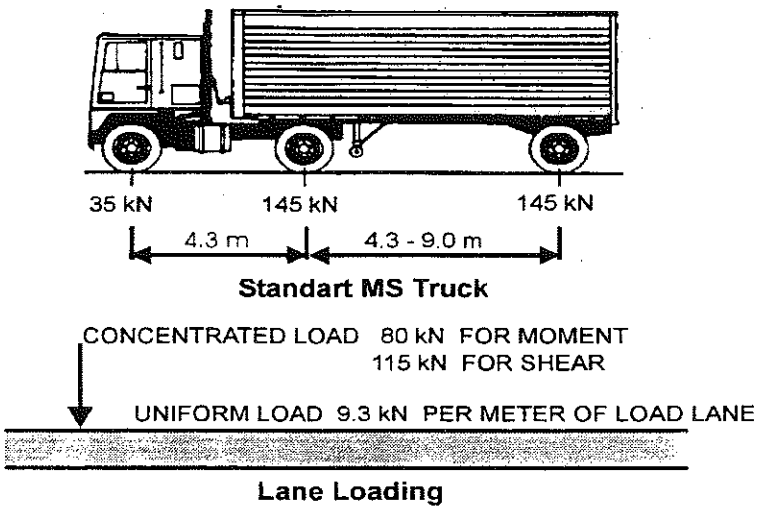

Fig. 2-1. Design Live Load MS18 in the Michigan Design Manual (1992).

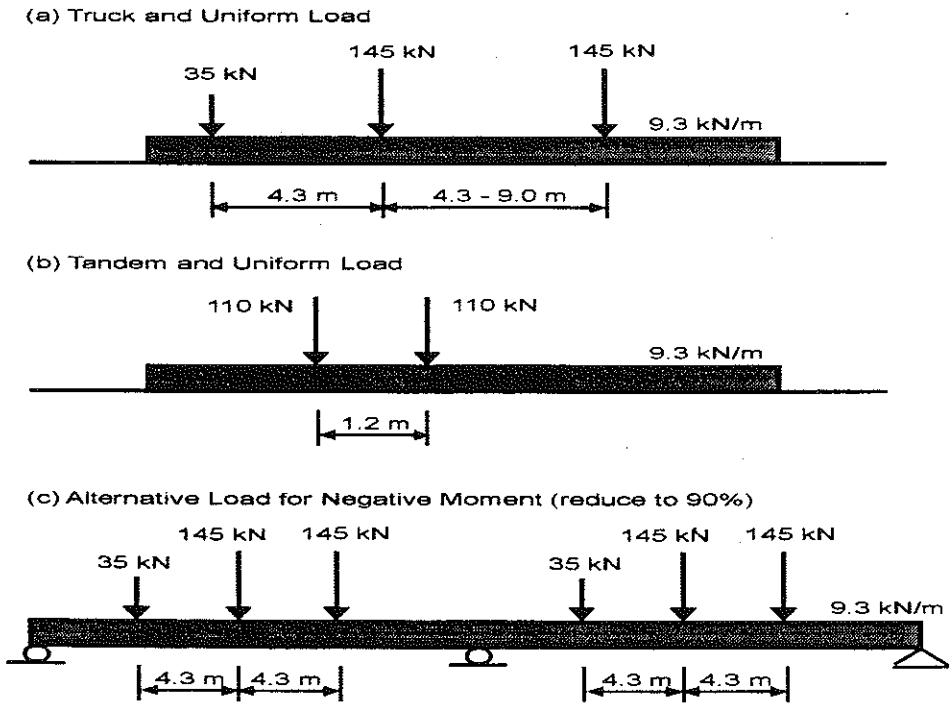

Fig. 2-2. Design Live Load HL-93 in AASHTO LRFD Code (1994).

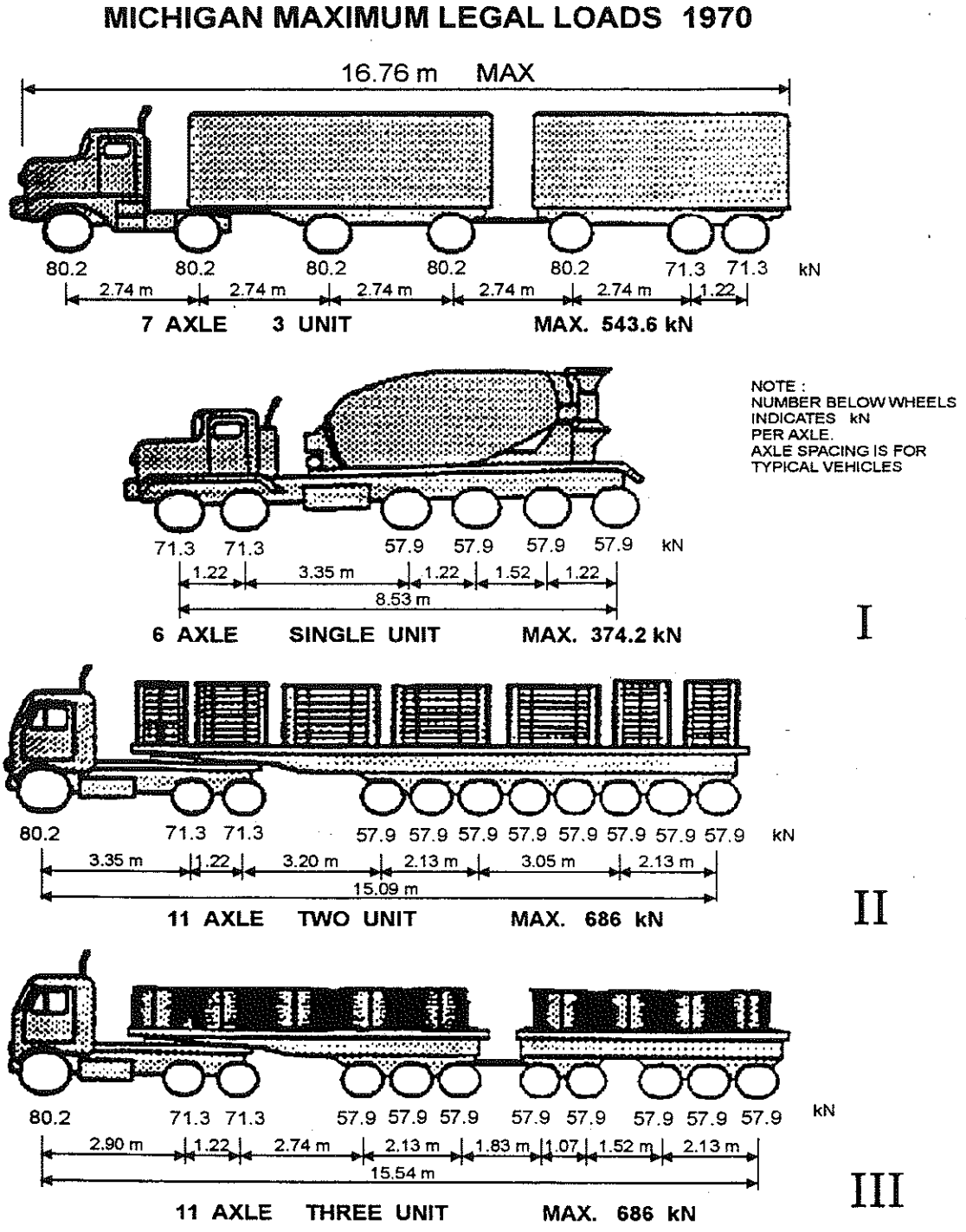

Fig. 2-3. Legal Loads (Michigan Bridge Analysis Guide 1983).

OTHER MAXIMUM LAGAL LOADS

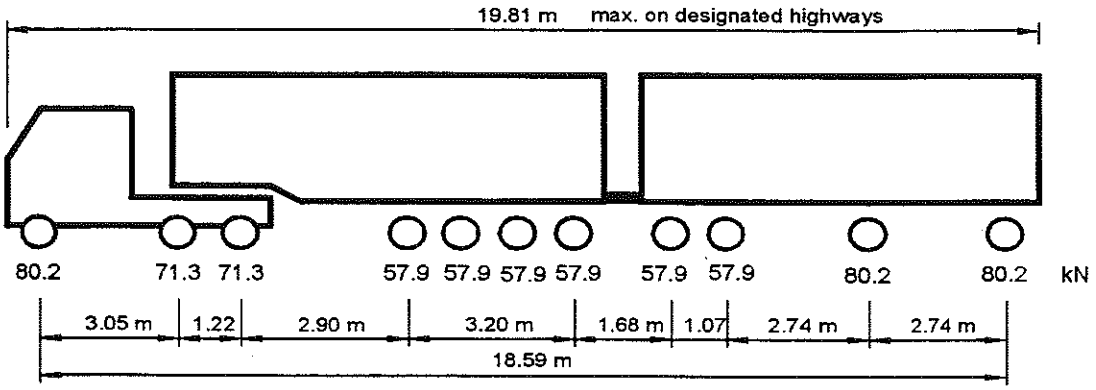

MICHIGAN 11 AXLE THREE UNIT MAX. 730.6 kN

(Moments are less than two unit 686 kN for spans less then 33.22 meters)

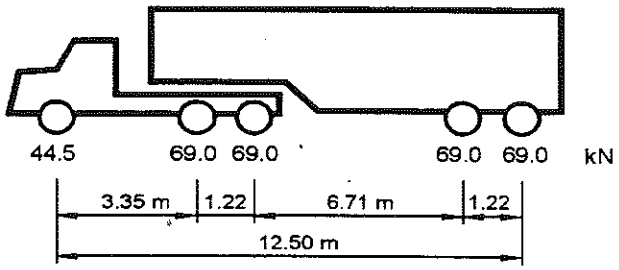

NOTE :
NUMBER BELOW WHEELS INDICATES kN PER AXLE.
AXLE SPACING IS FOR TYPICAL VEHICLES

AASHTO TYPE 3S2 **5 axle** **Max. 320.5 kN** II A

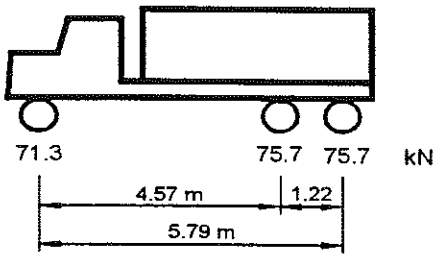

AASHTO TYPE 3 **3 axle** **222.7 kN** I A

MOMENTS FOR TYPE 3 & 3S2 on page 48 of AASHTO Manual.
If any bridge dates before about 1920 or has a known weakness (say less than 490 kN) the AASHTO type 3 and 3-S2 should be used for initial analysis.
If the resulting axle loads exceed legal loads then use veh. I & II.

Fig. 2-3. Legal Loads - Continued (Michigan Bridge Analysis Guide 1983).

Michigan Legal Loads are specified in the Michigan Bridge Analysis Guide (1983). Live load effects (moments and shear forces) are calculated for the trucks shown in Fig. 2-3.

For bridge evaluation, Michigan Legal Loads are recommended. All loads shown in Fig. 2-3 must be checked, and the governing load is to be used for evaluation. In the case of low traffic volume bridges (ADTT < 1,000), a simultaneous side-by-side occurrence of two fully loaded heavy trucks is unlikely, therefore, a single truck for load distribution can be used.

2.2.3. Dynamic Load

The dynamic load is calculated by multiplying live load (L) by the impact factor (I).

According to the AASHTO LRFD Code (1994), the dynamic load allowance (I) shall not be applied to pedestrian loads or to the design lane load. It shall be applied only to the truck and tandem load, and in this case it is taken as 0.33.

In the current AASHTO Code (1996), impact factor is specified as a function of span length only:

$$I = \frac{50}{3.28L + 125} \leq 0.30 \qquad (2\text{-}2)$$

where:

L = Length in meters of the portion of the span that is loaded to produce the maximum stress in the member; typically, this is the bridge or girder span.

Field measurements have indicated that the dynamic (impact) load component, calculated in terms of strain or deflection, stays relatively constant. Therefore, with increased heavy truck load (static component), the dynamic load factor decreases (Nowak et. al., 1996; Nassif and Nowak, 1995; Moses, 1987). In these studies, including the work done for Part I of this Guide, the dynamic factors for heavy 11-axle trucks were found to be less than 10 percent.

Therefore, for the evaluation of bridges loaded with heavy trucks, with spans longer than 6m, it is recommended to use an impact factor I = 0.10, unless case-specific data suggest otherwise.

2.3. Load Distribution

According to the AASHTO Standard Specifications (1996), the live load bending moment for each interior girder is calculated by applying to the girder the fraction of the truck weight. This fraction is the girder distribution factor (GDF). All GDF's in this report are specified based on the entire truck weight rather than a wheel line (1/2 truck) load. In the AASHTO Standard Specifications, for bridges with concrete decks, the corresponding GDF is:

For single lane loading:

Steel and prestressed concrete girders,	GDF = S / 4.27	(2-3a)
Concrete T-beams,	GDF = S / 3.96	(2-3b)

For multiple lane loading:

Steel and prestressed concrete girders,	GDF = S / 3.36	(2-3c)
Concrete T-beams,	GDF = S / 3.66	(2-3d)

where S = girder spacing (m).

Note that, in the 1996 AASHTO Standard Specifications, GDF's are specified for a wheel line load. However, the denominators in Eq.2-3 are given for the whole truck.

For bridges with four or more girders, The AASHTO LRFD Code (1994) specifies the girder distribution factor (GDF) as a function of girder spacing, span length, stiffness parameters, and bridge skew. For moment in interior girders, the GDF is as follows:

For single lane loading,

$$GDF = \left\{0.06 + \left(\frac{S}{4300}\right)^{0.4}\left(\frac{S}{L}\right)^{0.3}\left(\frac{K_g}{Lt_s^3}\right)^{0.1}\right\}\left\{1 - c_1(\tan\theta)^{1.5}\right\} \qquad (2\text{-}4)$$

For multi-lane loading,

$$GDF = \left\{0.075 + \left(\frac{S}{2900}\right)^{0.6}\left(\frac{S}{L}\right)^{0.2}\left(\frac{K_g}{Lt_s^3}\right)^{0.1}\right\}\left\{1 - c_1(\tan\theta)^{1.5}\right\} \qquad (2\text{-}5)$$

$$c_1 = 0.25\left(\frac{K_g}{Lt_s^3}\right)^{0.25}\left(\frac{S}{L}\right)^{0.5} \quad \text{if} \quad 30° < \theta < 60° \qquad (2\text{-}6)$$

$$c_1 = 0 \quad \text{if} \quad \theta < 30°$$

$$\text{use} \quad \theta = 0 \quad \text{if} \quad \theta > 60°$$

where:

S = girder spacing (mm)

L = span length (mm)

$K_g = n(I + Ae_g^2)$

t_s = depth of concrete slab (mm)

n = modular ratio between girder and slab materials

I = moment of inertia of the girder (mm^4)

A = area of the girder (mm^2)

e_g = distance between the center of gravity of the girder and slab (mm)

θ = skew angle in degrees, measured as the angle between the centerline of a support and a line normal to the roadway centerline.

Because the term $K_g/(Lt_s^3)$ implies more accuracy than exists for bridge evaluation, it is recommended that it be taken as 1.0. The applicability ranges for these equations are:

$$1100 \le S \le 4900 \qquad 110 \le t_s \le 300 \qquad 6000 \le L \le 73000$$

Finite element analyses previously performed at the University of Michigan indicated that the GDF's specified in the AASHTO Code (1996) are too conservative for longer spans and larger girder spacings [Nowak and Hong, 1991]. Similar results were obtained by Zokai et al. (1991). Values proposed by Zokai et al. (1991) were adopted as a basis for GDF's in the AASHTO LRFD Code (1994). Finite element analysis was performed by Bishara, Liu and El-Ali (1992). Bishara et al. (1992) considered 36 bridges with 2.7m spacing of girders, spans 22.5m, 30m and 37.5m, width 11.5m, 17m and 20m, and skew angles 0°, 20°, 40° and 60°. They also tested one bridge to validate analytical formulas. However, the resulting GDF's are unrealistically low, less than half of AASHTO (1996) or AASHTO LRFD (1994).

The actual GDFs were determined by field tests performed on five short span bridges (less than 18m), as described in Part I of this report (Nowak and Kim 1998). For three bridges, the obtained GDFs for two side-by-side 11-axle trucks were approximately S/3.36 (where S is in meters), and for two other bridges they were approximately S/5. FEM analyses cited above provided GDFs close to S/3.36 (Nowak and Hong, 1991; Zokai et al. 1991). Field test measurements are presented by Fu, Elhelbawey, Sahin and Schelling (1996). The measured GDF's are listed for four bridges. It is not possible to

compare the data with other test results because the spans and girder spacings are not provided.

For comparison, the GDF's obtained in field tests as a part of this study, are plotted versus analytical values calculated using AASHTO Specifications (1996), and AASHTO LRFD Code (1994). The results are shown in Fig. 2.4 for a single truck (one lane loaded), and for two trucks (two lanes loaded).

Many bridges in Michigan carry low volume roads. However current design and evaluation provisions are based on the assumption that two side-by-side fully loaded vehicles occur simultaneously. This event is unexpected on low volume trunkline and secondary roads. In particular, it is practically unlikely to have two very heavy vehicles simultaneously on the bridge. The actual probability of such an event can be calculated using the approach developed for the AASHTO LRFD Code (Nowak and Hong 1991; Nowak 1993; Nowak 1995).

The statistical data on heavy vehicles in Michigan is provided in the Michigan Department of Transportation position paper titled Trucks and Transportation (1998). There are approximately 108,000 commercial trucks registered in Michigan, with 15,000 capable to carry more than 360 kN. The total number of trucks operating in the state is estimated at 300,000. There are about 850 trucks registered to carry 720-740 kN (less than 1 out of every 350 trucks on the road).

On the major interstate highways 11-axle trucks constitute about 3-5% of all truck traffic. This percentage is much lower for low volume roads (less than 1%). Visual observations on interstate highways showed that about 2-4% of vehicles travel side-by-side (Nowak, Laman and Nassif 1994). These vehicles travel in the same direction using two or three parallel lanes. On low volume roads, with two traffic lanes in opposite directions, the probability of side-by-side

occurrence is even smaller (much less than 1%). Furthermore, the probability of having two 11-axle trucks side-by-side on low volume roads, P,

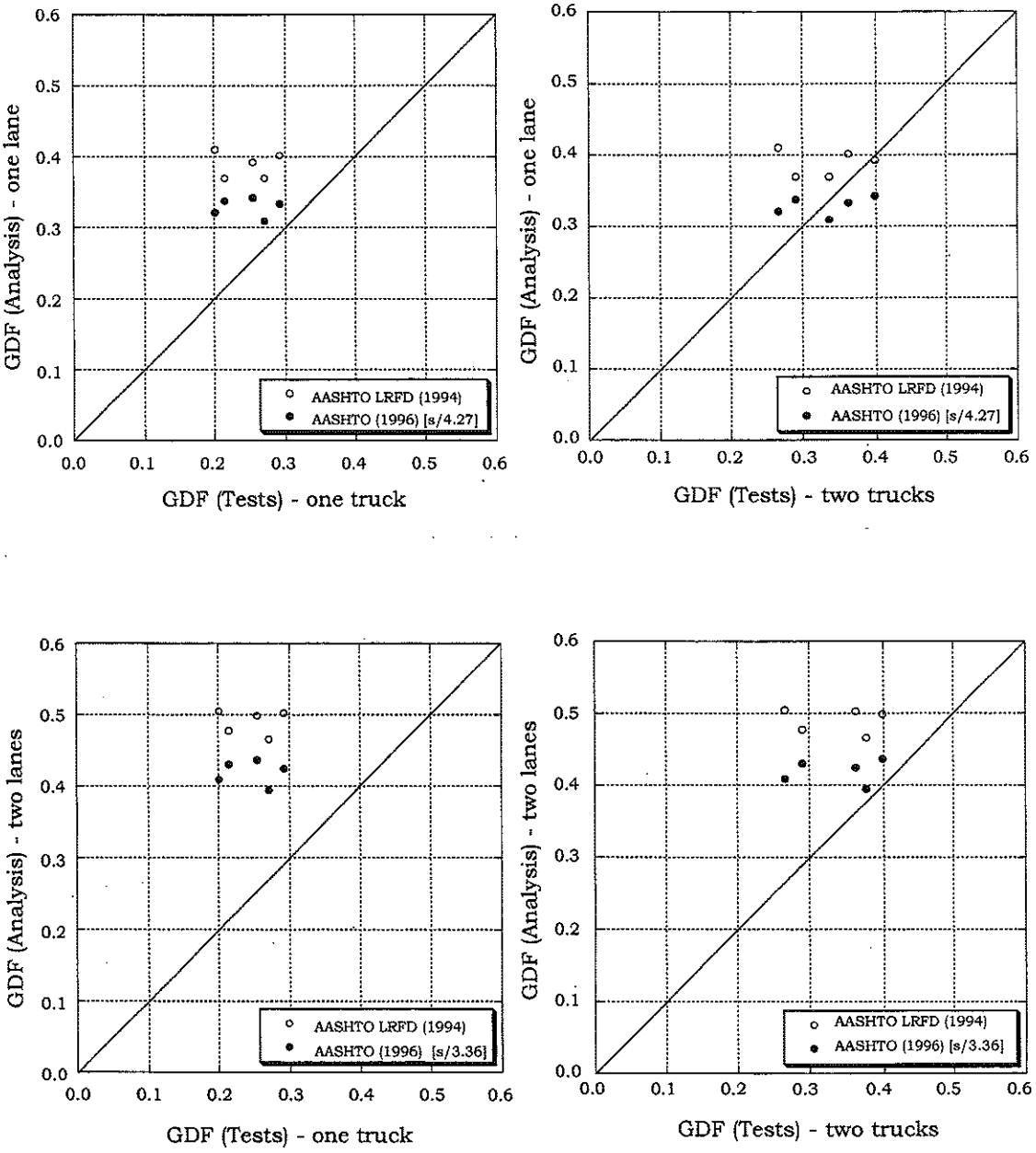

Fig. 2.4 GDF (Tests) vs. GDF (Analysis).

$$P < (0.01)(0.01)(0.01) = 0.000001 = 10^{-6} \quad (2\text{-}7)$$

where 0.01 = fraction of 11-axle trucks, 0.01 = percentage of side-by-side events, 0.01 = probability the other truck is an 11 axle vehicle. For low volume roads this means that it is practically unlikely to have two 11-axle trucks simultaneously on the bridge. This very low probability can be further reduced by considering a very low likelihood of two fully loaded trucks (as opposed to partly loaded). Therefore, it is recommended to evaluate low volume road bridges using a single heavy vehicle.

For the considered bridges, the girder distribution factors (GDF) for a single truck do not exceed 0.3, as observed in the field tests described in Part I of this report [Nowak and Kim 1998]. For a single truck, GDF is less than S/4.27. Therefore, it is recommended to use:

$$GDF = S/4.27 \quad (2\text{-}8)$$

when evaluating bridges carrying low traffic volume roads (ADTT<1000).

The recommended values of GDF are given in Table 2-1. For bridges with low traffic volume (ADTT < 1,000), S/4.27 can be used. For higher traffic volume (ADTT>1000), it is recommended that the GDF formulas specified in AASHTO LRFD Code (1994) can be used. However, for short span bridges (span < 15 m), based on the field test results performed in this project, AASHTO LRFD Code (1994) formula for one lane is adequate even for two lane bridges. For longer spans (larger than 15 m), there is a need for additional field tests to validate GDF's.

Table 2-1 Recommended GDF for Evaluation of Bridges

	GDF	
Span	ADTT < 1,000	ADTT > 1,000
Span < 15 m	S/4.27	AASHTO LRFD (1994) for one lane
Span > 15 m	S/4.27	AASHTO LRFD (1994) for two lanes

2.4. Load Carrying Capacity

The load carrying capacity of a bridge girder is to be calculated for moment and shear separately. It is recommended that bridges with steel girders be analyzed assuming composite action, even if designed non-compositely, unless signs of deterioration or slab-girder de-bonding suggest that composite action is lost. Field tests have indicated that steel-girder bridges exhibit composite action even if designed non-compositely [see Part I Report, Nowak and Kim 1998; Nowak and Saraf 1996].

The calculation of load carrying capacity of the structure is described in Appendix C. This value should be equal to or greater than the load effect. The calculation of load effect, and the appropriate load factors to use for this computation, are described in following paragraphs.

2.5. Interpretation of Results

The analytical evaluation of the bridge shall be made according to the expressions below. The left side of the inequality is the load effect, while the right represents load carrying capacity.

According to the 1996 AASHTO Standard Specifications:

$$1.3(M_D + M_{DW} + M_L + M_I) \le \phi M_n \quad \text{(2-9a)}$$

$$1.3(V_D + V_{DW} + V_L + V_I) \le \phi V_n \quad \text{(2-9b)}$$

where ϕ =1.0 for steel and prestress concrete.

According to the 1994 AASHTO LRFD Code:

$$1.25M_D + 1.50M_{DW} + 1.75(M_L + M_I) \le \phi M_n \quad \text{(2-10a)}$$

$$1.25V_D + 1.50V_{DW} + 1.75(V_L + V_I) \le \phi V_n \quad \text{(2-10b)}$$

where:

M_D = moment due to dead load except asphalt

M_{DW} = moment due to dead load of asphalt

M_L = moment due to live load

M_I = moment due to dynamic load

M_n or ϕM_n = moment carrying capacity

V_D = shear due to dead load except asphalt

V_{DW} = shear due to dead load of asphalt

V_L = shear due to live load

V_I = shear due to dynamic load

V_n or ϕV_n = shear carrying capacity

ϕ = resistance factor

According to the 1994 AASHTO LRFD Specifications, values of ϕ's shall be taken as:

ϕ = 1.00 (steel, prestressed concrete)

= 0.90 (reinforced concrete)

2.6. Rating Factor

Bridge members can have two different ratings, an operating rating and an inventory rating. Bridge rating formulas are not yet

available in the LRFD format. The basic formulas for the theoretical rating of a bridge member, as expressed in the AASHTO Manual For Condition Evaluation of Bridges, are as follows :

Operating rating :

$$RF = \frac{1}{L}\frac{C - 1.3D}{1.3(1+I)} \tag{2-11}$$

Inventory rating :

$$RF = \frac{1}{L}\frac{C - 1.3D}{2.17(1+I)} \tag{2-12}$$

where:

D = dead load effect on the member, calculated from data on the plans and supplemented by field measurements.

L = live load effect on the member. It is recommended that the Michigan Legal Loads be used for the calculation of rating factors.

I = the impact factor to be used with the live load effect. It can be calculated as it is described in the section 2.2.3.

C = the capacity of the member to resist the applied load effects. For compact sections, this value is equal to M_n, and for non-compact sections, it is equal to F_n. M_n and F_n are described in Appendix C.

2.7. Effect of Deterioration

2.7.1. Corrosion

During the field investigation, the corrosion level and pattern on the main structural members should be determined. There are three basic changes which can be occur in a steel bridge due to corrosion: loss of material, reduction of section parameters, and buildup of corrosion products.

Loss of material will result in a smaller net section, which may increase the stress level for a given load. When corrosion is localized, as in pitting, stress concentrations can occur and further increase the stress level.

A reduction in section area will also decrease the values of section properties, such as moment of inertia and radius of gyration. This change may occur in a nonlinear manner because the section properties are related to the square or cube of the dimension; just a slight loss of additional flange material can lead to large losses of bending capacity. Similarly, buckling capacity can be critically affected by the reduction in metal thickness.

The buildup of corrosion products can also adversely affect steel bridges. Rust formation may exert pressure on adjacent elements. This pressure can pry apart plates, causing stresses and eccentricities in the connected parts. The formation of "pack" rust around a bearing or hinge can lock the mechanism in place. A nonfunctional hinge may cause unintended stress in the structure.

These adverse effects of corrosion must be accounted for when calculating the load carrying capacity; the reduced sectional areas must be used. The buildup of corrosion and locking of supports should also be considered.

2.7.2. Fatigue

Produced by the cyclic loading of truck traffic, fatigue cracks are another common form of deterioration. Stress concentration spots around bolts and rivets are especially prone to develop fatigue cracks, as are corrosion-deteriorated locations.

When calculating the load carrying capacity of a bridge, the reduction of structural capacity of a member that has a fatigue crack should be determined.

3. Bridge Selection Criteria

There are two primary bridge tests: a weigh-in-motion (WIM) test and a load test. Because the tests have different objectives, bridge selection criteria differ for each, and are discussed below.

Weigh-In-Motion Test

A weigh-in-motion test is used to determine gross vehicle weight, axle weight, and the axle spacing of trucks that travel over the bridge. The following criteria should be considered for bridge selection:

- traffic speed - most measuring equipment requires a minimum vehicle speed of about 40 km/h, so the presence of stop lights near the bridge may cause a problem.
- accessibility - the installation/setup crew must be able to reach the girders, with or without mechanical assistance, for installation of the strain transducers.
- low dynamic effect - dynamic effect is filtered out and the results include only static effect. High dynamic load may affect the results.
- two lane bridges - the equipment is set for measurements on two lanes. If there are more lanes of traffic then only two are instrumented.
- girder type - acceptable types include steel or prestressed concrete, and conditionally acceptable are box girders or slab bridges. The selection depends on calibration data.

- skew - optimal is 0 to 10 degrees, but acceptable is 10 to 25 degrees, and conditionally acceptable is 25 to 45 degrees, however after inspection of calibration data, and it can be used with one influence line.
- span length - optimal is 10 to 20 m, but acceptable is 7.5 to 30 m.

- bridge type - simple span bridges are preferred, but continuos bridges can also be handled.

Before a bridge is selected, the Bridge Weigh-in-Motion (BWIM) manual should be studied for more information about restrictions of the software, since specific software limitations or strengths may influence bridge selection.

Load Tests

Load Tests refer to Load Distribution Tests, Dynamic Load Tests, Fatigue Load Test and Proof Load Tests. The main objective of these tests is to find an unknown bridge property such as load distribution factor, impact factor, or actual load carrying capacity. Bridges are often more suitable for load tests than WIM tests. The following criteria should be considered for bridge selection:

- accessibility (clearance, feature below, water level, etc.), the installation/setup crew must be able to reach the girders for installation of the strain transducers and LVDTs. If there is water below the bridge, a special technique must be used for LVDT placement.
- sign of deterioration (spalling concrete, cracks, corrosion, etc.), if any; bridges with higher deterioration levels are generally chosen first, if a bridge is badly deteriorated, however, such that its likelihood to survive the load test undamaged is questionable, it should be repaired before testing.
- missing design documents
- existence of a low load rating
- consequences of traffic interruption (bridge or lane closure); field work may affect the traffic flow
- age of bridge
- degree of heavy truck traffic

4. Truck Weight-in-Motion Measurement (WIM)

4.1. Procedure

The primary bridge live load is truck traffic. In the past, truck load data were collected by surveys. The most common survey method consisted of weighing trucks with static scales, present at weigh stations along fixed locations on major highways. The usefulness of this data is limited, however, because many drivers of overloaded trucks intentionally avoid the scales. This results in a load bias toward lighter trucks.

A weight-in-motion test attempts to gather unbiased truck traffic data, which includes axle weight, axle spacing, vehicle speed, multiple truck presence on the bridge, and average daily truck traffic (ADTT). Sensors measure strains in girders, and these data are then used to calculate the truck parameters at the given traffic speed.

4.2. Equipment

Beneath the deck, the WIM system is invisible to the truck drivers, and so overloaded trucks do not avoid the bridge. Unbiased results can thus be obtained. The system is portable and easily installed to obtain site-specific truck data.

The Bridge WIM system consists of three basic components: strain transducers, axle detectors (tape switches or infrared sensors), and the data acquisition and processing system (Fig. 4-1). The analog front end (AFE) acts as a signal conditioner and amplifier with a capacity of 8 input channels. Each channel can condition and amplify signals from the strain transducers (see Appendix A).

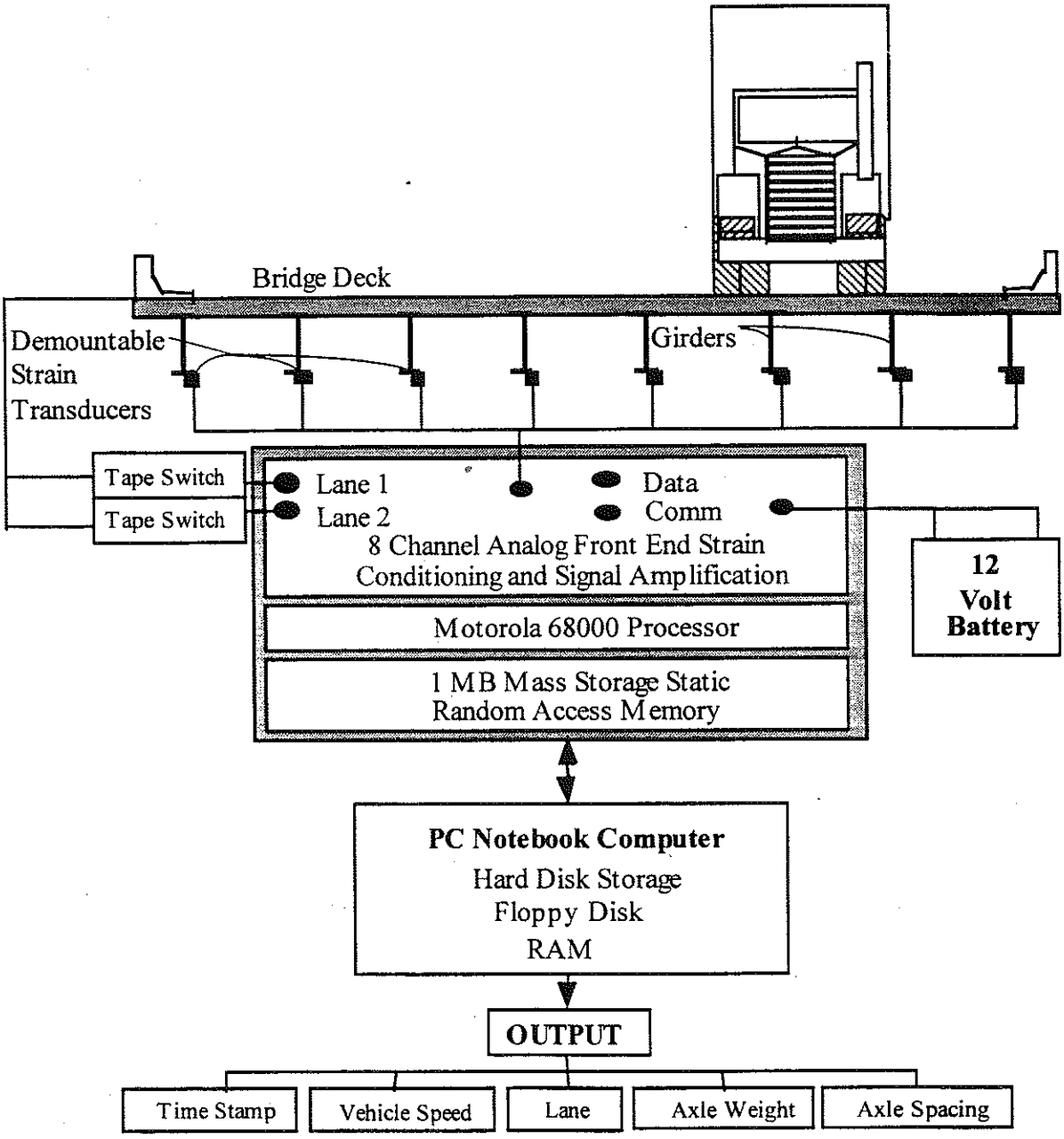

Fig. 4-1. Weigh-in-Motion Truck Measurement System.

During data acquisition, the AFE maintains the strain signals at zero. The auto-balancing of the strain transducers is activated when the first axle of the vehicle crosses the first axle detector. As the truck crosses the axle detectors, the speed and axle spacing are determined by the system. When the vehicle drives upon the bridge,

the strain sampling is activated. When the last axle of the vehicle leaves the instrumented bridge span, the strain sampling is turned off. Data received from strain transducers are digitized and routed to the computer. The strain time history is decomposed using an influence line algorithm to determine vehicle axle weights. These data do not include dynamic loads. This process takes from 1.5 to 3.0 seconds, depending on the instrumented span length, vehicle length, number of axles, and speed. The data are then saved by the computer.

4.3. Installation of Equipment

Strains are measured in the lower flanges of the girders, so the strain transducer must be clamped to the upper or lower surface of the bottom flange of the steel girder (Fig. 4-2a). For concrete beams, a Hilti-gun rather than clamps, is recommended for attachment as shown in Fig. 4-2b. All transducers are placed on the girders at the same distance from the abutment, in the middle third of a simple span. The vehicle speed, time of arrival, and lane of travel are obtained using tape switches on the roadway placed before the instrumented span of the bridge (Fig.4-3).

Two types of lane sensors can be used depending on the site conditions: tape switches and infrared sensors. Tape switches consist of two metallic strips that are held apart when the bridge is unloaded. As a vehicle wheel passes over the tape, it forces the metallic strips into contact and grounds a switch. By completing the circuit, a voltage is impressed across the switch, and a signal is obtained at the instant the vehicle crosses the tape. This signal is fed to a computer, where the speed, axle spacing, and number of axles are determined. The tape switches are placed perpendicular to the traffic flow and are also used to trigger the strain data collection.

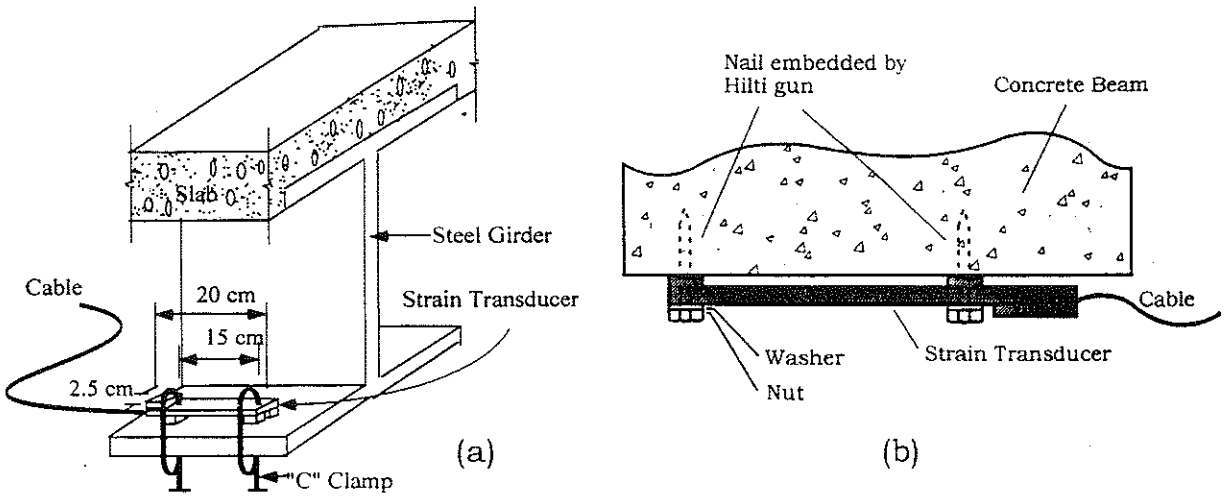

Fig. 4-2 Demountable Strain Transducer Mounted to the Lower Flange and Concrete Beam..

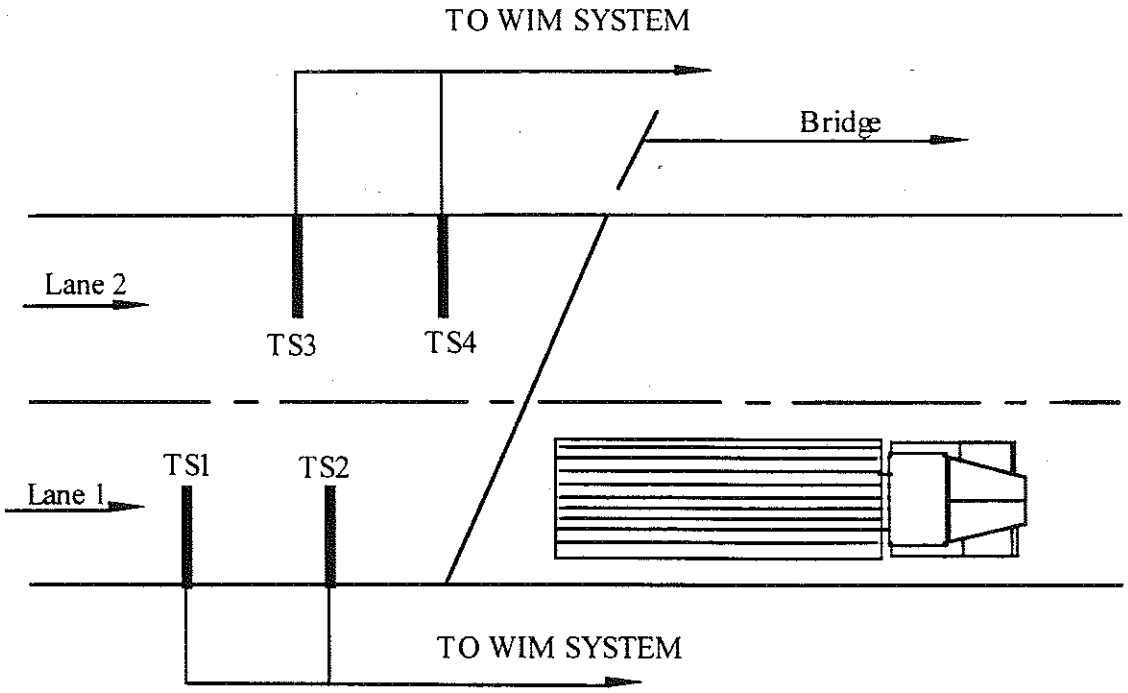

Fig. 4-3 Plan of Roadway Sensor Configuration.

The major problem with tape switches is their vulnerability to damage by moving traffic, particularly if the pavement is wet. Various alternative devices can be considered, one of which is the infrared sensor.

The infrared system consists of a infrared light beam source and a reflector. The light source is installed on the side of the road, and the reflector is installed in the center of the traffic lane. The infrared system, however, is still vulnerable to damage by moving traffic. It is also more difficult to install than tape switches, and trucks can easily move the reflector, interrupting the operation (at which point the light beam must be aligned). The infrared system is not reliable for operation during rain.

4.4. Measurements

The strain transducers are connected to the main unit using 5 shielded cables. Cables also connect the main unit to the lane sensors. AC power is provided by a portable gasoline-powered generator. Communication with the weigh-in-motion system is through a separate portable computer. All data concerning influence lines, girders, and other physical parameters are entered into the WIM computer and the system is instructed to begin the weighing operation.

The WIM equipment is calibrated by running calibration trucks over the bridge several times in each lane. The best results are obtained for calibration trucks which are fully loaded multi-axle vehicles. The readings are verified and calibration constants are determined so that the instrumentation will predict the correct axle weights and spacing. The comparison of the results indicates that the accuracy of measurements is within about 10 percent for 11-axle

trucks. For 5-axle trucks, gross vehicle weight (GVW) is within 5 percent, and axle loads are within 20 percent. The calibration is performed once for each tested structure.

The system is activated when the first tire triggers the lane sensor. Strain measurements are taken at the rate of 62.5 Hz. Vehicle speed is calculated from the time delay between the first and second tape signal. The number of axles and axle distances are computed by the system and recorded. The dynamic strains sampled from each channel are then decomposed into axle weights using preprogrammed influence lines. A smoothing technique is used to determine the static weights from the dynamic records. Results of axle spacing and weight calculations are stored in memory for later processing and summarization. The weighing operation results may be displayed in real time.

4.5. Results of WIM Tests

4.5.1. Gross Vehicle Weight Distributions

The WIM results can be presented in a traditional histogram (frequency or cumulative). Examples of frequency histograms are shown in Fig. 4-4 and 4-5. However, this approach does not allow for an efficient analysis of the extreme values (upper or lower tails) of the considered distribution. Therefore, results of gross vehicle weight (GVW) WIM measurements can also be shown as cumulative distribution functions (CDFs) on the normal probability paper as shown in Fig. 4-6. CDFs are used to present and compare the critical extreme values of the data. They are plotted on normal probability paper [Benjamin and Cornell, 1970], which is described as follows: The horizontal axis is the considered truck parameter (e.g. gross vehicle weight, axle weight, lane moment or shear force).

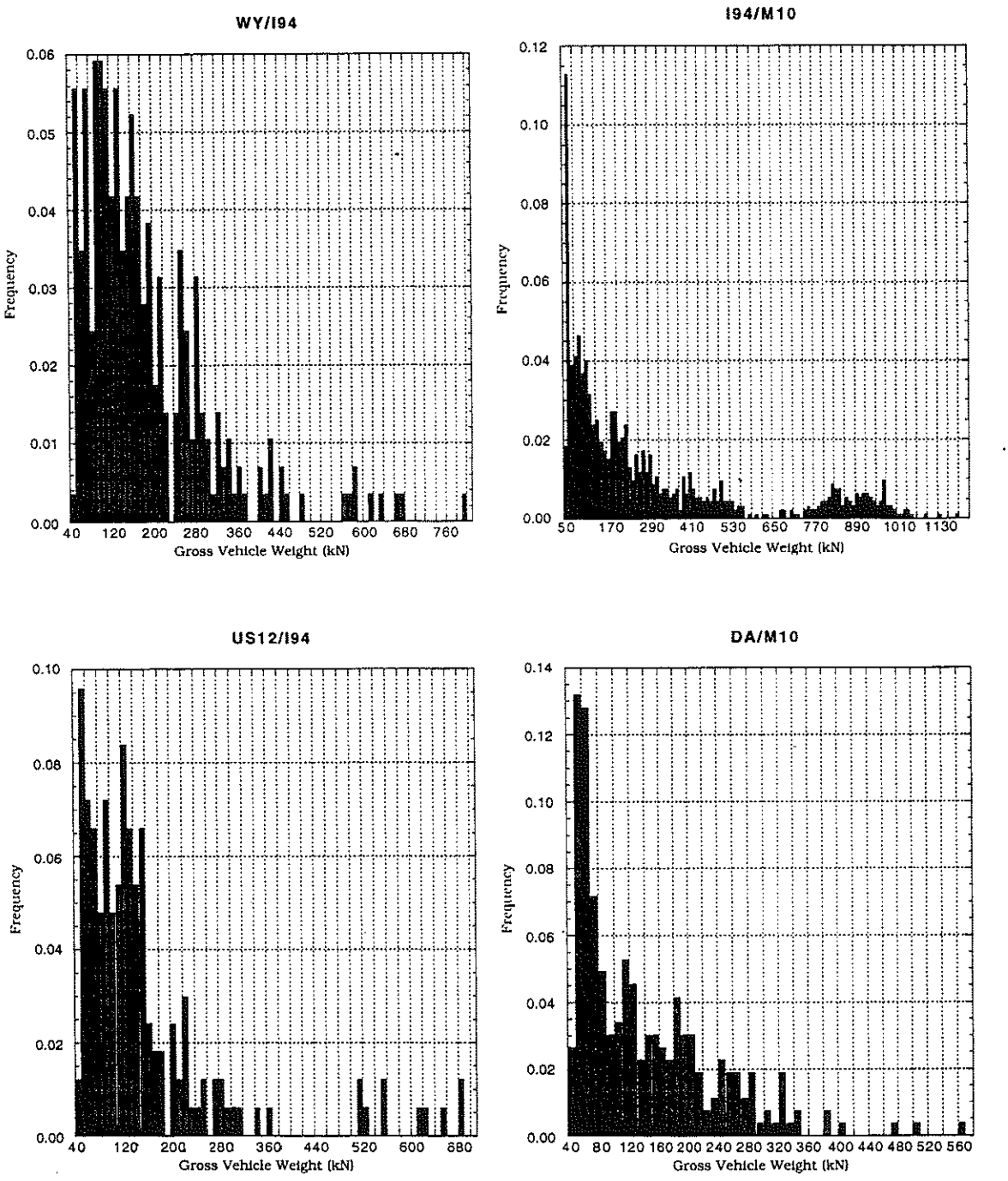

Fig. 4-4. Frequency Histograms of GVW for the Considered Bridges.

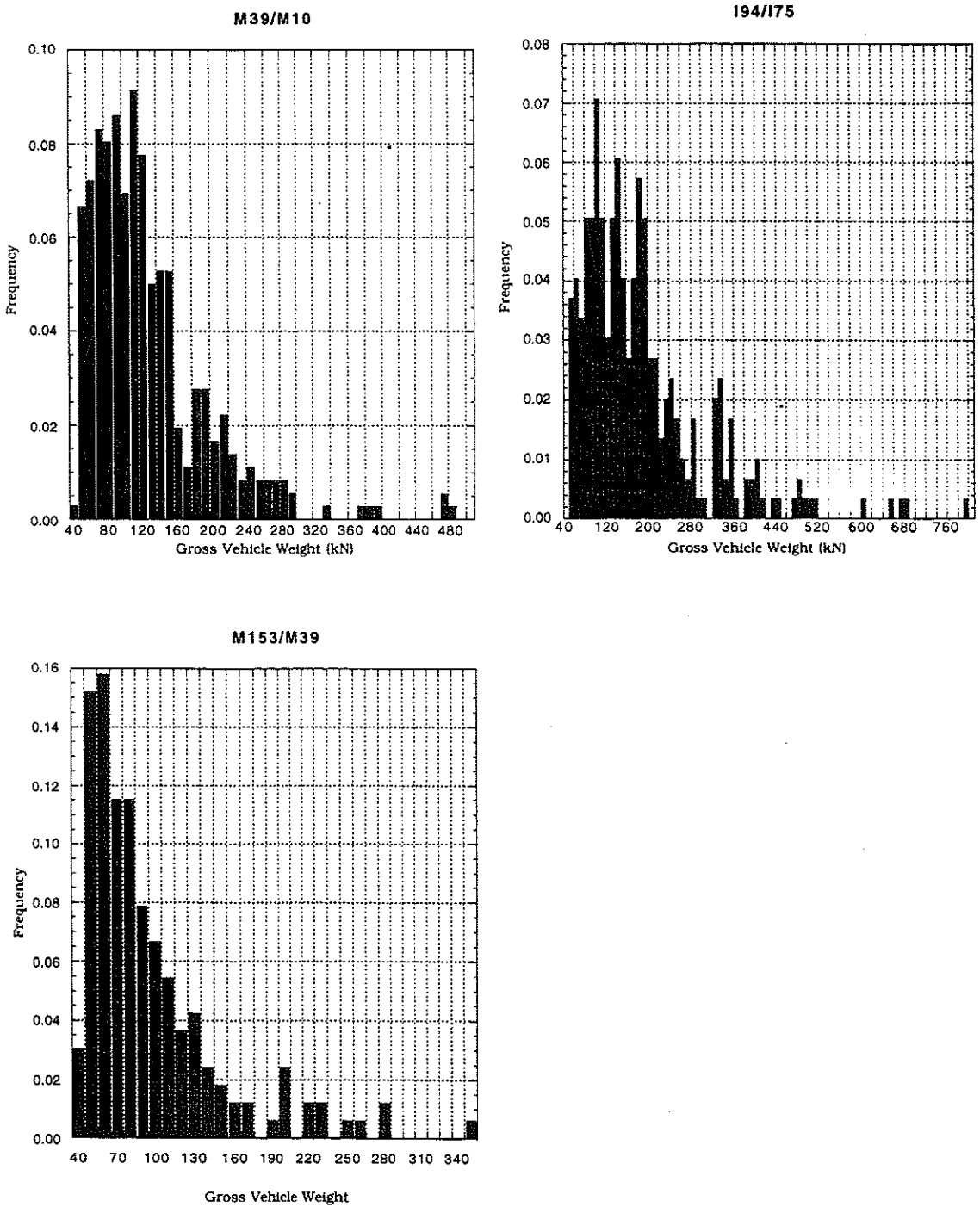

Fig. 4-5. Frequency Histograms of GVW for the Considered Bridges - Continued.

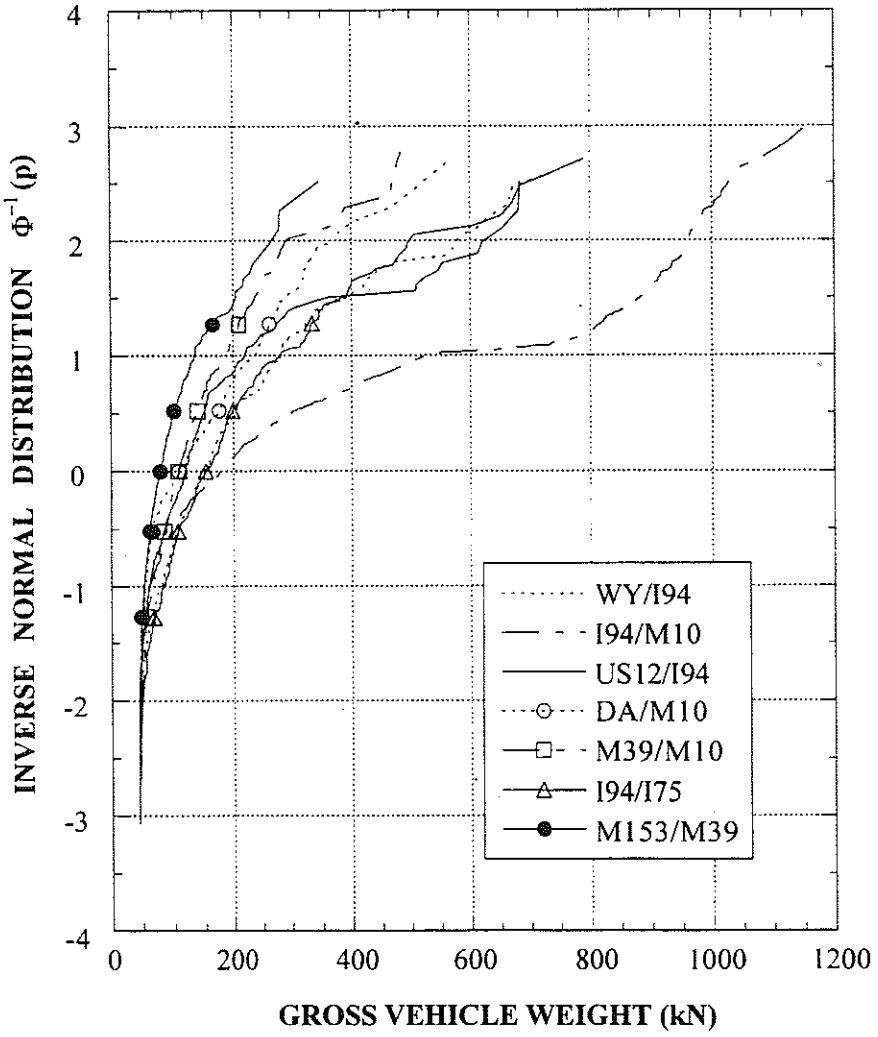

Fig. 4-6 CDFs of Gross vehicle Weight for the Considered Bridges.

The vertical axis represents the probability of a particular point being exceeded, p. The probability of being exceeded (vertical scale) is then replaced with the inverse standard normal distribution function denoted by $\Phi^{-1}(p)$. For example, $\Phi^{-1}(p) = 0$ corresponds to the probability of being exceeded $p = 0.5$, while $\Phi^{-1}(p) = 1$ corresponds to $p = 0.159$, and $\Phi^{-1}(p) = -1$ corresponds to $p = 0.841$, and so on. The construction and use of the normal probability paper is summarized in Appendix B.

The distribution of truck type by number of axles will typically bear a direct relationship to the GVW distribution; the larger the population of multiple axle vehicles (greater than five axles) the greater the GVW load spectra. Past research has indicated that 92% to 98% of the trucks are four and five axle vehicles. Three and four axle vehicles are often configured similarly to five axle vehicles, and when included with five axle vehicles, this group accounts for 55% to 95% of the truck population. In Michigan, between 0% and 7.4% of the trucks have eleven axles.

Most states in the US allow a maximum GVW of 355 kN, where up to five axles per vehicle are permitted. The State of Michigan legal limit allows for an eleven axle truck of up to 730 kN, depending on axle configuration.

4.5.2 Axle Weight Distributions

Potentially more important for bridge fatigue and pavement design are the axle weights and axle spacings of the trucks passing over the bridge. Fig. 4-7 presents the distributions of the axle weights of the measured vehicles.

4.5.3. Lane Moment and Shear Distributions

Once truck data has been collected by a WIM test, the results can be used to generate the expected moments and shears for any bridge span. Each truck in the data base is analytically driven across the desired span (using influence lines) to determine the maximum static bending moment and shear per lane. The cumulative distribution functions of these load effects for the same span are then determined. As an example, the resulting CDF's for a specific span (27m) are shown in Fig. 4-8 for lane moment and Fig. 4-9 for lane

shear. As a point of reference, the calculated load effects are divided by the values resulting from using the AASHTO LRFD (1994) design loads.

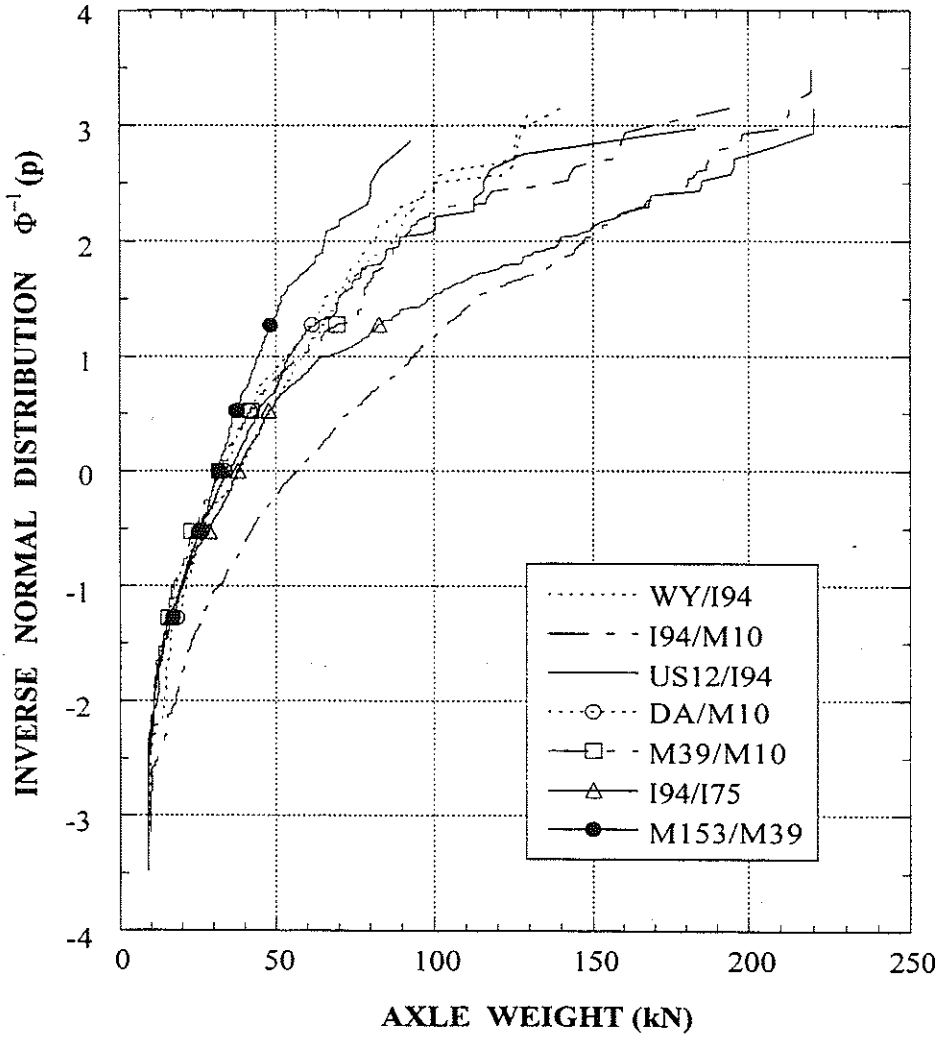

Fig. 4-7. CDFs of Axle Weight for the Considered Bridges.

Fig. 4-8 indicates that there is a wide variation of truck load distribution among the example bridges investigated. Maximum values of lane-moment-to-LRFD-moment ratio vary from 0.6 at M153/M39 to 2.0 at I94/M10. The variation of lane shears in Fig. 4-9 is similar to that of lane moments. For I94/M10, the extreme value exceeds 2.0. For the other bridges, the maximum shears can be seen to vary from 0.65 at M153/M39 to 1.5 at I94/I75.

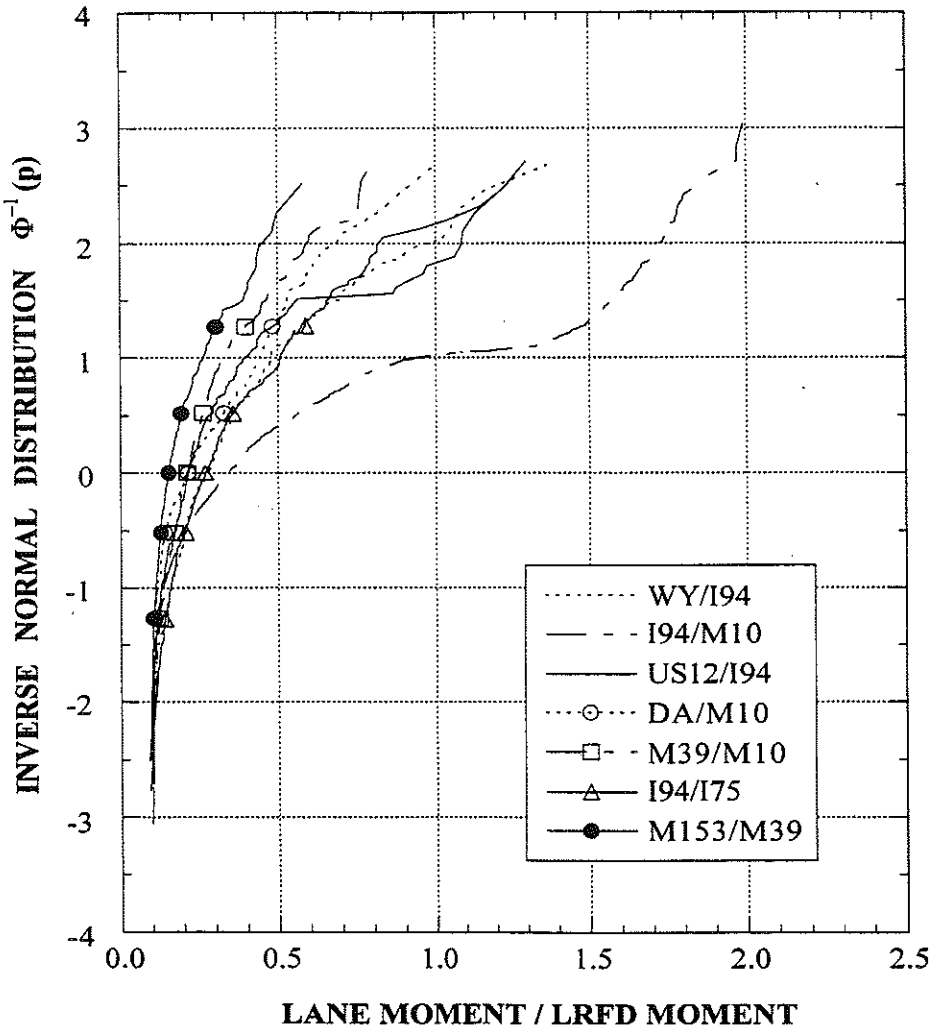

Fig. 4-8 CDFs of Lane Moment for the Span Length of 27 m.

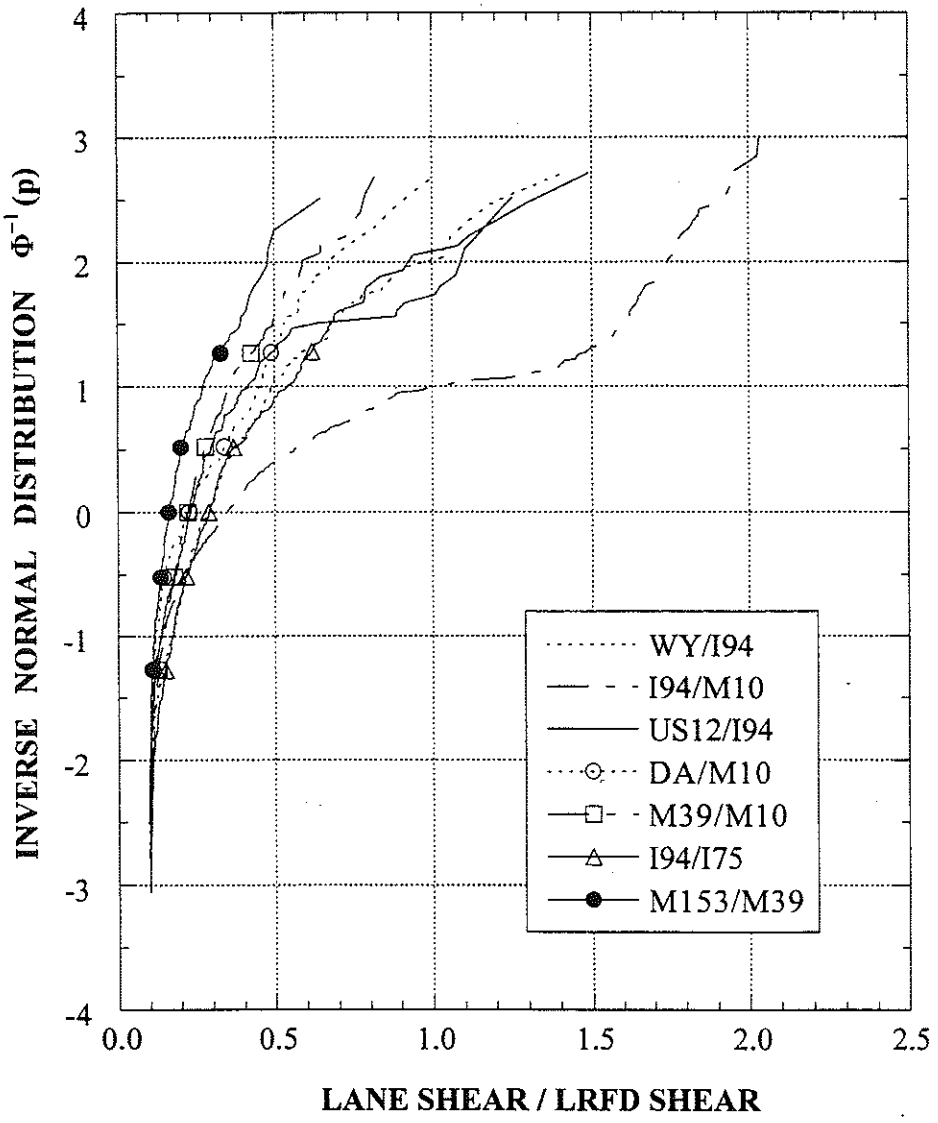

Fig. 4-9 CDFs of Lane Shear for the Span Length of 27 m.

Note:
Intentionally left blank

5. Dynamic Load Measurement

5.1. Procedure

The dynamic load can be a significant component of live load. Not only is it time variant and random in nature, but it depends on the vehicle type, vehicle weight, axle configuration, bridge span length, road roughness, and transverse truck position on the bridge. In a dynamic test, strain transducers are attached to the bridge girders, and stress values are recorded under actual moving traffic loads.

5.2. Equipment

The SCXI system, manufactured by National Instruments Corporation, can be used for a load distribution test. The SCXI system setup is shown in Fig. 5-1. In contrast to the WIM system, the SCXI system has neither an independent processor nor a memory module. The data acquisition mode is controlled from an external PC notebook computer, and the acquired data are processed and directly saved in the PC's hard drive.

The system is composed of 4 major components totaling 5 modules (Fig. 5-1): one SCXI-1000 chassis, one SCXI-1200 data acquisition module, two SCXI-1100 multiplexer modules, and one PC with LabView software. The power for all components is provided from a portable electric generator. The generator also supplies excitation for strain transducers through the AC to DC converter.

The SCXI-1000 chassis integrates the operation of multiple SCXI modules with a SCXI-1200 module. The chassis's bus includes guarded analog buses for signal routing and digital buses for transferring data and timing signals.

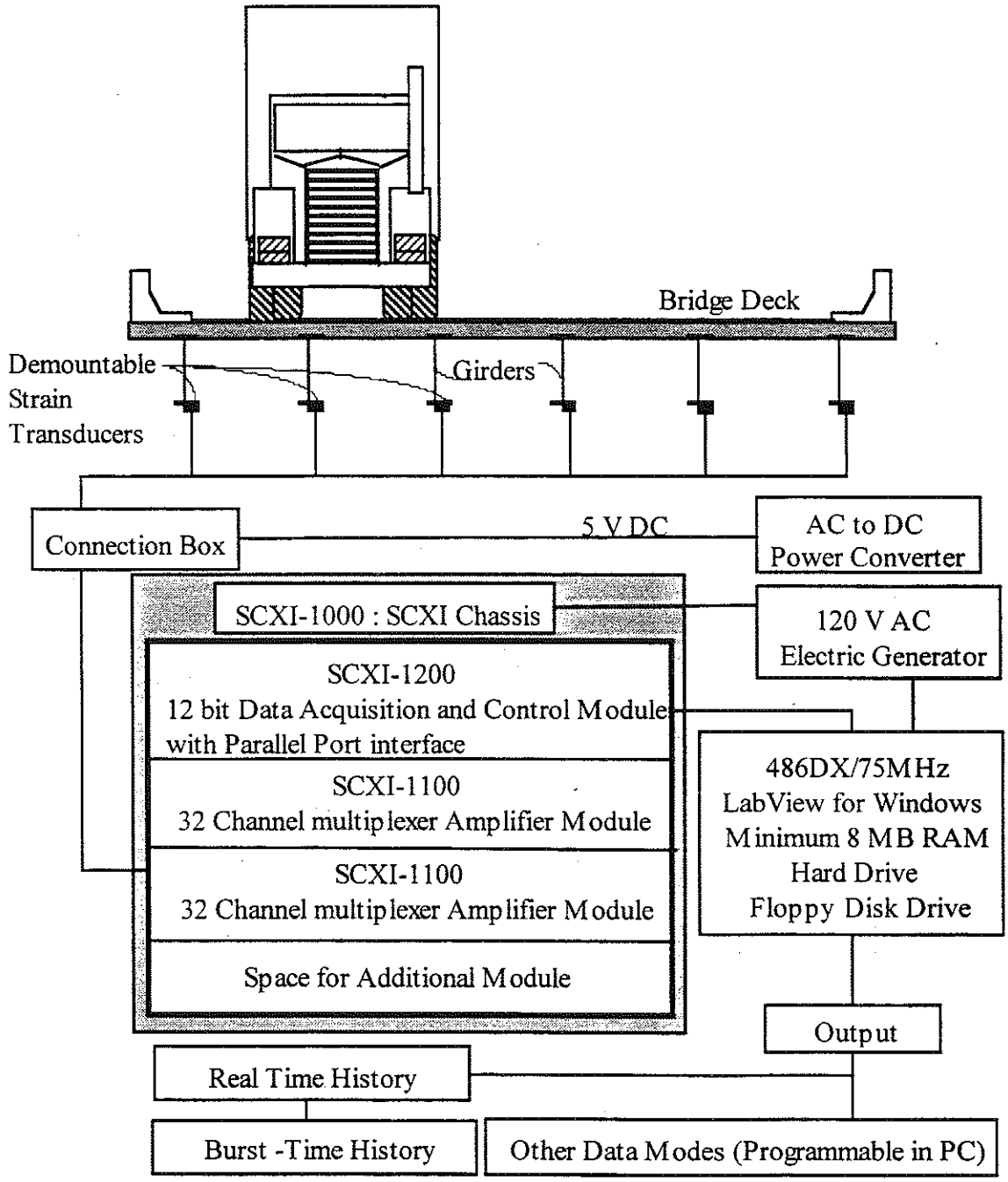

Fig. 5-1. SCXI Data Acquisition and Control System

The SCXI-1200 data acquisition module is a multifunction analog, digital, and timing module. It is connected directly to the standard PC parallel printer port. The module has a 12-bit analog to digital converter (ADC) and a sustained sampling rate of 20 kHz in the Standard Parallel Port (SPP) mode. It acquires data from and controls several SCXI signal conditioning modules installed in the same chassis.

The SCXI-1100 is a 32 differential channel multiplexer amplifier module. It can be configured to sample a variety of millivolt and volt signals by using the selectable gain and bandwidth settings. The signals from the strain transducers are connected to the SCXI-1100 module. Each SCXI-1100 module multiplexes the 32 channels into a single channel of the SCXI-1200 module. Several SCXI-1100 modules can be cascaded to multiplex hundreds of signals into a single channel on a SCXI-1200 module. Conditioned signals from the SCXI-1100 are passed along the SCXIbus in the back of the chassis to the SCXI-1200 data acquisition module. LabView is used to control the SCXI-1200 module and signal conditioning functions on the SCXI modules.

LabView is the data acquisition and control programming language installed on the PC. It has the necessary library functions for data acquisition, analysis, and presentation. The data acquisition parameters, such as sampling rate and data acquisition mode, are controlled with options in LabView. After data acquisition, the voltage data can be converted into strains by using the analysis routines in LabView. The results are displayed on the computer screen in real time and saved on the PC's hard drive. The SCXI system in conjunction with LabView has far more flexibility for data acquisition, analysis, and presentation than a system with built-in control software. With built-in control software, all routines are preprogrammed and unchangeable, while if LabView is used, the SCXI system can be controlled according to the user's specific needs and objectives.

5.3. Installation of Equipment

Strain transducers should be installed following the same procedure as described for a weigh-in-motion test, as explained in Chapter 4.3.

5.4. Measurement

This test can be carried out simultaneously with a weigh-in-motion test. Field measurements are taken by the SCXI system described above to determine the actual dynamic load effects and to verify the available analytical models [Hwang and Nowak, 1991; Nassif and Nowak, 1995; Kim and Nowak, 1997]. For each truck passage, the dynamic response is monitored by recording strain data. Truck weight, speed, axle configuration, and lane occupancy may also be determined and recorded from WIM measurements when a dynamic test is carried out. A suitable sampling rate for a dynamic test is 200 Hz.

5.5. Processing and Presentation of the Results

An example of the actual bridge response for a vehicle traveling at a highway speed is shown in Fig. 5-2. For comparison, also shown is an equivalent static response, which was developed from the same vehicle traveling at crawling speed.

There are different definitions for the dynamic load factor, as described by Bakht and Pinjarkar (1989). The dynamic load is usually considered as an equivalent static live load and it is expressed in terms of the dynamic load factor (DLF):

$$DLF = \varepsilon_{dyn} / \varepsilon_{stat} \qquad (5\text{-}1)$$

where ε_{dyn} is the maximum dynamic response (in terms of stress, strain or deflection) measured from the test data, and $\varepsilon_{dyn} = \varepsilon_{total} - \varepsilon_{stat}$. ε_{total} is the total response, and ε_{stat} is the maximum static response obtained from the filtered dynamic response.

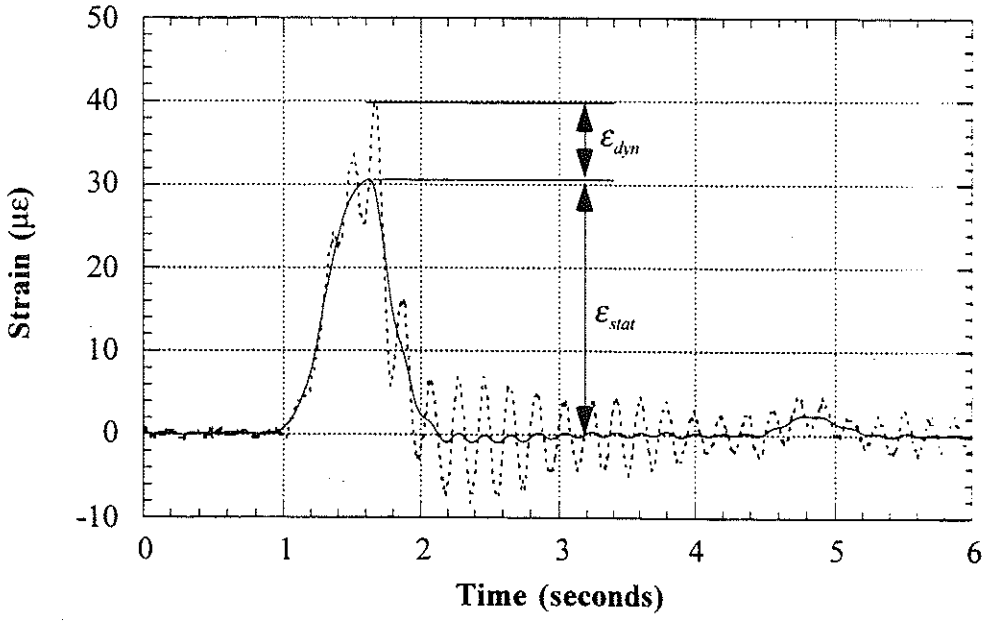

Fig. 5-2 Dynamic and Static Strain under a Truck Traveling at Highway Speed.

A numerical procedure is applied to filter and process collected data. The DLF is determined under normal truck traffic for various load ranges and axle configurations.

An example of the actual static and dynamic strains is shown in Fig. 5-3. In Fig. 5-4, the CDF of the static stress is plotted on normal probability paper. For each value of static stress, the corresponding

dynamic stress is also shown. The stress due to dynamic load is nearly constant and is not dependent on truck weight. Fig. 5-5 shows dynamic load factors as a function of static strains. Also shown in the figure is a power curve fit, which approximately represents mean values of the DLF's. In general, the DLF decreases as static strain increases. Therefore, the DLF is smaller for heavier trucks.

Dynamic load effects can also be illustrated versus girders of bridge (Fig. 5-6). Typically, very large values for impact factors are found for girders with the lowest static strains. Exterior girders most commonly display this behavior, and as discussed earlier, large impact factors in girders of low static strain are of no concern.

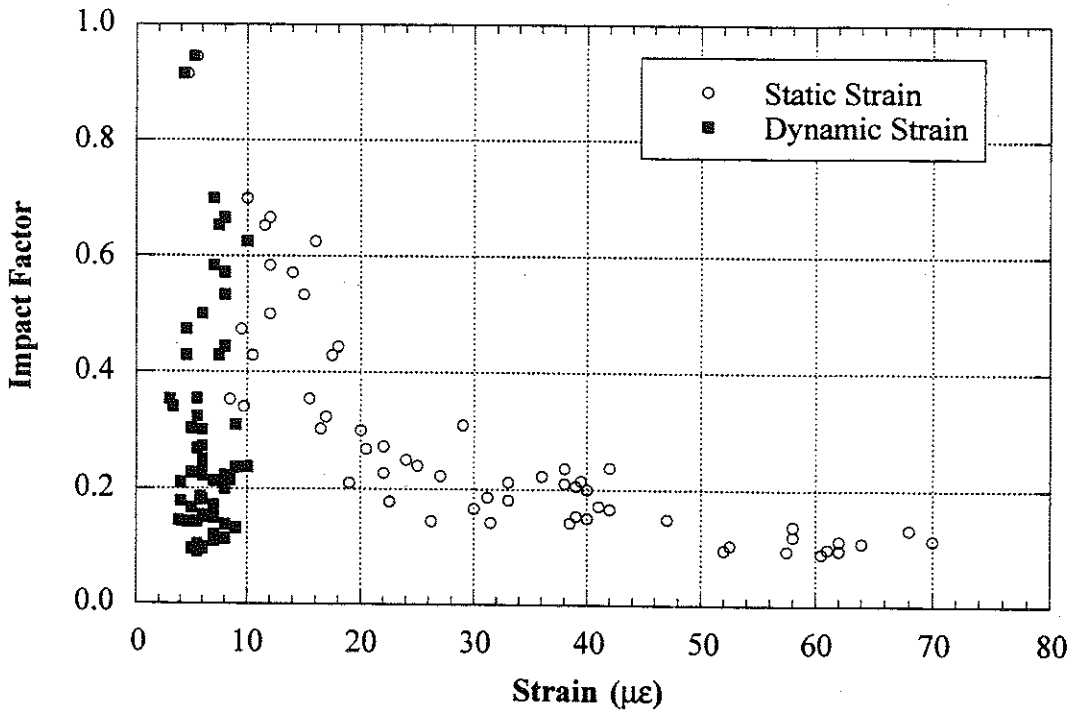

Fig. 5-3. Static and Dynamic Strains.

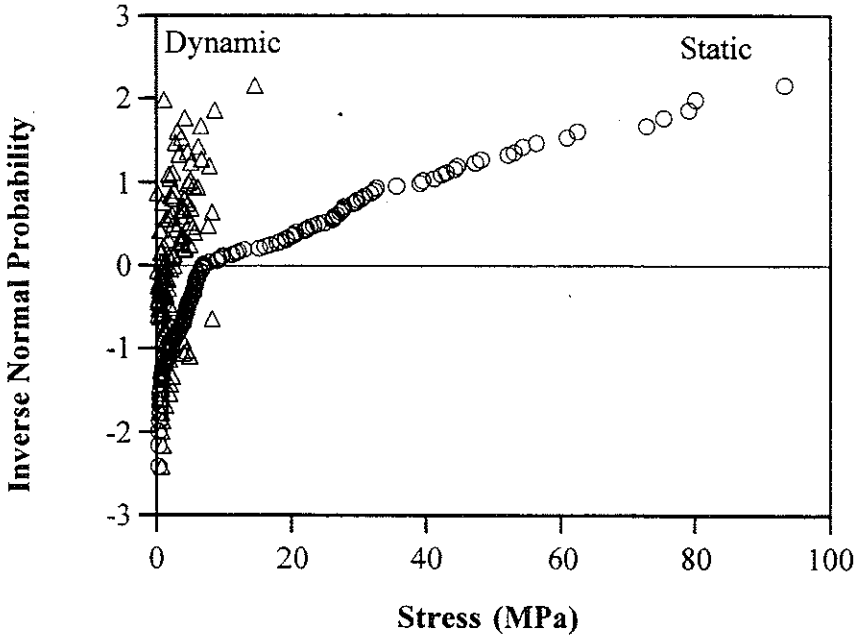

Fig. 5-4. Typical CDF of Static Stress and Corresponding Dynamic Stress.

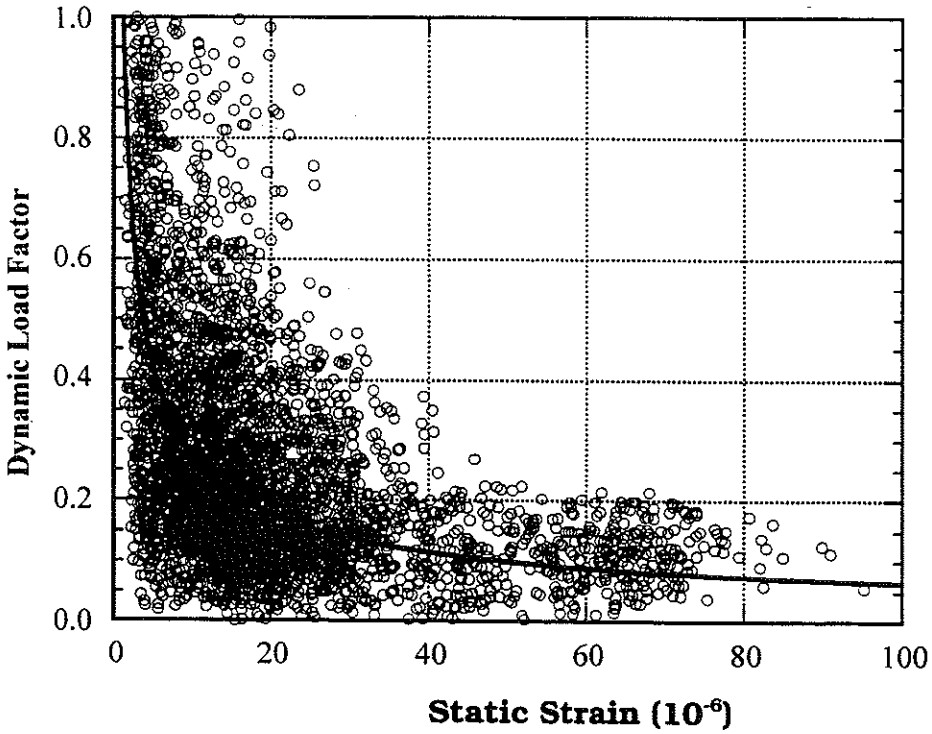

Fig. 5-5. Dynamic Load Factor versus Static Strain.

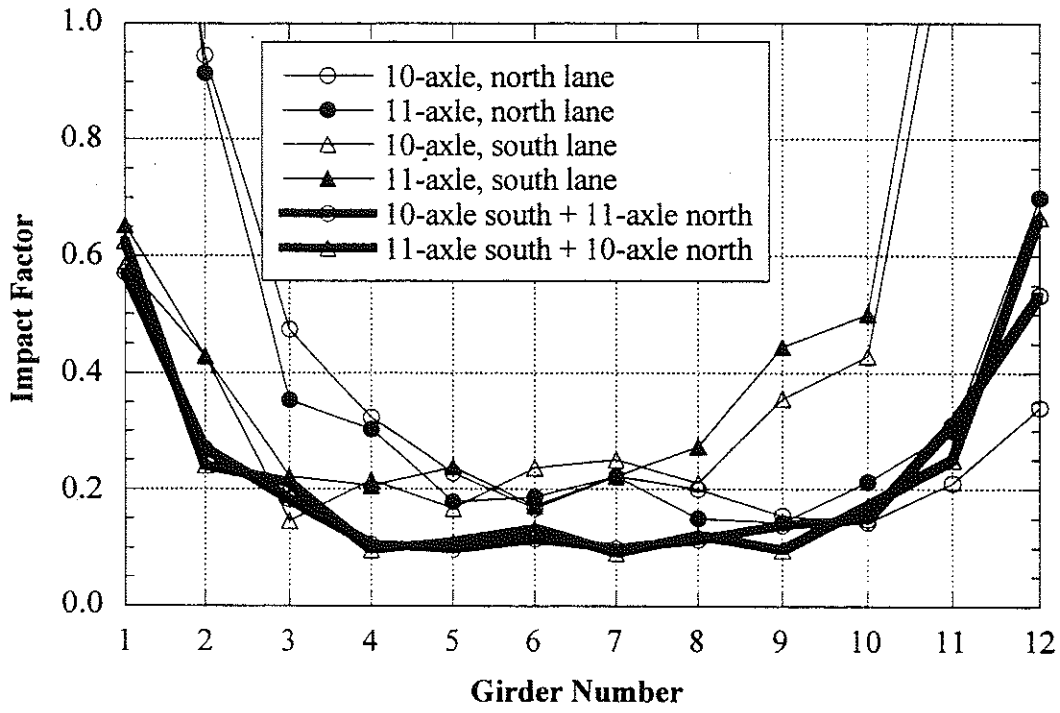

Fig. 5-6. Dynamic Load Factors vs. Girders

6. Fatigue Load Measurement

6.1. Procedure

Development of a probabilistic fatigue load model requires the collection of actual dynamic stress time histories for various members and components. Following a collection of time histories, the data must be processed into a usable form. The expected fatigue life of a component is then calculated using the rainflow method.

6.2. Equipment

The Stress Measuring System (SMS), with the main unit manufactured by the SoMat Corporation, is shown in Fig. 6-1. It collects component strain histories produced by actual traffic loads, and assembles the stress cycle histograms by the rainflow method of cycle counting and other counting methods. The data is then stored to memory and down-loaded at the conclusion of the test period. The rainflow method counts the number of cycles, n, in each predetermined stress range, S_i, for a given stress history. The SMS is capable of recording up to 4 billion cycles per channel for extended periods in an unattended mode. Strain transducers are attached to all girders at the lower mid-span flanges of a bridge.

The SoMat Corporation Strain Gage Module is shown in Fig. 6-1. It includes a power/processor/ communications module, a 1 Megabyte CMOS extended memory unit, and 8 strain gage signal conditioning modules. The system is designed to collect strains through 8 channels in both attended and unattended modes with a range of 2.1 mV to 12.5 mV. A notebook computer is used to communicate with the SoMat system to control the data acquisition mode, calibration, initialization, data display, and downloading of data. The SoMat system

has been configured specifically for the purpose of collecting stress/strain histories and statistical analysis for highway bridges. This application is particularly suitable because of the modular component arrangement of the SoMat system.

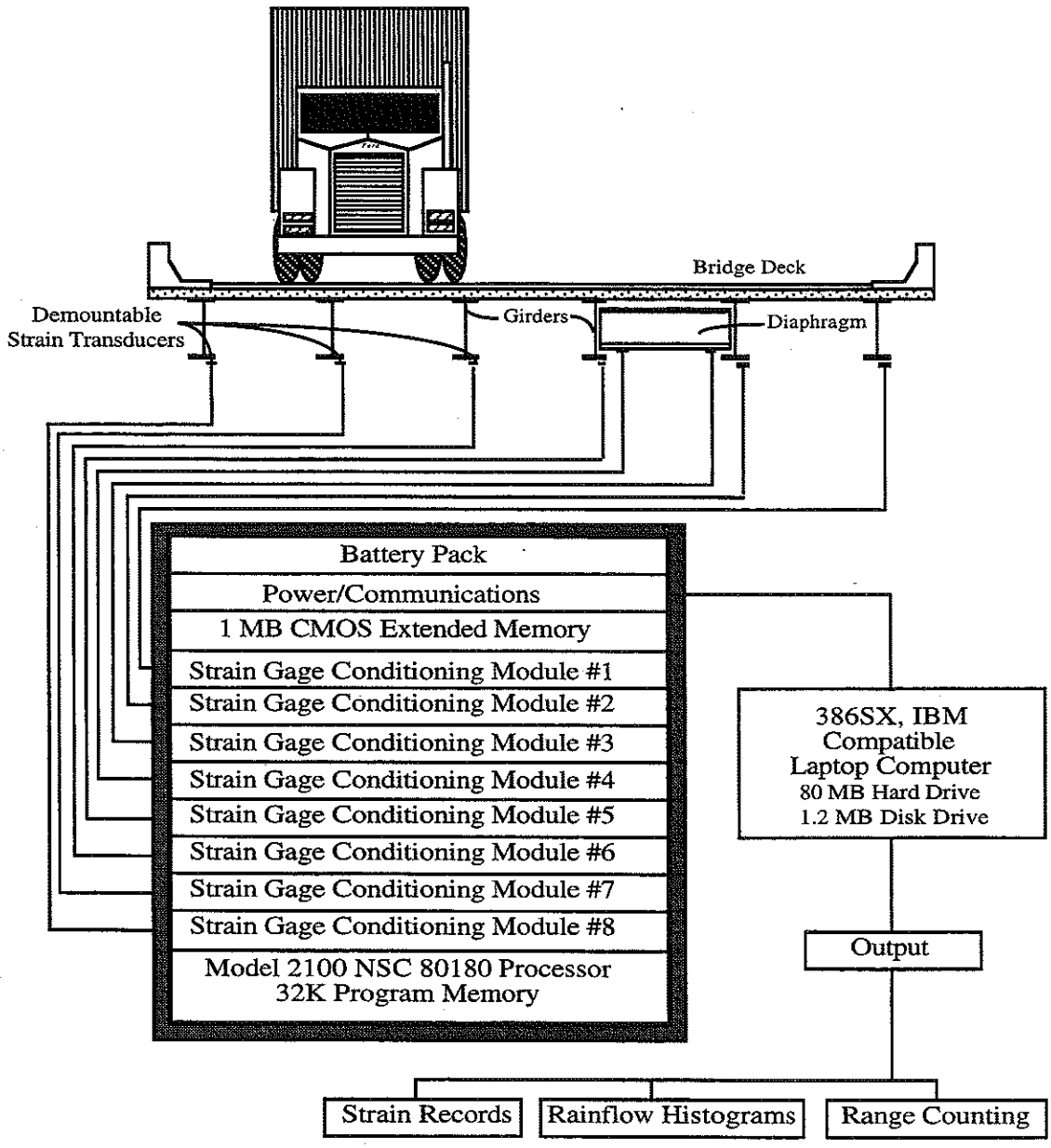

Fig. 6-1 SoMat Strain Data Acquisition System.

The data-acquisition system consists of five major components totaling 12 modules; eight strain transducer signal conditioning modules, and one each for a battery pack, a Power/Communications module, a 1MB CMOS Extended Memory module, and a Model 2100 NSC 80180 processor (see Fig. 6-9). Regulated power is supplied by a rechargeable 11.3 - 13.4 volt electrically isolated DC/DC converter. This unit powers all modules as well as provides excitation for the strain transducers. Serial communications via an RS 232C connector, and battery backup for memory protection, is provided by the Power/ Communications module. An Extended Memory Module of 1 megabyte, high speed, low power CMOS RAM with battery backup is included for data storage. The strain gage conditioning modules each provide 5-volt strain transducer excitation, internal shunt calibration resistors, and an 8-bit, analog-to-digital converter. Further information is given in Appendix A.

The strain measurement range is ± 2.1-mV minimum and ± 12.5 mV maximum. The processor module consists of 32 kilobytes of programmable memory and an NSC 80180 high speed processor capable of sampling data in simultaneous mode resulting in a maximum sampling rate of 3000 Hz. Communication to the PC is via RS 232C at 57600 baud. Data acquisition modes include time history, burst time history, sequential peak valley, time at level matrix, rainflow matrix, and peak valley matrix. Following collection, data are reviewed and downloaded to the PC hard drive for storage, processing, analysis, and plotting.

6.3. Installation of Equipment

Strain transducers should be attached to the point of maximum moment of each girder. For simple spans, however, a midspan placement is sufficiently close to the point of maximum moment, and

this can be used for attachment. The attachment technique is described in Chapter 4.3. Since the stresses are to be recorded over an extended period of time (a minimum of 1 week), the data acquisition system must be attached to a reliable and secure location on the bridge.

6.4. Measurements

Strain histories usually must be collected continuously for periods of at least one week long, although this time can be reduced using the rainflow algorithm [Nowak, Nassif and Frank, 1993; Nowak, Laman and Nassif, 1994; Laman and Nowak, 1996]. 50 Hz is a sufficient sampling rate for a fatigue load test. Data should be collected for each bridge girder.

6.5. Processing and Presentation of the Results

6.5.1. Rainflow Method of Cycle Counting

Commonly occurring load histories in fatigue analysis often are categorized as either narrow band or wide band processes. Narrow band processes are characterized by an approximately constant period, such as that shown in Fig. 6-2(a). Wide band processes are characterized by higher frequency small excursions superimposed on a lower, variable frequency process, such as that shown in Fig. 6-2(b). For steel girder highway bridges, where the loading is both random and dynamic, the stress histories are wide band in nature.

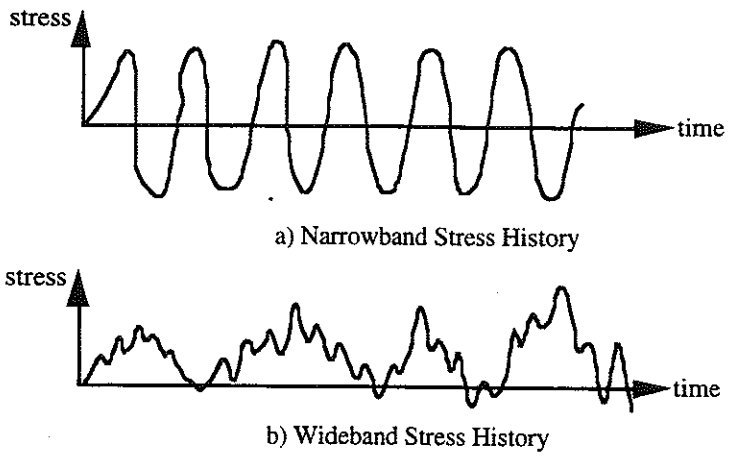

Fig. 6-2 Example of Narrow and Wide Band Stress Histories.

Stress histories which are wide band in nature do not allow for simple cycle counting. The cycles are irregular with variable frequencies and amplitudes. Several cycle-counting methods are available for the case of wide band and nonstationary processes, and each are successful to a degree in predicting the fatigue life of a structure. The rainflow method is preferred due to the identification of stress ranges within the variable amplitude and frequency stress histogram, which are associated with closed hysteresis loops. This is important when comparing the counted cycles with established fatigue test data obtained from constant amplitude stress histories.

The rainflow method counts the number of cycles, n, in each predetermined stress range, S_i, for a given stress history. Rules of counting are applied to the stress history after orienting the trace vertically, with the positive time axis pointing downward. This convention facilitates the flow of "rain" due to gravity along the trace and is merely a device to aid in the understanding of the method. Rules for the rainflow method are as follows (see Fig. 6-3):

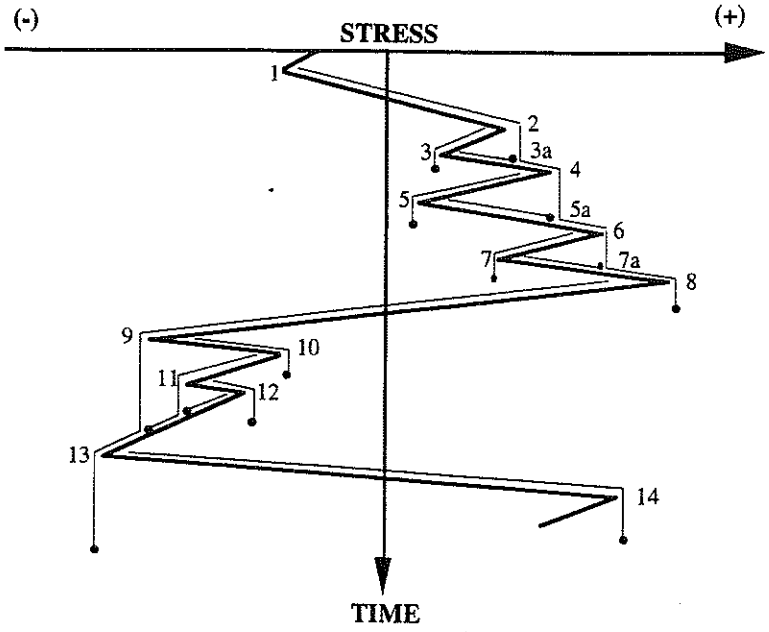

Fig. 6-3 Rainflow Counting Diagram.

1. All positive peaks are evenly numbered.
2. A rainflow path is initiated at the inside of each stress peak and trough.
3. A "rainflow" progresses along a slope and "drips" down to the next slope.
4. A "rainflow" is permitted to continue unless the flow was initiated at a minimum more negative than the minimum opposite the flow, and similarly for a rainflow initiated a maximum. For example, path 1-8, 9-10, 2-3, 4-5, and 6-7.
5. A "rainflow" must stop if it meets another flow that flows from above. For example, path 3-3a, 5-5a, and 7-7a.
6. A "rainflow" is not initiated until the preceding flow has stopped.

Following the above procedure, each segment of the history is counted only once. Half cycles are counted between the most negative minimum and positive maximum, as well as the half cycles or interruptions between the maximum and minimum. As shown in Fig.6-3, all negative trough-initiated half cycles will eventually be paired

with a peak-initiated cycle of equal magnitude. For a more detailed explanation and discussion of the rainflow method and others, introductory texts on fatigue analysis are available [Banantine, Comer and Handrock, 1992].

6.5.2. Results of Strain Spectra Testing

To aid interpretation of the results, the CDFs of strain cycles and the corresponding equivalent stress values are plotted on normal probability paper (Fig. 6-4). For each bridge, the CDFs are shown for strains in girders numbered from 1 (exterior, on the right-hand side looking in the direction of the traffic).

As a means of comparison of fatigue live load, the equivalent stress, s_{eq}, is calculated for each girder using the following root mean cube (RMC) formula:

$$Seq = \sqrt[3]{\sum p_i \cdot S_i^3} \qquad (6\text{-}1)$$

where S_i = midpoint of the stress interval i and p_i = the relative frequency of cycle counts for interval i. The stress, S_i, is calculated as a product of strain and modulus of elasticity of steel. s_{eq} values are shown on a graph for each girder (Fig. 6-5).

Stress spectra considerably vary from girder to girder (component-specific). Therefore, the expected fatigue life is different depending on girder location. Exterior girders experience the lowest load spectra.

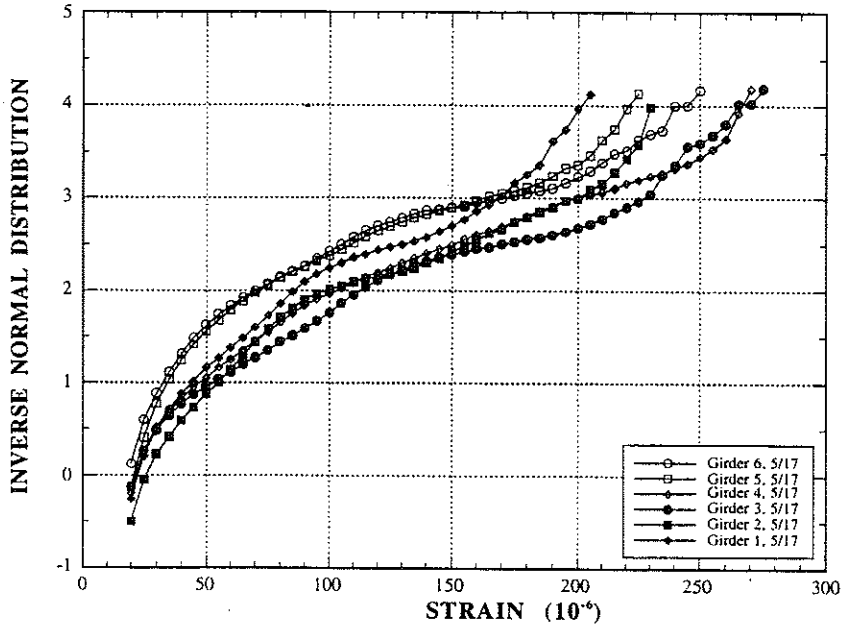

Fig. 6-4 Strains for Girders in Bridge US23/HR.

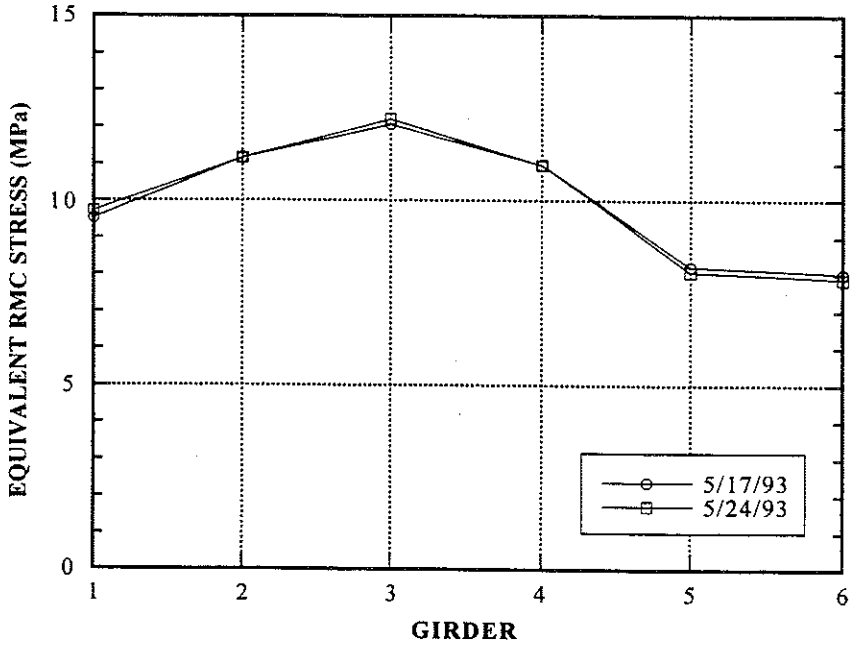

Fig. 6-5 Equivalent Stresses for Girders in Bridge US23/HR.

7. Load Distribution Tests

7.1. Procedure

The objective of this test is to determine the distribution of load to each girder. One or two trucks of known weight are used as the test load, and the resulting strains are collected from all girders. To determine the distribution of load transversely on the bridge, at least one strain value must be taken from each girder. To determine the longitudinal load distribution, strain values at the ends and quarter points of the girders are also necessary.

7.2. Testing Equipment

In load distribution tests, the SCXI data acquisition system described in Chapter 5.2, can be used with strain transducers.

7.3. Installation of Equipment

A typical installation layout for a highway bridge is shown in Fig. 7-1. The number and placement of instruments on the bridge may vary according to the test objective, but in general, transducers are placed to determine the distribution of load to the girders transversally and longitudinally, and to find the maximum load effects. Attachment of strain transducers is described in Chapter 4.3.

As with previous tests, the strain transducers are attached to the lower flanges of each girder at midspan, assuming that the bridge is a simple span. Although midspan is not the location of maximum stress, it is sufficiently close for test measurements. For continuous spans, the locations of maximum effect should be estimated analytically, and the transducers should be placed there.

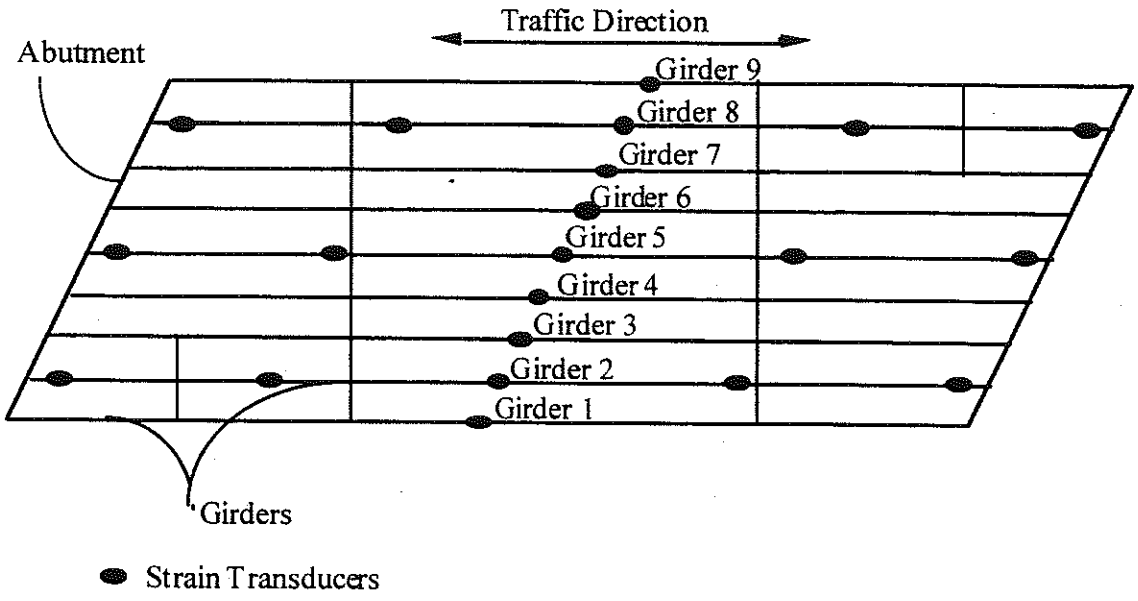

Fig. 7-1. Typical Bridge Disposition Plan

Additionally, for at least one of the girders, strain transducers should be attached at each quarter point to determine influence line of girder. If the degree of support fixity is to be determined, it is also necessary to attach a strain transducer next to each support.

Since the locations of maximum load effect are to be determined, a visual inspection of the bridge girders may yield additional points of desirable gauge placement. If there is significant corrosion damage on the girders, for example, locations with the smallest remaining flange thickness should be monitored with a transducer.

All spans of multi-span structures should be tested. Although the simple spans of multi-span bridges can be tested individually, it would be useful to instrument neighboring spans to check for unintended continuity. If the spans are continuous, the measurements should be made simultaneously on all spans. In this case, strain transducers should also be attached around each pier.

If there is a lack of equipment or time to instrument all that is desired, points on the structure that are expected to provide the smallest load response should be eliminated first. External steel girders with concrete facia often fall into this category, as do concrete girders that has extensive cracks or damage, which are not suitable for strain measurement. Additionally, it is sometimes not possible to attach displacement transducers at some spans, if there is deep water or un-reroutable traffic below.

7.4. Measurements

During the test, the trucks are driven across the bridge at crawling speed, which will generate the maximum static stresses. High-speed tests are used to determine impact factors and variations in response. 50 Hz is an appropriate sampling rate for this test.

The following load combinations may be performed for bridges which have two lanes. These loadings may be repeated at high speed.

- A truck along the center of the first lane
- A truck close to the curb of the first lane
- A truck along the center of the second lane
- A truck close to the curb of the second lane
- A truck along the center of the first lane and another truck along the center of the second lane.

To determine girder distribution and impact factors, strain data taken from the bottom-flanges of mid-span girders are adequate. For a complete bridge diagnostic test, however, displacement data (via LVDT's) is also necessary. During the tests, transducer signals are recorded continuously with suitable amplification and sampling rates.

7.5. Processing and Presentation of The Results

7.5.1. Load Distribution Factor Calculation from Test Results

Girder Distribution Factors (GDF) are calculated from the maximum strain obtained from the static loading at each girder at the same section along the length of the bridge. Ghosn *et al.* (1986) assumed that GDF was equal to the ratio of the static strain at the girder to the sum of all the static strains. Stallings and Yoo (1993) used the weighted strains to account for the different section modulus of the girders. The GDF for the *i*th girder, GDF_i, can be expressed as follows:

$$GDF_i = \frac{M_i}{\sum_{j=1}^{k} M_j} = \frac{ES_i\varepsilon_i}{\sum_{j=1}^{k} ES_j\varepsilon_j} = \frac{\frac{S_i}{S_\ell}\varepsilon_i}{\sum_{j=1}^{k} \frac{S_j}{S_\ell}\varepsilon_j} = \frac{\varepsilon_i w_i}{\sum_{j=1}^{k} \varepsilon_j w_j} \qquad (7\text{-}1)$$

where M_i = bending moment at the *i*th girder; E = modulus of elasticity; S_i = section modulus of the *i*th girder; S_ℓ = typical interior section modulus; ε_i = maximum bottom-flange static strain at the *i*th girder; w_i = ratio of the section modulus of the *i*th girder to that of a typical interior girder; and k = number of girders.

When all girders have the same section modulus (that is, when weight factors, w_i, are equal to one for all girders), Eq. (7-1) is the equivalent to that of Ghosn *et al.* Because of the edge stiffening effect due to sidewalks and barrier walls, the section modulus in exterior girders is slightly greater than that in interior girders. In other words, the weight factors, w_i, for exterior girders are greater than one. Therefore, from Eq. (7-1), if the weight factors, w_i, are assumed equal to one, the GDFs in interior girders will be slightly overestimated, and slightly underestimated in the exterior girders.

Measured GDFs can be compared with the values calculated according to the current design codes, expressions for which are given in Chapter 2.

7.5.2. Summarizing Results

The test and calculation results can be summarized graphically. The two charts of Fig. 7-2, for example, show stresses measured from girder mid-points and their resulting distribution factors. These graphs are prepared for each lane, and each line in a graph is drawn for a different truck position. A separate set of graphs can display the results of two-lane loading (Fig. 7-3). The superposition of single lane loadings is also shown in this graph. The similarity between the superposition and two-lane loading curves indicates linear behavior of the structure.

Another important graphical summary is the distribution factor envelope, in which the maximum distribution factor for each girder found from any single-lane load test is plotted. The process can be repeated for the two-lane load test. The more flat the resulting graph, the more even the load is distributed to each of the girders.

The code-specified GDF can also be plotted on this graph for comparison (Fig. 7-4). The formulas for GDF in AASHTO (1996) and AASHTO LRFD Code (1994) are given in Chapter 2 of this report.

Another group of graphs can show the longitudinal distribution for each lane and two-lane loading (Fig. 7-5). In these graphs, the x axis represents the girder length, and the y axis represents strain. Each line shows a different load case. In Fig. 7-5, the negative strains at the west end indicate partial fixity at the support.

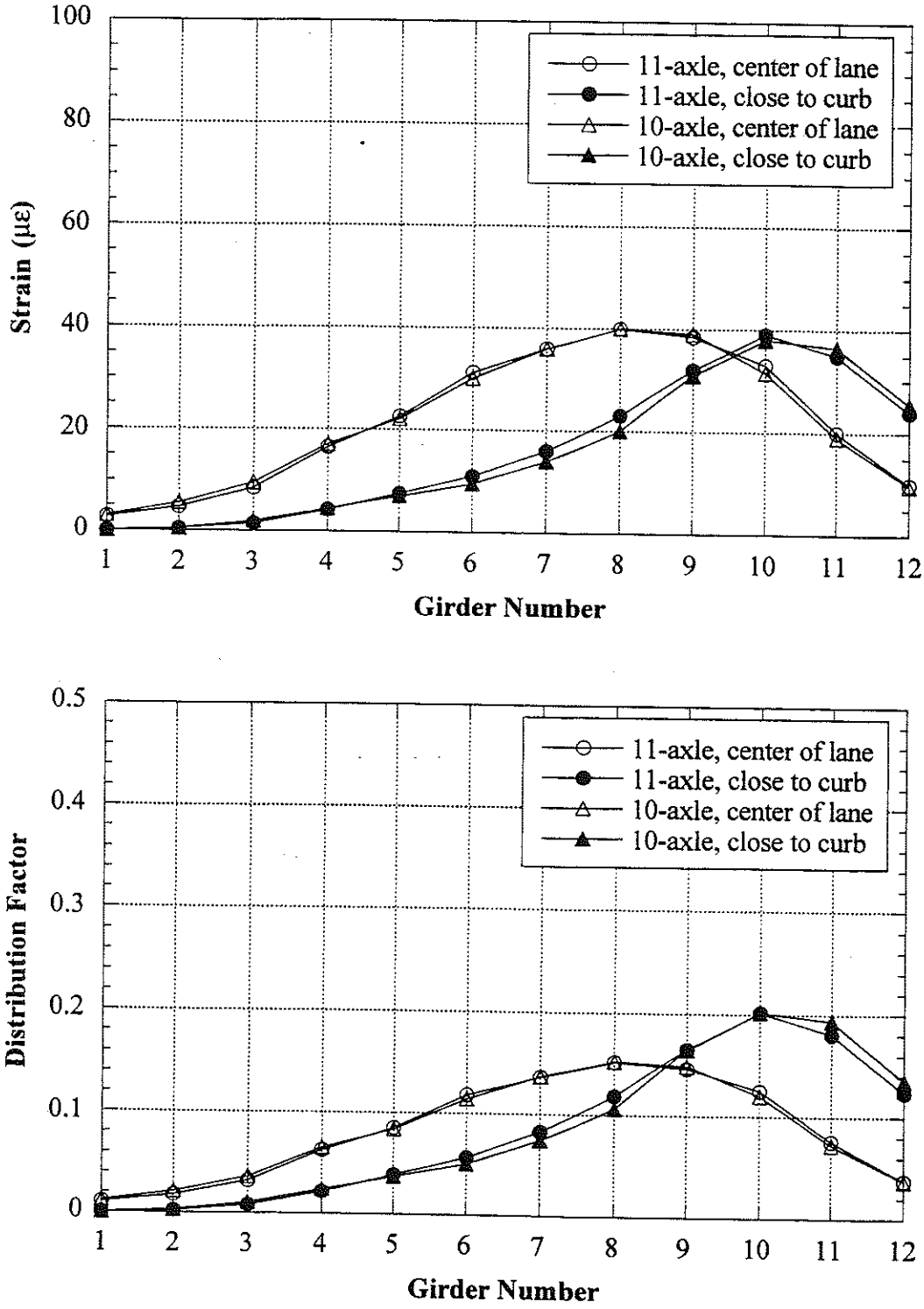

Fig. 7-2. Stress values measured from mid-span of girders while any lane was loaded and their distribution factors. This graphs should be prepared for other lanes

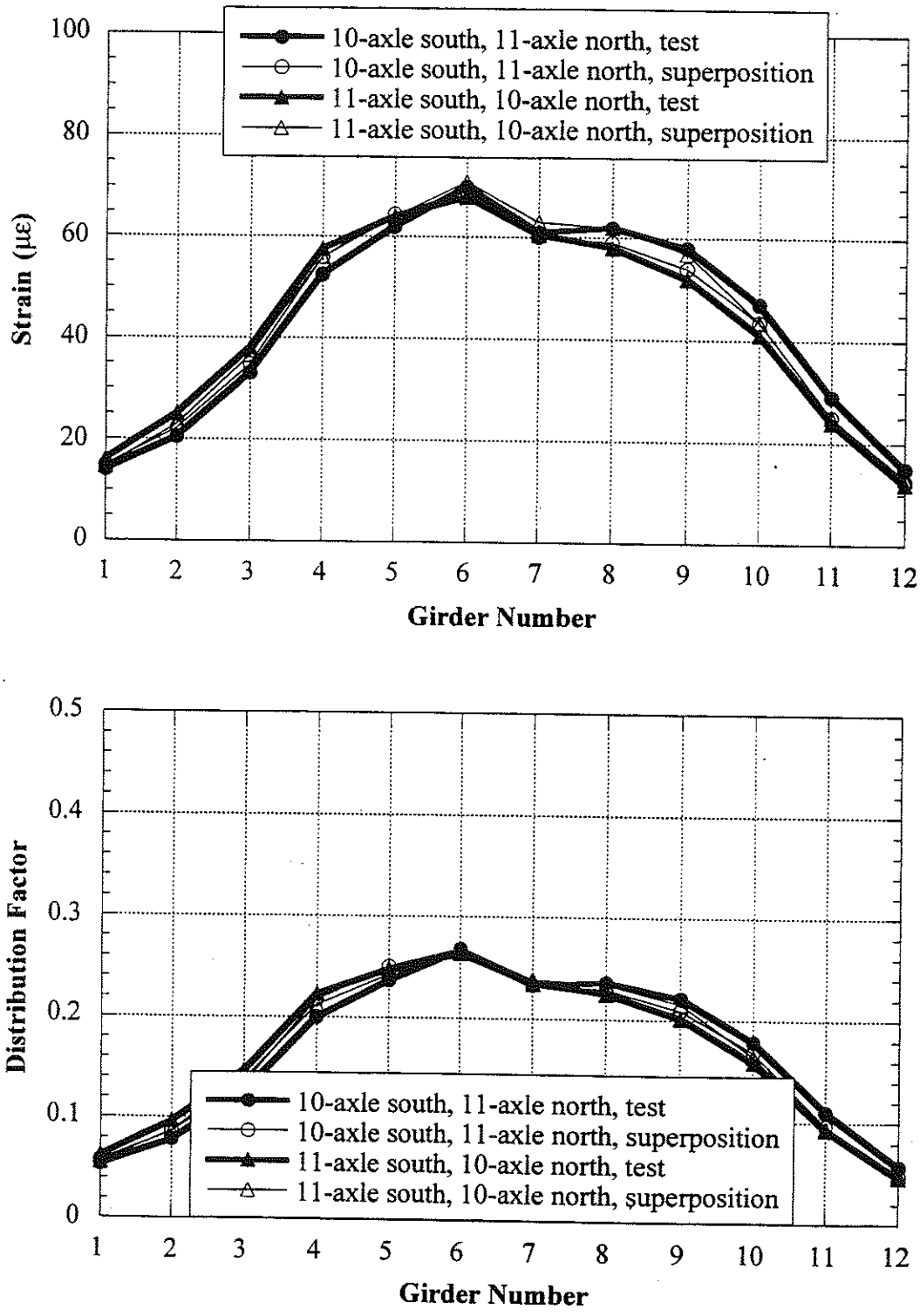

Fig. 7-3. Stress values measured from mid-span of girders while two of lanes was loaded and their distribution factors.

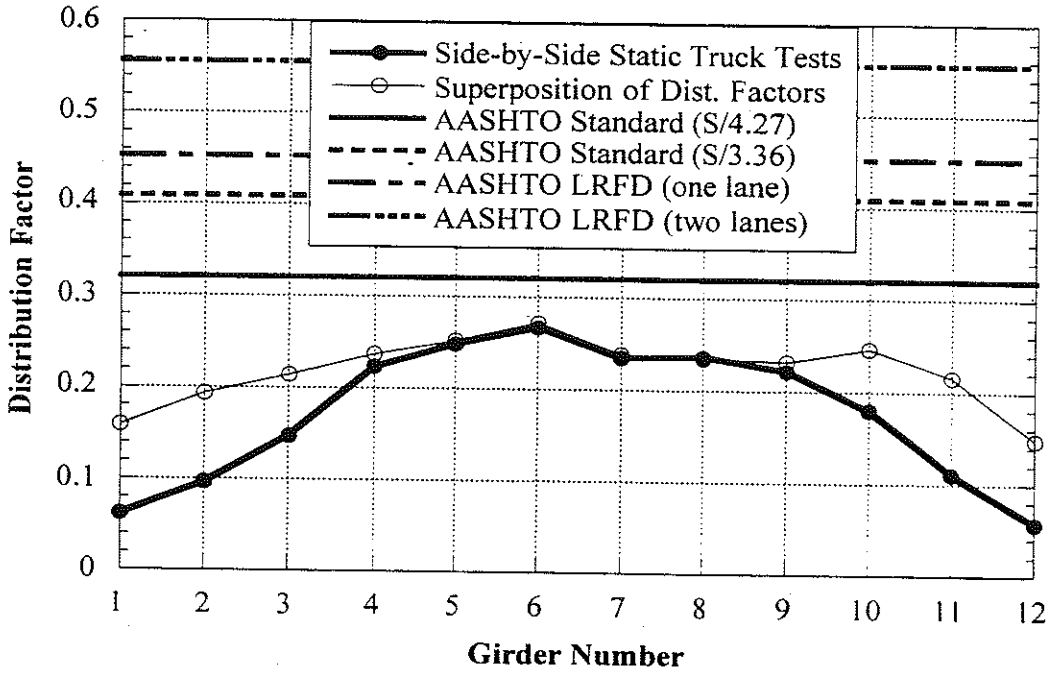

Fig. 7-4. Comparison with Code Specified Distribution Factor.

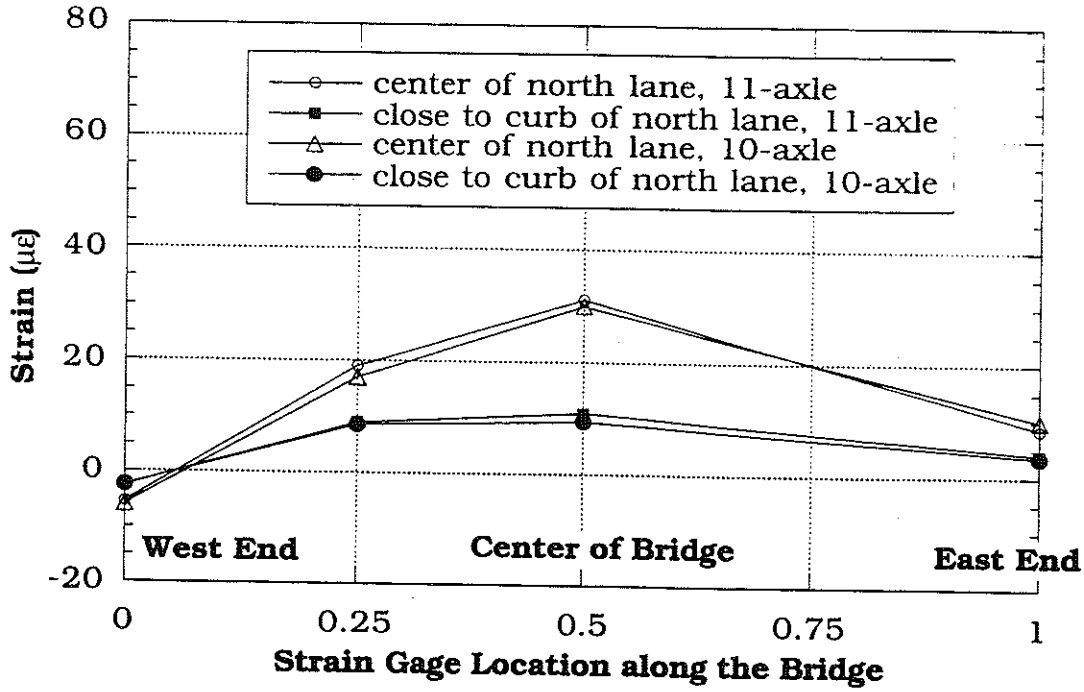

Fig. 7-5. Strain profile on any girder along the bridge, North Lane, tatic or crawling speed. This graph should be also prepare for South Lane and two-lane loading.

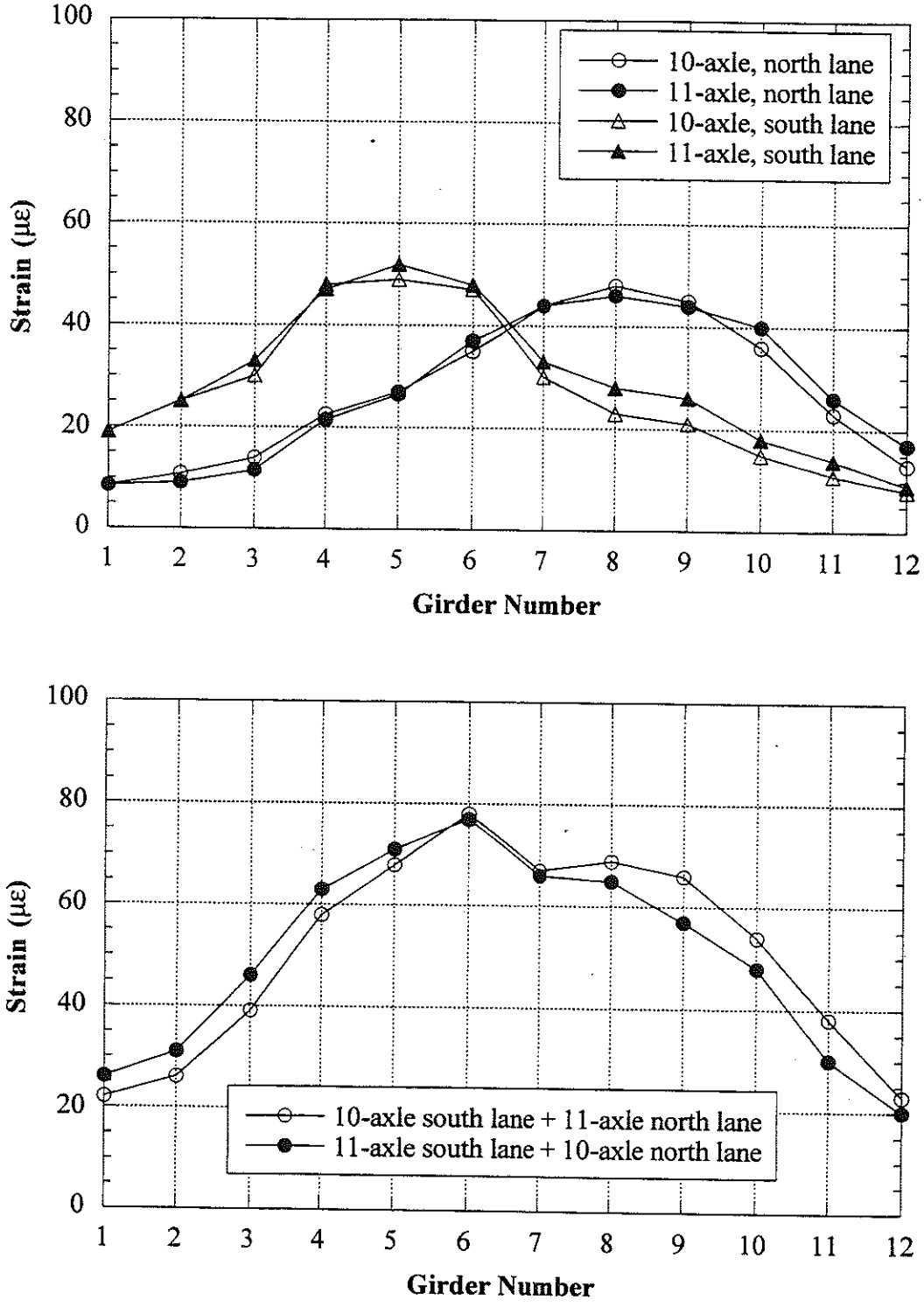

Fig. 7-6. Strains under one truck or side-by-side truck loading at high speed.

Note:
Intentionally left blank

8. Proof-Load Test

8.1. Procedure

The rating calculations and a preliminary design check of the selected bridges are carried out using the available design details and the deterioration (section loss) observed during site inspection. Proof load testing can be used either to find the yield capacity of the structure, or to check its ability to carry a specified live load. Usually, the yield capacity of a bridge is very high and requires exceptionally heavy loads, which make the tests uneconomical and slow. In this case, proof load tests are carried out to verify if the bridge can safely carry the maximum allowable legal load. Before the proof load tests, the target proof load is calculated as per Section 8.4.1. The type and placement of load, instrumentation and data acquisition setup would depend on the target proof load level.

8.2. Equipment

In proof load tests, the SCXI data acquisition system manufactured by National Instruments Corporation, can be used with strain transducers and displacement transducers (LVDT). The data acquisition system is described in Chapter 5.2. The information about displacement transducers (LVDT) can be found in Appendix A.

8.3. Installation of Equipment

A strain transducer is attached at midspan of each girder. Although this is not the location of maximum moment, it is sufficiently close for testing. It is also necessary to attach an LVDT next to each strain gauge to monitor displacement and verify the linearity of the structure's behavior. The sleeve of the LVDT is supported by a tripod

beneath the measurement position. A tensioned steel wire connect the LVDT core to the bridge girder, so movement of the girder cause simultaneous movement of the core. To maintain tension in the wire, the other end of the transducer core is anchored to a heavy steel plate on the ground, via another wire and spring (Fig. 8-1). All transducers are placed on the girders at the same distance from the abutment. The attachment technique of strain transducers is given in Chapter 4-3, and a typical data acquisition setup is shown in Fig. 8-1.

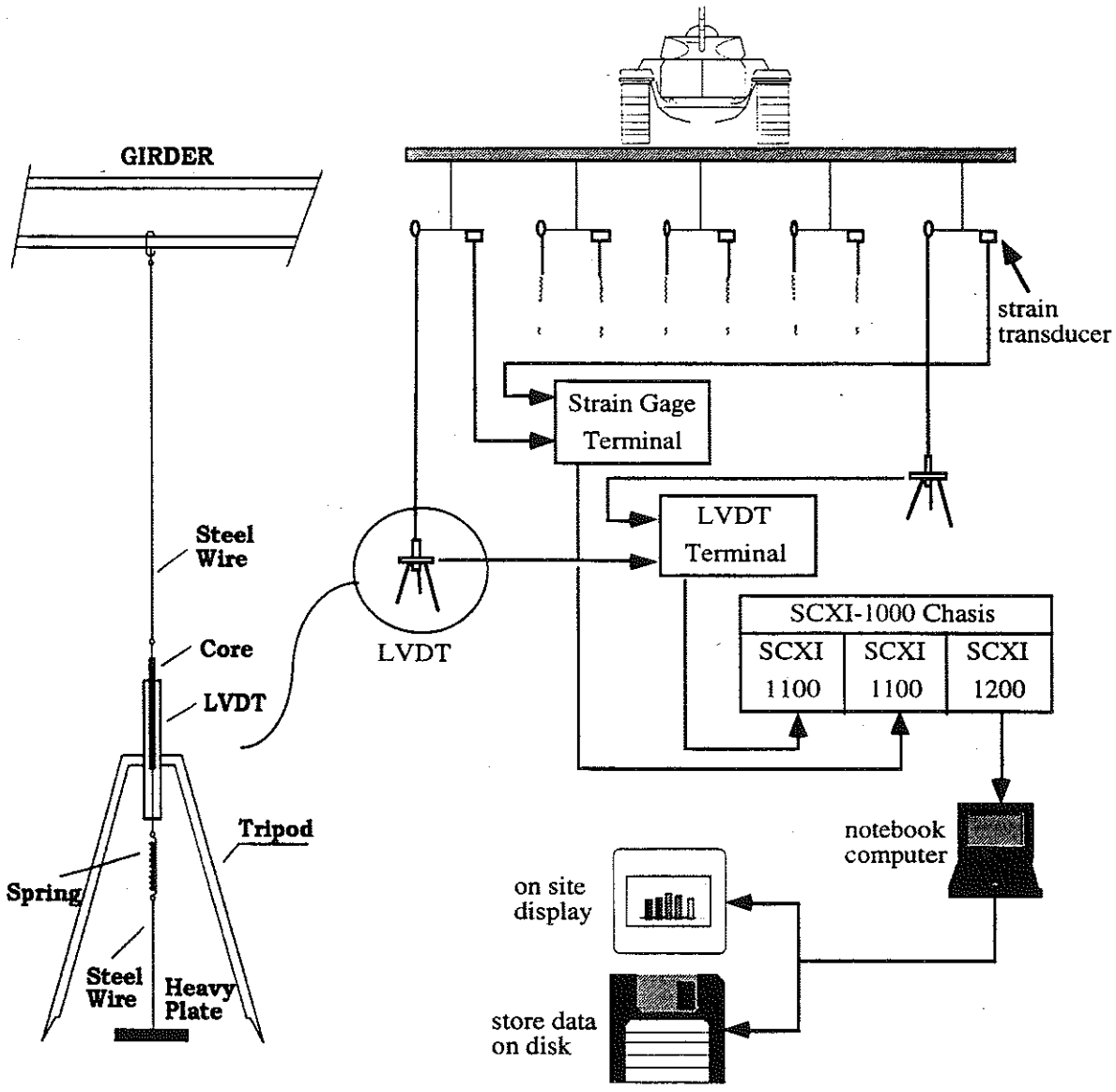

Fig. 8-1. Typical Data Acquisition Setup.

8.4 Load Selection

8.4.1 Calculation of Proof Load

In Michigan, the maximum moment in medium span bridges is caused by two unit 11-axle trucks. For such an 11-axle truck, the gross vehicle weight (GVW) can be up to 730 kN. It is more than twice the MS18 design load (Michigan Design Guide: Bridge Design, 1992).

The proof load level should be sufficiently higher than that from a two-unit 11-axle truck, to ensure the desired safety level. The final draft of the report NCHRP No:12-28(13)A [Lichtenstein, 1993] provides guidelines for calculating the target proof load level. It suggest that the maximum allowable legal load should be multiplied by a factor X_p, which represents the live load factor needed to bring the bridge to an operating rating factor of 1.0. The guide recommends that X_p should be 1.4 before any adjustments are made. It also recommends the following adjustments to X_p, which should be considered in selecting a target live load magnitude.

- Increase X_p by 15 percent for one lane structures or for other spans in which the single lane loading augmented by an additional 15 percent would govern.
- Increase X_p by 10 percent for spans with fracture critical details. A similar increase in X_p shall be considered for structures without redundant load paths.
- Increase X_p by 10 percent if inspections are to be performed less often than 2-year frequency.
- Reduce X_p by 5 percent if the structure is ratable and there are no hidden details, and if the calculated rating factor exceeds 1.0.

Application of the recommended adjustment factors, leads to the target live load factor X_{pa}. The net percent increase (Σ) in X_p, is found by summing the appropriate adjustments given above. Then

$$X_{pa} = X_p [1 + (\Sigma/100)] \quad (8\text{-}1)$$

The target proof load (L_t) is then:

$$L_t = X_{pa} (1 + I) L_r \quad (8\text{-}2)$$

$$1.3 \leq X_{pa} \leq 2.2 \quad (8\text{-}3)$$

where Σ = net percent increase in X_p, i.e. summation of the appropriate adjustments, L_r = the live load due to the rating vehicle for the loaded lanes, I = impact factor, and X_{pa} = the target live load factor.

8.4.2 Selection of Proof Load

In the tests of some researchers (Juntunen and Isola, 1995), concrete barrier blocks, each weighing about 22 kN, were used as load. However, in most cases, the required number of concrete blocks would be so large (5 or 6 layers) that it is not feasible to fit them on one truck. Other types of loads, such as steel coils, sand and gravel etc., loaded on an 11-axle truck, can be considered, but it would require considerable effort to place or move the load. In addition, expensive and heavy equipment is needed to load the trucks. Other options, such as building a water tank on top of the bridge and using water as the proof load, are also possible. Two significant drawbacks of all of these options are the considerable resources required, and the need for a complete bridge closure to traffic for a long period of time.

In addition, if the test procedure is carried out over an extended time period, temperature variations may be considerably large and can cause measuring inaccuracies.

As mentioned earlier, the moment at mid-span can be used as the critical value considered as the load effect for the proof load test. For a particular bridge, any load vehicle can be used that will generate a mid-span moment equivalent to that which would be produced by a vehicle of the maximum allowable legal load (L_r). The required mid-span moments needed for a proof load are calculated using report NCHRP 12-28(13)A [Lichtenstein, 1993].

M-60 military tanks are recommended as load in proof load tests. Since the mid-span moment can be increased by moving the tanks further onto the bridge, the load steps can be as small as desired, lowering the risk of collapse. The tanks can be placed accurately and quickly as compared to other load methods (such as concrete blocks), which results in a faster test and less traffic disruption. On average, one bridge can be tested in three hours. The use of tanks also allows for the passage of traffic over one lane of the bridge when the tanks are being positioned; a full closure is required only at the critical time of maximum load.

Each tank weighs 504.2 kN and the load is distributed over a track length of 4.5 m, a load configuration that can generate high moments at mid-span. For some short-span bridges, just one tank is enough to generate the required proof load moment, while for moderate spans, two or more tanks are required. If two lanes of any bridge are loaded simultaneously, the required 15 percent increase for single lane loading is not applied. In past tests, tanks were provided by the Michigan National Guard. The front and side views of the M-60 tanks are shown in Fig. 8-2.

Tank tracks may cause damage to the bridge wearing surface. To avoid this damage, the tanks can be placed on flat bed trailers. Fig. 8-3 and 8-4 show the two different trailers used during a proof load test. Only the four rear axles of these trailers were used to load this specific bridge. For some tests, if the trailers are unavailable, or when the tanks must be positioned closely together to generate the required moment, the tanks can be placed directly on the pavement. Past tests indicate that the tanks do not always damage the pavement, and the tanks alone are easier to position than the tank/trailer combinations. Although the tanks are wider than the 11-axle trucks, the girder distribution factors for both vehicles are about the same for both composite and noncomposite structures [Saraf, Sokolik and Nowak, 1997].

Prior to the testing of each bridge, the axle weights of the four rear axles of a trailer/tank combination, shown in Figure 8-3 and 8-4, must be measured at a weigh station. If available, a portable scale can be used on site to improve the accuracy of the axle weights. As an example, typical axle weight values are shown in Fig. 8-3 and 8-4. The weight of the tank is specified in Michigan National Guard documents as 504.2 kN.

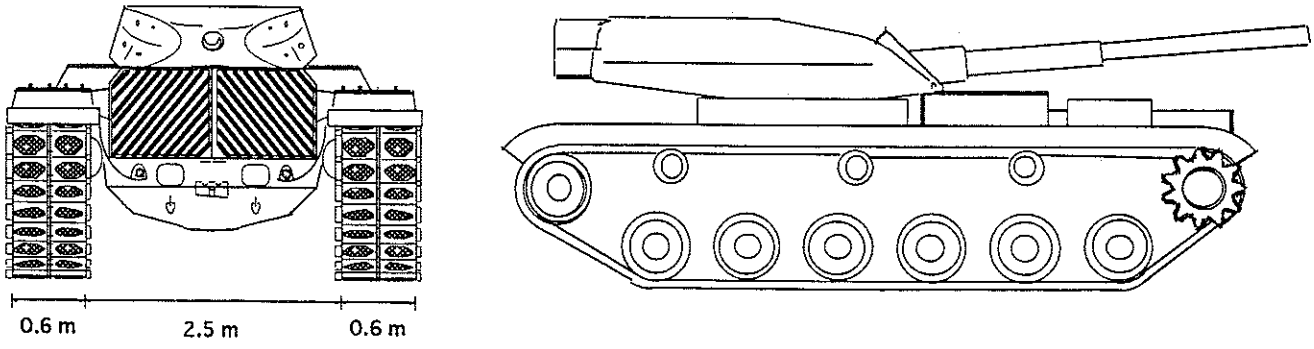

Fig. 8-2. M-60 Tank.

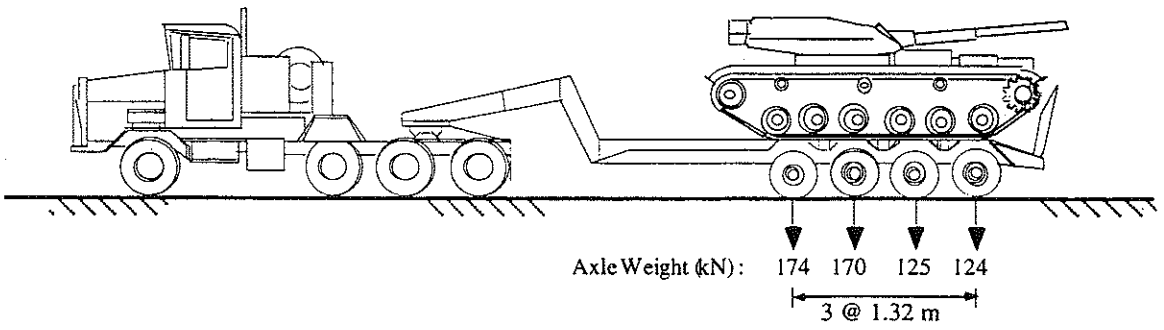

Fig. 8-3. Tank on a Military Trailer.

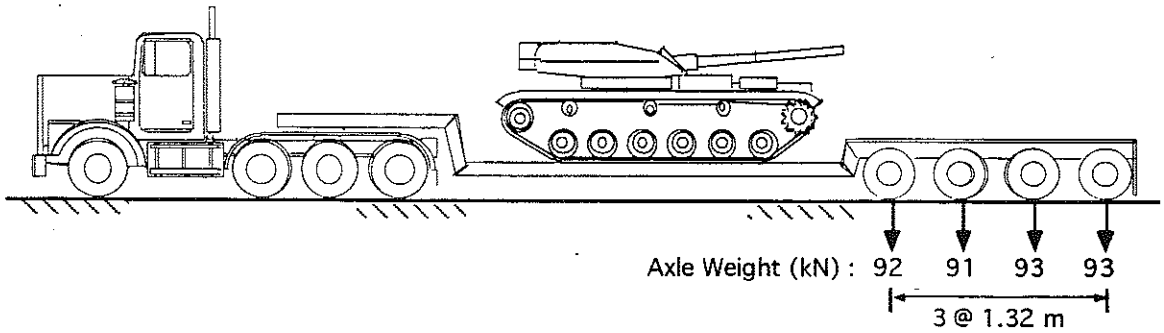

Fig. 8-4. Tank on a Commercial Trailer.

8.5. Measurements

8.5.1. Load Positions

As noted earlier, the proof load should be applied by gradually increasing the load until the target proof load level is reached. Tanks alone or on trailers should be moved from the supports to the mid-span in several steps to gradually increase the mid-span moment. Each step is referred to as a load position. For bridges that require more than two tanks to generate the required proof load moment,

adequate concrete barrier blocks can be placed close to the curbs on each side.

Tanks should be also placed in different locations in the transverse direction to check all girders. Generally, three locations are enough as shown in Fig. 8-5.

- upstream (tanks closer to the upstream railing)
- center and (tanks in center of the bridge)
- downstream (tanks closer to the downstream railing)

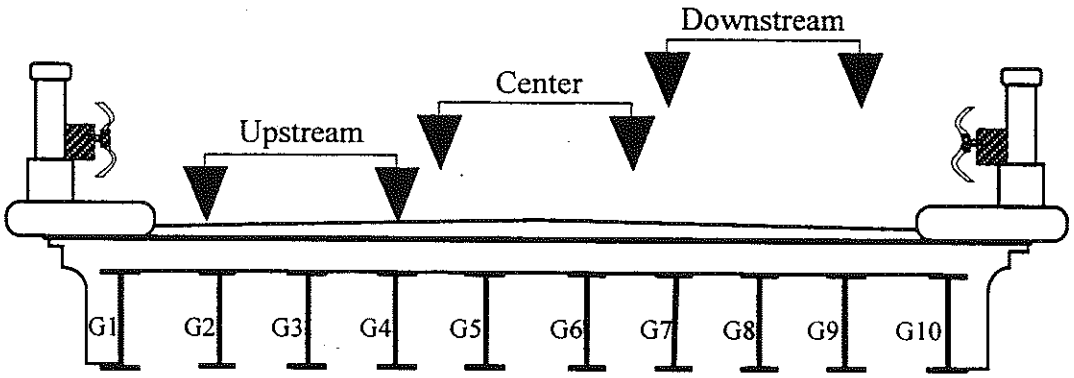

Fig. 8-5. Transverse Load Positions

8.5.2. Testing Procedures

The operator of the data acquisition system should have a clear view of the bridge deck. If this is not possible, good radio communication needs to be established. Before loading, it should be verified that all transducers and their connections are in working order. All problems should be resolved before the test begins. The noise levels of all channels should be checked, and mechanical or electrical noise sources should be eliminated. Some significant but

weak signals can be masked by a high noise level. 50 Hz should be used as the sampling rate.

As the load is gradually applied, strains and displacements are recorded for each load position. At all stages of field testing, the bridge response should be closely monitored and compared to analytically predicted values. If an unreasonable difference or a serious nonlinear behavior becomes apparent, the test should be stopped and the loads removed from the bridge. Other visible signs of distress, such as a buckling pattern appearing in a compressive zone of a steel member, or cracking in concrete, clearly indicate that the carrying capacity of bridge was exceeded.

8.6. Processing and Presentation of the Results

During the test, a large amount of data are recorded on some type of magnetic media. These data are then converted to format which is more suitable to process, and extraneous noise is filtered out.

Graphs are then prepared which present the results. If both strain and displacement are measured, the separate graphs should be prepared for each. If there is a lack data for a particular location, perhaps caused by a transducer failure, it is often possible to interpolate to these values.

There are two sets of stress-displacement graphs that can be prepared. The first set is prepared for each girder. Every line on this set of graphs will indicate a different transverse loading, such as downstream, center or upstream vehicle position. Although a small amount of nonlinear behavior is normal, the relation between the applied load and the deflection or stress should be nearly linear. If a nonlinearity displays an increase of rigidity, this may indicate that

composite action increases with the load level, or that support fixity increases with load level. Conversely, a decreasing rigidity may indicate that composite action is being lost as the load increases, or that there are some points on the bridge which have yielded.

The second set of stress-displacement graphs are used to compare experimental and analytical results. One line on these graphs should show the maximum experimental results, while other lines can show the results of different analytical or numerical models. For example, several possible bridge models for comparison with the true results are: a composite structure, a non-composite structure, a bridge with pinned supports, with fixed supports, or a combination of these. By comparing these models with the experimental results, it becomes more clear which condition the actual bridge most closely resembles. These graphs are prepared for each girder and each transverse loading case.

Examples of these graphs are shown in Fig. 8-6, 8-7, 8-8, and 8-9.

Observed experimental deflections are compared with those predicted using the analytical model and AASHTO deflection limits.

The operating rating factor of the bridge is calculated for the moment produced by a two-unit, 11-axle truck. According to the report NCHRP No:12-28 (13) A [Lichtenstein, 1993], the operating rating factor at the conclusion of the proof load test should be calculated as follows:

$$OP = \frac{K_0 L_p}{X_{PA}} \qquad (8\text{-}4)$$

where,

OP = operating level capacity.

L_p = actual maximum proof load applied to the bridge.

X_{pa} = the target live load factor (see Section 8.4.1).

K_0 = 1.00 if target load is reached.

= 0.88 if a distress level is reached prior to reaching the target load.

Therefore, the operating rating factor (ORF) would be

$$ORF = OP / L_r (1+I) \qquad (8\text{-}5)$$

where L_r = maximum allowable legal load (e.g. maximum moment caused by a two-unit 11-axle truck). If the operating rating factor is bigger then 1, then the bridge is considered safe for legal truck traffic.

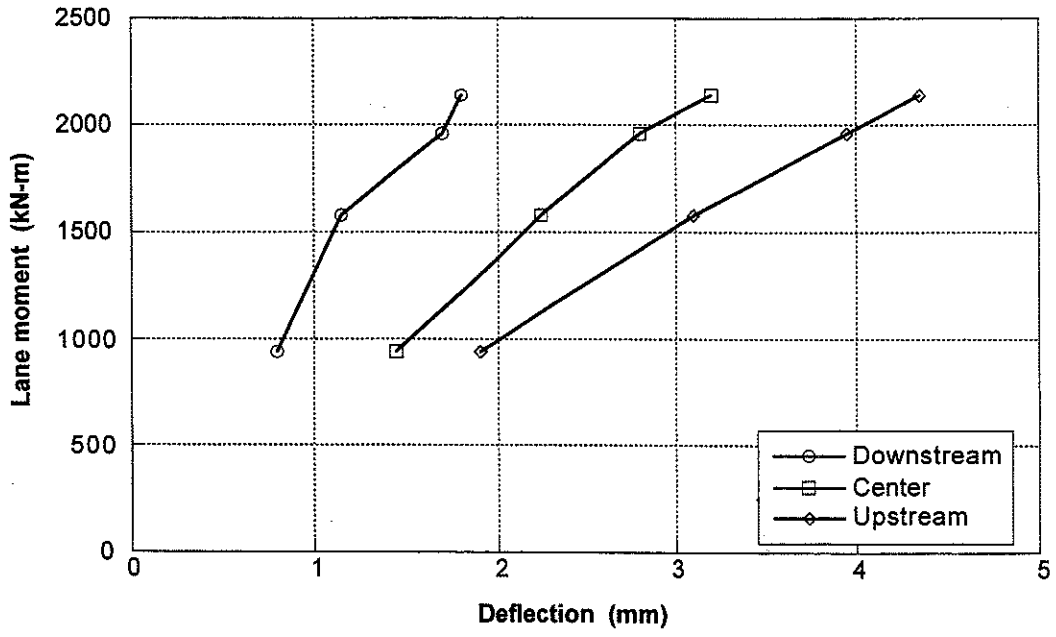

Fig. 8-6. Deflection vs. Lane Moment for any girder of the tested bridge.

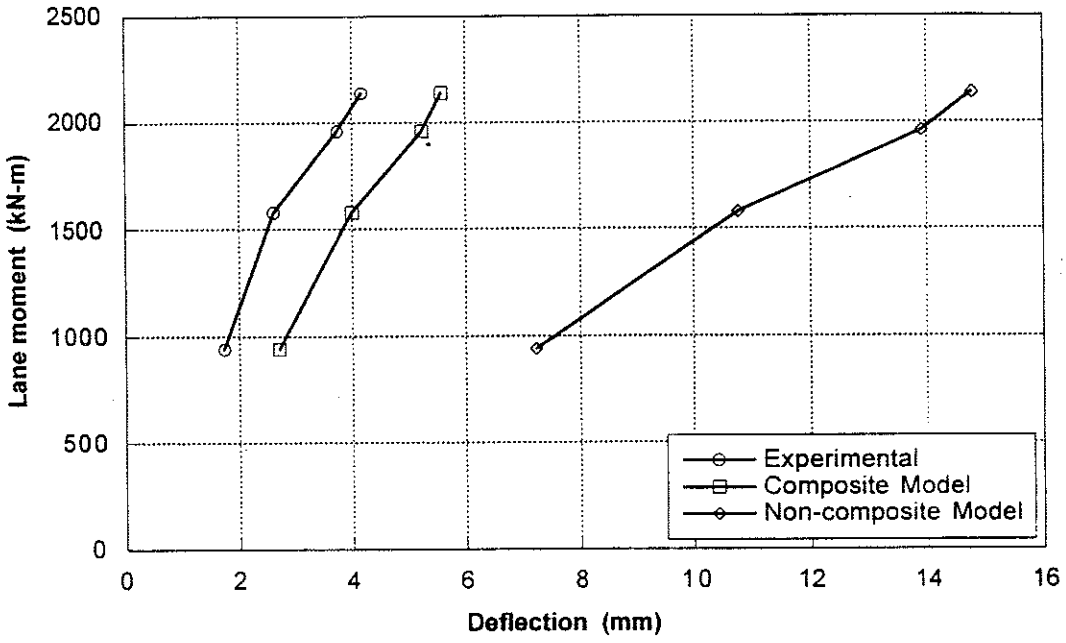

Fig. 8-7. Experimental and Analytical Deflections of any girder of the tested bridge for Downstream [or Center or Upstream] Loading

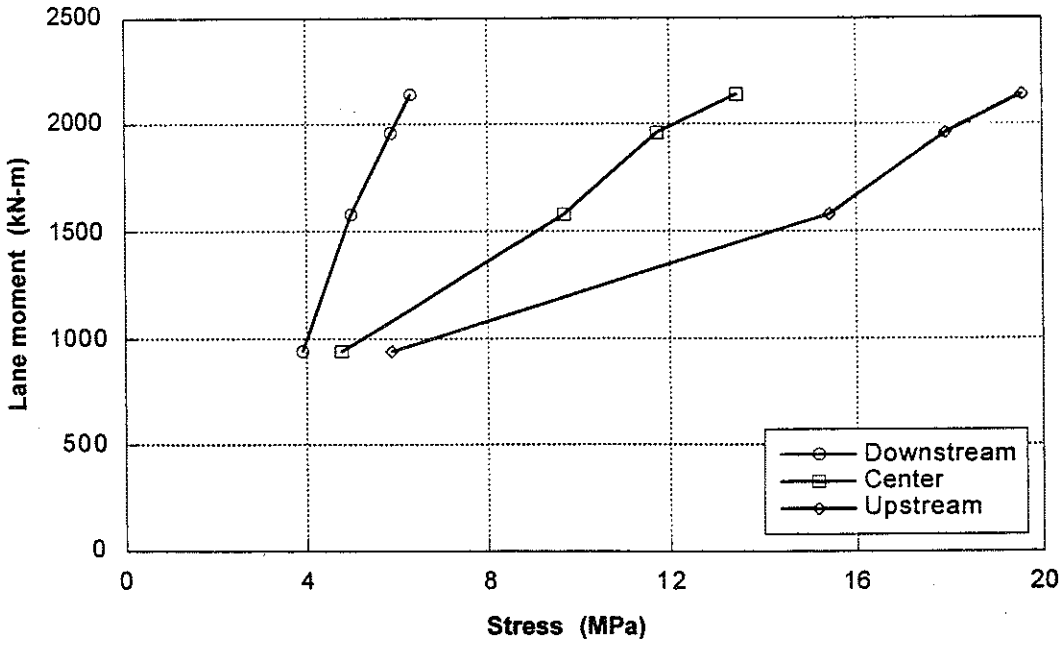

Fig. 8-8. Stress Lane Moment of any girder of the tested bridge at mid [or quarter or end] point.

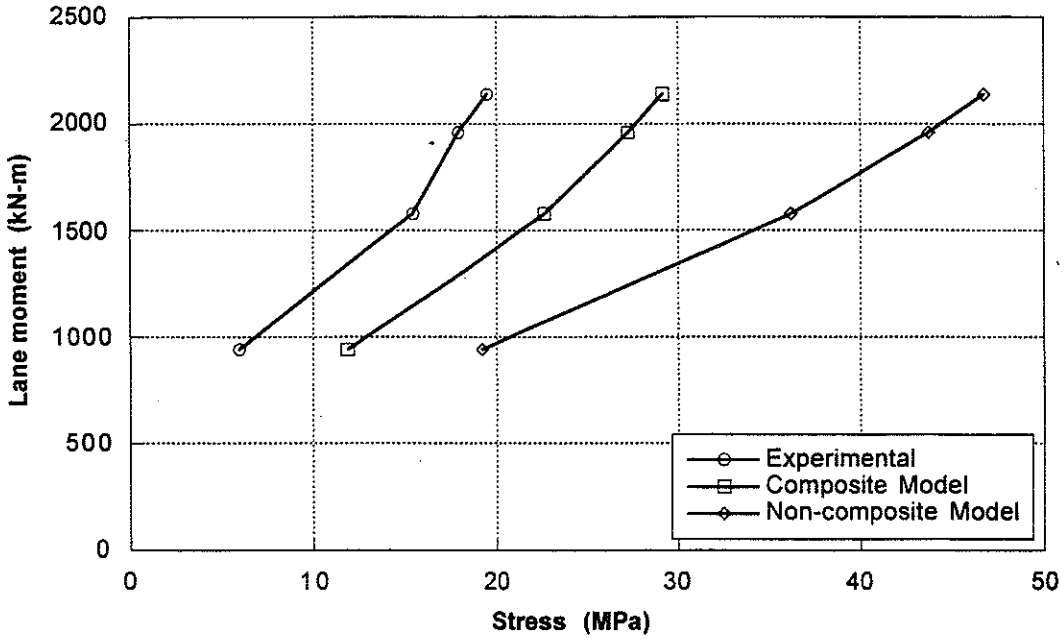

Fig. 8-9. Experimental and Analytical Stresses of any girder of the tested bridge for Downstream [or Center or Upstream] Loading.

Note:
Intentionally left blank

9. Safety and Summary of Field Tests

9.1 Safety during Field Tests

During any load test, the bridge and the investigators experience some risk of injury. This is especially true for proof load tests, when loading is high and the bridge behavior is ultimately unknown. The risk increases when information about material strengths and as-built details is missing. In assessing the risk, consideration should be given to the following: the safety of personnel, possible structural damage, loss of equipment, and traffic disruption. The degree of risk involved depends upon the bridge type, condition, and location, the loading method and anticipated behavior.

Of particular importance is the degree of redundancy of the structure. Redundant bridges provide reserve strength that may prevent the failure of the entire structure upon the failure of a single element.

In the final draft report NCHRP No:12-28(13)A [Lichtenstein, 1993], the risks involved are classified in three groups:

- Minimum : Bridge sustains superficial damage requiring minimum repairs. No equipment damage or loss of life.
- Medium : Bridge sustains tolerable damage requiring minor repairs and traffic disruption. Possible equipment damage but no loss of life.
- Major : Bridge sustains significant damage requiring major repairs and rerouting of traffic for an extended period. Possible loss of equipment and loss of life.

The safety of the test personnel, the bridge, and the equipment are paramount during a test. Precautions should be taken to control and regulate traffic and pedestrians during the test. Generally, public vehicles and pedestrians should not be allowed on or under the bridge during testing.

Some specific safety measures for the bridge, the test equipment, and the test personnel are the following:

For Bridge :

Before the load test, structural weak points should be determined. In some cases, analytic or numeric models of the bridge may have to be constructed to facilitate this. Transducers should be attached to these areas and monitored continuously.

Likely failure mechanisms of the bridge should be identified, and can be used to determine where most safety measures should be considered. Bridge deterioration should be included.

Areas of structural deterioration or damage should be closely monitored during a load test. If crack growth or member deformation is observed, such as a wrinkle in the compression flange of a steel girder, the test must be stopped and the loads immediately removed. Moreover, if the structure emits noise during the loading, this may indicate component breaking or settling.

In a proof load test, the load should be gradually increased. At the end of each load step, measured values should be checked against those predicted, and the linear behavior of the structure should be verified. Between two load steps, when the load on the bridge is fixed,

if displacements are increasing or if stresses are changing, this may indicate that the structure is not behaving elastically.

For Test Equipment :

To avoid damage, strain transducers should not be attached to uneven or twisted surfaces.

LVDT displacement transducers should be mounted carefully. If the core rubs on the body of the LVDT, its sensitivity may decrease, especially during dynamic measuring. Moreover, if the transducer body is not vertically aligned with the guide wire, the device may be damaged.

Cables and connectors should be protected direct sunlight, heat, moisture, and dust. They should also be protected from traffic and pedestrians.

If a power generator is used for the test, the output voltage should be monitored throughout the test. It should also be checked before powering the test equipment.

After every test, all equipment should be cleaned and oiled if it is necessary. Damaged cables and equipment should be clearly marked at the field and later repaired.

For Personnel :

Personnel who work on, under, or around the bridge should wear a bright reflective vest and hard hat, even if the traffic has stopped.

If equipment needs to be placed on a bridge lane or any place higher then two meters under the bridge, at least two people should be present for the task. The second worker is needed to observe traffic, hold a ladder, or otherwise monitor the activity to avoid accidents.

A first-aid kit should be kept close to test area, and a nearby telephone should be found in case it is needed in an emergency.

9.2 Summary of Field Testing

In general, the actual performance of bridges is different than predicted by the analytical calculations. There are several factors that effect the actual behavior of bridges. Many of these factors are not considered in the design and load rating, although they can improve the bridge response to applied load. However, such increase of strength may not be present at the higher load levels. These affects can be summarized as follows.

- *Unintended Composite Action*

  Most bridges build before 1950 were designed without shear connectors between the main load carrying girders and the concrete deck. Nevertheless, field tests have shown that such noncomposite decks consistently behave compositely. Although in all load tests to date this unintended composite action has been maintained, it is possible that this effect could be lost during the test. In this case, a sudden increase in stress may be observed. It is recommended that bridges with steel girders be analyzed assuming composite action, even if designed non-compositely, unless signs of deterioation or slab-girder de-bonding suggest that composite action is lost.

- *Load Distribution Effects*

  An important part of the rating equation concerns the distribution of the live load to the main load-carrying members of the bridge, and to the individual components of a multi-component member. Typically, in design and rating, load distribution to main supporting members is based on the AASHTO Specifications distribution factors. However, this distribution is affected by several variables which greatly complicate the analysis. Except by field testing, it is impossible to find exact values of girder distribution factors.

- *Differences in Material Properties*

- *Unintended Continuity*

  For simply-supported bridges it is assumed that the ends are supported on idealized rollers and do not carry any moment. However, tests have shown that there can be significant end moments attributable to the continuity provided by the deck slab as well as frozen bearings.

- *Participation of Secondary Members, Parapets, Railing, Curbs and Utilities*

  Secondary bridge members are those members which are not directly in the load path of the structure, and includes lateral bracing members, diaphragms, wind bracing, parapets, railing, curbs and utilities. In some bridge types, secondary members enhance the load-carrying system by increasing the stiffness of the bridge.

- *Effects of Skew*

  The conventional AASHTO Specifications (1996) live load distribution factors may not be applicable to girder system with large skews (20° or more).

- *Effects of Deterioration and Damage to Structural Members*

- *Portion of Load Carried By Deck*

  Depending on the bridge span and the thickness of the deck, there may be a portion of the load carried directly by the deck slab spanning between end supports of the bridge.

- *Unintended Arching Action Due To Frozen Bearings*

References

1. AASHTO. (1994a). *Manual for the Condition Evaluation of Bridges*, American Association of State and Transportation Officials, Washington, D.C.
2. AASHTO. (1994b). *LRFD Bridge Design Specifications*, American Association of State and Transportation Officials, Washington, D.C,
3. AASHTO. (1996). *Standard Specifications for Highway Bridges, Bridge Design Specifications*, American Association of State and Transportation Officials, Washington, D.C.
4. Bakht, B. and Pinjarkar, S. G. (1989). "Dynamic testing of highway bridges - a review.", *Transportation Research Record*, 1223, 93.
5. Bannantine, J. A., Comer, J. J., and Handrock, J. L. (1992). "Fundamentals of metal fatigue analysis.", *Prentice Hall*, New Jersey.
6. Benjamin, J. R., and Cornell, C. A. (1970). "Probability, statistics and decision for civil engineers.", *McGraw-Hill*, New York.
7. Bishara, A.G., Liu, M.C. and El-Ali, N.D. (1993). "Wheel load distribution on simply supported skew I-beam composite bridges.", *Journal of Structural Engineering, ASCE*, Vol. 119, No. 2, pp. 399-419.
8. Fu, C.C., Elhelbawey, M., Sahin, M.A. and Schelling, D.R. (1996). "Lateral distribution factor from bridge field testing." *Journal of Structural Engineering, ASCE*, Vol. 122, No. 9, pp. 1106-1109.
9. Goshn, M., Moses, F., and Gobieski, J. (1989). "Evaluation of steel bridges using in-service testing." *Transportation Research Record 1072, Transportation Research Board*, Washington, D.C., pp. 71-78.
10. Hwang, E-S. and Nowak, A.S. (1991). "Simulation of dynamic load for bridges." *Journal of Structural Engineering, ASCE*, Vol. 117, No. 5, pp. 1413-1434.

11. Juntunen, D.A., and Isola, M.C. (1995). "Proof load test of R01 of 61131 M-37 over CSX Railroad, south of Bailey, Michigan.", *Michigan Department of Transportation*, Lansing, MI.

12. Kim, S., and Nowak, A. S. (1997). "Load distribution and impact factors for I-girder bridges." *Journal of Bridge Engineering, ASCE.* 2, 97.

13. Laman, J. A., and Nowak, A. S. (1996). "Fatigue-load models for girder bridges." *Journal of Structural Engineering, ASCE*, 122, 726.

14. Lichtenstein, A.G. (1993). "Manual for bridge rating through nondestructive load testing - Final Draft." *NCHRP Project Number: 12-28(13)A, A.G. Lichtenstein and Associates, Inc.*, Fair Lawn, New Jersey.

15. *Michigan Bridge Analysis Guide.* (1983). Michigan Department of Transportation, Lansing.

16. *Michigan Design Manual: Bridge Design.* (1992) Michigan Department of Transportation, Lansing.

17. Moses, F. (1987). "Fatique evaluation procedures for steel bridges.", *NCHRP Rep. No:299, Transportation Research Board*, Washington, D.C.

18. Nassif, H. and Nowak, A.S. (1995). "Dynamic load spectra for girder bridges." *Transportation Research Record*, No. 1476, pp. 69-83.

19. Nassif, H. and Nowak, A.S. (1996). "Dynamic load for girder bridges under normal traffic." *Archives of Civil Eng.*, Vol.XLII, No.4, pp. 381-400.

20. Nowak, A.S. and Hong, Y-K. (1991). "Bridge live load models." *Journal of Structural Engineering, ASCE*, Vol. 117, No. 9, pp. 2757-2767.

21. Nowak, A.S. (1993). "Live load model for highway bridges." *Journal of Structural Safety*, Vol. 13, Nos. 1+2, pp. 53-66.

22. Nowak, A.S., Nassif, H. and Frank, K.H. (1993). "Fatigue load spectra for steel girder bridge." *Transp. Research Record*, No. 1393, pp. 154-161.

23.Nowak, A.S., Kim, S-J., Laman, J., Saraf, V. and Sokolik, A.F. (1994). "Truck loads on selected bridges in the Detroit area.", *Final Report submitted to MDOT*, University of Michigan, Ann Arbor, Michigan.

24.Nowak, A. S., Laman, J. A., and Nassif, H. (1994). "Effect of truck loading on bridges." *Report UMCE 94-22. Dep. of Civil and Environmental Engineering*, University of Michigan, Ann Arbor, Michigan.

25.Nowak, A.S. (1995). "Calibration of LRFD bridge code." *Journal of Structural Engineering, ASCE*, Vol. 121, No. 8, pp. 1245-1251.

26.Nowak, A.S., Kim, S-J. and Stankiewicz, P.R. (1996). "Huron Parkway Bridge study.", *Report submitted to McNamee, Porter and Seeley and City of Ann Arbor*, Ann Arbor, Michigan.

27.Nowak, A.S. and Saraf, V. (1996). "Load testing of bridges.", *UMCEE 96-10, Final Report submitted to Mich. Dep. of Transp*, University of Michigan, Ann Arbor, Michigan.

28.Nowak, A.S., Kim, S-J. (1998). "Development of a guide for evaluation of existing bridges - Part I." *Report UMCE 98-12. Dep. of Civil and Env. Engineering University of Michigan*, Ann Arbor, Michigan.

29.Saraf, V. and Nowak A.S. (1997). "Field evaluation of a steel girder bridge." *Transportation Research Record*, No. 1594, pp. 140-146.

30.Saraf, V., Sokolik, A.F., and Nowak, A.S. (1997). "Proof load testing of highway bridges." *Transportation Research Rec.* No.1541, pp. 51-57.

31.Stallings, J.M., and Yoo, C.H. (1993). "Test and ratings of short-span steel bridges." *Journal of Structural Engineering, ASCE*, Vol. 119, No. 7, pp. 2150-2168.

Note:
Intentionally left blank

Appendix A. Information On Data Acquisition

A.1. Signal Types

Signals are often described as being either analog or digital. They are defined by how they convey useful data. Attributes such as amplitude, state, frequency, pulse-width, and phase can represent data.

A.1.1. Analog Signals

While all signals can be assumed to be changing with time, analog signals are the only ones that convey information within their incremental amplitude variations. In instrumentation and control applications, most analog signals are in the range of -10V to +10V or 4 to 20mA. Analog inputs can indicate how high a level is or how much stress is occurring in a girder.

A.1.2. Digital Signals

A digital signal is also called pulse. Digital and pulse signals have binary amplitude values; that is, they are represented by only two possible states - low and high. While low and high states can be represented by any voltage level, transistor-transistor-logic (TTL) levels are most often used. TTL levels are approximately 0V and 5V. The actual allowable ranges for TTL signals are :

Low level = 0V to 0.8V
High level = 2.0V to 5.0V

Thus, with analog signals what is important is how high the signal is, while with digital signals it matters only whether the signal is high or low (on or off, true or false). Figure A-1 illustrates the differences between analog and digital signals.

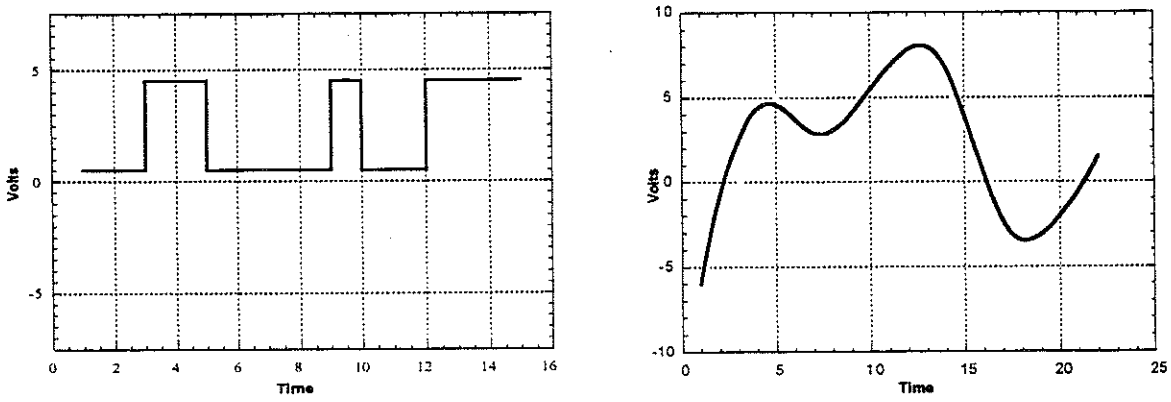

Fig. A-1. Digital and analog signals

A.2. Transducers

Sensors and transducers change physical phenomena into electrical signals. Therefore, they play a vital role in the electronic measuring systems. It is necessary to use different transducers to measure different physical values. A physical value may be force, stress, displacement, temperature, etc. The electrical equivalents produced by input transducers are most commonly in the form of voltage, current, charge, resistance or capacitance.

As will be shown, the process of signal conditioning will further convert these basic signals into voltage signals. This is important because the interior blocks of the data acquisition can only deal with voltage signals. Transducers which represent the measured value by means of the change of a physical property are called "passive transducers". The strain gauge transducer belongs to this category.

Transducers which deliver a voltage or current proportionate to the measured quantity are "active transducers".

A.2.1. Strain Gages and Transducers

The strain gauge is one of the most important tools of the electrical measurement technique applied to the measurement of mechanical quantities. The strain of a body is always caused by an external influence or an internal effect. Strain might be caused by forces, pressures, moments, heat, structural changes of the material and the like.

Figure A-2 shows the principle construction of a standard strain gauge. Embedded between two plastic strips is the measuring grid, the active part of the gauge, and is made from a thin metal foil which is electrically conducting. The separate layers of the gauge are bonded together. The functioning of metallic strain gauges is basically a strain effect on the resistance of electrical conductors. The strain gauge must be mounted on the surface of the specimen of which the stress shall be determined. This is normally done with the aid of special cements. For any problem, a few gauge designations are be preferred. As an example, in Figure A-3, three designations are shown for a tensile load.

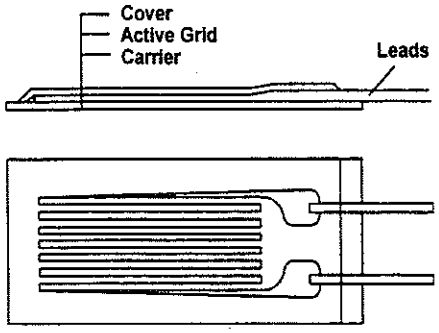

Fig. A-2. Schematic construction of an embedded foil gauge

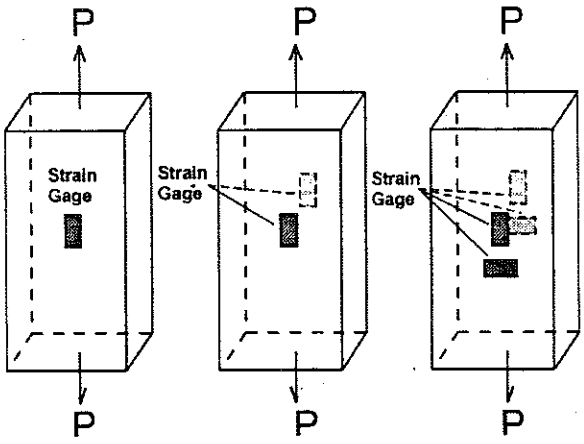

Fig. A-3. Gauge designations of the tensile rod

Additional circuitry and instruments are needed to further process the measured value of the strain gauge. In 1843 the English physicist Sir Charles Wheatstone (1802-1875) found a bridge circuit for the measurement of electrical resistance. The Wheatstone bridge is well suited also for the measurement of small changes of resistance and, therefore, is also suitable to measure the resistance change in a strain gauge. The form of this electronic circuit depends on gauge designation (Fig. A-4).

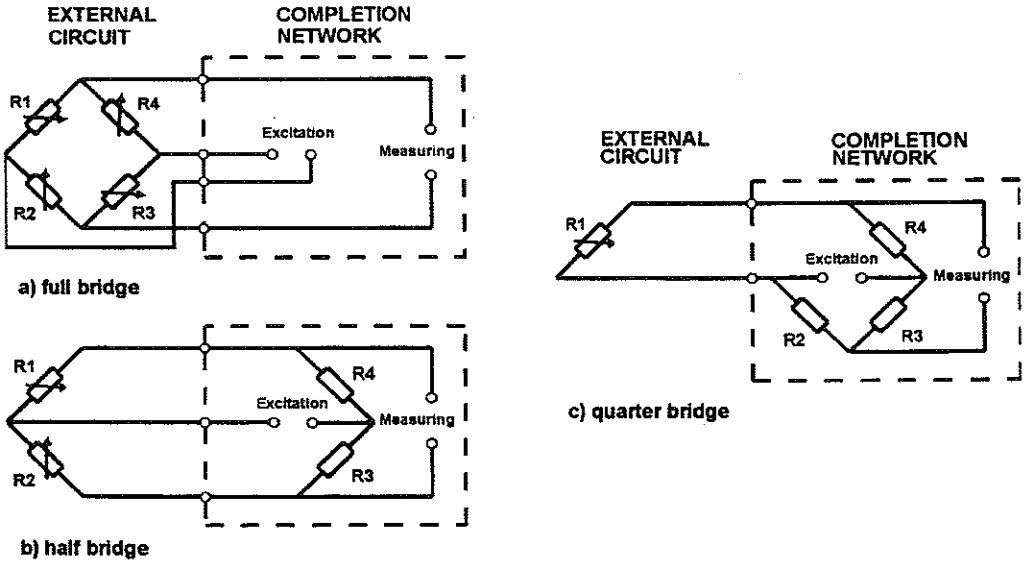

Fig. A-4. Different version of the Wheatstone bridge circuit

Special transducers can be designed for the measurement of strains. The transducer generally contains a properly formed spring element which produces a clear relation between the measured quantity and the strain on a suitable spot on the spring element (Fig. A-5). They are designated with a full bridge strain gauge configuration to increase their sensibility and to eliminate temperature effects.

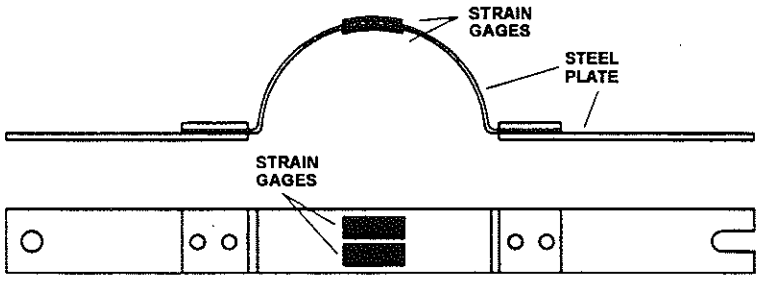

Fig. A-5. An example of Strain Transducer

A.2.2. Linear Variable Differential Transformers (LVDT)

This transducer can convert the rectilinear motion of an object to which it is coupled mechanically into a corresponding electrical signal. An LVDT has one primary and two secondary coils. The magnetic core inside the coil winding assembly provides the magnetic flux path linking the primary and secondary coils (Fig. A-6). Secondary coils are connected serially to each other. When the LVDT is in its null position, the two voltages of secondary coils are of equal and opposite polarity. Thus, output voltage is zero. When the magnetic core is displaced from the null position, an electromagnetic imbalance occurs. This imbalance generates a differential AC output voltage across the secondary coils which is linearly proportional to the direction and magnitude of the displacement. Some LVDTs are designed together with their signal conditioning unit. In this case, this LVDSs need DC voltage as power, and they produce DC voltage.

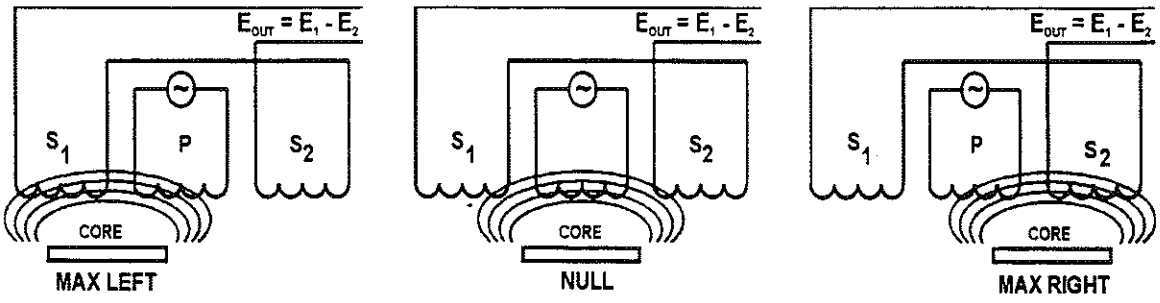

Fig. A-6. Working principle of an LVDT

A.3. Signal Conditioning

Devices which is convert analog signal to digital are usually designed to accept voltage inputs in the range of ±10V. Other signal ranges and signal types such as resistance or impedance changing generally require preprocessing to make them compatible. This task is known as signal conditioning and this unit first part of a data acquisition system after transducers. Signal conditioning accessories amplify low-level signals, isolate, filter, excite and complete bridge transducers to produce high-level signals for analog to digital devices.

A.3.1. Amplification

The most common type of conditioning is amplification. Most A/D converters are designed to operate with high-level input signals. Common A/D ranges include 0 to 10V, ±5, ±10V. When the maximum input signal is below 1V, accuracy is degraded. For the highest possible accuracy, the signal should be amplified so that the maximum voltage range of the conditioned signal equals the maximum input range of the A/D converter.

At the same time, every amplifier unit produces some noise. The amount of this noise depends on the amplification level and amplifier quality. Generally, noise increases faster after a specific value of gain factor. Therefore, there is an upper bound of amplification level. Most often used as a unit of amplification is the decibel (dB). This unit is specified as follows :

$$Gain(dB) = 20 \log \frac{V_{out}}{V_{in}}$$

Where V_{in} and V_{out} are voltage values of the signals entering and leaving the amplifier, respectively.

Single-Ended and Differential Signals

Analog signals can be configured as either single-ended or differential input. Single ended inputs all share a common return or ground line. Only the high ends of the signals are connected to the amplifier. The low ends of the signals return to the amplifier through the system ground connections. This arrangement works well for high-level signals when the difference in ground potential is relatively small. Problems arise when there is a large difference in ground potentials. This is usually caused by current flow (a ground loop) through the ground conductor.

A differential arrangement allows both the noninverting (+) and the inverting (-) inputs of the amplifier to make connections to both ends of the actual signal source. In this way, any ground-loop-induced voltage appears as a common-mode signal and is rejected by the differential properties of the amplifier. While differential connections can greatly reduce the effects of ground loops, they consume the equivalent of two single-ended inputs. Thus, a 16-channel, single-ended system can handle only 8 differential inputs.

A.3.2. Isolation

Another common application for signal conditioning is to isolate the transducer signals from the other divisions of the data acquisition system for safety purposes. The system being monitored may contain high-voltage transients that could damage the computer.

An additional reason for needing isolation is to make sure that the readings from the data acquisition device are not affected by differences in ground potentials or common-mode voltages. When the two channels of data acquisition system are each referenced to different grounds, problems occur if there is a potential difference between the two grounds. This difference can lead to what is known as a ground loop, which may cause inaccurate representation of the acquired signal, or if too large, may damage the measurement system. Using isolated signal conditioning modules eliminates the ground loop and ensures that the signals are accurately acquired.

A.3.3. Filtering

Filtering is used to separate desired signals from undesired signals, such as when an AC line frequency picks up and radio or TV station interference. All such signals are referred to as noise. Filtering can be performed, prior to the A/D conversion, using physical devices consisting of resistors, capacitors, inductors, and amplifiers. Filtering can also be accomplished, after conversion, using mathematical algorithms that operate on the digital data within the computer. This is known is digital signal processing (DSP).

Averaging is a simple example of DSP that is useful for reducing unwanted data fluctuations. By averaging a series of incoming data points, the signal-to-noise ratio can be effectively increased. Averaging will be most effective in reducing the effect of random, non-periodic noise. It is less affective in dealing with 50 or 60 Hz or other periodic noise sources. When the desired signal has lower frequency components then the error sources, a low-pass filter can be used. This includes the case where the real input signal frequency components can equal, or exceed, half the sampling rate. Here the filter is used to prevent sampled-data aliasing (Fig. A-7).

Aliasing results in the generation of spurious signals within the frequency range of interest that cannot be distinguished from real information. Hence, serious errors in the interpretation of the data can occur. Noise-filtering techniques, whether implemented in hardware or software, are designed to filter specific types of noise. In addition to low-pass filters, high pass and notch (band-reject) filters can also be used. For example, if the frequency band of interest includes the AC line frequency, a notch filter could be used to selectively remove this one component.

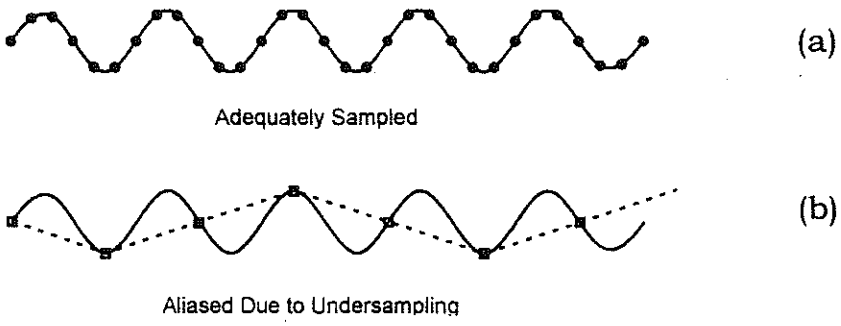

Fig. A-7. Effects of Too Low Sampling Rate

A.3.4. Excitation

Signal conditioning also generates excitation for some transducers. Strain gauges, strain transducers and displacement transducers, for example, require external voltage or current excitation. Signal conditioning modules for these transducers usually provide these signals. Strain gauges are resistance devices in a Wheastone bridge configuration, which often require bridge completion circuitry and excitation sources. Some LVDT type displacement transducers which has inductive components, require high frequency excitation voltage.

A.3.5. Linearization

Another common signal conditioning function is linearization. Many transducers have a nonlinear response to changes in the phenomenon being measured. Some conditioners contain electronic circuits to linearize the response of the related transducer. But, generally, this process is done with software after measuring.

A.4. Analog to Digital Conversion

A.4.1. Multiplexing

The multiplexer is simply a switch arrangement that allows many input channels to be serviced by one amplifier and one A/D converter (Fig. A-8). Software or auxilary hardware can control this switch to select any one channel for processing at a given time. Because the amplifier and A/D converter are shared, the channels are read sequentially, causing the overall speed of the system to be reduced. The rated speed of amplifier and A/D converter will be divided by the number of input channels serviced. Therefore, the throughput rate is

defined as the sample rate (per-channel speed) multiplied by the total number of channels.

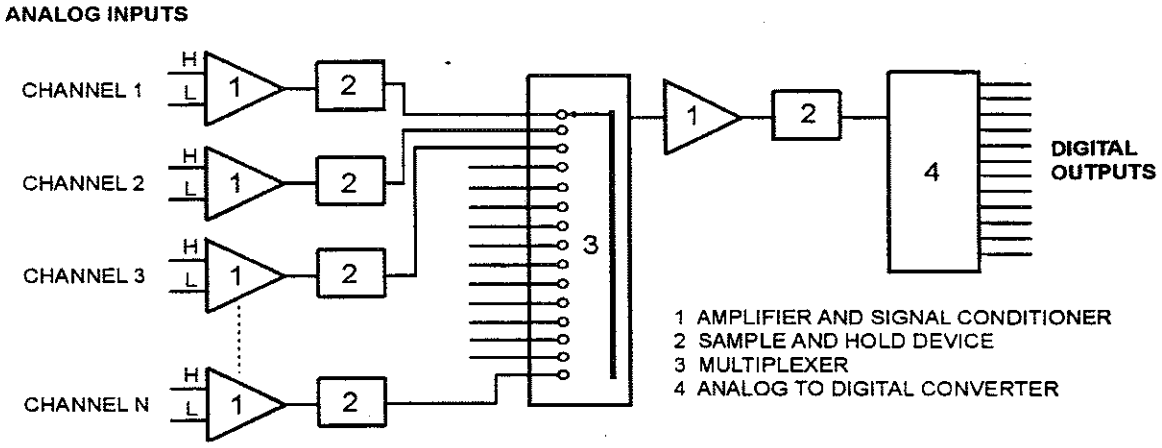

Fig. A-8. A general data acquisition system

In an ideal system, all of the input channels would be read at the same instant in time. However, multiplexing inherently generates a time difference between each channel's reading. In general, many applications can tolerate the time difference between readings. However, some applications are very sensitive to time skew. In such time-critical applications, the simultaneous sample/hold architecture is ideal (Fig. A-8). In these systems, each sample is held by a separate device before multiplexing.

A.4.2. Resolution

The number of bits that the analog to digital converter uses to represent the analog signal is the resolution. The higher the resolution, the higher the number of divisions the voltage range is broken into, and therefore, the smaller the detectable voltage changes. Figure A-9 shows a sine wave and its corresponding digital image as obtained by an ideal 3-bit ADC. A 3-bit converter divides the analog range into 2^3, or 8 divisions. Each division is represented by a binary

code between 000 and 111. The digital representation is not a good representation of the original analog signal because information has been lost in the conversion. By increasing the resolution to 16 bits, however, the number of codes from the ADC increases from 8 to 65,536.

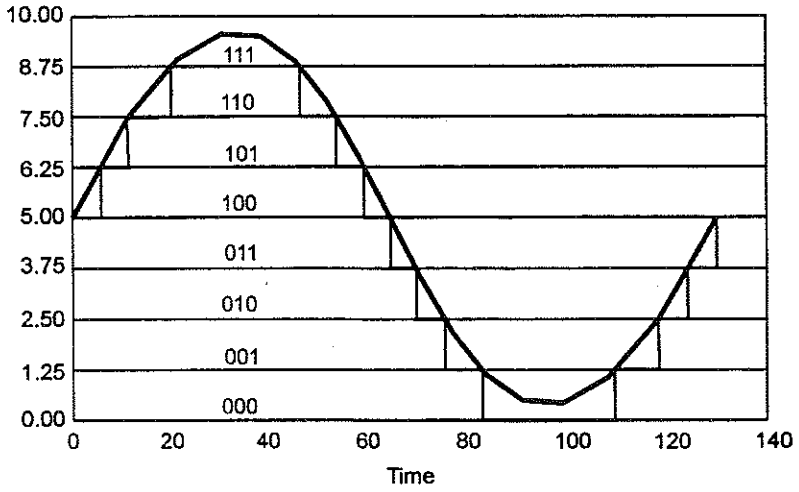

Fig. A-9. Digitized sine wave with 3-bit resolution

A.4.3. Sampling

This parameter specifies how often conversion can take place. Using a faster sampling rate, you will acquire more points in a given time, providing a better representation of the original signal. As shown in Figure A-7a, you must sample all input signals at a sufficiently fast rate to faithfully reproduce the analog signal.

Obviously, if the signal is changing faster than the digital to analog converter is digitizing, errors are introduced into the measured data. In fact, data that is sampled too slowly can appear to be at a completely different frequency. This distortion of the signal is referred to as aliasing (Fig. A-7b).

According to the Nyquist theorem, a signal must be sampled at least twice the rate of the maximum frequency component to prevent aliasing. The frequency that is one-half the sampling frequency is referred to as the Nyquist frequency. Theoretically, it is possible to recover information about signals with frequencies at or below the Nyquist frequency. Due to aliasing, frequencies above the Nyquist frequency appear between the DC and Nyquist frequencies.

A.5. Recording

Last process of data acquisition is the recording of digitized signals. As a first step, these digital values are sent to semi-conductor memories called buffers. In the systems integrated in a micro computer, at the same time, they are also sent to the computer's memory or directly to its hard disk. In general, recording to the computer memory is slower compared to the conversion time of the A/D system. Thus, buffer memories assure uninterrupted measuring and recording.

The separate systems which haven't magnetic media, such as a hard disk, record the signals in their internal memories. Their memory is generally big enough for at least a few measurings. They are often down loaded to the computer. This kind of measuring systems is also called as logger.

A.6. Noise

Signals entering a data acquisition and control system include unwanted noise. Whether this noise is troublesome depends on the signal-to-noise ratio and the specific application. In general, it is desirable to minimize noise to achieve high accuracy. Digital signals

are relatively immune to noise because of their discrete and high-level nature. In contrast, analog signals are directly influenced by relatively low-level disturbances.

The major noise transfer mechanisms include conductive, inductive (magnetic), and capacitive coupling. Some noise transfer examples are:

- Switching high-current loads in nearby wiring can induce noise signals by magnetic coupling (transformer action).
- Signal wires running close to AC power cables can pick up 50 or 60 Hz noise by capacitive coupling.
- Allowing more than one power or signal return path can produce ground loops that inject errors by conduction.

Interference via capacitive or magnetic mechanisms usually requires that the disturbing source be close to the affected circuit. At high frequencies, however, radiated emissions (electromagnetic signals) can be propagated over long distances.

In all cases, the induced noise level will depend upon several user-influenced factors:

- Signal source output impedance
- Signal source load impedance (the input impedance to the data acquisition system)
- Lead-wire length, shielding, and grounding
- Proximity to noise source(s)
- Signal and noise amplitude

Another noise source is triboelectric induction. This refers to the generation of noise voltage due to friction. All commonly used

insulators can produce a static discharge when moved across a dissimilar material. This effect is very slight in most cases. However, it should not be ignored as a possible source of noise when motion of the cables or vibration of the system is involved. Special low-noise cables are available that use graphite lubricant between the inner surfaces to reduce friction.

In Table A-1, possible problems about noise and their solutions are summarized.

Table A-1. Troubleshooting guide for noise

Observation	Suspect	Possible Solution
Noise a Function of Cable Location	Capacitive coupling Inductive coupling	Use shielded or twisted pair. Reduce loop area; use twisted pair or metal shield
Average Value of Noise : Is not zero Is zero	 Conductive paths or ground loops Capacitive coupling	 Faulty cable or other leakage. Eliminate multiple ground connections Use shielded or twisted pair.
Shield Inserted Ground Significant Ground Insignificant	 Capacitive coupling Inductive coupling	 Use shielded or twisted pair. Reduce loop area; use twisted pair or metal shield.
Increasing Load Reduces Error Increases Error	 Capacitive coupling Inductive coupling	 Use shielded or twisted pair. Reduce loop area; use twisted pair or metal shield.
Dominant Feature Low Frequency High Frequency	 60 Hz AC line, motor, etc. Electromagnetic radiation	 (1) Use shielded or twisted pair (2) Reduce loop area; use twisted pair or metal shield (3) Faulty cable or other leakage; eliminate multiple ground connections. Complete shield.
Noise a Function of Cable Movement	Triboelectric effect	Rigid or lubricated cable.
Noise is "White" or 1/f	Electronic amp., etc.	Not a cable problem.

Note:
Intentionally left blank

Appendix B - Normal Probability Paper

The objective of this Appendix is to provide additional information on the construction and use of the normal probability paper. The construction of the normal probability paper is shown in Fig. B-1 and B-2.

B.1 Role of the normal probability paper

It is used for an efficient interpretation of statistical data

- applications in bridge engineering:
- evaluation of existing structures
- selection of repair/rehab materials
- to evaluate test data (material tests)
- to evaluate truck weight data
- to evaluate stress (or strain) data

B.2 Basic properties

Normal probability paper is a special scale, so that a normal distribution is represented by a straight line:

- any normal distribution is represented by a straight line
- any straight line represents a normal distribution.

For any distribution function, the mean and standard deviation can be read directly from the probability paper as shown in Fig. B-3.

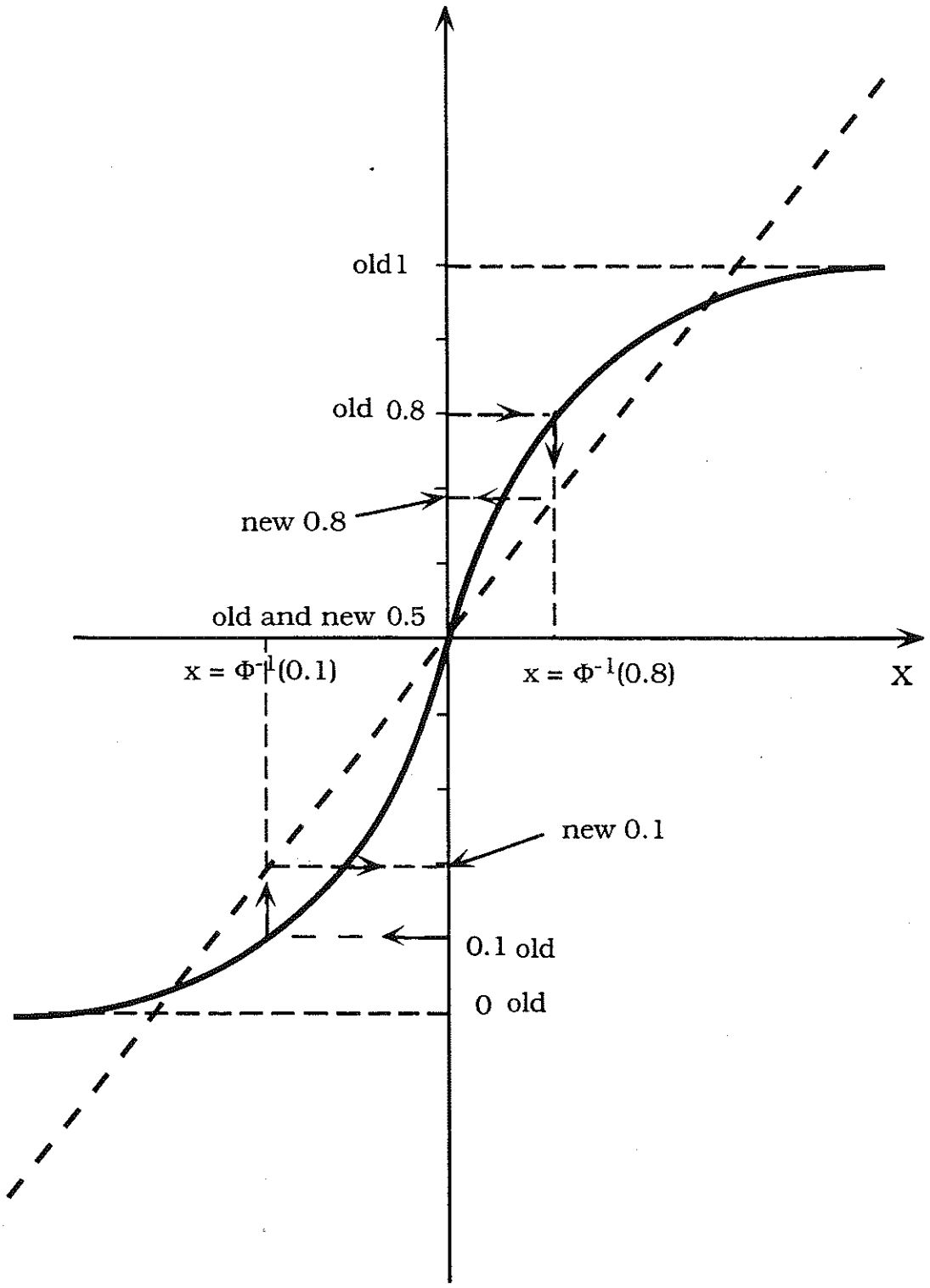

Fig. B-1. Development Of Probability Paper Using Standard Normal Distribution.

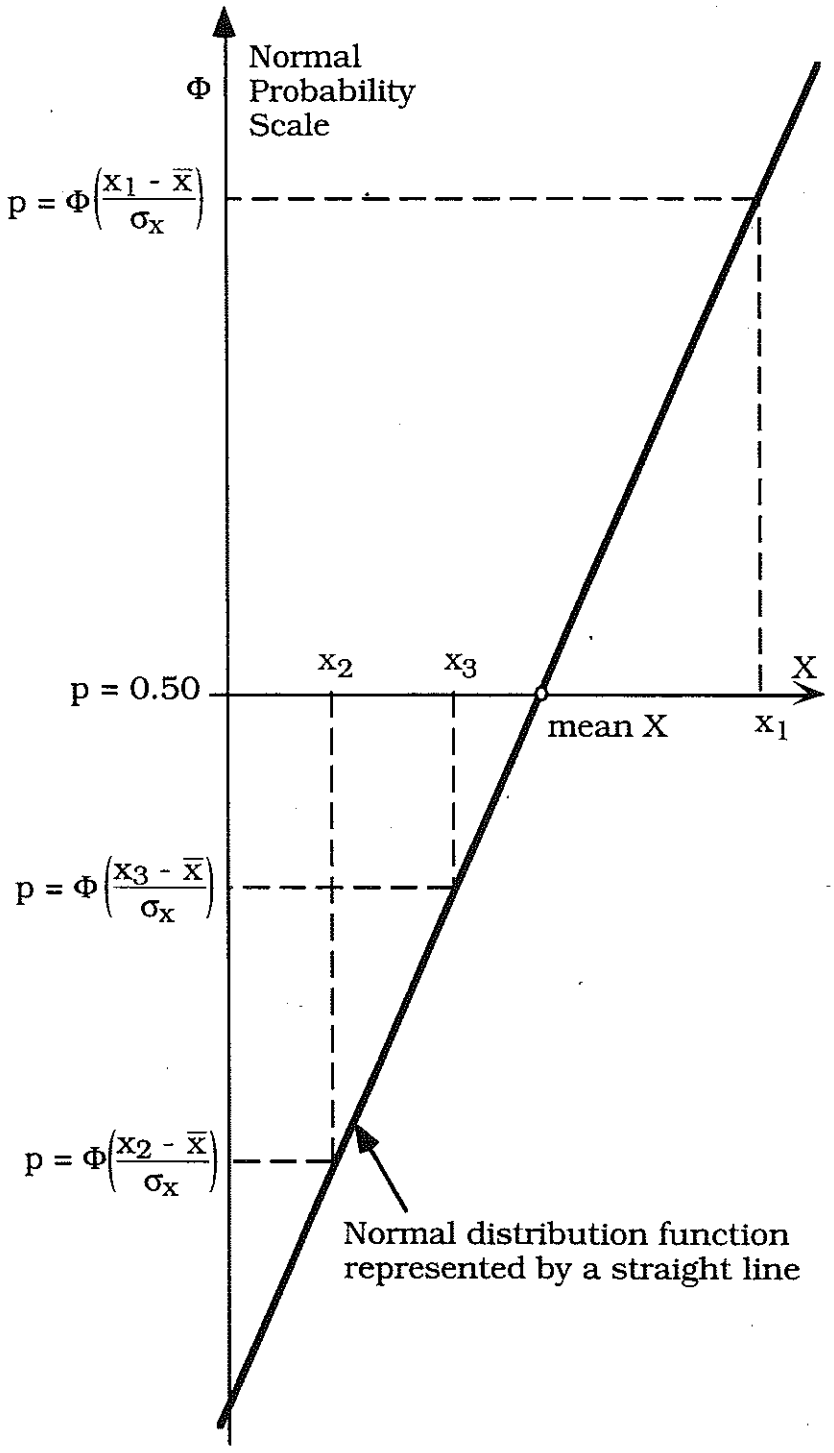

Fig. B-2. Development Of Probability Paper Using Any Normal Distribution.

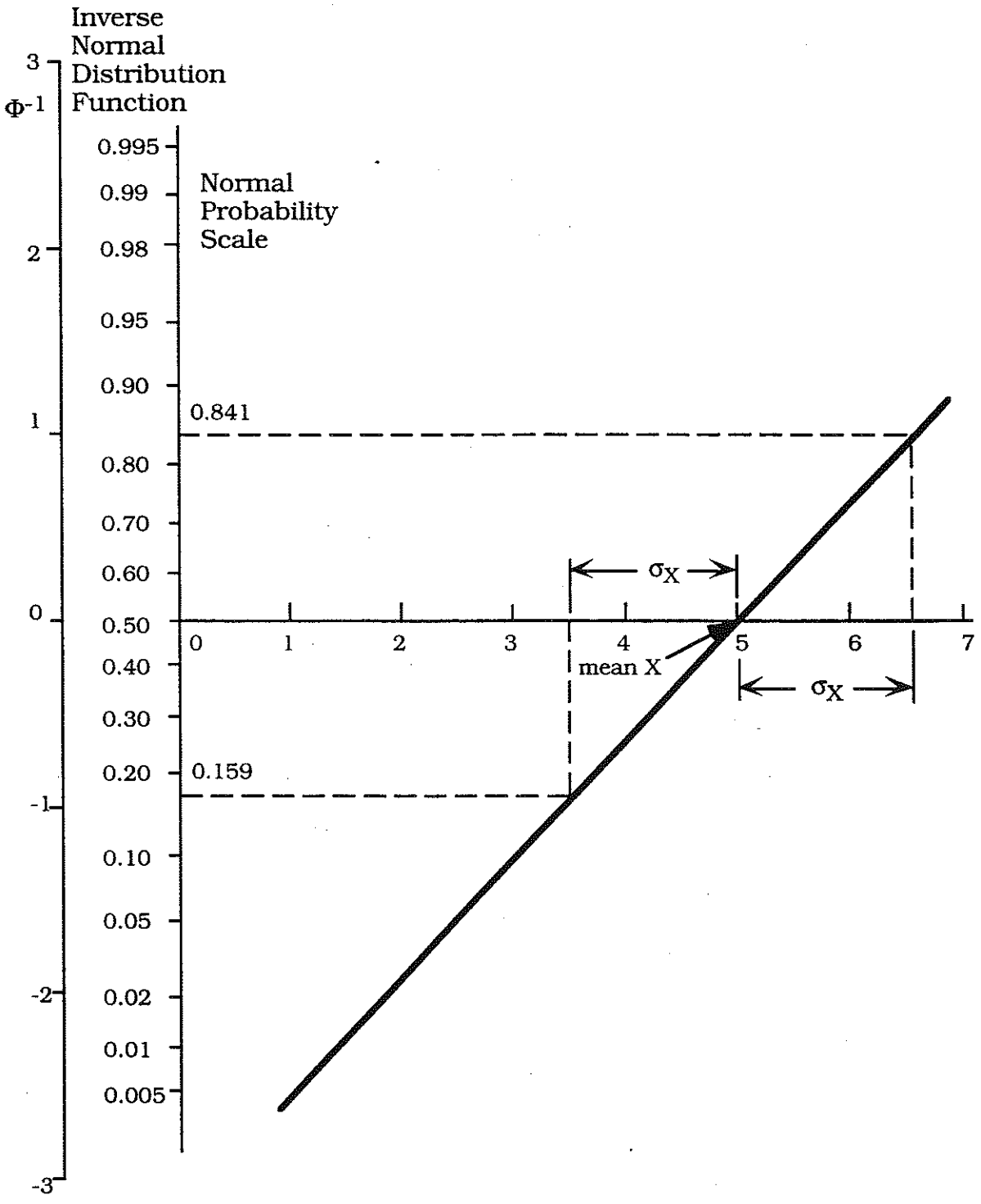

Fig. B-3. Mean And Standard Deviation Of A Normal Random Variable On Normal Probability Paper.

B.3 Use Of Normal Probability Paper

Manual procedure:

1. Collect the data to be plotted (e.g. n test results)

   $a_1, a_2, \ldots, a_n$.

2. Rank a_i's, from the minimum to the maximum value. the rearranged a_i's, are represented by

   $b_1, b_2, \ldots, b_n$

   so that

   $b_1 \leq b_2 \leq \ldots \leq b_n$

3. For each b_i, calculate the probability corresponding to i,

   $p_i = i/(n+1)$

4. Plot b_i vs. p_i, for i = 1,..., n.

Computer procedure:

1. Prepare the file with original data to be plotted (e.g. n test results)

   $a_1, a_2, \ldots, a_n$.

2. Use rank command to rearrange a_i's, from the minimum to the maximum value. the rearranged a_i's, are represented by

   $b_1, b_2, \ldots, b_n$

   so that

   $b_1 \leq b_2 \leq \ldots \leq b_n$

3. For each b_i, calculate the probability corresponding to i,

   $p_i = i/(n+1)$

4. For each p_i calculate the corresponding value of the inverse standard normal function (available on most computers, if not then use the formula given on next page)

$$F_i^{-1} = \Phi^{-1}(P_i)$$

5. Using computer, plot b_i vs. F_i^{-1}, for i = 1,..., N.

Example

Plot Test Results On The Normal Probability Paper

original data:	5.9,	6.5,	7.2,	5.5,	6.4,	6.5,	5.3,	6.8,	5.9
rearranged data:	5.3,	5.5,	5.9,	5.9,	6.4,	6.5,	6.5,	6.8,	7.2
i	1	2	3	4	5	6	7	8	9
$p_i = i/(n+1)$	0.1	0.2	0.3	0.4	0.5	0.6	0.7	0.8	0.9

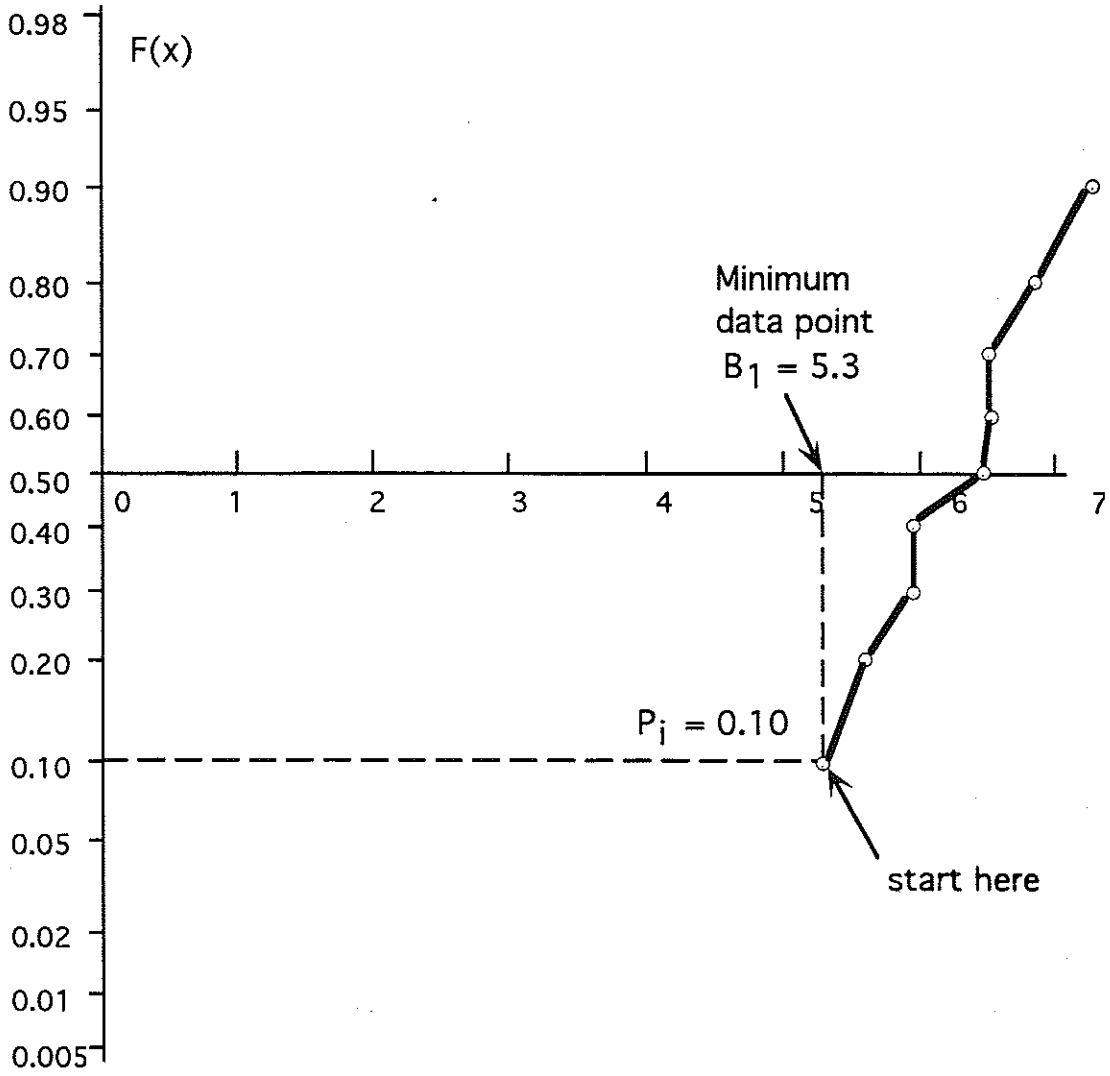

Fig. B-4. Example Of Data Plotted On The Nomral Probability Paper

B.4 Inverse Standard Normal Function

$$x = \Phi^{-1}(p)$$

where p is probability.

for $p < 0.5$,

$$x = \Phi^{-1}(p) = -t + \frac{c_0 + c_1 t + c_2 t^2}{1 + d_1 t + d_2 t^2 + d_3 t^3}$$

where $c_0 = 2.515517$
$c_1 = 0.802853$
$c_2 = 0.010328$
$d_1 = 1.432788$
$d_2 = 0.189269$
$d_3 = 0.001308$
$t = \sqrt{- \ln p^2}$

For $p > 0.5$, Φ^{-1} is calculated for $(1 - p)$, and then

$$\Phi^{-1}(p) = - \Phi^{-1}(1 - p)$$

Normal random variable

Table B-1, $\Phi(x)$ for selected values of x.

X	$\Phi(X)$
4.0	0.9999683
3.0	0.99865
2.0	0.9772
1.0	0.841
0.0	0.5
- 1.0	0.159
- 2.0	0.0228
- 3.0	0.00135
- 4.0	0.0000317

Appendix C. Calculations of Load Carrying Capacities According to AASTHO LRFD Code.

C.1. Flexural Resistance

C.1.1. Prestressed Concrete Girders

The nominal resistance of prestressed concrete girders shall be taken as:

$$Mn = Apsfps\left(dp - \frac{a}{2}\right) + Asfy\left(ds - \frac{a}{2}\right) - As'fc'\left(ds' - \frac{a}{2}\right) + 0.85fc'(b - bw)\beta 1hf\left(\frac{a}{2} - \frac{hf}{2}\right) \quad \text{(C-1)}$$

where:

M_n = nominal resistance specified for compact composite and compact non-composite sections (N-mm).

A_{ps} = area of prestressing (mm^2)

f_{ps} = average stress in prestressing steel at nominal bending resistance (MPa).

d_p = distance from extreme compression fiber to the centroid of prestressing tendons (mm)

A_s = area of non-prestressed tension reinforcement (mm^2)

f_y = specified yield strength of reinforcing bars (MPa)

d_s = distance from extreme compression fiber to the centroid of non-prestressed tensile reinforcement (mm).

A_s' = area of compression reinforcement (mm^2)

f_y' = specified yield strength of compression reinforcement (MPa)

d_s' = distance from extreme compression fiber to the centroid of compression reinforcement (mm).

f_c' = specified compressive strength of concrete at 28 days, unless another age is specified (MPa).

b = with of the compression face of the member (mm).

b_w = width of web (mm).

β_1 = stress block factor

h_f = compression flange depth of an I or T member (mm)

a = $c\beta_1$: depth of the equivalent stress block (mm)

$$f_{ps} = f_{pu}\left(1 - k\frac{c}{d_p}\right) \tag{C-2}$$

for which:

$$k = 2\left(1.04 - \frac{f_{py}}{f_{pu}}\right) \tag{C-3}$$

for T-section behavior:

$$c = \frac{A_p f_{pu} + A_s f_y - A_s' f_y' - 0.85\beta_1 f_c'(b - b_w)h_f}{0.85 f_c' \beta_1 b_w + k A_{ps}\frac{f_{pu}}{d_p}} \tag{C-4}$$

for rectangular section behavior:

$$c = \frac{A_{ps} f_{pu} + A_s f_y - A_s' f_y'}{0.85 f_c' \beta_1 b_w + k A_{ps}\frac{f_{pu}}{d_p}} \tag{C-5}$$

where:

f_{pu} = specified tensile strength of prestressing steel (MPa)

f_{py} = yield strength of prestressing steel (MPa)

c = distance between the neutral axis and the compressive face (mm).

$$\begin{aligned} &\beta_1 = 0.85 && \text{if } f_c' \le 28\text{MPa} \\ &\beta_1 = 0.85 - 0.05\left(\frac{f_c' - 28}{7}\right) && \text{if } 28\text{MPa} < f_c' < 56\text{ MPa} \\ &\beta_1 = 0.65 && \text{if } f_c' \ge 56\text{ MPa} \end{aligned} \tag{C-6}$$

C.1.2. Compact Steel I-Sections

For a non-composite compact steel I-section, nominal resistance shall be taken as:

$$M_n = F_y Z_x \tag{C-7}$$

where:

Fy = yield strength of steel

Zx = plastic section modulus

For a composite compact steel I-section, nominal resistance shall be taken as:

$$M_n = M_p \qquad \text{(C-8)}$$

M_p = plastic moment capacity, which can be calculated as described in section A6 -1 of the 1994 AASHTO LRFD Code.

The sections providing the flexural resistance of Eq.C-7 and 8 shall satisfy the following three checks:

a. Web slenderness check:

$$\frac{2D_{cp}}{t_w} \leq 3.76\sqrt{\frac{E}{F_{yc}}} \qquad \text{(C-9)}$$

where:

D_{cp} = depth of the web in compression

F_{yc} = specified minimum yield strength of the compression flange (MPa)

t_w = web thickness (mm)

E = modulus of elasticity of steel (MPa)

D_{cp} shall be calculated as follows:

a.1. For non-composite sections:

$$D_{cp} = \frac{D}{2A_w F_{yw}}(F_{yt}A_t + F_{yw}A_w - F_{yc}A_c) \quad \text{if} \quad F_{yw}A_w \geq \left|F_{yc}A_c - F_{yt}A_t\right| \qquad \text{(C-10)}$$

otherwise,

$$D_{cp} = D \qquad \text{(C-11)}$$

where:

D = web depth (mm)

A_t = area of the tension flange (mm^2)

A_c = area of the compression flange (mm^2)

A_w = area of the web (mm^2)

F_{yt} = specified minimum yield strength of the tension flange (MPa)

F_{yc} = specified minimum yield strength of the compression flange

F_{yw} = specified minimum yield strength of the web

a.2. For composite sections:

- for sections in positive flexure, where the plastic neutral axis is in the web, D_{cp} shall be taken as:

$$D_{cp} = \frac{D}{2}\left[\frac{F_{yt}A_t - F_{yc}A_c - 0.85 f_c' A_s - F_{yr}A_r}{F_{yw}A_w} + 1\right] \qquad \text{(C-12)}$$

where:

D_{cp} = depth of the web in compression at the plastic moment (mm)

A_s = area of the slab (mm^2)

A_t = area of the tension flange (mm^2)

A_c = area of the compression flange (mm^2)

A_w = area of the web (mm^2)

A_r = area of the longitudinal reinforcement included in the section (mm^2)

F_{yt} = specified minimum yield strength of the tension flange (MPa)

F_{yr} = specified minimum yield strength of the longitudinal reinforcement included in the section (MPa)

f'_c = specified minimum 28-day compressive strength of the concrete (MPa)

- For all other sections in positive flexure, D_{cp} shall be taken equal to 0 and the web slenderness requirement shall be considered to be satisfied.

- For sections in negative flexure, where the plastic neutral axis is in the web:

$$D_{cp} = \frac{D}{2A_w F_{yw}}\left(F_{yt}A_t + F_{yw}A_w + F_{yr}A_r - F_{yc}A_c\right) \qquad \text{(C-13)}$$

- For all other sections in negative flexure, D_{cp} shall be taken equal to D.

b. Compression flange slenderness check:

For composite sections in positive flexure, this requirement is considered satisfied. For composite sections in negative flexure, or either positive or negative flexure cases of non-composite sections:

$$\frac{b_f}{2t_f} \le 0.382\sqrt{\frac{E}{F_{yc}}} \qquad \text{(C-14)}$$

where:

b_f = width of the compression flange (mm)

t_f = flange thickness (mm)

c. Compression flange bracing check:

For composite sections in positive flexure, this requirement is considered satisfied. For composite sections in negative flexure, or either positive or negative flexure cases of non-composite sections, the compression flanges of sections shall be braced to satisfy:

$$L_b \leq \left(0.124 - 0.0759\left(\frac{M_L}{M_P}\right)\right)\left(\frac{r_y E}{F_{yc}}\right) \qquad \text{(C-15)}$$

where:

L_b = the unbraced length (mm)

r_y = minimum radius of gyration of the steel section, with respect to the vertical axis (mm).

M_l = the lower moment due to the factored loading at either end of the unbraced length (N-mm).

M_p = plastic moment

F_{yc} = specified minimum yield strength of the compression flange at the section where r_y is determined (MPa).

C.1.3. Non-Compact Steel Sections

The nominal resistance of a non-compact section is taken as:

$$M_n = F_n S \qquad \text{(C-16)}$$

where:

S = section modulus

For non-compact sections, bending stress rather then absolute moment is evaluated. The nominal flexural stress of each flange is defined as:

$$F_n = R_b R_h F_{yf} \qquad \text{(C-17)}$$

where:

F_n = nominal stress specified for non-compact composite and non-compact non-composite sections (MPa).

R_b and R_h = flange-stress reduction factors

F_{yf} = specified minimum yield strength of the flange (MPa)

Hybrid Factor for Positive Flexure and Composite Sections, R_h

For flexural resistance of composite hybrid sections in positive flexure, the hybrid reduction factor shell be taken as:

$$R_h = 1 - \left[\frac{\beta\psi(1-\rho)^2(3-\psi+\rho\psi)}{6+\beta\psi(3-\psi)} \right] \qquad \text{(C-18)}$$

where:

ρ = F_{yw}/F_{yb}

β = A_w/A_{fb}

ψ = d_n/d

d_n = distance from outer fiber of bottom flange

d = depth of steel section (mm)

F_{yb} = specified minimum yield strength of bottom flange (MPa)

F_{yw} = specified minimum yield strength of web (MPa)

A_w = web area (mm2)

A_{fb} = bottom flange area (mm2)

Hybrid Factor for Negative Flexure and Composite Sections or All Cases of Non-composite Sections, R_h

If the neutral axis of a composite hybrid section is located within 10% of the web depth from mid-depth of the web, or the section is non-composite, the hybrid factor shall be taken as:

$$R_h = \frac{12+\beta(3\rho-\rho^3)}{12+2\beta} \qquad \text{(C-19)}$$

where:

ρ = F_{yw}/f_{fl}

β = $2A_w/A_{tf}$

f_{fl} = lesser of either the specified minimum yield strength, or the stress due to the factored loading in either flange (MPa)

A_{sf} = total area of both steel flanges and the longitudinal reinforcement included in the section (mm^2)

For other composite hybrid sections in negative flexure, the hybrid factor shall be taken as:

$$R_h = \frac{M_{yr}}{M_y} \qquad \text{(C-20)}$$

where:

M_y = yield resistance in terms of moment, when web yielding is disregarded (N-mm)

M_{yr} = yield resistance in terms of moment, when web yielding is accounted for (N-mm).

Load Shedding Factor for Compression Flanges, R_b

For composite sections, if either a longitudinal stiffener is provided, or equation the below is satisfied, then R_b shell be taken as 1.0.

$$\frac{2D_c}{t_w} \leq \lambda_b \sqrt{\frac{E}{f_c}} \qquad \text{(C-21)}$$

If either of the above requirements are not satisfied or the section is non-composite, R_b shall be taken as:

$$R_b = 1 - \left(\frac{a_r}{1200 + 300a_r}\right)\left(\frac{2D_c}{t_w} - \lambda_b \sqrt{\frac{E}{f_c}}\right) \qquad \text{(C-22)}$$

for which

$$a_r = \frac{2D_c t_w}{A_{fc}} \qquad \text{(C-23)}$$

where:

λ_b = 5.76 for members with a compression flange area equal to orgreater then the tension flange area

λ_b = 4.64 for members with a compression flange area less then the tension flange area

f_c = stress in the compression flange due to the factored loading (MPa).

A_{fc} = compression flange area (mm^2)

Load Shedding Factor for Tension Flanges, R_b

For tension flanges, R_b shall be taken as 1.0.

The sections providing the flexural resistance of Eq.C-17 shall satisfy the following three conditions:

a. Web slenderness check:

$$\frac{2D_c}{t_w} \le 6.77\sqrt{\frac{E}{f_c}} \qquad \text{without longitudinal stiffeners} \qquad \text{(C-24)}$$

$$\frac{2D_c}{t_w} \le 11.63\sqrt{\frac{E}{f_c}} \qquad \text{with longitudinal stiffeners} \qquad \text{(C-25)}$$

where:

D_c = depth of the web in compression in the elastic range (mm)

f_c = stress in the compression flange due to the factored loading (MPa)

b. Compression flange slenderness:

For composite sections in positive flexure, this requirement is considered satisfied. For composite sections in negative flexure, or either positive or negative flexure cases of non-composite sections:

$$\frac{b_f}{2t_f} \leq 1.38\sqrt{\frac{E}{f_c\sqrt{\frac{2D_c}{t_w}}}} \qquad \text{(C-26)}$$

c. Compression flange bracing check:

For composite sections in positive flexure, this requirement is considered satisfied. For composite sections in negative flexure, or either positive or negative flexure cases of non-composite sections, the compression flanges of the section shall be braced to satisfy:

$$L_b \leq 1{,}76 r_t\sqrt{\frac{E}{F_{yc}}} \qquad \text{(C-27)}$$

where:

L_b = distance between points bracing the compression flange (mm).

R_t = minimum radius of gyration of the compression flange of the steel section, plus one-third of the web in compression taken about the vertical axis (mm).

F_{yc} = specified minimum yield strength of the compression flange at the section where r_t is determined (MPa).

C.2. Shear Resistance

C.2.1. Concrete Sections

The nominal shear resistance, Vn, shell be determined as the lesser of the following two equations:

$$V_n = V_c + V_s + V_p \quad \text{(C-28)}$$

$$V_n = 0.25\, f'_c\, b_v\, d_v + V_p \quad \text{(C-29)}$$

for which:

$$V_c = 0.083\beta\sqrt{f'_c}\, b_v d_v \quad \text{(C-30)}$$

$$V_s = \frac{A_v f_y d_v (\cot\theta + \cot\alpha)\sin\alpha}{s} \quad \text{(C-31)}$$

where:

b_v = effective web width taken as the minimum web width, with the depthd_v, modified for the presence of ducts where applicable (mm)

d_v = effective shear depth taken as the distance, measured perpendicular to the neutral axis, between the resultants of the tensile and compressive forces due to flexure, but it need not be taken less then the greater of $0.9d_e$ or $0.72h$ (mm)

s = spacing of stirrups (mm)

β = factor indicating ability of diagonally cracked concrete to transmit tension

θ = angle of inclination of diagonal compressive stresses (DEG)

α = angle of inclination of transverse reinforcement to longitudinal axis (DEG).

A_v = area of shear reinforcement within a distance s (mm^2)

V_p = component in the direction of the applied shear of the effective prestressing force, positive if resisting the applied shear (N)

For non-prestressed concrete sections not subjected to axial tension and containing at least the minimum amount of transverse reinforcement, or which have an overall depth less than 400 mm, the following values may be used:

$\beta = 2.0$

$\theta = 45°$

The minimum transverse reinforcement shall be taken as:

$$A_v = 0.083\sqrt{f_c'}\frac{b_v s}{f_y} \qquad \text{(C-32)}$$

where:

A_v = area of a transverse reinforcement within distance s (mm^2)

s = spacing of transverse reinforcement (mm)

f_y = yield strength of transverse reinforcement (MPa)

C.2.2. Steel Sections

The nominal shear resistance of unstiffened webs of hybrid and homogeneous girders shall be taken as:

$$V_n = V_p = 0.58F_{yw}Dt_w \quad \text{if} \quad \frac{D}{t_w} \le 2.46\sqrt{\frac{E}{F_{yw}}} \qquad \text{(C-33)}$$

$$V_n = 1.48t_w^2\sqrt{EF_{yw}} \quad \text{if} \quad 2.46\sqrt{\frac{E}{F_{yw}}} < \frac{D}{t_w} \le 3.07\sqrt{\frac{E}{F_{yw}}} \qquad \text{(C-34)}$$

$$V_n = \frac{4.55t_w^3E}{D} \quad \text{if} \quad \frac{D}{t_w} > 3.07\sqrt{\frac{E}{F_{yw}}} \qquad \text{(C-35)}$$

where:

F_{yw} = specified minimum yield strength of the web (MPa)

D = web depth (mm)

t_w = thickness of web (mm)